TABLE DES MATIERES

LISTE DES FIGURES

LISTE DES TABLEAUX

GLOSSAIRE DES TERMES ET DES SYMBOLES

ANOVA	Analyse de variance
ASTM	American Society for Testing and Materials
C1	carbone lié avec un seul atome d'oxygène non carbonyle, ou avec un atome d'hydrogène
C2	carbone lié avec un atome d'oxygène
C3	carbone lié avec un atome d'oxygène (liaison double) ou avec deux atomes d'oxygène
C4	carbone lié avec deux atomes d'oxygène (une liaison simple et une liaison double)
ΔE	Énergie d'activation
DMA	analyse dynamique mécanique
DRIFTS	spectroscopie infrarouge à transformée de Fourier, couplée à la technique de réflectance diffuse
DSC	calorimétrie différentielle à balayage
DTG	thermogravimétrie en dérivation
E′	module dynamique de stockage
E″	module dynamique de perte
FLD	distribution de la longueur des fibres
FQA	analyseur de la qualité des fibres
FTIR	spectroscopie infrarouge à transformée de Fourier
FTIR-EGA	technique couplée de spectroscopie infrarouge à transformée de Fourier et analyseur des gaz émis
HDPE	polyéthylène haute densité
ICTA	International Confederation for Thermal Analysis

iPP	polypropylène isotactique
J	complaisance de fluage
Lw	longueur pondérée
MAPE	copolymères greffés éthylène-anhydride maléique (MAPE)
MOE	module d'élasticité
MOR	module de rupture
O/C	ratio atomique oxygène/carbone
PE	polyéthylène
R	universal gas constant
RB	résistance à la rupture
Rm	résistance maximale à la flexion
SEM	Microscope électronique à balayage
tan δ	facteur de perte
TGA	analyse thermogravimétrique
TTSP	Principe de superposition temps-température
WPC	composite bois/plastique
wt%	pourcentage par poids total
XPS	spectroscopie de photoélectrons avec rayons X
ε RB	élongation maximale à la rupture
χ_c	cristallinité
ω	fréquence d'oscillation

ABSTRACT

The potential of wood fibers from sawmill residues as reinforcing component for thermoplastic composites was investigated. Wood species (*Thuja occidentalis L.*, *Pinus banksiana* lamb. and *Picea mariana* (Miller)), type (heartwood, sapwood, bark), load (25, 35 and 45 wt %) size (24, 42 and 64 mesh) and processing method (injection molding, extrusion, compression molding) were the main variables analyzed. An incomplete factorial experimental design was used to make composites. The Production of wood plastic composite samples was carried out in two steps: (i) a compounding stage and (ii) injection molding, molding thermo-compression and single-screw extrusion stage.

Diffuse reflectance infrared Fourier transform spectroscopy (DRIFTS) and X-ray photoelectron spectroscopy (XPS) were used to investigate the variability in the surface chemical composition. Both DRIFTS and XPS showed high variability in fiber surface chemical composition between species and between fiber types (sapwood, heartwood, and bark). However, DRIFTS failed to assess surface modification by esterification reaction using a maleic anhydride polyethylene (MAPE) treatment. XPS results showed that MAPE treatment increased the surface hydrocarbon concentration of jack pine wood fiber as indicated by a decrease in oxygen-carbon ratio and an increase in relative intensity of the C1 component in the C1s signal. Lignin concentration on the fiber surface was found to be the major inhibitor factor for esterification.

Thermal sensitivity of wood fibers was investigated using thermogravimetric analysis and the nucleating ability and non-isothermal crystallization of high density polyethylene (HDPE) were studied using differential scanning calorimetry. Results showed that wood degrades at a lower temperature than HDPE. The most dissimilarity was observed between wood and bark in the decomposition rate at processing temperature around 300°C and the peak temperature location for cellulose degradation. The higher degradation rate for bark is explained by the devolatilization of extractives and the degradation of lignin. Nucleating ability for various wood fillers was evaluated by crystalline weight fraction, crystal conversion, half-time crystallization and crystallization temperature of the HDPE matrix. Nucleation activity improved with the addition of wood particles to the HDPE matrix. However, no effect of wood species on crystal conversion was found.

Selected mechanical and physical properties of wood plastic composites were studied. All tested properties vary significantly with fiber origin. Higher fiber size produces

higher strength and elasticity but lower toughness and elongation. The effect of fiber size on water uptake is minimal. Increasing fiber load improves the strength and stiffness of the composite but decreases elongation and toughness. Water uptake increases with increasing fiber proportion.

The sensitivity of wood particles (eastern white cedar, black spruce, jack pine and jack pine bark) to composite processing was analyzed. Because of their higher thermal sensitivity, bark particles showed higher propensity to generate fines than wood particles. The major reduction in mean particle length was found to occur in the compounding process, while extrusion and injection molding contributed to particle length reduction to a lesser extent. The relationship between the structure and properties of high density polyethylene (HDPE) filled with the various wood fiber species in relation to processing techniques was also investigated. The main reduction of the effective mean particle length was observed after the compounding process, while extrusion and injection molding influence length distribution, which was shifted toward shorter length.

The effects of wood filler characteristics and processing methods on either the mechanical relaxation and the creep behavior of the thermoplastic matrix were investigated. It was concluded that this behavior was related to the chemical composition on the surface of the wood fibers and the efficiency of the adhesion mechanism between fibers and HDPE.

Dynamic mechanical properties of wood particle/HDPE composites were investigated. Jack pine-based composites showed the highest storage modulus. This behavior was attributed to better interfacial adhesion between jack pine wood fiber and HDPE matrix. In HDPE, the α-relaxation peak shifted to high temperature regions with the addition of wood fiber and resultant loss modulus (E″) increased by 17% to 30%, indicating more viscous dissipation. Cooling rate of extruded samples significantly affected α-peak temperature. Storage modulus (E′) increased with increasing frequency, whereas loss factor (tan) δ and E″ decreased. Moreover, α-peak tended to shift to lower temperatures as frequency decreased. A slight increase in activation energy (ΔE) was detected after wood particle addition, which may be explained by the increase in crystallinity due to the nucleation efficiency of wood filler.

Creep behavior of wood particles/ (HDPE) composites was investigated. Short-term creep tests at different temperature levels were carried out and modeled using Bürger's model and Findley's power law. Jack pine fibers based composites exhibited the best creep reduction, which is related to the chemical composition on the surface of wood fibers and the efficiency of the adhesion mechanism between fibers and HDPE. Master curves, constructed by applying the time-temperature superposition principal (TTSP), and Findley-extrapolated data did not depict similar tendencies. Dynamic mechanical behavior has been calculated from the short-term creep

measurement and a good agreement between calculated and predicted values was observed only at moderate frequency (0.5 to 1.5 Hz).

RÉSUMÉ

Ce travail est une analyse comparative du potentiel de fibres de bois issues de résidus de première transformation dans la fabrication des composites bois/thermoplastiques. Les fibres analysées proviennent des essences suivantes : le thuya occidental (*Thuja occidentalis* L.), le pin gris (*Pinus banksiana* Lamb.) et l'épinette noire (*Picea mariana* Mill.). Les effets des facteurs suivants sur la performance des matériaux composites bois/thermoplastique ont été analysés : l'essence de bois, l'origine des fibres (fibres de duramen ou d'aubier), la taille des particules de bois, les proportions dans le mélange et les procédés de mise en forme (injection, extrusion et thermo-compression), selon un dispositif factoriel incomplet.

La production des échantillons de composites bois plastique a été réalisée en deux étapes : (i) une étape de mélange et mise en granules et (ii) une étape de mise en forme proprement dite des échantillons par moulage par injection, moulage par thermo-compression ou par extrusion mono-vis. L'effet de la variabilité spécifique de la surface des fibres de bois sur la qualité de l'interface bois/thermoplastique a été étudié moyennant l'utilisation de la spectroscopie infra rouge en mode réflexion diffuse par Transformée de Fourier (DRIFTS) et spectroscopie des photoélectrons par rayons X (XPS). Les deux techniques ont montré une grande variabilité dans la composition de la surface des fibres issues de différentes espèces et aussi à l'intérieur d'une même espèce (aubier, bois de duramen, écorce). La surface des fibres a été modifiée par réaction d'estérification en utilisant le polyéthylène modifié à l'anhydre maléique (MAPE). Les modifications de surface n'ont pas été détectées par DRIFTS, cependant les résultats de XPS ont montré que le traitement par le MAPE augmente la concentration des molécules d'hydrogène et d'oxygène notamment sur la surface des fibres de pin gris indiquée par une diminution du rapport oxygène-carbone et une augmentation de l'intensité relative de la composante C1 dans le signal C1s. Une concentration élevée de lignine et d'extractibles sur la surface des fibres a été présentée comme principal facteur qui inhibe l'établissement d'un lien entre l'agent de couplage à base d'anhydride et le bois.

La stabilité thermique des fibres de bois a été étudiée par analyse thermogravimétrique, alors que la capacité de nucléation et la cristallisation non-isotherme du polyéthylène haute densité (PEHD) à différentes charges de bois ont été étudiées par calorimétrie différentielle à balayage. Les résultats ont montré que le bois se dégrade à une température nettement inférieure à celle du PEHD. Toutefois, la

cinétique de la décomposition thermique était similaire entre les essences de bois. Les divergences les plus remarquables ont été observées entre le bois et l'écorce aux alentours d'une température de 300°C qui correspond à la température de dégradation de la cellulose. Le taux élevé de la dégradation de l'écorce a été expliqué par le dégazage de matières extractibles et la dégradation de la lignine. La capacité de nucléation, à différents taux de charges en fibres de bois, a été évaluée grâce à la variation de la fraction cristalline, au taux de conversion en cristal, au demi-temps de conversion et à la température de cristallisation du PEHD. Il a été remarqué que la nucléation a été améliorée avec l'ajout de particules de bois à la matrice du PEHD. Cependant, aucun effet de l'essence de bois sur le taux de conversion en cristal n'a été trouvé. Les effets d'une variation du type des fibres, de leur taille et de leur proportion dans le mélange sur les propriétés mécaniques et physiques des composites bois-plastique ont été étudiés. Les résultats ont montré que toutes les propriétés testées varient de façon significative avec l'essence de la fibre. Une forte granulométrie des fibres donne des composites plus résistants et plus rigides, mais moins tenace et ayant un taux d'élongation à la rupture inférieur. Par contre, la granulométrie des fibres n'a pas d'effet significatif sur le taux d'absorption d'eau des composites bois/plastique. L'augmentation de la charge de fibres améliore la résistance et la rigidité du composite, mais diminue l'allongement et la ténacité. La teneur en eau augmente significativement avec l'augmentation de la charge en fibres de bois dans le mélange. Par ailleurs, l'analyse du développement des fibres de bois, avant et au cours de leur mise en forme, a montré que l'intégrité des fibres, en termes d'attrition de la forme et de la longueur, a été tributaire des caractéristiques intrinsèques des fibres de bois et des procédés utilisés.

Les résultats des propriétés mécaniques dynamiques des composites bois/PEHD ont montré que le module de stockage (E') diminue avec une augmentation de la température. Toutefois, les composites à base de fibres de pin gris ont montré le module de stockage le plus élevé. Ceci a été expliqué par une meilleure compatibilité entre les fibres de bois de pin gris et le polymère thermoplastique. Le pic de relaxation de type α a légèrement décalé vers les hautes températures en réponse à une addition des fibres de bois. Au contraire, le module de perte (E") qui en résulte a augmenté de 17% à 30%, indiquant ainsi plus de dissipation visqueuse. La vitesse de refroidissement des échantillons extrudés affecte la température du pic de la relaxation α. E' augmente avec une augmentation de la fréquence de sollicitation, alors que le facteur des pertes (tan δ) et E" ont diminué pour le même effet. En outre, la température relative au pic de la relaxation α a diminué en réponse à une diminution de la fréquence. La légère augmentation de l'énergie d'activation ΔE, détectée après l'ajout de particules de bois, a été expliquée par l'augmentation de la cristallinité due à l'efficacité de nucléation des particules de bois.

Des essais de fluage à court terme pour différentes températures ont été réalisés sur des éprouvettes de composites et des modèles d'analogie (modèle de Burger et la loi de puissance de Findley) ont été utilisés afin de décrire leur comportement mécanique différé. Le fluage des composites augmente avec la température. Ceci s'explique par la mobilité de la fraction amorphe du polymère. Globalement, les particules de bois permettent de réduire le niveau de fluage des composites dépendamment du type des fibres utilisées. La variation de la résistance au fluage entre les composites est lié à la composition chimique de la surface des fibres du bois et donc, l'efficacité du mécanisme d'adhésion entre les fibres et le PEHD. Les Courbes maîtresses, construites en appliquant le principe de superposition temps-température (TTSP), ont présentées des divergences avec celle obtenues par extrapolation de la loi de Findley. Enfin, les résultats de mesure du fluage à court terme ont été utilisés pour prédire les propriétés mécaniques dynamiques, toutefois une bonne concordance entre les valeurs calculées et les valeurs prédites n'a été observée qu'à des fréquences modérées (0,5 à 1,5 Hz).

CHAPITRE 1

INTRODUCTION

Le marché nord-américain des composites bois/polymères (WPC) est marqué par une forte croissance ces dix dernières années. En effet, en 2005, le volume de vente de ces matériaux aurait dépassé un milliard de dollars, aux États-Unis seulement (Smith et Wolcott, 2006). Les deux tiers de la quantité produite étaient sous forme de planchers et de clôtures. Le marché nord-américain continue à progresser avec une moyenne annuelle de croissance de 14% pour, au moins, le reste de la décennie (Anonymous, 2003).

Présenté comme une alternative au bois, sans ses inconvénients, les composites bois/polymères qui contiennent une forte proportion de bois (jusqu'à 80 %) peuvent être utilisés à la place de ce matériau, mais avec une durabilité à l'extérieur semblable à celle des plastiques et avec des frais de maintenance très réduits.

En réalité, plusieurs autres facteurs demeurent derrière cette volonté vers le remplacement du bois massif traditionnel par de nouveaux matériaux: D'une part, les forêts s'épuisent au niveau mondial, et d'autre part, l'engouement pour les produits en bois augmente avec l'augmentation du niveau de vie et l'industrialisation de plusieurs pays émergents comme la Chine, l'Inde, et les pays de l'Europe de l'Est. Par ailleurs, les ressources disponibles ne satisferont plus à une demande accrue des

consommateurs qui se penchent de plus en plus vers les matériaux écologiques pour divers soucis environnementaux. En outre, pour un arbre abattu, seulement la moitié du volume est transformée en planches. Le reste est utilisé dans différents usages incluant la production de pâtes à papier, les panneaux à base de bois, l'énergie, l'utilisation comme litières pour animaux ou mulch agricole. Bien qu'une quantité appréciable de ces résidus soit effectivement utilisée dans la production des panneaux de particules ou de fibres à haute valeur ajoutée, un fort potentiel de réutilisation de ces résidus demeure disponible pour soutenir une industrie de composites bois/polymères. Ceci est d'autant plus intéressant que le prix du pétrole augmente, obligeant ainsi les transformateurs à rechercher des éléments de charge bon marché pour réduire le coût des plastiques (Clemons, 2002; Stokke et Gardner, 2003; Pritchard, 2004; Ashori, 2008).

Cela dit, les fibres de bois sont aujourd'hui utilisées dans la formulation de plusieurs thermoplastiques comme renfort du matériau, en remplacement des fibres minérales, telles que les fibres de verre. Étant plus légères, elles présentent également des propriétés mécaniques comparables à celles du verre (résistance à la traction, résilience ...) et une facilité d'usinage et de mise en forme.

Si les matériaux composites bois plastiques sont aujourd'hui d'utilisation courante dans des secteurs tels que l'automobile, la décoration et les terrasses, leurs applications structurales dans le domaine de construction des bâtiments et du génie civil restent embryonnaires. Ils se heurtent aux conditions de mise en œuvre et aux exigences techniques de construction des bâtiments. En effet, la sensibilité à la température et à l'humidité ainsi que les problèmes de compatibilité avec les polymères synthétiques limitent encore l'utilisation des fibres de bois dans de telles applications. Ceci est ajouté à de fortes contraintes en termes de coût, du fait de la concurrence des matériaux traditionnels.

Cette étude s'intéresse au potentiel des fibres de bois issues de résidus de sciage comme élément de renfort pour les polymères thermoplastiques. L'objectif principal est alors d'établir une relation entre la variabilité intrinsèque des résidus de sciage, notamment la variabilité spécifique, la variabilité entre fibres issues du bois de duramen, du bois de l'aubier ou de l'écorce, et la performance des composites qui en résultent. Les objectifs spécifiques se résument dans les quatre points suivants :

- Enquêter sur l'effet de l'interface bois/polymère sur les propriétés mécaniques du composite ;
- Étudier les effets de la morphologie et de la charge des fibres de bois sur le développement des propriétés physico-mécaniques des matériaux composites bois/thermoplastique ;
- Étudier l'effet des procédés de fabrication des composites sur la structure des fibres de bois et aussi sur les propriétés mécaniques aussi bien statiques que dynamiques du matériau composite produit ;
- Étudier le comportement mécanique différé (dit aussi comportement viscoélastique) des composites á base de fibres de bois par analogie avec des modèles rhéologiques «puissance» et «exponentiel».

L'hypothèse de recherche sur laquelle repose ce projet est que la variabilité intrinsèque des fibres naturelles explique, en grande partie, la divergence des caractéristiques mécaniques et physiques des matériaux composites. Nous supposons ainsi que, selon les espèces, les fibres de bois ne présentent pas la même compatibilité avec les polymères synthétiques. Une connaissance approfondie de l'état de surface des trachéides permettra alors de classer ces matériaux selon leur aptitude à établir une meilleure adhésion avec les polymères.

Afin d'atteindre ces objectifs, ce travail a été subdivisé en huit parties. Tout d'abord, parce que le bois est un matériau complexe et dans le but de l'utiliser efficacement

comme élément de renfort pour des polymères thermoplastiques, les aspects fondamentaux incluant les caractéristiques anatomiques et chimiques, sont indispensables. Pour cela, une revue bibliographique a été consacrée à l'analyse des principaux éléments anatomiques clés qui peuvent affecter l'interaction entre les fibres de bois et les polymères thermoplastiques, tels que la longueur des fibres et la structure de leur paroi cellulaire (**Chapitre II**). Les techniques d'analyse des caractéristiques intrinsèques des fibres de bois ont été brièvement discutées dans une deuxième partie de ce même chapitre. La nature de l'interface et les mécanismes d'adhésion entre les deux phases du composite ont été révisés aussi dans ce chapitre.

Dans le **Chapitre III**, la variabilité de la composition chimique de la surface des fibres chez différentes espèces de bois (thuya occidental, pin gris, et épinette noire) issues de résidus de sciage a été étudiée moyennant le recours à la spectroscopie infrarouge à transformée de Fourier, couplée à la technique de réflectance diffuse (DRIFTS) et la spectroscopie de photoélectrons avec rayons X (XPS). Le **Chapitre IV** est dédié à l'effet de cette variabilité du point de vue aptitude à réagir avec un agent de couplage : le polyéthylène greffé anhydride maléique (MAPE). À la fin de ce chapitre, une classification de ces fibres selon la composition de leur surface et donc, selon leur aptitude à former une liaison chimique avec d'autres composants, a été dressée.

Dans le **Chapitre V,** la sensibilité thermique et le pouvoir d'initier la cristallisation du HDPE pour les différentes particules de bois utilisées dans cette étude ont été analysés. Pour ce faire, la technique d'analyse thermogravimétrique et la technique de l'analyse par calorimétrie différentielle à balayage ont été utilisées, respectivement. Le but essentiel de cette partie était de déterminer les limites de la stabilité thermique des fibres de bois qui seront soumises à un fort gradient de température lors du procédé de fabrication des composites et aussi d'évaluer le potentiel des particules de

bois comme agent de nucléation lors du refroidissement du polymère semi-cristallin : le HDPE.

Le **chapitre VI** est consacré à l'évaluation de l'effet de la variabilité spécifique du facteur forme et des proportions de charge sur quelques propriétés mécaniques et physiques des échantillons de composites bois/HDPE. Des méthodes statistiques conventionnelles ont été utilisées dans cette investigation et les relations entre la microstructure (la cristallinité), la chimie de surface de ces échantillons et les propriétés macro-mécaniques a été mise en évidence.

Parce que les caractéristiques intrinsèques des fibres de bois, comme éléments de renfort ou de charge d'un polymère thermoplastique, varient en fonction des espèces, de la structure et de la densité des parois cellulaires, leur vulnérabilité vis à vis les conditions opératoires ne peut pas être la même. Pour cela, dans le **Chapitre VII**, nous avons étudié la modification des particules de bois, en termes de variation de la distribution des dimensions géométriques, au cours des différents procédés de fabrication des composites, notamment les procédés de défibrage mécanique, de mise en granules, d'extrusion, d'injection et de thermo-consolidation.

Les propriétés mécaniques dynamiques et les mécanismes de relaxation des chaînes moléculaires sont souvent utilisés pour déterminer les caractéristiques de l'interface des systèmes polymériques hétérogènes (Mohanty *et al.*, 2006). En effet, la relation entre la température et les paramètres dynamiques, tels que le module dynamique de stockage (E'), le module de perte (E'') et le facteur de perte (tanδ) fournissent des éléments d'information permettant d'évaluer le degré d'interaction entre les différents composants du système composite (Mohanty *et al.*, 2006). Conformément à ce concept, le **Chapitre VIII** est dédié, en général, à l'étude de l'effet de l'ajout des fibres de bois sur le comportement mécanique dynamique du composite et, en particulier, sur les mécanismes de relaxation du HDPE.

Étant donné que la structure moléculaire instable des polymères thermoplastiques change en fonction du temps, plusieurs propriétés mesurées dans des conditions statiques seront inefficaces dans certaines applications où les composites bois/plastiques encourront l'épreuve d'un changement persistant de la température et de l'humidité (mode dynamique). C'est pourquoi, prédire le fluage du composite bois plastique qui, par évidence, augmente quand les molécules de la matrice bougent et aussi quand les éléments de renfort glissent ou se délocalisent, demeure une mesure indispensable pour identifier les champs d'utilisation potentielle des matériaux produits. Ainsi, l'effet de variation de l'origine des particules, de leur taille, leurs proportions dans le mélange ainsi que l'effet les procédés de mise en forme sur le comportement au fluage des composites bois plastiques ont été développés dans une dernière partie de cette thèse (**Chapitre IX**).

CHAPITRE 2

REVUE DE LITTERATURE

2.1 Introduction

Ces dernières années, l'industrie forestière canadienne, notamment québécoise, passe par une phase de transition qui se marque par une restructuration de toute la filière bois. Cette restructuration était imminente suite à l'interférence de plusieurs facteurs défavorables dont : un déclin en quantité et en qualité des ressources lignocellulosiques, accès restreint aux marchés internationaux à cause de l'amélioration de la compétitivité des produits issus des pays en voie de développement, d'une part et l'augmentation des taxes sur les frontières, d'une autre part. Face à ces difficultés, il est évident que la solution doit passer impérativement par l'établissement d'une stratégie pour l'amélioration de la compétitivité qui sera basée sur l'innovation, dans laquelle la deuxième transformation des produits forestiers doit jouer un rôle clef. En effet, l'industrie du bois est appelée aujourd'hui à relever plusieurs défis allant du développement de produits innovateurs, performants et donc compétitifs, tout en adoptant de nouvelles technologies de conception et de fabrication, jusqu'aux nouvelles pratiques qui conduisent à la réduction des coûts de production et ce au même titre que la protection de l'environnement.

Parmi plusieurs produits forestiers ayant une valeur ajoutée potentielle, les matériaux composites à base de bois et de plastiques s'inscrivent parfaitement dans cette même

perspective. En effet, la réutilisation des fibres de bois issues des résidus de sciage, des résidus de pâtes et papiers, ou encore des résidus de coupes forestières est une pratique qui génère non seulement des retombées économiques, mais aussi environnementales.

Au Québec, les scieries génèrent d'énormes quantités de résidus de sciage. Malgré la concurrence avec le secteur de bioénergie, le potentiel du stock en matière ligneuse reste convenable pour maintenir une industrie de composites durable. Comme le montre le Tableau 2.1, les résidus lignocellulosiques produits dans la province en 2004 sont estimés à 6 669 tonnes anhydres (TA). Seulement 100 000 TA (1.5%) ont été inventoriées comme un surplus, tandis que 169 000 TA (2.5%) ont été exportés au États-Unis (Anonymous, 2005). Malgré que le rapport national sur les résidus de sciage au Canada ait prévu un déclin dans la génération des résidus de sciage au Québec, suite à la décision du Gouvernement québécois du 18 mars 2005 de réduire les possibilités annuelles de coupe des résineux de 20%, l'impact de cette décision peut être comblé par le recours à des sources non-conventionnelles d'approvisionnement en fibres de bois, par exemple à partir des boues papetières.

Tableau 2.1. Bilan de l'année 2004 des résidus de sciage au Québec: production, consommation, exportation et surplus en TA. (Anonymous, 2005)

	Ecorce	Sciures	Copeaux	Total
Production	3 472,645	1 655,862	1 540,640	6 669,146
Consommation				6 400,146
Exportation				169,000
Surplus				100,000

En plus des avantages liés à la protection de l'environnement, les produits composites bois-plastiques doivent leur succès à plusieurs facteurs de performance. En effet, comparés aux produits composés entièrement de polymères, les composites bois-plastiques sont moins coûteux, plus léger, ayant une meilleurs résistance mécanique à

l'impact et au fluage ainsi qu'une facilité de fabrication selon les technologies de plasturgie conventionnelles. Par rapport au bois, ces matériaux sont moins hydrophobes, dimensionnellement plus stables et plus résistants aux attaques fongiques (Caulfield *et al.*, 2005).

Toutefois, les principaux obstacles à la progression de ce type de produits par rapport aux applications traditionnelles du bois solide sont en grande partie liés à sa résistance mécanique inférieure à celle du bois et aussi à son prix de vente élevé. L'incompatibilité entre les fibres de bois et le polymère synthétique demeure la principale cause du manque de performances mécaniques des matériaux composites. Ainsi, l'amélioration de l'interface demeure un défi majeur pour l'industrie des composites à base de fibres naturelles et un champ de recherche interdisciplinaire fertile (Bledzki *et al.*, 1996; Gassan et Bledzki, 1997; Bledzki *et al.*, 1998b; Bledzki et Gassan, 1999).

Le bois est souvent considéré comme un matériau composite formé d'une structure fibreuse complexe. À leur tour, les fibres de bois sont aussi des structures composites dans lesquelles la structure cristalline des microfibrilles joue le rôle de l'élément de renfort, alors que la matrice est principalement composée de lignines et hémicelluloses et, dans une proportion beaucoup plus faible, elle contient aussi des extractibles, des protéines et certains composés inorganiques. Étant donnée la multidisciplinarité des domaines impliqués dans l'examen d'un matériau composite à base de fibres naturelles aux différentes étapes de production, il n'est pas réaliste de penser qu'une étude bibliographique, aussi complète soit elle, puisse être exhaustive sur le sujet. Notre attention sera accordée aux aspects liés aux caractéristiques des fibres ligneuses et aux facteurs permettant leur « adhésion » avec une matrice thermoplastique. Cela dit, dans cette revue bibliographique, nous nous proposons d'analyser les éléments anatomiques du bois qui peuvent influencer l'interaction entre les fibres de bois et la matrice thermoplastique. Ainsi, l'analyse sera basée sur une

anatomie comparative de quelques essences canadiennes, notamment le thuya occidental (*Thuja occidentalis* L.), le pin gris (*Pinus banksiana* lamb) et l'épinette noire. (*Picea mariana* (Mill.)). Dans une seconde partie, on porte attention à la surface des fibres de bois tant pour sa complexité structurelle que pour son rôle déterminant dans l'amélioration de l'interface bois-polymère.

2.2 Les éléments anatomiques clés influençant la performance des composites à base de fibres courtes et polymère thermoplastique

2.2.1 Introduction à l'anatomie des conifères

Par opposition aux feuillus, le bois des résineux (gymnospermes) présente une structure anatomique relativement simple, uniforme et régulière. Cela lui permet d'être convenable pour différentes applications (Panshin et De-Zeeuw, 1980). Seulement deux principaux types de cellules constituent les plans ligneux de tous les résineux : les trachéides qui constituent 90% de l'ensemble des cellules du bois des résineux et les cellules de parenchyme. Étant donné que le bois des résineux ne contient pas des éléments de conduction spécifiques (les vaisseaux), les trachéides remplissent le double rôle de conduction verticale de la sève brute et de soutient mécanique de la structure, alors que les rayons ligneux servent d'éléments de stockage et de distribution de réserves horizontalement (Core *et al.*, 1979). Le xylème des résineux contient aussi des cellules de parenchyme à paroi cellulaire mince. Ces cellules entourent les canaux résinifères radiaux et longitudinaux. En réalité, ces derniers ne forment pas des éléments proprement dit du bois mais une cavité entourée par des groupes de cellules de parenchymes et épithéliales excrétrices organisées pour former un canal où les substances secrétées sont rejetées dans sa cavité (Panshin et De-Zeeuw, 1980) (Figure 2.1.a). La variation du nombre, de la manière avec laquelle les canaux résinifères sont regroupés, de leur taille ainsi que de la taille et le type des

cellules épithéliales ne dépendent pas seulement de l'espèce, de l'âge de l'arbre et du taux de croissance, mais aussi des accidents d'origine quelconque. En effet, en cas de lésion, les résineux élaborent des tissus spéciaux de cicatrisation autre que les canaux résinifères. Ces canaux sont appelés des canaux traumatiques souvent alignés tangentiellement (Figure 2.1.b). De nombreux genres sont dépourvus de canaux résinifères, par exemple, Cedrus, Abies, … (Core *et al.*, 1979)

Figure 2.1. a) Coupe transversale d'un canal résinifère longitudinal (à gauche) avec des cellules épithéliales à parois cellulaires minces chez *Pinus banksiana* lamb. (x20). b) À droite, canaux résinifères traumatiques chez *Picea mariana* (Mill.) (x5).

Comme le montre la Figure 2.2.a, les trachéides longitudinales dans le plan ligneux d'un gymnosperme, exemple du *Thuja occidentalis* L., sont arrangées en structure uniforme. Dans le bois initial, les trachéides longitudinales sont hexagonales, ayant une paroi cellulaire relativement mince et un diamètre plus étendu dans la direction radiale (figure 2.2.b). Dans la direction tangentielle, le diamètre demeure sensiblement constant dans un même cerne annuel et ne varie que légèrement avec l'âge de l'arbre (Panshin et De-Zeeuw, 1980). Lorsqu'on passe du bois initial au bois final, on remarque une diminution radiale de la cellule accompagnée d'une

augmentation de l'épaisseur des parois. La transition d'un type à l'autre entre une saison de végétation et la suivante est toujours abrupte tandis qu'à l'intérieur d'une saison de végétation, elle est relativement graduelle (*Thuja occidentalis* L), (Figure 2.2.a) ou abrupte (*Pinus banksiana* lamb), (Figure 2.2.b).

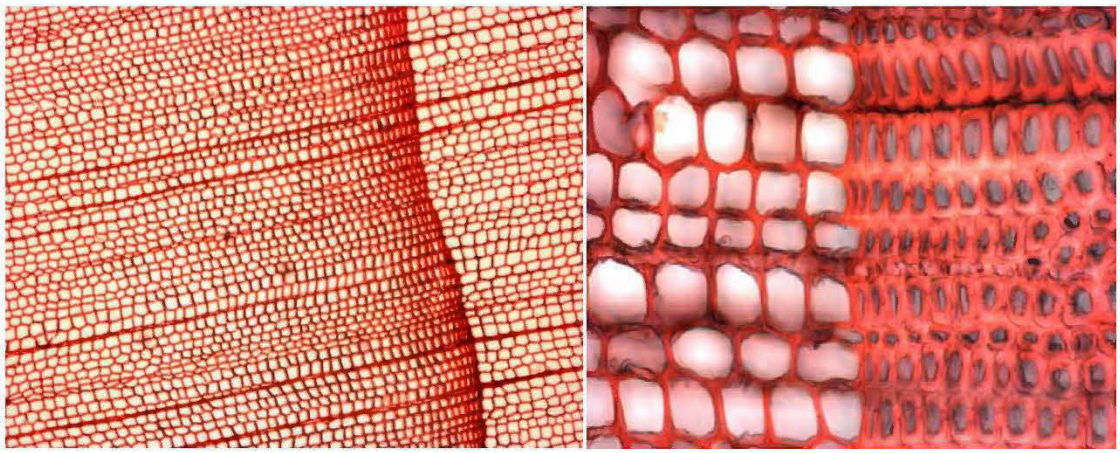

Figure 2.2. a) Exemple de transition graduelle du bois initial au bois final sur une coupe transversale de *Thuja occidentalis* L. (x1.5, à gauche). b) Transition abrupte du bois initial au bois final d'une coupe transversale de bois de *Pinus banksiana* lamb. (x20, à droite).

Les faces radiales des trachéides longitudinales portent de nombreuses ponctuations aréolées, permettant les échanges de cellule à cellule (Figure 2.3.a et b). Ces ponctuations sont moins abondantes sur la face tangentielle. Chez les résineux, le flux dans la direction axiale qui se fait à travers les ponctuations aréolées est de 50 à 200 fois plus rapide que dans les deux autres directions (Stamm, 1953). Les échanges dans la direction tangentielle sont contrôlés par les ponctuations situées sur la face radiale de la paroi des trachéides (Banks, 1970; Watanabe, 1998; Olsson *et al.*, 2001) alors que la communication entre les trachéides longitudinales et les parenchymes radiaux se fait à travers les ponctuations des champs de croisement (Panshin et De-

Zeeuw, 1980). En outre, Malkov et *al*. (2003) ont comparé la vitesse de pénétration de l'eau dans des cubes de bois d'aubier et bois de duramen. Ils ont observé que la pénétration dans le bois d'aubier est beaucoup plus rapide que dans le bois de duramen. Ils ont expliqué cela par la différence de capillarité entre ces deux types de bois.

2.2.2 Longueur des trachéides

La relation entre la taille des trachéides et l'âge cambial est souvent discutée (Lindström, 1997; Lindström *et al.*, 1998; Sirviö et Kärenlampi, 2001). Bien qu'il ait été démontré que la variation des dimensions physiques de la trachéide est prédominée par la maturité du cambium (Panshin et De-Zeeuw, 1980; Lindström *et al.*, 1998), on retient dans cette étude bibliographique que les longues fibres (trachéides) de résineux ont une paroi relativement plus épaisse que les fibres courtes. En effet, les trachéides atteignent une longueur minimale dans la zone de bois initial alors qu'un maximum de longueur est observé dans la zone de bois final : où la paroi des trachéides atteint également un maximum d'épaisseur (Panshin et De-Zeeuw, 1980). Tel que illustrée par la figure 2.4, la variation des dimensions des trachéides suit une courbe de forme typique des résineux. En effet, cette courbe peut être divisée en deux phases : (i) une phase initiale, aux alentours de la moelle, qui correspond au bois juvénile et durant laquelle une augmentation rapide des dimensions des trachéides a été observée et (ii) une seconde phase qui reflète la période de stabilité de fonctionnement du cambium mature. Durant cette dernière phase, la longueur des trachéides est plus ou moins constante (Panshin et De-Zeeuw, 1980).

Il est entendu que l'optimisation des propriétés mécaniques dépend étroitement de l'efficacité du transfert de charge entre les fibres et la matrice (Sanschagrin *et al.*, 1988; Tze *et al.*, 2007). Ce transfert de charge est souvent défini en termes de longueur critique des fibres (*lc*). Toutefois, il ne faut pas négliger le rôle de

l'interaction physico-chimique, établie au niveau de l'interface, qui joue aussi un rôle clé dans la détermination du degré du transfert de charge et, par conséquent, sur la valeur de *lc*. D'ailleurs, c'est la raison pour laquelle plus l'adhésion entre les fibres et la matrice est grande, plus la longueur critique est faible (Nardin et Schultz, 1993).

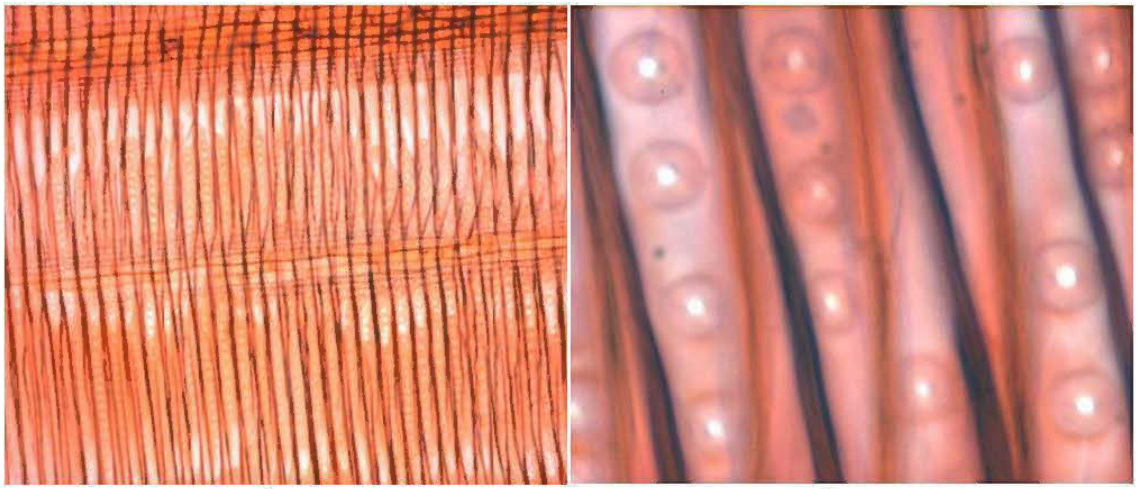

A b

Figure 2.3. Coupe longitudinale radiale du bois initial de *Pinus banksiana* lamb. a) À gauche, vue d'ensemble des trachéides et les rayons (éléments horizontaux) communiquant par des ponctuations au niveau de champs de croisement (x5). b) À droite, détails des ponctuations aréolées sur coupe longitudinale radiale (x40).

Le concept de la longueur critique développé par Kelly et Tayson (Kelly et Tyson, 1965) a été couramment appliqué dans l'objectif de déterminer la relation entre la longueur des fibres et les propriétés mécaniques des matériaux composites renforcés par des fibres unidirectionnelles. Cette longueur critique est définie comme la longueur minimale de la fibre pour laquelle la contrainte de traction appliquée au composite peut atteindre la résistance maximale à la traction de la fibre. En d'autres termes, *lc* est la longueur au-dessus de quelle la fibre, située symétriquement de part et d'autre du plan de rupture, se casse plutôt que de s'arracher (Carlsson et Lindstrom, 2005). La longueur critique s'écrit alors de la façon suivante (Kelly et Tyson, 1965):

$$l_c = \frac{\sigma_f d_f}{2\tau_\emptyset} \qquad (2.1)$$

Où σ_f est la contrainte axiale appliquée sur la fibre, d_f est le diamètre de la fibre et $\tau_\emptyset$ est la cission à l'interface fibre-matrice.

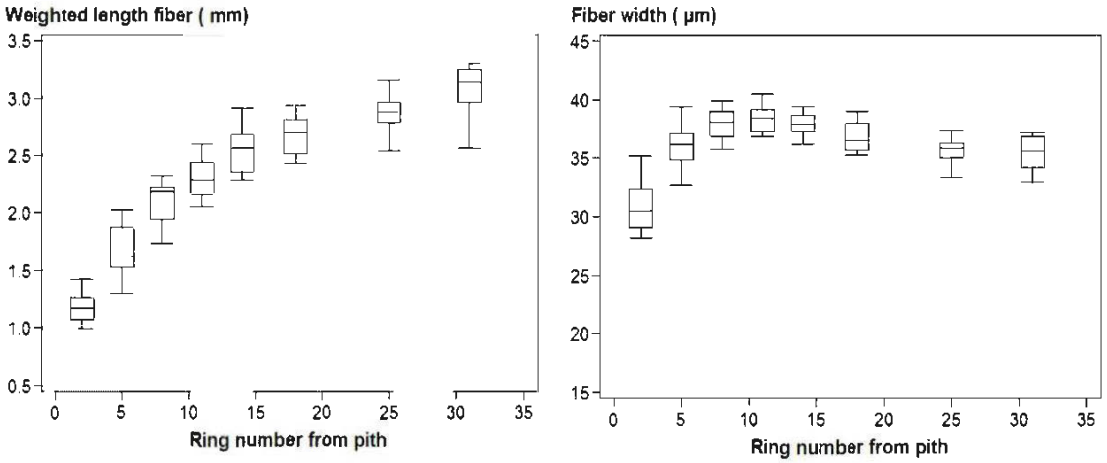

Figure 2.4. Moyenne, 1.5 x quantile, maximum et minimum de dimensions des fibres du bois de *Pinus banksiana* lamb en fonction de l'âge cambial [1].

Selon la simple règle des mélanges appliquée aux contraintes, lorsque les fibres ont une longueur inférieure à la longueur critique ($l < l_c$), elles sont considérées trop courtes pour que la contrainte maximale à laquelle elles sont soumises atteignent la valeur critique nécessaire pour aboutir à leur rupture. Par conséquent, en cas de rupture du composite, toutes les fibres qui chevauchent le plan de rupture seront arrachées de la matrice polymère. Dans ce cas, la résistance à la traction du polymère renforcé par des fibres courtes alignées de longueur $l < lc$ est donnée par l'expression suivante (Kelly et Tyson, 1965):

[1]Bouafif, H. A. Koubaa, H. Kasraoui, J. Samson-Morasse, S. Alain et S. Brais. (2007). Variations des propriétés du bois du *Pinus banksiana* (Lamb.) en milieu boréal. Stand Thématique Carrefour de la recherche forestière, 19 et 20 septembre 2007, Québec, QC, Canada.

$$\rho_c = V_f \tau_{\emptyset} \frac{l}{d_f} + \left(1 - V_f\right) E_m A_f, \qquad l < l_c \qquad (2.2)$$

Où V_f est la fraction volumique des fibres de renfort, E_m est le module d'élasticité de la matrice et A_f est la limite de contrainte à la traction de la fibre.

Quand les fibres de renfort dépassent largement la longueur critique ($l > l_c$), elles agissent de la même manière que des fibres continues, en termes de contribution à la rigidité du composite (Robinson et Robinson, 1994). Dans ce cas, la règle des mélanges s'applique au module d'élasticité du matériau composite. En effet, un composite où toutes ces fibres de renfort sont suffisamment longues pour atteindre la limite de contrainte à la traction est défini comme ayant un rendement au renforcement de 100%. Toutefois, quand les fibres varient entre fibres courtes et fibres continues, le rendement au renforcement varie entre 0 et 100%. Dans le cas de rupture du composite, seules les fibres dont les extrémités se trouvent à une distance inférieure à $l_c/2$ du plan de rupture seront arrachées de la matrice polymère. Le cas contraire, c-à-d les extrémités se trouvant à une distance supérieure de $l_c/2$ du plan de fracture, les fibres seront cassées. Statistiquement, si les fibres sont réparties de façon homogène dans la matrice, la fraction des fibres qui sera arrachée est égale à l_c/l, alors que le reste sera rompue (Carlsson et Lindstrom, 2005). La résistance à la traction du composite avec des fibres longues alignées s'écrira ainsi (Carlsson et Lindstrom, 2005):

$$\rho_c = V_f \sigma_f \left(1 - \frac{l_c}{2l}\right) + \left(1 - V_f\right) E_m A_f, \qquad l > l_c \qquad (2.3)$$

Toutefois, pour ce qui est de la résistance à la traction ρ_c du composite, il est nécessaire d'avoir une fraction volumique critique V_f^* de renfort pour que le composite possède une résistance à la traction au moins égale à la résistance à la traction ρ_m de la matrice (Baïlon et Dorlot, 2000). Cette fraction volumique critique est donnée par l'expression suivante

$$V_f^* = \frac{\rho_c - (\sigma_m)_{A_f}}{\rho_f - (\sigma_m)_{A_f}} \qquad (2.4)$$

Où

- ρ_c est la résistance à la traction du composite;
- ρ_f est la résistance à la traction des fibres;
- $(\sigma_m)_{A_f}$ est la contrainte s'exerçant sur la matrice à la rupture des fibres.

Pour toute valeur de la fraction volumique V_f inférieure à cette valeur critique V_f^*, le composite aura une résistance à la traction ρ_c inférieure à celle de la matrice. Cela veut dire que l'effet de renfort peut être bénéfique pour la rigidité et la limite d'élasticité du composite, mais peut s'avérer néfaste pour la résistance à la traction de ce dernier si la fraction volumique de renfort est inférieure à V_f^* (Baïlon et Dorlot, 2000). Dans un tel cas, on considère la matrice comme un milieu contenant une fraction volumique V_f de vide puisque le renfort s'étant rompu et ne transmettant plus les contraintes (Baïlon et Dorlot, 2000). Ainsi, la variation de la résistance à la traction du composite en fonction de cette fraction volumique est donnée par l'équation suivante :

$$\rho_c = (1 - V_f)\rho_m \qquad (2.5)$$

Cela dit, la notion de fraction volumique critique est différente de la fraction volumique maximale. En effet, cette dernière indique le volume maximal de charge que peut contenir une matrice. En pratique, il y a deux méthodes simples pour calculer la fraction volumique maximale : La première est basée sur le modèle de mailles carrées; la deuxième est basée sur le modèle de mailles hexagonales (Figure 2.5). Dans le cas de ces deux modèles, les éléments de renfort prennent une forme

sphérique régulière. La fraction volumique est le rapport de l'aire des fibres par l'aire de la matrice.

$$V_f = \frac{aire\ des\ fibres}{aire\ de\ la\ matrice} \qquad (2.6)$$

Ainsi dans le cas de structure en **maille hexagonale**

$$V_f = \frac{3.\frac{\pi r^2}{6}}{\frac{1}{2}L.Lsin\left(\frac{\pi}{3}\right)} = \frac{2\pi r^2}{\sqrt{3}L^2} \qquad (2.7)$$

Le maximum de présence de fibre est atteint une fois toutes les fibres se touchent, i.e., L = 2r.

D'où,

$$V_{f(max)} = \frac{\pi}{2\sqrt{3}} = 0{,}907 \qquad (2.8)$$

Dans le cas de structure en **maille carrée**

$$V_f = \frac{\pi r^2}{L^2} \qquad (2.9)$$

Et,

$$V_{f(max)} = \frac{\pi}{4} = 0{,}786 \qquad (2.10)$$

À partir de l'analyse de ces deux figures, il s'est avéré impossible d'incorporer plus que 90 % par fraction de volume de renfort dans une matrice thermoplastique. D'ailleurs, même une fraction volumique de renfort de 78 % apparait très difficile à réaliser. En pratique, la fraction volumique ne dépasse pas 60% dans le cas des fibres

de renfort unidirectionnelles et 40 % dans le cas des fibres en arrangement aléatoire (Ramakrishna *et al.*, 2004).

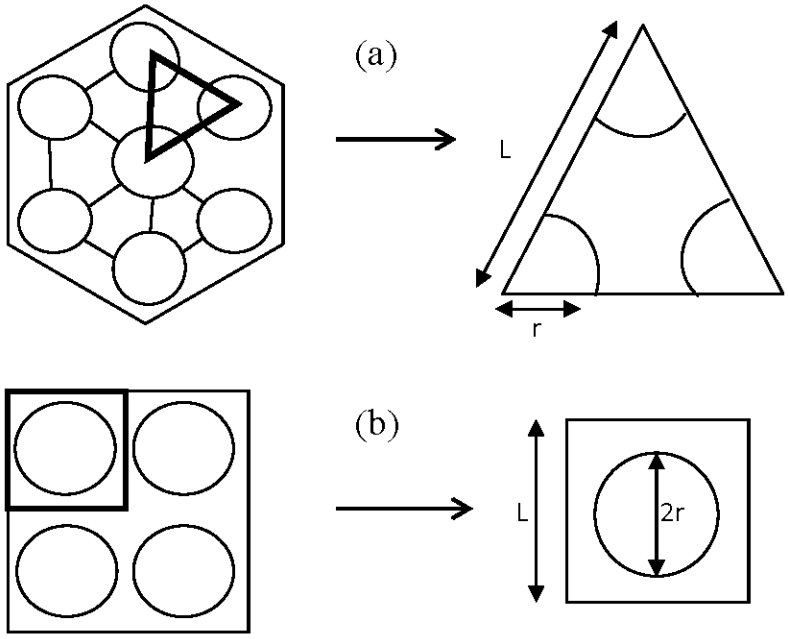

Figure 2.5. Représentation schématique de la disposition des particules de bois (a) en maille hexagonale et (b) en maille carrée (Ramakrishna *et al.*, 2004).

2.2.3 Paroi de la trachéide

À cause des contraintes de cisaillement qui se développent au cours des procédés de fabrication des composites bois plastique (raffinage, mélange, extrusion, injection…), les fibres de bois changent de forme. Le niveau de changement et d'endommagement subi par les fibres dépend de leur diamètre et aussi de leur longueur. De plus, compte tenu de la variabilité intra et interspécifique, les fibres de bois peuvent avoir la même rigidité mais avec des diamètres différents. Par ailleurs, la présence d'un facteur de forme (l/d) critique, plutôt que la longueur critique (l_c), sera plus important à considérer lorsqu'on étudie l'influence des fibres de bois sur le comportement mécanique du matériau composite. D'ailleurs, Stark et Rowlands (2003) ont comparé

l'effet de particules de bois tendre et de bois dur sur le comportement en traction des matériaux composites mis en forme par injection. Il a été conclu que le facteur de forme est plus important au développement des propriétés mécaniques que la longueur des particules. Les mêmes constatations ont été rapportées par Sanschagrin et al. (1998).

Toutefois, étant donnée leur structure tubulaire, la paroi cellulaire est largement responsable du comportement physique et mécanique des trachéides. En effet, au cours du procédé de raffinage mécanique, par exemple, les fibres de bois initial, ayant une paroi mince, ont dû changer leur forme transversalement en manifestant un plus grand degré d'aplatissement et un affaissement (collapse) de leur paroi. Inversement, les fibres de bois final, aux parois cellulaires plus épaisses, sont plus résistantes à de tels changements au cours du raffinage (Mohlin, 1997). Elles conservent souvent leur forme originale bien qu'une certaine diminution de l'épaisseur des parois et une fibrillation excessive apparaissent souvent sur ce dernier type de fibres (Laine *et al.*, 2004).

La cellule ligneuse complètement différenciée présente une structure pluristratifiée. La représentation schématique des différentes couches constituant la paroi est donnée à la figure 2.5. De l'extérieur vers l'intérieur, on peut distinguer une couche intercellulaire qui sert à souder deux cellules adjacentes. Ensuite, une fine paroi primaire de structure fibreuse se plaque sur la couche intercellulaire, tandis que la paroi secondaire se dépose sur la paroi primaire. Par sa structure et son volume, la paroi secondaire constitue la partie de cellule la plus résistante mécaniquement. Elle est dense, rigide et contient une forte proportion de cellulose. Cette paroi est généralement composée de trois couches fibreuses qui se distinguent facilement par le degré d'inclinaison de leur angle de microfibrilles (Salmén et Burgert, 2009):

- La couche S1 contient des microfibrilles de cellulose disposées en hélice. L'orientation des microfibrilles est variable. Elle atteint dans la zone la plus interne 60 à 80° par rapport à l'axe de la cellule (Panshin et De-Zeeuw, 1980). Elle représente au total 5 à 10% de l'épaisseur totale de la membrane cellulaire;
- La couche S2 constitue la partie la plus volumineuse de la paroi. Elle représente 75 à 85 % de l'épaisseur totale de la paroi cellulaire (Panshin et De-Zeeuw, 1980). Elle est formée d'une structure dense de microfibrilles de cellulose disposées en hélices relativement parallèles dont l'angle avec l'axe de la cellule est compris entre 5 et 30° (Panshin etDe-Zeeuw, 1980). Cette couche est tenue largement responsable du comportement physique de la paroi de la cellule ligneuse (Panshin et De-Zeeuw, 1980; Salmén, 2004).
- La couche S3 est relativement mince. Elle a aussi une structure lamellaire mais, contrairement à la couche S2, les microfibrilles y sont moins parallèles entre elles. Elles font ressortir un angle par rapport à l'axe de la cellule d'environ 60 à 90° (Panshin et De-Zeeuw, 1980).

La déposition spécifique des microfibrilles de cellulose est supposée être contrôlée par les contraintes géométriques du périmètre cellulaire, le nombre des unités de cellulose synthétisées et la distance latérale entre les fibrilles (Emons et Mulder, 1998; 2000). Une coupe transversale d'un plan ligneux montre une grande variabilité de l'épaisseur de la paroi des trachéides entre bois initial et bois final. Alors que dans une même structure de croissance saisonnière, la variabilité de l'épaisseur des parois cellulaires est expliquée par la structure effilée de la trachéide.

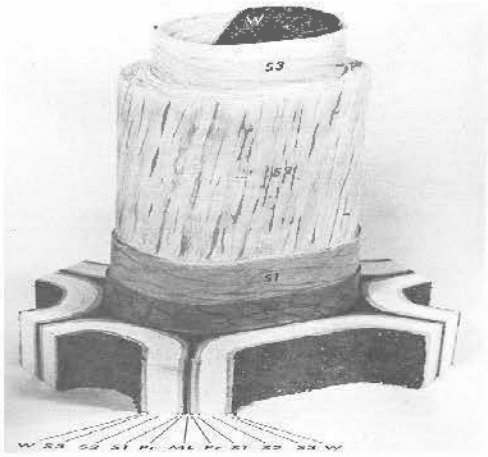

Figure 2.6. Modèle de structure de la paroi cellulaire d'une trachéide de résineux (Panshin et de-Zeeuw, 1980)

Le traitement d'images a été largement utilisé pour mesurer les dimensions des cellules (Moëll et Donaldson, 2001; Reme et Helle, 2001; Reme et Helle, 2002; Rahman *et al.*, 2005). C'est dans cette même perspective que nous avons utilisé les images issues de microscope électronique environnemental afin de comparer l'épaisseur de la paroi cellulaire ainsi que l'ouverture du lumen chez trois essences nord américaines (figure 2.6). Les résultats présentés dans le tableau 2.2 montrent que les trachéides du bois initial chez le thuya occidental ont, en moyenne, les parois les plus minces. Le plan ligneux du pin gris contient des cellules deux fois plus épaisses que le thuya occidental. Le pourcentage de la section relative au lumen indique que le bois final de l'épinette noire est le plus compact. Par conséquent, nous pouvons prédire que, durant la fabrication des composites bois plastique, les fibres du bois du thuya présenteront plus de susceptibilité à la rupture que le pin gris à cause de leurs parois minces. Les fibres de bois final de l'épinette noire seront les plus résistantes à l'endommagement. Le bois final représente la partie d'un cerne dont le bois est le plus dense, à cellules plus petites (Panshin et de-Zeuuw 1980).

2.2.4 Ponctuations et perforations des parois cellulaires

Définies par Panshin et De Zeeuw (1980), les ponctuations aréolées sont des décollements vers l'intérieur de la paroi secondaire par rapport à la paroi primaire. La perforation, proprement dite, se trouve au centre du bombement et n'affecte que la paroi secondaire. Ces structures forment une paire de ponctuations de part et d'autre de la paroi de deux cellules adjacentes. Généralement, plus le diamètre de la trachéide est grand plus le nombre de ponctuations est élevé (Panshin et De-Zeeuw, 1980). Cela dit, le nombre et la taille de ces ponctuations constituent des irrégularités qui affaiblissent la structure des trachéides. Sirviö et Kärenlampi (1998) ont montré que la taille et la densité des ponctuations augmentent également aux alentours des extrémités effilées des trachéides. Cela explique la vulnérabilité des fibres de bois dans ces endroits. Les ponctuations, et ce au même niveau que les autres ouvertures (lumens et déchirures), jouent un rôle clé dans l'ancrage mécanique entre la matrice thermoplastique et les fibres de bois. En effet, les observations au microscope électronique à balayage ont montré une pénétration d'un adhésif à base de thermoplastique (polypropylène) à travers les larges ouvertures, y compris les ponctuations du bois (Smith *et al.*, 2002). En outre, l'adhésif pénètre le tissu poreux du bois sur plus de 150 µm pour un diamètre d'ouverture de 15 µm. La profondeur de pénétration est d'autant plus grande que le diamètre de l'ouverture est large. Toutefois, l'adhésion mécanique entre l'adhésif thermoplastique et la surface du bois dépend en outre de la porosité du bois, de la viscosité, de la pression appliquée et de la durée du procédé (Smith *et al.*, 2002).

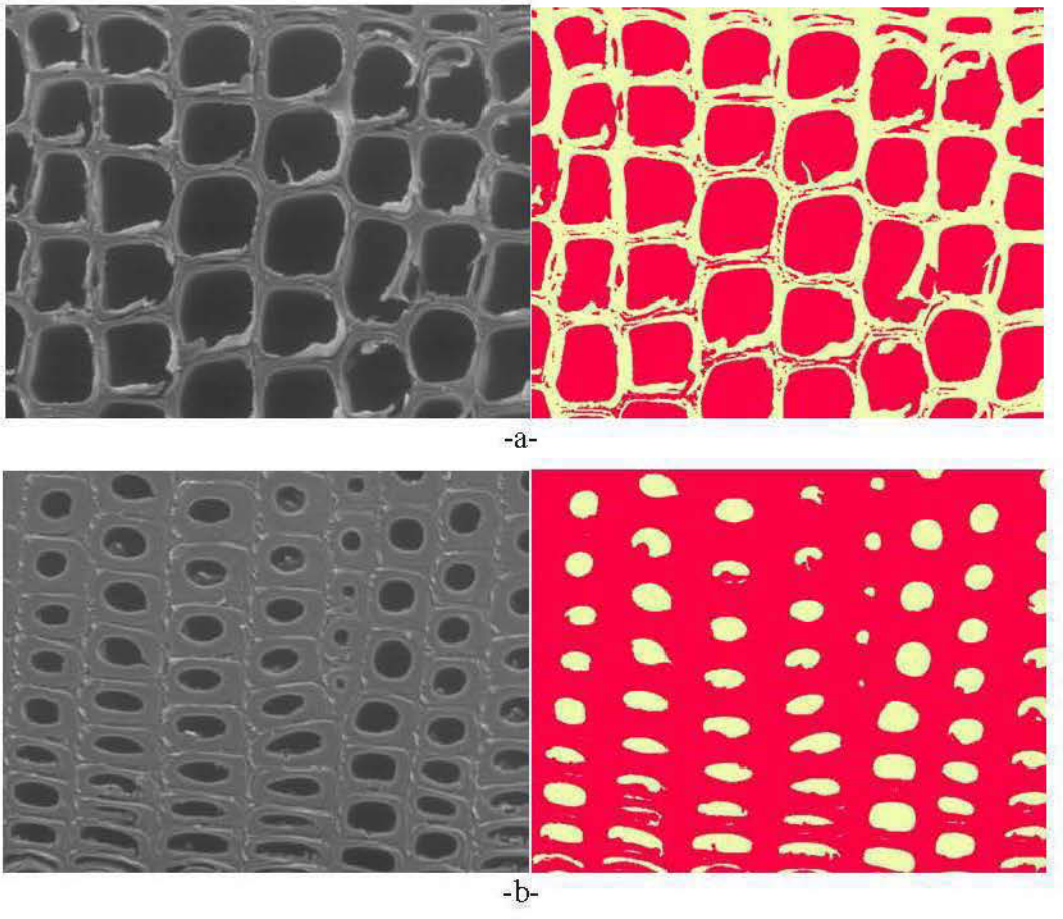

-a-

-b-

Figure 2.7. Exemple de traitement d'images de microscope electronique environnemental de bois de pin gris afin de déterminer l'épaisseur de la paroi cellulaire. Avant traitement (à gauche) et après classification en deux classes (à droite). (a) plan transversal du bois initial; (b) bois final.

Tableau 2.2. Moyennes et écarts-type (entre parenthèses) de l'aire de section de paroi et de lumen mesurées suite au traitement d'image sur des coupes transversale de bois de résineux.[2]

	Thuja occidentalis L. (n= 1012 cellules)		*Picea mariana* (Mill.) (n=766 cellules)		*Pinus banksiana* Lamb. (n = 987 cellules)	
	Bois initial	Bois final	Bois initial	Bois final	Bois initial	Bois final
Aire de section de paroi (μm^2)	172,70 (18,22)	567,32 (29,62)	228,32 (71,25)	263,70 (53,96)	366,60 (43,21)	391,92 (37,45)
Aire du lumen (μm^2)	503,94 (22,21)	228,30 (26, 15)	385,75 (32,31)	80,09 (28,19)	642,79 (112,23)	34,30 (61,05)
Lumen (%)	74	29	63	24	64	46

Cela dit, l'efficacité de l'ancrage mécanique dépend aussi bien de la rugosité de la surface des fibres que de la facilité du mouvement du polymère visqueux à travers les pores du bois (Frihart, 2005). Le mouvement d'un fluide dans le bois se fait de deux manières : par diffusion à travers la paroi cellulaire et par écoulement dans le lumen (Hunter, 1993; Watanabe, 1998). La loi de Darcy a été utilisée pour décrire le mouvement d'un fluide visqueux dans une structure poreuse, telle que le bois (Gibson etAshby, 1997). L'expression de cette relation s'écrit de la façon suivante :

$$u = -\frac{K}{\mu}\frac{dp}{dx} \qquad (2.11)$$

Où u (m^3/s) est le flux, K (m^2) est la perméabilité absolue du bois, μ est la viscosité dynamique (Pa.s) du liquide et dp/dx est un gradient de pression.

Tesoro et al. (1974) ont comparé la perméabilité de plusieurs espèces résineuses et feuillues et ont constaté que, chez les résineux, plus le rayon effectif des pores est

[2] Données mesurées dans le cadre de cette étude

faible plus en est la perméabilité. Ils ont rapporté que la perméabilité dépend également du type des ponctuations et de la présence de torus. En supposant que, pour un flux longitudinal (à travers le lumen) ou transversal (diffusion à travers les ponctuations), le fluide passe par une ouverture de diamètre *d*. La perméabilité du bois devient (Tesoro *et al.*, 1974):

$$K = Ad^2\left(1 - {}^{\rho}/_{\rho_s}\right)^{3/2} \qquad (2.12)$$

Où A est une constante générale égale à 0.4, et ρ et ρ_s sont, respectivement, la densité du bois et la densité de la paroi cellulaire.

2.2.5 Surface des fibres

Il est communément entendu que l'incompatibilité entre les fibres de bois, en tant qu' élément de renfort, et la matrice thermoplastique demeure de loin la majeure contrainte qui contrarie le développement des matériaux composites bois/plastique et limite leur utilisation à des applications non structurales (Sain *et al.*, 1994; Gassan etBledzki, 1997; Matuana *et al.*, 1998; Mahlberg *et al.*, 2001b). En effet, la différence d'énergie libre de surface, également appelée tension superficielle, entre les fibres de bois (forte tension superficielle) et polymère (faible tension superficielle) est à l'origine de la distinction au niveau de l'interface bois/polymère. Lors de la phase de mélange des fibres de bois et du thermoplastique, en absence de compatibilité, la cellulose qui est le majeur constituant de la paroi cellulaire tend à réagir avec d'autres molécules de polysaccharides ou avec des molécules d'eau (Rowell *et al.*, 2005). Ainsi, la matrice thermoplastique entoure les fibres de bois sans y adhérer. La résultante est un manque de transfert de charge au niveau de l'interface, ce qui donne un matériau cassant.

L'amélioration de la compatibilité entre les fibres naturelles et le polymère synthétique est un champ de recherche très actif. Parmi les pistes enquêtées figurent

l'amélioration de l'interface par modification chimique de la surface des fibres. Ces méthodes et bien d'autres seront revues plus en détails dans le paragraphe suivant alors qu'un exemple de modification chimique par estérification a été étudié (***Chapitre IV***).

2.3 Compatibilité et adhésion des fibres de bois avec les polymères thermoplastiques

2.3.1 Chimie de la paroi de trachéides

La paroi cellulaire se présente sous forme de structure lamellaire. La paroi secondaire présente également une structure en couche. L'angle d'inclinaison des microfibrilles de cellulose est le principal paramètre qui discrimine les différentes couches. Parce qu'il est impossible de prédire un plan préférentiel de rupture des échantillons de bois (Fahlén et Salmén, 2002), différents états de surfaces pourront affleurer après le cycle de défibrage mécanique ou de raffinage. Par ailleurs, l'analyse de la structure moléculaire de la paroi cellulaire et plus précisément les différentes surfaces qui peuvent apparaître au cours du procédé de fabrication des composites est indispensable pour une meilleure compréhension du potentiel technologique des fibres de renfort et les moyens permettant l'amélioration de leur compatibilité avec les matrices de polymères.

La cellulose est un polysaccharide formé d'une succession d'unités de (1 → 4)-β-D-glucopyranose. Elle constitue l'élément majoritaire de la paroi cellulaire. Entre 50 et 60% de sa structure est cristalline (Newman, 2004). Sa disposition en microfibrilles expliquerait la forte résistance à la traction transversale de la paroi cellulaire (Panshin et De-Zeeuw, 1980). Bien que Newman (2004) a rapporté que la différence de cristallinité de la cellulose dans le bois initial et le bois final chez le *Pinus radiata* est quasi absente, Lee (1961) et Wimmer *et al.* (1997) ont rapporté que la cristallinité de cellulose du bois initial est systématiquement moins élevée que celle du bois final

chez les épinettes. En outre, Newman (Newman, 2004) a conclu que la faible diminution de la cristallinité de la cellulose au niveau de la moelle ou dans le bois de compression peut être interprétée en termes de rapidité de croissance dans ces zones, tandis qu'une faible vitesse de croissance pourrait augmenter la cristallinité de la cellulose. De nouvelles investigations sur les différentes régions de la paroi cellulaire, moyennant l'analyse des images Raman, ont montré que la concentration de cellulose varie aussi bien entre les différentes régions de la paroi cellulaire que dans une même région (Agarwal, 2006). Il a été montré également que la distribution de cellulose dans la paroi cellulaire suit un modèle inverse à celui de la lignine (Agarwal, 2006). Contrairement aux proportions de cellulose, le degré de cristallinité est considéré homogène non seulement dans un même arbre mais aussi entre les arbres (Agarwal, 2006).

Les lignines constituent le second constituant le plus abondant chez les plantes végétales. Il est généralement admis que les lignines sont issues d'une réaction de condensation entre trois unités structurales majeures : coumaryl, coniferyl, et sinapyl. La distribution topo-chimique de la lignine à travers la paroi cellulaire des trachéides a été largement étudiée surtout chez les résineux (Fergus *et al.*, 1969; Fukazawa et Imagawa, 1981; Westermark *et al.*, 1988; Donaldson, 1991; Downes *et al.*, 1991; Donaldson, 1995; Donaldson, 2001; Donaldson, 2002; Ruel *et al.*, 2006). En effet, il a été rapporté que la lamelle moyenne est plus lignifiée que la paroi secondaire. Elle contient plus que 50% de lignines tandis que la couche S2 en contient seulement 20% (Donaldson, 2001). De plus, il a été largement admis que les coins de la lamelle moyenne sont souvent plus lignifiés que le reste de la couche avec une concentration qui atteint 70% (Fergus *et al.*, 1969; Fukazawa et Imagawa, 1981; Saka et Thomas, 1982a; Westermark *et al.*, 1988; Donaldson, 1995). Fergus et al. (1969) ont déterminé la distribution quantitative de la lignine dans une section transversale de 0,5 µm de la paroi des trachéides de l'épinette noire en utilisant la microscopie UV. Ils ont remarqué que la concentration moyenne de la lignine dans la lamelle mitoyenne et au

niveau de ses coins est à peu près deux à quatre fois celle de la paroi secondaire. Toutefois, cette disproportion dans la distribution topo-chimique de la lignine est éclipsée par le volume de la paroi secondaire qui atteint 80% de la totalité de la paroi cellulaire. Conformément à Fergus *et al.* (1969), Agarwal (2006) a remarqué une nette différence dans la distribution de la lignine entre les coins de la lamelle moyenne et la paroi secondaire. Toutefois, cet auteur n'a pas remarqué une variation significative entre le reste de la lamelle moyenne et la paroi secondaire, en termes de concentration de lignine. Bien qu'il soit souvent admis que la couche S2 est uniformément lignifiée, elle peut présenter des irrégularités de concentration de lignine (Daniel et Nilsson, 1984). La lignification de la couche S1 chez le *Pinus radiata* a été décrite par Donaldson (1995). En effet, ce dernier a montré que cette couche est moins lignifiée que la couche S2. La limite entre les deux couches S1 et S2 est l'endroit le moins lignifié. D'ailleurs, cette carence en lignine sur la frontière entre la couche S1 et S2 a été retenue comme explication potentielle de la fracture de la paroi cellulaire durant le raffinage des fibres du *Pinus radiata.* Les analyses quantitatives ont montré que, chez les pinacées, la couche S3 présente souvent un degré plus élevé de lignification que la couche S2 adjacente (Saka et Thomas, 1982b; Donaldson, 2001). Toutefois, elle demeure moins lignifiée que la lamelle moyenne. De plus, il est important de noter que la lignine de la lamelle moyenne a une masse moléculaire et une teneur en oxygène plus élevées que la lignine de la paroi secondaire (Sorvari *et al.*, 1986). Contrairement au bois juvénile et au bois mature, la différence entre le bois initial et le bois final ne révèle pas une variation dans la distribution de la lignine (Fukazawa et Imagawa, 1981; Donaldson, 1995; Gindl et Tschegg, 2002). Chez le genre piceas, des teneurs élevées en lignine et des composants à base de p-hydroxyphenyl, typiques du bois de compression, ont été détectées dans le bois final de plusieurs cernes de croissance et dans certaines directions des troncs d'arbre (Pranovich *et al.*, 2005). Conformément à la différence morphologique entre le bois initial et le bois final, la paroi secondaire très développée des trachéides du bois final réduit la contribution de la lamelle moyenne dans la

détermination de la teneur en lignine totale de la cellule, ce qui engendre une légère diminution de la teneur en lignine dans le bois final par rapport au bois initial (Bertaud et Holmbom, 2004). Les plus récentes informations sur la distribution quantitative de la lignine chez l'épinette noire ont montré que pour le bois initial, 72% de la totalité de lignine se trouve dans la paroi secondaire alors que la quantité qui reste (28%) est localisée dans la lamelle moyenne et les coins des cellules. Dans le bois final, ces valeurs correspondent à 82% et 18%, respectivement (Fergus *et al.*, 1969).

Après la cellulose, les hémicelluloses constituent le groupe des polysaccharides le plus important dans les cellules végétales. Les hémicelluloses diffèrent de la cellulose par des unités différentes d'oses, par des chaines beaucoup plus courtes et par des ramifications sur la chaîne principale. Les hémicelluloses et la lignine se déposent aux alentours des microfibrilles de cellulose, reproduisant ainsi le rôle d'une matrice. L'interaction entre la cellulose et les hémicelluloses a fait l'objet de plusieurs investigations (Salmen et Olsson, 1997; 1998; Åkerholm et Salmén, 2001). Tokoh et al. (Tokoh *et al.*, 2002) ont comparé la taille des cristallites et les espaces intra-cristallins (*d-spacing*) de cellulose obtenue par culture *in vitro* d'Acetobacter *xylinum* dans un milieu nutritif de Schramm/Hestrin contenant de la pectine et du xylane ou du glucomannane. Ils ont conclu que le xylane et le glucomannane affectent la taille et la structure de la cristallite des microfibrilles de cellulose. De plus, étant donné l'association intime de la lignine avec les hémicelluloses, le modèle de distribution de ces derniers suit le même modèle que la lignine (Ruel *et al.*, 2006). En effet, l'élimination du xylane, qui avec la lignine constitue le complexe lignine-polysaccarides, augmente la susceptibilité des fibres à la déformation tandis que la séparation du glucomannane, qui est plutôt associée à la cellulose, affecte souvent les propriétés mécaniques, notamment la résistance de la fibre à la traction (Rauvanto *et al.*, 2006).

Les extractibles recouvrent une large gamme de constituants qui peuvent être extraits avec des solvants polaires et apolaires. Malgré leur faible concentration, ces substances extractibles marquent profondément les caractéristiques du bois. En ce qui nous concerne, les extraits sont souvent considérés comme des contaminants de la surface des fibres qui affectent la compatibilité bois-polymère. Saputra *et al* (2004) ont remarqué qu'une simple extraction des fibres de sapin Douglas a permis d'améliorer les propriétés mécaniques du composites bois/polypropylène. Ils ont expliqué que le mélange des fibres sans extraction avec le polypropylène qui se fait à haute température accélérerait la migration des substances extractibles vers la surface des trachéides et une accumulation au niveau de l'interface bois/polymère. D'autres études ont attribué la réduction de la perméabilité du bois de duramen à l'accumulation des substances extractibles ayant une masse moléculaire élevée au niveau des ponctuations (Olsson *et al.*, 2001).

2.3.2 Relation entre la composition de la surface et son énergie libre

Il est souvent admis que l'adhésion à des polymères thermoplastiques est limitée à des liaisons secondaires (liaison entre deux atomes ou molécules autre que la liaison covalente) (Frihart, 2005). Toutefois, vu la grande variabilité de la surface des trachéides, une connaissance de leur énergie libre de surface est essentielle afin d'optimiser les propriétés de l'interface et, par conséquent, la performance du matériau composite. En effet, les propriétés de l'interface sont assujetties à de fortes variations même pour des variations minimes de l'énergie libre de surface (Liu *et al.*, 1995). L'affleurement d'un état de surface riche en lignine ou encore, riche en carbohydrates, est à l'origine de la variation de la tension superficielle des fibres de trachéides (Matuana *et al.*, 1998). En d'autres termes, la complexité du système multicouche et les différentes irrégularités et défauts de la paroi cellulaire sont des facteurs intrinsèques qui enrichissent la variabilité de la composition chimique de la surface des trachéides. Cette variabilité se traduit par un état de surface présentant des

groupes fonctionnels allant de groupements phénoliques, hydroxyles jusqu'au groupements carboxyles ou encore carbonyles (Liu *et al.*, 1998). En outre, les substances extractibles, telles que les acides gras, peuvent effectivement donner une propriété oléfine à la surface des fibres (Liu *et al.*, 1998; Takeshita *et al.*, 2000) et donc changer son énergie libre (Saputra *et al.*, 2004). D'autre part, Liu et *al.* (Liu *et al.*, 1995) ont rapporté que l'adsorption des impuretés, que ce soit à partir des gaz ou suite à une contamination durant la transformation, a aussi des impacts sur l'interface fibres/polystyrène.

L'angle de contact est la technique la plus répandue pour l'évaluation de l'énergie libre de surface des solides (Koljonen et Stenius, 2005; Mohammed-Ziegler *et al.*, 2006; Gupta *et al.*, 2007; Kutnar *et al.*, 2008; Wolkenhauer *et al.*, 2009). Une revue de littérature des différentes méthodes et grandeurs de mesures de l'énergie libre de surface pour différents types de bois a été établie par De-Meijer et al. (2000). Il a été rapporté que la tension de surface critique «dynamique» pour la plupart des espèces varie entre 40 et 55 $mJ.m^{-2}$. Cependant, la somme de l'énergie libre de surface, en considérant aussi bien les composants polaires que dispersifs, a montré une large variation non seulement entre les différentes espèces mais aussi dans la même essence. Elle est généralement plus grande que la tension de surface critique (De Meijer *et al.*, 2000). Le caractère acido-basique de tension de surface des fibres de bois a été interprété en termes de présence de composants accepteurs d'électron ou donateurs d'électron (Gindl et Tschegg, 2002). Cela dit, l'énergie libre de surface est essentiellement composée de composants de Lifshitz-van der-Waals (polaires et dispersifs). Cependant, plusieurs essences de bois montrent également un caractère basique et beaucoup moins un caractère acide (De Meijer *et al.*, 2000). Au delà du caractère complexe de la surface des trachéides, une large partie de la variation des grandeurs de mesures entre les essences du bois peut être expliquée par la différence des méthodes de mesures. De-Meijer *et al* (2000) ont présenté une analyse comparative sur l'effet des méthodes de détermination de l'énergie libre de surface.

Bien que les méthodes de mesure et de calcul aient un grand impact sur les résultats, il a été conclu que l'énergie libre de surface, indépendamment de l'essence étudiée, se situe typiquement entre 30 et 50 $mJ.m^{-2}$.

Tel que mentionné auparavant, la tension superficielle des fibres de bois change aussi avec le degré d'endommagement des fibres au cours de leur transformation. Sinn et al. (2004) ont montré que le sablage de la surface du bois augmente l'énergie libre de surface en augmentant l'occurrence du carbone C1s (carbone lié avec un seul atome d'oxygène non carbonyle, ou avec un atome d'hydrogène), alors que Gérardin et al. (2007) ont montré qu'un traitement thermique du bois modifie les propriétés de surface en augmentant l'hydrophobicité et en réduisant nettement les composants acido-basiques.

2.3.3 L'adhésion bois/thermoplastique

Bien que l'adhésion interfaciale entre les fibres naturelles, en général, et les matrices thermoplastiques fût largement étudiée, plusieurs points demeurent en controverse autour des mécanismes d'adhésion. En effet, une large partie des recherches admettent que ni le principe d'adhésion par ancrage mécanique ni l'établissement des liaisons covalentes, qui sont largement adoptées pour expliquer l'adhésion bois/polymère thermodurcissable, ne peuvent être valides dans le cas de mélange des fibres de bois et de polymère thermoplastique. Par contre, certaines recherches admettent que les propriétés de l'interface ainsi que les performances du matériau composite sont la résultante des interactions spécifiques qui s'établissent entre les deux phases (Bledzki *et al.*, 1996; Kazayawoko *et al.*, 1999a; Dányádi *et al.*, 2007).

Peu d'études ont fait allusion au modèle d'adhésion par ancrage mécanique dans le cas de composites bois/thermoplastique. Smith et al. (2002) ont étudié l'interaction mécanique entre le bois et un adhésif thermoplastique (un mélange de propylène isotactique et éthylène-propylène copolymère). Ils ont conclu que le système adhésif-

adhérant ne peut être expliqué que par la théorie d'adhésion mécanique appliquée à des surfaces rugueuses et poreuses. Récemment, Escobar (2008) a étudié l'interaction physique entre matrice thermoplastique et bois massif. Les résultats ont montré une forte corrélation entre le diamètre et le nombre des ponctuations, d'une part, et la mobilité du thermoplastique à l'intérieur des porosités, d'autre part. De plus, l'auteur a identifié les affaissements dans certaines essences de bois comme possible facteur qui limite la pénétration du thermoplastique et donc les propriétés de l'interface.

Etant donné la non-compatibilité, due à la faible énergie libre de surface des éléments de renfort et du polymère (Chtourou *et al.*, 1992; Bledzki *et al.*, 1998b; Kazayawoko *et al.*, 1999a), les interactions chimiques demeurent très faibles entre les deux composants. En conséquence, l'amélioration de l'interface est une piste inévitable pour l'amélioration des performances du composite. La modification de l'état de surface des fibres naturelles, en général, et des fibres de bois en particulier reste la principale voie pour l'amélioration de l'interface. La modification des fibres de bois a fait l'objet de plusieurs investigations et revues bibliographiques (Maldas et Kokta, 1991; Sain *et al.*, 1994; Matuana *et al.*, 1998; Kazayawoko *et al.*, 1999a; Razi *et al.*, 1999; Li et Matuana, 2003b). Plusieurs techniques ont été utilisées, ou au moins testées, afin d'améliorer l'interface. La modification chimique des fibres de bois consiste à substituer les groupements hydroxyles de la surface par des groupements fonctionnels d'un comptabilisant adéquat, tel que les copolymères greffés éthylène-anhydride maléique (MAPE). Cela dit, les modifications chimiques dans ce cas ne prennent pas en considération les imprégnations chimiques (imprégnation par des monomères qui se polymérisent *in situ* sans nécessairement établir des liaisons chimiques avec la paroi cellulaire), le revêtement et le traitement thermique (Rowell, 2004). Les polymères fonctionnalisés avec l'anhydre maléique sont souvent greffés au niveau de l'interface bois/thermoplastique de la façon suivante : les groupes fonctionnels interagissent fermement ou même réagissent chimiquement avec la surface du bois tandis que les longues chaînes alkyles se diffusent dans la matrice en

assurant un transfert adéquat de charge (Kazayawoko *et al.*, 1997; Gauthier *et al.*, 1998; Simonsen *et al.*, 1998; Ellis et O'Dell, 1999; Ichazo *et al.*, 2001; Mahlberg *et al.*, 2001a; Balasuriya *et al.*, 2002; Li et Matuana, 2003a; Yuan *et al.*, 2008; Zhang *et al.*, 2009).

Des revues exhaustives des agents de couplages utilisés dans la fabrication des composites bois plastiques ont été réalisées. (Lu, 2003; Nabi Saheb et Jog, 1999). Une liste contenant plus de 40 agents de couplage a été spécifiée. En effet, on peut trouver : (i) les agents de couplage organiques tels que les isocyanates, les anhydrides, les amides, les imides acrylates, les chlorotriazines, les époxides, les acides organiques, les monomères, les polymères et les copolymères ; (ii) les agents de couplage inorganique, tels que les silicates et (iii) les agents de couplages organiques-inorganiques incluant les silanes, et les titanates (Lu, 2003). Les agents de couplage agissent comme un pont qui lie les fibres de bois à la matrice thermoplastique par un ou plusieurs des mécanismes suivants : liaisons covalentes, enchevêtrement avec la chaîne moléculaire du polymère, et fortes liaisons secondaires telles que les liaisons hydrogènes (Raj *et al.*, 1988; Maldas *et al.*, 1989a). Généralement, la structure moléculaire de l'agent de couplage comprend au moins deux groupes fonctionnels. En effet, une face comprend les groupes fonctionnels tels que (-N=C=O) des isocyanates, [-$(CO)_2$ O-] des anhydrides maléiques, et (-Cl-) des dérivées de diclorotriazine, interagissent avec les groupes hydroxyles (-OH) de la cellulose et de lignine pour former des liaisons covalentes ou des liaisons hydrogènes (Lu *et al.*, 2000). Par l'autre face, les agents de couplage peuvent se lier à la matrice thermoplastique par greffage des copolymères sur la chaine moléculaire du thermoplastique. Ce type de mécanisme est typique des agents de couplage commercialisés et ils assurent un bon remède pour le manque de compatibilité entre les fibres de bois et les polymères synthétiques.

L'estérification est un autre type de prétraitement des fibres naturelles afin d'améliorer leur potentiel adhésif. Elle consiste à convertir les groupements hydroxyles de la surface des fibres en groupements esters grâce à une addition nucléophile d'un groupement anhydride. Toutefois, cette addition doit se faire en respectant la nature de la matrice thermoplastique afin d'assurer un bon rendement de la réaction d'estérification. Par exemple, l'anhydride maléique greffé à trans-1,4-isoprène pour la matrice du caoutchouc trans-1,4-isoprène, l'anhydride acétique pour la cellulose acétate butyrate, l'anhydride phtalique pour le polystyrène, l'anhydride maléique pour le styrène-éthylène-butylène et le MAPE pour le polyéthylène (Lu, 2003),(Kazayawoko *et al.*, 1999a; Matuana *et al.*, 2001; Li et Matuana, 2003b; Carlborn et Matuana, 2006). Les différents mécanismes d'adhésion qui peuvent avoir lieu dans un composite bois-thermoplastique sont donnés dans un tableau récapitulatif (tableau 2.3).

2.3.4 Pratiques de modification des fibres de bois

Généralement, le traitement des fibres de bois a lieu avant ou durant le procédé de formulation (*compounding*). Avant le procédé de formulation, le prétraitement des fibres peut être conduit selon deux méthodes : (i) par recouvrement (coating) de la surface des fibres grâce à un agent de couplage (Maldas *et al.*, 1988a; Maldas etKokta, 1990; 1991), ou (ii) par greffage des copolymères sur la surface des fibres dans une solution aqueuse (Gauthier *et al.*, 1998; Kazayawoko *et al.*, 1999a; Keener *et al.*, 2004). Le traitement durant le procédé commence quand la température du mélange atteint celle de fusion de la matrice thermoplastique, tandis que le temps de résidence dans l'extrudeuse (ou le mixeur) influence beaucoup l'établissement des liaisons chimiques (Lu, 2003; Kazayawoko *et al.*, 1999a; Matuana *et al.*, 2001; Li et Matuana, 2003b; Carlborn et Matuana, 2006). Étant donnés la simplicité, la rapidité et le coût moins élevé, cette dernière pratique est couramment utilisée dans l'industrie des composites. En général, les agents de couplage comptent pour un à 3% de la masse

totale du composite. Au-delà de cette concentration, une diminution des propriétés mécaniques a été observée (Maldas *et al.*, 1988a; Paunikallio *et al.*, 2003; Keener *et al.*, 2004). Il est opportun de noter aussi que le nombre de sites acide, qui représentent la quantité réactionnelle dans l'agent de couplage, et le poids moléculaire sont deux propriétés importantes qui influencent l'efficacité du couplage entre fibres naturelles et polymère thermoplastique (Lu *et al.*, 2005b).

Tableau 2.2. Différents schémas de mécanismes d'adhésion entre fibres de bois et matrices thermoplastiques (Lu, 2003).

Type d'adhésion	Structure à l'interface	
Adhésion mécanique	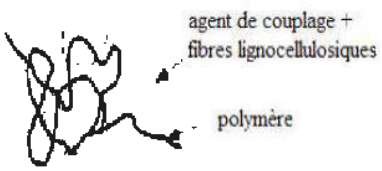 enchevêtrement de la chaîne moléculaire	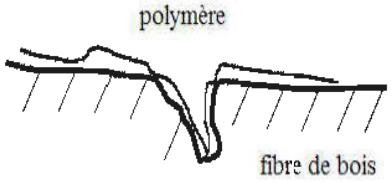 Ancrage mécanique
Liaisons secondaires (<10 Kcal/mol)	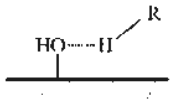 Liaison hydrogène	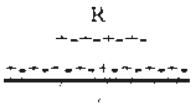 forces de van der Waals
Liaisons Covalentes (>50 Kcal/mol)	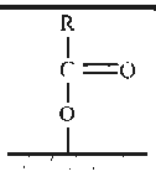 Estérification	

2.4 Techniques d'analyse des caractéristiques intrinsèques des fibres de bois

2.4.1 Techniques d'analyse de la morphologie des fibres de bois

Étant donnée sa forte susceptibilité à la dégradation sous l'influence de la température et des contraintes de cisaillement générées lors du procédé de mise en forme des composites bois-thermoplastique, la détermination de la distribution des longueurs de fibres est importante pour déduire la relation entre la performance mécanique du composite et les conditions opératoires utilisées. Plusieurs techniques ont été utilisées pour caractériser la distribution des propriétés morphologiques des fibres de bois après leur mélange avec une matrice thermoplastique. Les techniques basées sur les principes optiques (Olson *et al.*, 1995; Robertson *et al.*, 1999) sont les techniques les plus couramment utilisées. Guay *et al.* (2005) a présenté une étude comparative de différentes marques de fabrication d'analyseur optique de longueur de fibres. Carvalho *et al.* (1997) a comparé la méthode optique d'analyse des fibres à la méthode basée sur l'analyse des images vidéo. Des nouvelles techniques basées sur le traitement numérique des images sont également rapportées par (Karlsson, 2008). Dans le **chapitre VII**, nous avons présenté une revue de littérature assez exhaustive concernant ces techniques.

2.4.2 Techniques d'analyse de la composition chimique de la surface des fibres

4.4.2.1 Spectroscopie infrarouge à transformée de Fourier

La spectroscopie infrarouge à transformée de Fourier (ou FTIR, Fourier Transformed InfraRed spectroscopy) est basée sur l'absorption d'un rayonnement infrarouge par le matériau analysé. L'interprétation des fonctions chimiques présentes dans le matériau s'effectue via la détection des vibrations caractéristiques des liaisons chimiques (Gordon et Macrae, 1989). Le domaine infrarouge, entre 4000 cm^{-1} et 400 cm^{-1},

correspond au domaine de l'énergie de vibration des molécules. Lorsque l'énergie apportée par le faisceau infrarouge est voisine de l'énergie de vibration de la molécule, cette dernière absorbe le rayonnement et la diminution de l'intensité réfléchie ou transmise sera alors enregistrée. Toutefois l'absorption du rayonnement IR dépend aussi de la géométrie de la molécule et en particulier de sa symétrie (Colthup *et al.*, 1975). Par conséquent, à une molécule de composition chimique donnée correspond une bande d'absorption caractéristique permettant de l'identifier. L'ensemble des bandes d'absorption forme le spectre d'absorption d'un matériau donné. Les informations tirées des spectres sont généralement qualitatives. En effet, elles permettent l'identification des longueurs d'onde auxquelles l'échantillon absorbe qui sont caractéristiques des groupes chimiques présents dans le matériau analysé. Des tables permettant d'attribuer les absorptions aux différents groupes chimiques présents dans les fibres de bois sont données dans le **Chapitre IV** de ce document. Néanmoins, des informations quantitatives peuvent aussi être tirées du spectre d'absorption IR. En effet, l'intensité de l'absorption à la longueur d'onde caractéristique (l'aire du signal) est souvent reliée à la concentration du groupe chimique responsable de l'absorption (Solomon et Carangelo, 1982; Drumond *et al.*, 2006; Cornel *et al.*, 2008).

Parce qu'il est doté d'une structure chimique très complexe, le bois fait partie des matériaux les plus analysés par cette technique. Certaines études ont simplement utilisé le FTIR pour élucider les différents groupes chimiques présents sur la surface des fibres de bois (Barker et Owen, 1999; Ferraz *et al.*, 2000; Ajuong et Redington, 2004; Colom et Carrillo, 2005; Toivanen et Alén, 2006). Dans d'autres études, cette technique a été utilisée comme outil de vérification de l'établissement des liaisons chimiques (i.e., liaison ester) entre le bois et d'autres composants chimiques à base d'anhydride (Kazayawoko *et al.*, 1997; Pandey, 1999; Carlborn et Matuana, 2006; Dominkovics *et al.*, 2007). Dans une autre perspective, Raiskila *et al.* (2007) ont utilisé la spectroscopie IR pour déterminer la teneur en lignine dans le bois de

duramen et le bois de l'aubier de trois clones de *Picea abies,* tandis que Rodrigues *et al.* (1998) ont servi de cette technique pour déterminer la teneur en monosaccharide chez l'*Eucalyptus globulus*.

Grâce à la grande diversité des montages expérimentaux (montage de réflexion totale atténuée (ATR), montage de réflexion/transmission (DRIFT)), la spectrométrie IR permet d'analyser aussi bien les matériaux organiques que les matériaux inorganiques indépendamment de leur état physique ou de surface.

4.4.2.2 Spectroscopie de photoélectrons excités par rayons X

L'analyse par XPS (X-ray photoelectrons spectroscopy) est la méthode la plus utilisée dans l'analyse des surfaces. Elle peut fournir la composition atomique d'un échantillon ainsi que la nature des liaisons chimiques présentes et leur distribution, et ce jusqu'à une profondeur de 10 nanomètres (Andrieu et Müller, 2005). Ainsi, l'analyse chimique par XPS permet de connaitre la distribution des différents types de liaisons chimiques présentes. Par exemple, pour un échantillon de bois, il sera possible de déterminer les abondances relatives des liaisons C-C par rapport aux liaisons C=C ou C-O, etc.

Le principe de cette technique est basé sur l'irradiation d'un échantillon par un faisceau de rayons X issu d'une source monochromatique. Les énergies les plus courantes sont 1486.6 Ev (Al) et 1253.6 eV (Mg). Sous l'effet des photons ayant l'énergie la plus haute, les électrons des couches électroniques peuvent être excités et éjectés des atomes. Les électrons ainsi libérés possèdent une énergie cinétique qui varie en fonction de (i) l'énergie du photon X et de (ii) l'énergie de liaison du niveau où se trouvait l'électron (Yip-wah, 2001). L'éjection des électrons hors de l'échantillon permet leur collection et leur analyse grâce à un analyseur d'électrons. Après un balayage de la gamme des énergies, un spectre des énergies de liaison est alors reconstitué (voir exemple de spectres dans le **chapitre IV**). Le spectre

comprend des pics qui correspondent aux énergies de liaison des niveaux électroniques des atomes. Ces pics sont caractéristiques des atomes dont ils proviennent, permettant ainsi de déterminer les éléments qui composent la surface d'un matériau.

Koubaa *et al.* (1996) ont eu recours à la technique de XPS afin d'analyser l'effet d'un pressage et séchage simultanés sur la composition chimique des fibres obtenues par le procédé chimio-thermomécanique (CTMP). Les spectres ont montré une augmentation de la teneur en lignine et une diminution des polysaccharides des fibres pressées-séchées à une température de 175 °C. Plus tard, Johansson *et al.* (1999) a utilisé la spectroscopie de photoélectrons excités par rayons X comme indicateur de la teneur en lignine résiduelle sur la surface des fibres ayant subit différents procédés chimiques de mise en pâtes. Il a été conclu que l'efficacité de cette technique reste tributaire du niveau de contrôle de la contamination qui pourrait avoir lieu lors des mesures. Dans une autre perspective, Tserki *et al.* (2005) ont étudié l'effet du traitement par acétylation et propionylation sur la surface des fibres naturelles moyennant le recours à la technique XPS. La variation du ratio O/C a été utilisée comme principal indicateur de changement de la surface des fibres par estérification. Une discussion plus détaillée de l'application de cette technique a été présentée dans le **chapitre IV** de ce document.

En réalité, plusieurs autres méthodes spectroscopiques sont aussi utilisées pour déceler la composition chimique de la surface des matériaux. En effet, pour déterminer les groupements fonctionnels, la RMN, Raman, UV-visible, en plus de la spectroscopie Infrarouge, sont les techniques les plus couramment utilisées, alors que les informations sur la nature des liaisons chimiques au niveau superficiel peuvent être obtenues par les techniques (autre que la XPS) de spectroscopie d'ions rétrodiffusés (ISS, ion scattering spectroscopy), spectrométrie de masse à ionisation secondaire (SIMS), spectroscopie électronique à distribution angulaire (ADES,

angular-distribution electron spectroscopy). Le microscope à force atomique (ou AFM pour atomic force microscope) a été récemment utilisé pour visualiser la topographie de la surface d'un échantillon.

2.4.3 Techniques d'analyse thermique et calorimétrique des fibres de bois et des composites bois/thermoplastique

2.4.3.1 Analyse thermogravimétrique (TGA)

Parce que les fibres de bois et les polymères synthétiques peuvent éprouver une dégradation de leurs propriétés mécaniques sous l'influence de augmentation excessive de la température (Wielage *et al.*, 1999), l'optimisation de la température lors de la mise en forme du composites est ainsi indispensable. La méthode par variation thermogravimétrique (TGA) est une technique de routine dans ce genre d'analyse. Le principe consiste à mesurer la masse d'un échantillon en fonction d'un gradient ascendant de température. Ce principe est couramment utilisé non seulement dans l'analyse compositionnelle des matériaux et la détermination des températures de décomposition (Shafizadeh et Bradbury, 1979; Shafizadeh, 1982; Horne et Williams, 1996; Orfão *et al.*, 1999), mais aussi dans l'objectif de tester la stabilité thermique des fibres de bois utilisées comme renfort pour des matrices thermoplastiques (Wielage *et al.*, 1999; Jakab *et al.*, 2000).

2.4.3.2 Calorimétrie différentielle à balayage (DSC)

La calorimétrie différentielle à balayage (DSC, Differential Scanning Calorimetry) sert à étudier les transitions thermiques d'un polymère. En effet, la DSC est utilisée pour déterminer le taux de cristallinité des polymères ainsi que leur température de fusion, de transition vitreuse et de cristallisation (Sturtevant, 1987). Ainsi, l'enregistrement du flux de chaleur dégagée pendant une réaction de polymérisation pour une température donnée, permet de déterminer la conversion en fonction du temps et d'analyser l'influence des additifs sur la cinétique correspondante.

Plusieurs études ont eu recours à la technique de DSC afin de déterminer l'effet de l'addition des fibres de bois sur la cristallisation de la matrice formé d'un polymère semi-cristallin (Bouza *et al.*, 2006; Sombatsompop *et al.*, 2006; Borysiak, 2007). Harper et Wolcott (2004) ont utilisé la DSC pour analyser l'effet de l'interaction entre agent de couplage et lubrifiant sur la cristallisation du polypropylène. Palaniyandi et Simonsen (2007) ont utilisé cette méthode afin de déterminer l'effet de l'addition d'un agent de compatibilité sur la cinétique de cristallisation d'un composite formé de cellulose et de HDPE.

Une discussion plus détaillée sur les avantages et les limites de l'application de ces deux dernières techniques dans l'étude du comportement thermique des composites bois-thermoplastiques a été présentée dans le **chapitre V** de ce document.

2.4.4 Techniques d'analyse des relaxations mécaniques des composites bois-thermoplastiques par analyse dynamique mécanique (DMA)

Du fait de sa large gamme de fréquences accessibles, l'analyse mécanique dynamique est particulièrement bien adaptée à l'étude de la dynamique de chaîne des polymères qui se caractérise par des modes de relaxation complexes (Degallaix *et al.*, 2007) Le principe de la méthode consiste à appliquer une contrainte périodique et mesurer la déformation correspondante. La réponse en amplitude diminue, et apparait avec un décalage (δ) dans le temps, dû aux propriétés visqueuses des polymères (Degallaix *et al.*, 2007). Il en résulte un module complexe qui peut être divisé en deux composantes :

$$E = E' + iE'' \qquad (2.13)$$

Où, E′ et E″ désignent respectivement les modules de stockage et de perte. Le rapport entre ces deux composantes (E″/ E′) est désigné par tan δ ou facteur de perte.

L'application de cette méthode dans la détermination des différents modes de relaxation moléculaire des polymères pures, ou renforcés par des fibres naturelles, a été largement rapportée dans la littérature. En effet, l'analyse des relaxations α, β, et γ (voir **chapitre VIII**) de plusieurs polymères (HDPE, LPDE, PP, etc.), moyennant le recours à l'analyse mécanique dynamique, a été rapporté dans plusieurs études (Boyd, 1984; Popli *et al.*, 1984b; Khanna *et al.*, 1985). D'autres études ont utilisé l'analyse dynamique mécanique comme outils de caractérisation de l'interface entre la matrice thermoplastique et les éléments de renfort (Kubat *et al.*, 1990; Pegoretti *et al.*, 2000; Bengtsson *et al.*, 2005; Mohanty *et al.*, 2006).

2.5 Conclusion

Afin d'optimiser l'utilisation des fibres de bois comme éléments de charge ou de renfort d'un polymère thermoplastique, la connaissance de la structure anatomique et des caractéristiques chimiques du bois est essentielle. Les éléments anatomiques qui affectent l'interaction entre les fibres de bois et la matrice thermoplastique ont été énumérés. La longueur des fibres, l'épaisseur et la structure de la paroi cellulaire ainsi que son état de surface ont été présentés comme les principaux attributs clés qui peuvent influencer les propriétés mécaniques et physiques des composites à base de fibres courtes et polymères thermoplastiques. La connaissance de la chimie de surface des trachéides est indispensable pour l'amélioration de l'interface et la compatibilité entre les fibres naturelles et le polymère synthétique. Les agents de couplage jouent un rôle important dans l'amélioration de l'affinité interfaciale entre les fibres lignocellulosiques polaires et les polymères synthétiques apolaires. Les anhydrides maléiques greffés sont les agents de couplage les plus populaires. Au niveau de l'interface, les liaisons covalentes, les liaisons secondaires, l'enchevêtrement des chaînes moléculaires ainsi que l'ancrage mécanique sont les principales formes d'adhésion entre les fibres de bois et les matrices thermoplastiques. La principale forme de liaisons covalentes entre fibres de bois et l'agent de couplage, tel que le

MAPE, se fait par estérification. Toutefois, il a été montré que la liaison peut être aussi mécanique si le polymère thermoplastique pénètre les ouvertures et les ponctuations ou le lumen des trachéides. Différentes méthodes de spectroscopie ont été utilisées pour caractériser aussi bien la structure chimique de la surface des fibres de bois que l'interface fibres de bois-polymères thermoplastiques.

CHAPTER III

MATERIALS AND METHODS

3.1 Introduction

In order to limit our analysis to only the effect of the intrinsic characteristics of wood fiber on wood/polymer composites (WPC) final properties, processing parameters (such as temperature profiles, screw speed of the extruder, etc.) were maintained constant for all sample preparations. The setting parameters of the machines, cited below, represent the optimum conditions that were chosen after numerous preliminary investigations. The choice of these processing parameters was based on the integrity of wood particles after processing and the characteristics of the polyolefin matrix.

3.2 Materials

Four types of wood sawdust were investigated: eastern white cedar (*Thuja occidentalis L.)*, jack pine (*Pinus banksiana* Lamb.) residue which divided into wood sawdust and bark shavings, and black spruce (*Picea mariana* Mill.) sawdust. These lignocellulosic materials were supplied by softwood sawmills located in Abitibi-Témiscamingue in the province of Quebec, Canada. Wood sawdust and bark shavings were hammer-milled into particles at FPInnovations, Division Forintek (QC, Canada). Particles were then screened and classified into 3 mesh particle groups (Table 3.1)

using an oscillating multideck-type screen classifier. At this stage, moisture content of the particle filler was calculated at around 10.5%. Wood particle fillers were not extracted.

An HDPE polymer (Goodfellow Corp., USA) was used as the matrix. This is a semicrystalline material (typically 70% to 80%) with 0.95 density, 9.0 g/10 min melt index, and 135 °C melting point.

Ethylene-Maleic Anhydride Copolymer (MAPE, A-C® 575A), supplied by Honeywell (Minneapolis, MN, USA), was used as the coupling agent. It has a 0.92 specific gravity and a 104 °C to 107 °C melting point. A modified fatty acid ester (STRUKTOL® TPW 113) was used as internal lubricant to facilitate extrusion.

Table 3.1. Classification of hammer-milled particles.

Mean class	Class interval	
	mesh	μm
24 mesh	]20,28]	]850, 600]
42 mesh	]35,48]	]425, 300]
65 mesh	]48,100]	]300, 150]

3.3 Methods

3.3.1 Experiment design

A 3^3 factorial split-block experimental design was used for each wood component (Figure3.1). The first factor is wood particle loading at 3 contents: 25 wt%, 35 wt%, and 45 wt%. The second factor is wood particle size at 3 distributions: 24, 42, and 65 mean mesh distributions. The last factor is the processing method, i.e., injection molding, compression molding, or extrusion. The complete design structure involves

108 possible combinations (4 x 3^3). However, due to the structure of the available experimental material, it was impossible to use a classic split-block design, so an incomplete design based on the split-block structure was used (Table 3.2).

Table 3.2. Factor combinations for the incomplete factorial design.

Species	Cedar heartwood			Cedar sapwood			Jack pine bark			Jack pine			Black spruce		
Size (mesh)	24	42	65	24	42	65	24	42	65	24	42	65	24	42	65
Load (wt%)	25	25	25	25	25	25	25	25	25	25	-	-	-	25	-
	35	35	-	35	35	35	35	35	35	-	35	-	35	-	-
	45	45	-	45	45	45	45	45	45	-	-	45	-	-	45

3.3.2 Processing methods

3.3.2.1 Compounding process

Similar sized wood particles were compounded into pellets at 25%, 35%, and 45% by weight of HDPE using a Coperion Werner & Pfleiderer ZSK-25 WLE co-rotating twin-screw extruder (Stuttgart, Germany). Coupling agent content was fixed at 2 wt% for all experimental design blocks. The choice of this latter weight percentage was based on state of art literature for WPC (Lu et *al.*, 2005, Maldas et Kokta, 1991) Wood particles, coupling agent, and polymer were fed to the extruder separately using a Colortronic GmbH gravimetric feeder (Germany) at temperature ranges 1 and 4, respectively. Barrel temperatures of the four zones were 180 °C, 180 °C, 180 °C, and 190 °C from feeding to die zone. Screw speed was 240 rpm and melt pressure at the die varied from 15 to 25 bars, depending on wood particle content (Appendix 1). Vacuum venting (-40 kPa) at temperature range 10 was used to minimize volatile extractives (Appendix 2). Residence time was determined experimentally in the preliminary experiments and was maintained constant at 240 seconds and material feed rate was 15 kg/h. Extrudates were air-cooled and pelletized into a nominal pellet size of 5 mm.

feed rate was 15 kg/h. Extrudates were air-cooled and pelletized into a nominal pellet size of 5 mm.

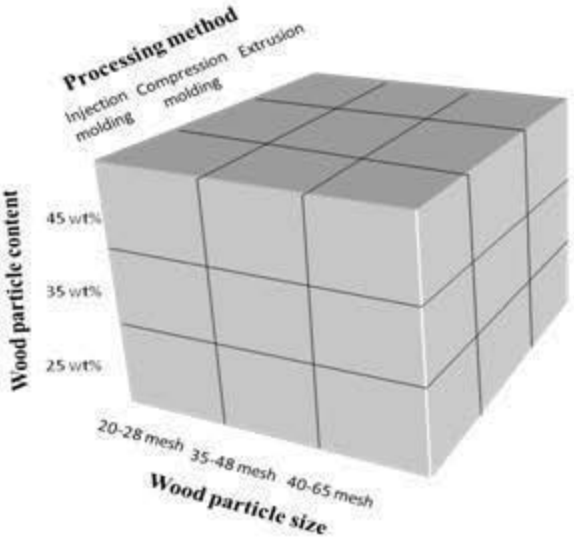

Figure 3.1. Split-block experimental design

3.3.2.2 Injection molding process

Injection molding experiments were carried out using a reciprocating-screw injection molding machine (Toshiba ISE60P, USA) with a maximum clamping force of 60 tons. Machine settings are shown in Table 3.3. The 3-cavity test specimen mold was designed to conduct the experiments according to ASTM standard specifications for tensile testing, flexural testing, and Izod Impact testing. Samples were cooled under room conditions.

Table 3.3. Injection molding machine settings.

Mold temperature: fixed/mobile	38 °C/38 °C
Injection pressure	900 kPa
Injection pressure time	10 *s*
Hold pressure	900 kPa
Hold pressure time	4 *s*
Barrel temperature profile: feed-zone1-zone2- nozzle	160-190-190-190 °C

3.3.2.3 Extrusion process

Plastic and wood particles pellets were extruded with various lubricant concentrations (0 wt %, 2 wt %, and 5 wt %). A single screw extruder from the AMUT EA48 series (Marano Ticino, Italy) was used. Screw diameter was 48 mm and length to diameter ratio (L/D) was 24:1. The rectangular die was 13 x 6 mm in size. Temperature profiles and screw speed conditions of the extruder were maintained constant for all sample preparations, as shown in Table 3.4. Extrudates were quenched in water and samples were collected for analysis.

Table 3.4. Single screw extruder conditions.

Screw speed	80 rpm
Feed zone temperature	170 °C
Compression zone temperature	180 °C
Metering zone temperature	190 °C
Die temperature	200 °C

3.3.2.4 Compression molding process

Pellets were compression molded on a preheated press (Fontyne TP 1000, Holland) into plaques according to ASTM D4703-03[3]. Machined-cavity flash molding was used to prepare 3.2 mm thick plaques. The mold was preheated to 180 °C. The material was then spread to slightly overfill the mold and the press was closed for 8 min to preheat the material by applying contact pressure. A molding pressure of 0.58 MPa was then applied for 5 minutes. Cooling rate of the mold was maintained at 10 ±2 °C/min. Test specimens were cut using a standard blanking die.

[3] ASTM.D4703-03, Standard Practice for Compression Molding Thermoplastic Materials into Test Specimens, Plaques, or Sheets. (2003).

CHAPTER IV

ANALYSIS OF AMONG-SPECIES VARIABILITY IN WOOD FIBER SURFACE USING DRIFTS AND XPS TECHNIQUES: EFFECTS ON ESTERIFICATION EFFICIENCY*

4.1 Abstract

Variability in the chemical composition of surface properties of various wood fibers (eastern white cedar, jack pine, black spruce, and bark) was investigated using diffuse reflectance infrared Fourier transform spectroscopy (DRIFTS) and X-ray photoelectron spectroscopy (XPS). Both DRIFTS and XPS showed high variability in fiber surface composition between species and between fiber types (sapwood, heartwood, and bark). Fiber surface was modified by esterification reaction using a maleic anhydride polyethylene (MAPE) treatment. DRIFTS failed to assess surface modification, while XPS results showed that MAPE treatment increased the surface hydrocarbon concentration of jack pine wood fiber, indicated by a decrease in oxygen-carbon ratio and an increase in relative intensity of the C1 component in the C1s signal. Lignin concentration variability on the fiber surface was determined as the major factor that prevents esterification from taking place.

---

* Reprinted in part with permission from Bouafif, H., Koubaa, A., Perré, P., Cloutier, A., & Riedl, B. (2008). "Analysis of among-species variability in wood fiber surface using DRIFTS and XPS: Effects on esterification efficiency. Journal of Wood Chemistry and Technology, 28(4), 296-315"

4.2 Résumé

La variabilité de la composition chimique de la surface des fibres de différentes essences de bois (thuya occidental, pin gris, épinette noire et écorce de pin gris) a été étudiée moyennant l'utilisation de la spectroscopie infra rouge en mode réflexion diffuse par transformée de Fourier (DRIFTS) et par la spectroscopie des photoélectrons par rayons X (XPS). Ces deux techniques ont montré une grande variabilité dans la composition de la surface des fibres issues de différentes espèces et aussi à l'intérieur d'une même espèce (aubier, bois de duramen, écorce). La surface des fibres a été modifiée par réaction d'estérification en utilisant le polyéthylène modifié à l'anhydre maléique (MAPE). Les modifications de la surface n'ont pas été détectées par DRIFTS, cependant les résultats de XPS ont montré que le traitement par la MAPE augmente la concentration des molécules d'hydrogène et d'oxygène sur la surface des fibres de pin gris indiquée par une diminution du rapport oxygène-carbone et une augmentation de l'intensité relative de la composante C1 dans le signal C1s. Des teneurs élevées en lignine sur la surface de la fibre ont été déterminées comme facteur contraignant le bon déroulement de la réaction d'estérification.

4.3 Introduction

Surface chemical properties of wood play an important role in fiber-to-fiber adhesion and fiber adhesion to thermoplastic and thermoset polymers (Rowell *et al.*, 2005). However, the variability of wood chemical composition in the fiber cell wall and on the fiber surface is very high. The main components of wood are cellulose, hemicelluloses, and lignin fractions, which vary widely among and within species (Rowell *et al.*, 2005). Hemicelluloses are known as the main sites of interaction with water for hydrogen bonding due to their greater accessibility (Rowell *et al.*, 2005). Lignin and other extractives (phenolic-OH) found in wood act as antioxidants

through resonance stabilization of free radicals, thus inhibiting grafting and copolymerization (Bhattacharya and Misra, 2004).

The surface properties of wood fibers are dependent not only on intrinsic characteristics of wood species but also on the method of preparation. For instance, mechanical and thermomechanical fiber separations usually display lignin-rich fiber surfaces, while chemical separation processes result in carbohydrate-rich surfaces (Koljonen, 2004). The surface tension of chemically produced fibers is often higher than that of mechanically produced fibers (Tze *et al.*, 2006). Subsequently, the functional groups, on the surface of chemically produced fibers are capable of stronger secondary interactions with other polymers, such as reported for polyolefins (Lu and Wu, 2005).

Several studies have focused on the effect of lignin content on wood-based composite properties. Luo et *al.* (2006) studied the effect of high lignin content on HDPE/lignin composites. They found that elongation at break of the composites gradually increased with lignin content. Bending modulus and bending strength increased with lignin dosage by 17.3 % and 12.2 %, respectively. They also observed that bending strength reached a maximum value of 16.1 MPa at the lignin mass fraction of 2.5 %, and subsequently declined with increasing lignin dosage, while tensile strength of the HDPE/lignin composite increased by 8.0 %.

Similarly, Le Digabel and Avěrous (2006) noted a decrease in stress at the limit of elasticity with increasing lignin content, while elongations at break and at the yield point increased with lignin content. Nevertheless, they concluded that the increased moduli in the biocomposites were mainly caused by cellulose filler rather than lignin content.

Although extractives constitute a small weight percentage of the chemical composition, they dominate the surface chemistry of wood fibers. Depending on chemical nature and concentration, extractives are considered as surface

contaminants, with deleterious effects on wood-polymer compatibility. Saputra and co-workers (2004) investigated how the removal of extractives from pine and Douglas fir can affect the mechanical properties of wood–polypropylene (PP) composites, and they reported that mixing wood flour or wood fibers and thermoplastics at high temperatures allowed extractives to migrate to the wood flour surface and accumulate in the wood-plastic interphase. Subsequent removal of this weak boundary layer led to a significant improvement in interfacial shear strength between the polypropylene matrix and the extracted wood filler (Saputra *et al.*, 2004).

Poor interfacial bonding and weak compatibility between wood-based materials and the most commonly used polymers are by far the greatest limiters of wood plastic composite (WPC) applications. Since polymers and wood fillers are incompatible, certain surface modifications, mostly using coupling agents, are required to improve the service performance of composites (Maldas *et al.*, 1988a; Gassan and Bledzki, 1997; Kazayawoko *et al.*, 1999a; Lu *et al.*, 2005b). Maleic anhydride grafted polyethylene and maleic anhydride grafted polypropylene (MAPE and MAPP, respectively) are mostly used as coupling agents in extruded WPC or lignocellulosic-based composite materials performed in liquid phase (Lu *et al.*, 2005a; Sombatsompop *et al.*, 2005).

Although all researchers agree on the need to make changes to the surface of wood fillers, there is a lack of consensus on the effects of concentration and type of functionalized polymer on composite properties. Lu et al. (Lu *et al.*, 2005b) observed that tensile strength and flexural storage moduli pass through a maximum as a function of concentration of the coupling agent. Similar behavior was also observed by Sombatsompop et al. (2005) at low concentration. However, others authors have found that composite stiffness was not significantly influenced by the presence of the functionalized polymer, and only strength was considerably increased (Kazayawoko *et al.*, 1999a; Bledzki *et al.*, 2005).

Compared to the number of studies on coupling mechanisms and interfacial characterization, few studies have investigated the effects of the intrinsic characteristics of wood fillers according to wood species and type (sapwood, heartwood, and bark-based particles).

This study investigates between-species variability in wood fiber surface composition by spectral characterization using Diffuse Reflectance Fourier Transform Infrared Spectroscopy (DRIFTS) and X-ray photoelectron spectroscopy (XPS). Variations in the grafting efficiency of maleic anhydride polyethylene with wood species and type are also discussed.

4.4 Experimental

4.4.1 MAPE grafting

MAPE grafting of wood flour (42 mesh) was conducted in a reactor in the presence of a solvent according to the method described by Kazayawoko et al. (1997; 1999b) and Chuai et al. (2001). Before grafting, the wood flour was oven-dried at 105°C for 24 h. The reaction procedure used to modify the wood flour was as follows: 250 ml of xylene was placed in a 500 ml reactor and stirred continuously to 130–140°C, at which point 5g of MAPE (A-C® 575A) and 30 g of wood flour were placed in the reactor. One gram of sodium hypophosphite hydrate was added as an esterification catalyst. The reaction was carried out for two hours at 130–140°C. As shown in the reaction schematic (Figure 4.1), two reactions were possible between MAPE and wood particles: a single site reaction, which led to monoester formation in addition to the carboxylic acid groups (Figure 4.1-a); or diester formation without the carboxylic acid groups (Figure 4.1-b) (Carlborn and Matuana, 2006). After the reaction, the mixture was filtered to isolate the reacted wood flour. The treated wood flour was treated by soxhlet extraction with xylene for 8 h to remove the unreacted anhydride, then oven-dried at 70°C for 24 h.

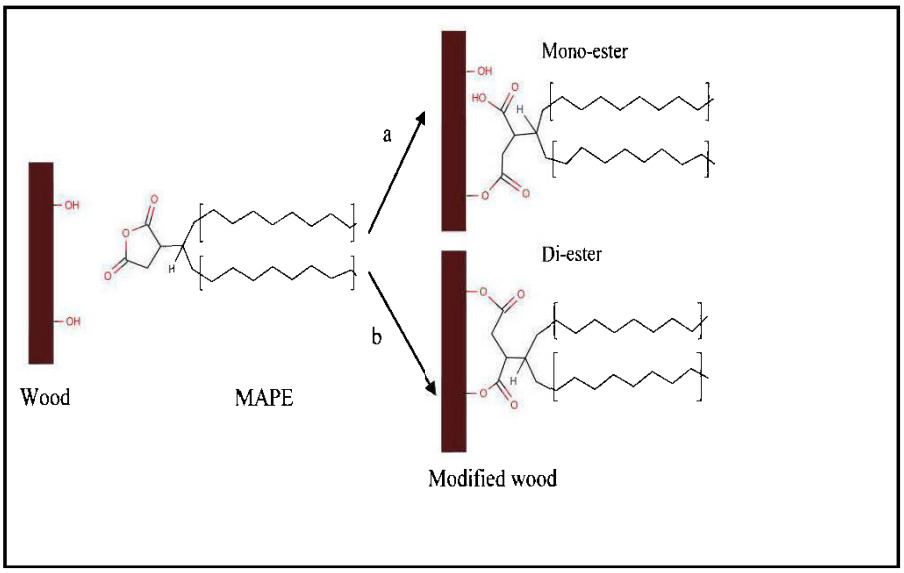

Figure 4.1. Model of the esterification reaction between wood fiber and maleic anhydride polyethylene (Carlborn and Matuana, 2006)

4.4.2 DRIFT measurements

Diffuse reflectance infrared Fourier transform spectroscopy (DRIFTS) was performed in order to: i) provide detailed information on the functional groups present at the surface of the wood particle samples; and ii) confirm whether esterification reaction occurred between wood flour and maleic polyethylene. DRIFTS was conducted on a Tensor 27 FT-IR system (Bruker Optics, Germany) equipped with a deuterated triglycine sulfate (DTGS) detector. For each sample, spectra were recorded by collecting 164 scans in the range of 4000–400 cm^{-1} at 4 cm^{-1} resolution. Pure powdered potassium bromide (KBr) was used as a reference substance. Since the DRIFTS spectra of wood powders in KBr are substantially influenced by both particle size and concentration (Faix and Böttcher, 1992), samples for DRIFTS were carefully prepared in microcups as follows: 1 mg of each wood flour (100 mesh) was mixed with KBr in the proportion of 1/100 (% by weight) in an agathe mortar and

then transferred to a 4-mm diameter cup where it was lightly compressed and leveled using a spatula. Tilted baselines of the original spectra were not altered.

4.4.3 XPS measurements

X-ray photoelectron spectroscopy (XPS) was also used for surface analyses of the wood and bark samples. Bleached Kraft fibers were included to provide more information. Prior to XPS analysis, samples were oven-dried. XPS spectra of unmodified and modified wood flour were recorded with an X-ray photoelectron spectrometer (Kratos Axis Ultra, UK). All spectra were collected using a monochromatic Al Kα X-ray source (1486.6 eV). The lateral dimensions of the samples were 800 microns x 400 microns, corresponding to those of the Al Kα X-ray used, and probing depth was approximately 5 nanometers. For each sample, two spectra in the fixed analyzer mode were recorded: (i) survey spectra (0-1150 eV and pass energy 120 eV) were recorded to estimate composition; and (ii) high-resolution spectra (within 20 eV and pass energy 20 eV) were recorded to obtain information on chemical bonds. From the survey spectra, the atomic concentration ratio of oxygen to carbon was determined by integrating the area under the curve after removal of the linear background (Dorris and Gray, 1978a; dorris and gray, 1978b; Johansson *et al.*, 2004). High resolution analysis of the carbon chemical bonds was performed by iterative convolution, using a non-linear least-squares procedure based on the Levenberg-Marquardt algorithm. Peak synthesis was performed with CasaXPS. Peak intensities at a given bending energy were generated as a Gauss-Lorentz product function peak. The Gauss-Lorentzian ratio was set at 0.30 for all curve fittings.

4.5 Results and Discussion

4.5.1 Surface and interface characterization by DRIFTS

4.5.1.1 FTIR spectra of untreated wood fibers

Figure 4.2 shows the FTIR absorption spectra of untreated wood particles for different species in the 4000 and 400 cm^{-1} range. Because bark and wood have similar chemical compositions, the bark absorption bands were assigned to specific chemical functions analogous to those of wood (Haussard *et al.*, 2003). Although an overview of all wood samples shows similar IR spectra, high resolution analysis reveals several divergences in the fingerprint region of the spectra (<1500 cm^{-1}). Differences are observed mainly between the bark spectrum and the rest of the wood spectra.

Spectra of the untreated wood particles show the presence of a broad stretching band for intermolecular bonded hydroxyl groups at 3400 cm^{-1}. The OH groups may include absorbed water, aliphatic primary and secondary alcohols found in carbohydrates and lignin, aromatic primary and secondary alcohols in lignin and extractives, and carboxylic acids in extractives (Faix and Böttcher, 1992; Kazayawoko *et al.*, 1997; Pandey and Theagarajan, 1997). This OH stretching band is flanked by prominent methylene/methyl bands appearing at 2904 cm^{-1}. In the case of bark particles, these bands are shifted and divided into two peaks at 2925 cm^{-1} and 2847 cm^{-1}, respectively.

A broad, medium intensity ester carbonyl vibration appears at 1735 cm^{-1}, which is presumed to emanate from carbonyl (C=O) stretching of acetyl groups in hemicelluloses and carbonyl aldehyde in lignin and extractives (Pandey and Theagarajan, 1997; Pandey, 1999; Pandey and Pitman, 2004; Silverstein, 2005). Kazayawoko and co-workers (1997) also attributed this vibration to carbonyl (C=O) stretching of carboxyl groups in hemicelluloses, lignin, and extractives, as well as esters in lignin and extractives. In the case of the particle bark spectrum, weak

carboxylic carbonyl functionality at 1717 cm^{-1} is superimposed as a shoulder, with a broad carbonyl band appearing at 1735 cm^{-1}. The bands around 1608 cm^{-1} and 1510 cm^{-1} can also be distinctly identified due to the aromatic C=C skeletal vibrations mainly linked to the lignin structure (Marcovich *et al.*, 1996; Barker and Owen, 1999; Ferraz *et al.*, 2000; Moore and Owen, 2001; Ajuong and Redington, 2004; Colom and Carrillo, 2005; Papp *et al.*, 2005).

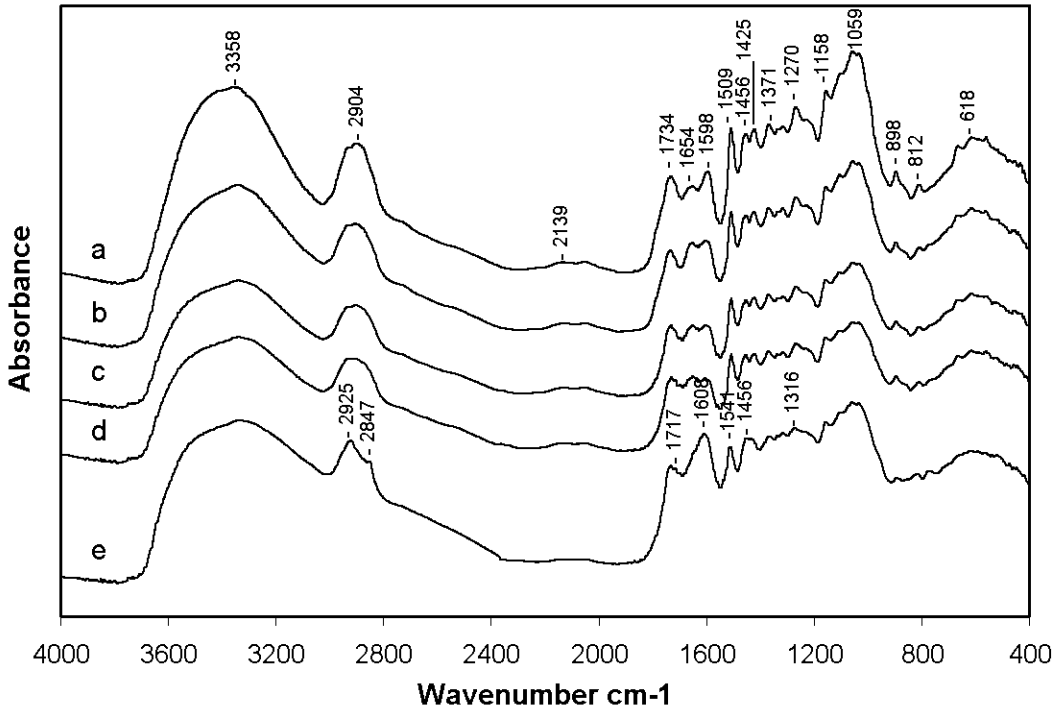

Figure 4.2. FTIR spectra of untreated fibers: eastern white cedar; heartwood (a) and sapwood fibers (b), jack pine wood fibers (c), black spruce wood fibers (d), and jack pine bark fibers (e).

In the fingerprint region between 1600 and 400cm^{-1}, many sharp and discrete absorption bands due to various functional groups present in the wood constituents are observed. The medium intensity bands around 1456cm^{-1}, 1425cm^{-1} and 1371cm^{-1} are associated with methylene deformation and methyl asymmetric and methyl

symmetrical vibrations (Faix and Böttcher, 1992; Kazayawoko *et al.*, 1997; Pandey and Theagarajan, 1997; Ajuong and Breese, 1998). The broad, strong bands appearing at 1270 cm^{-1} are due to either carbon single bonded oxygen stretching vibration or an interaction vibration between carbon single bonded oxygen stretching and in-plane carbon single bonded hydroxyl bend in carboxylic acids (Ajuong and Breese, 1998).

Papp et al. (2005) attributed bands containing no other nearby absorption maxima to one chemical component (1510 cm^{-1}: aromatic rings, 1270 cm^{-1}: guaiacyl units, 1158 cm^{-1}: C–O–C bonds in the cellulose). The observed absorption band at 1158 was identified as a result of the asymmetric stretching of C-O-C in the cellulose and hemicelluloses (Kazayawoko *et al.*, 1997; Bräs *et al.*, 2004). However, Ajuong and Breese (1998) suggested that this medium intensity absorption may arise from saturated fatty acid ester carbon single bonded oxygen stretching, in association with the ester carbonyl discussed earlier at lower wavenumber. Strong intensity bands at 1059 cm^{-1} and 1036 cm^{-1} are essentially in the positions corresponding to those observed by Chen and Jakes (2002) in the IR spectra of single cotton fibers. Finally, the vibrations appearing further down the field at 898 cm^{-1} and 812 cm^{-1} may arise from disubstituted ring stretching and out-of-plane carbon single bonded hydrogen (Ajuong and Breese, 1998).

DRIFTS was used as a semi-quantitative method to compare the chemical composition of the untreated wood particle surfaces. The following bands were selected as the most characteristic: 1) 1735 cm^{-1} for lignin and extractives; 2) 1605 cm^{-1} and 1510cm^{-1} for lignin and aromatic skeletal components; 3) 1271 and 1231 cm^{-1} for guaiacyl units of lignin; and 4) 1158 cm^{-1} for fatty acids. Figure 4.3 shows the area under peak, without linear background, of the selected band spectra for wood (the band area around 1735 cm^{-1} is presented separately in the next part of this paper). It confirms the variability of particle surface, not only between species, but also within tree types (sapwood vs. heartwood).

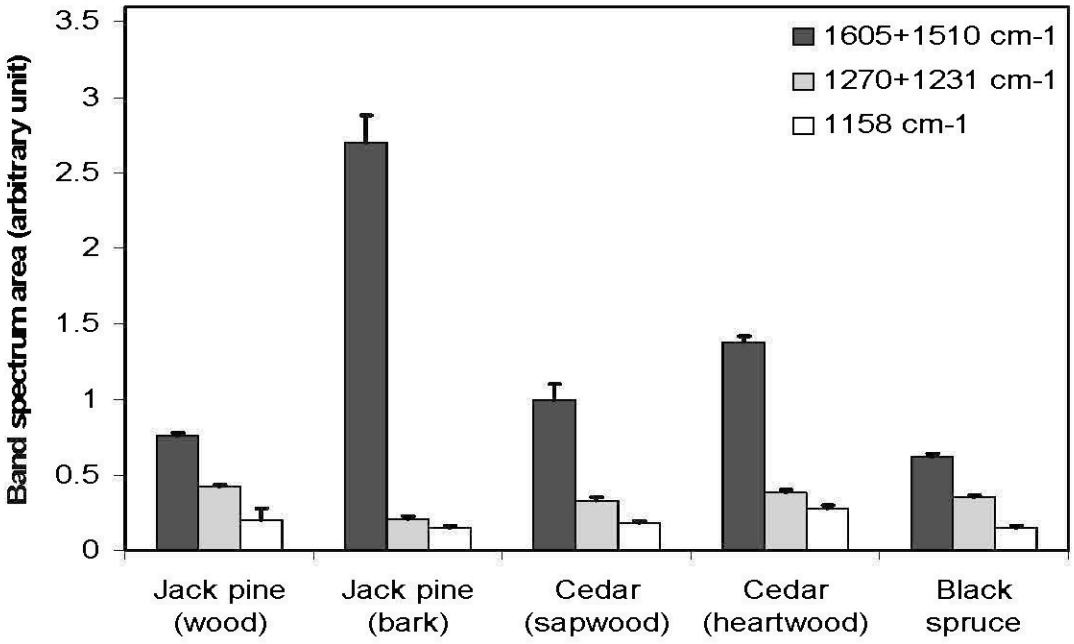

Figure 4.3. Area under the peak of the most important absorption band spectra of the studied wood and bark fibers.

The FTIR spectra of untreated wood were compared with those of bleached Kraft fibers. Figure 4.4 shows the FTIR spectra of untreated jack pine wood and bleached Kraft fibers. As can be seen, the greatest differences are located around 1735 cm^{-1}, which, as discussed earlier, may be linked to carbonyl (C=O) stretching of carboxyl groups in hemicelluloses, lignin, and extractives and/or to esters in lignin and extractives. This absorption band is absent in the FTIR spectra of bleached Kraft fibers. The observed absorption band at 1647 cm^{-1} arises when the semi-acetal hydroxyl group of the cellulose molecule transforms into aldehyde (Pandey, 1999). However, others studies have assigned this vibration to absorbed water (Kazayawoko *et al.*, 1997; Kazayawoko *et al.*, 1999a).

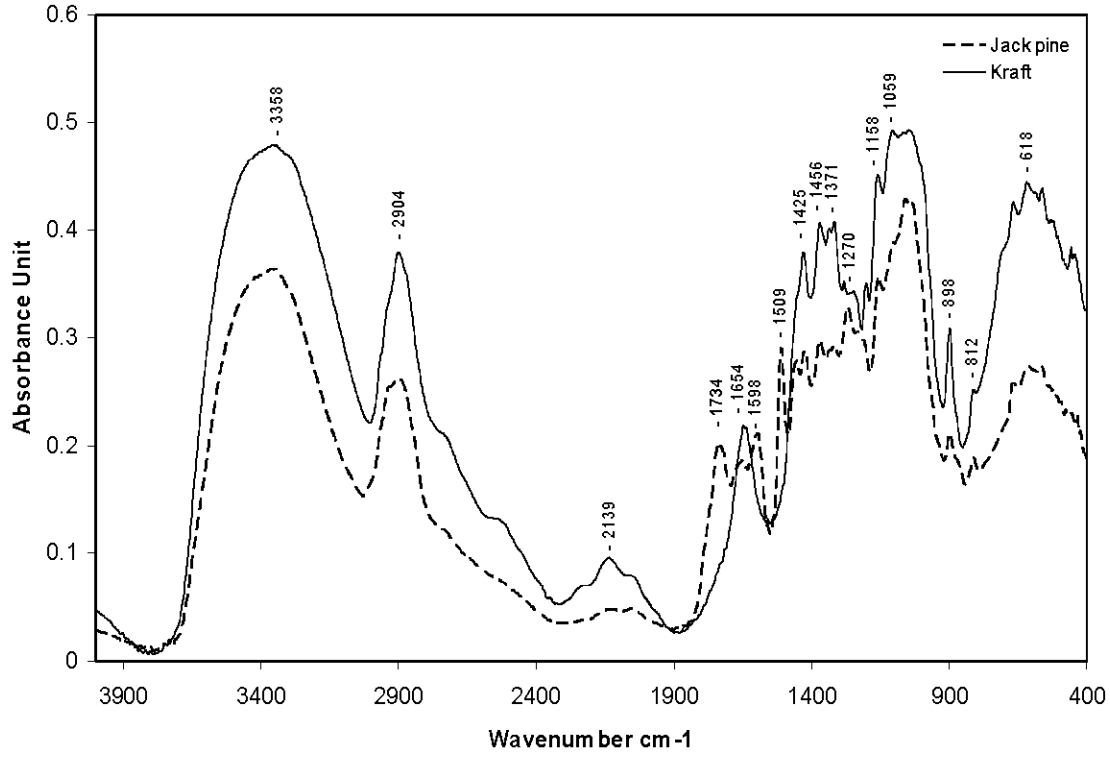

Figure 4.4. FTIR spectra of bleached softwood Kraft versus untreated jack pine fibers

3.5.1.2 FTIR spectra of Maleic Anhydride Polyethylene

Figure 4.5 shows the MAPE absorption spectra (MAPE, A-C® 575A). The most characteristic assignments of absorption bands are presented in Table 4.1. The strong intensity bands at 2920 cm^{-1} and 2851 cm^{-1} are characteristic of CH_2 stretching vibrations in polyethylene chains. The vibration at 1772 cm^{-1} is associated with the anhydre carbonyl (C=O) symmetric and asymmetric stretching, while bands near 1716 may be assigned to carbonyl stretching vibrations of carboxyl groups (Kazayawoko *et al.*, 1999a; Carlborn and Matuana, 2006; Sheshkali *et al.*, 2007).

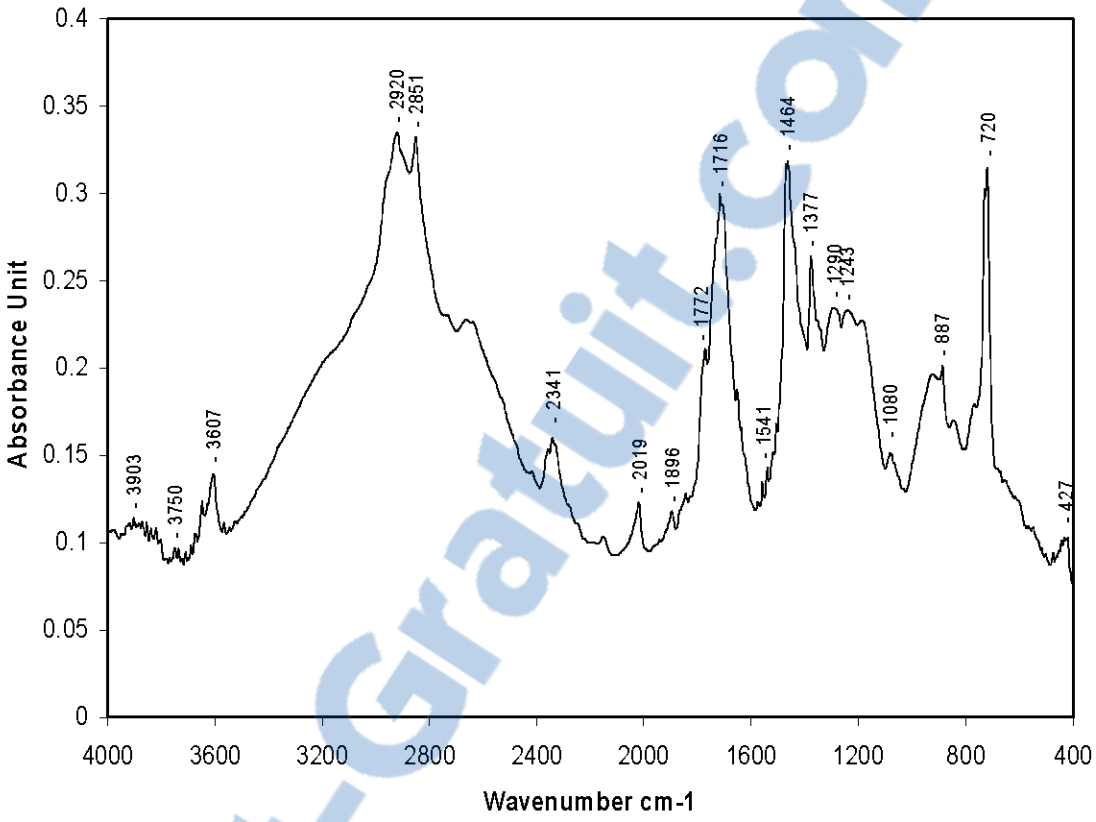

Figure 4.5. FTIR spectra of pure maleic anhydride polyethylene (MAPE, A-C® 575A)

The digital subtraction of the FTIR wood spectra after and before treatment with MAPE did not indicate the presence of any distinctive absorption bands around 1735 cm^{-1} that may be assigned to ester bonds between hydroxyl groups of wood fibers and maleic anhydride polyethylene. However, the peak around 1740 cm^{-1} confirms an effective esterification reaction between hydroxyl groups of bleached Kraft fibers and anhydride groups of the MAPE.

Table 4.1. FTIR Absorption Bands and Assignments of Pure MAPE (Kazayawoko *et al.*, 1999a; Carlborn and Matuana, 2006).

Wave number (cm^{-1})	**Assignment**
2920-2851	CH stretching of CH_2, CH_3
1772	Anhydride C=O stretching
1716	C=O stretching (carboxyl group)
1464	CH_2 deformation
1377	CH_2 deformation
720	$(CH_2)_n$ rocking vibration ($n > 3$)

4.5.1.3 Comparison between treated and untreated fiber surfaces

Although DRIFTS was successfully used to characterize the main chemical bonds on the fiber surface, it failed to confirm esterification between wood particles and maleated polyethylene. This could be explained by many factors. (i) The C=O bonding resulting from esterification can be overlapped by those already present in extractives and lignin. (ii) The sensitivity of DRIFTS limits measurement reproducibility and repeatability. Faix and Böttcher (1992) found that carbohydrate intensities, mainly around $1100cm^{-1}$, are strongly influenced by variations in wood concentration in the dispersing KBr matrix and the particle size of the milled wood. Otherwise, in the wavenumber range above 1150 cm^{-1}, intensity depends solely on the content of the chemical components (Pandey and Theagarajan, 1997). This may explain why researchers have often been interested in this wave range when characterizing the chemical composition of lignocellulosic materials (Rodrigues *et al.*, 1998; Rodrigues *et al.*, 2001; Tucker *et al.*, 2001; Pandey and Pitman, 2004; Nuopponen *et al.*, 2006; Polovka *et al.*, 2006; Raiskila *et al.*, 2007). (iii) The vibration intensity of each selected component depends on which part of the fiber surface has been scanned. In other words, it depends on how the fiber wall was fractured during mechanical grinding or milling. Many surface types are created,

because the cracks in the fibers are usually related to the stiffness of the cell wall, and especially the thickness of the S2 layer, which depends on wood species and type.

4.5.2 Surface and interface characterization by XPS

Typical XPS spectra for eastern white cedar, bark, and bleached Kraft fibers are shown in Figure 4.6. As expected, in all spectra, only oxygen and carbon can be clearly identified. However, relatively weak peaks of other major elements such as nitrogen, silicon, magnesium, phosphor, and calcium are also observed, possibly arising from sites during tree growth or from contamination during sample preparation. In the case of bleached Kraft, the presence of mineral elements can be attributed to residual magnesium salts and sodium silicate, which are frequently added to improve bleaching with alkaline peroxide. The survey spectra of the other wood species (black spruce and jack pine) exhibit similar trends to eastern white cedar.

The C1s signal is usually deconvoluted into four components according to oxidation level (Table 4.2): C1 refers to unoxidized carbon (i.e., C–C and/or C–H), C2 corresponds to carbon with one bond to oxygen (i.e. O–C), C3 is assigned to carbon with two bonds to oxygen (i.e., O–C–O and C=O), and C4 refers to carbon with three bonds to oxygen (i.e., O–C=O). C2 and C3 components arise mainly from carbohydrates, and C1 and C4 components arise mainly from lignin and wood extractives. Area percentages of the three C1s components are shown (Table 4.2) for treated and untreated samples. The binding energy values of C1, C2, C3, and C4, which correspond respectively to 285 ± 0.01 eV, 286.6 ± 0.1 eV, 288 ± 0.3, and 289 ± 0.6 eV, are in good agreement with those reported in the literature (Dorris and Gray, 1978a; dorris and gray, 1978b; Kamdem *et al.*, 1991; Koubaa *et al.*, 1996).

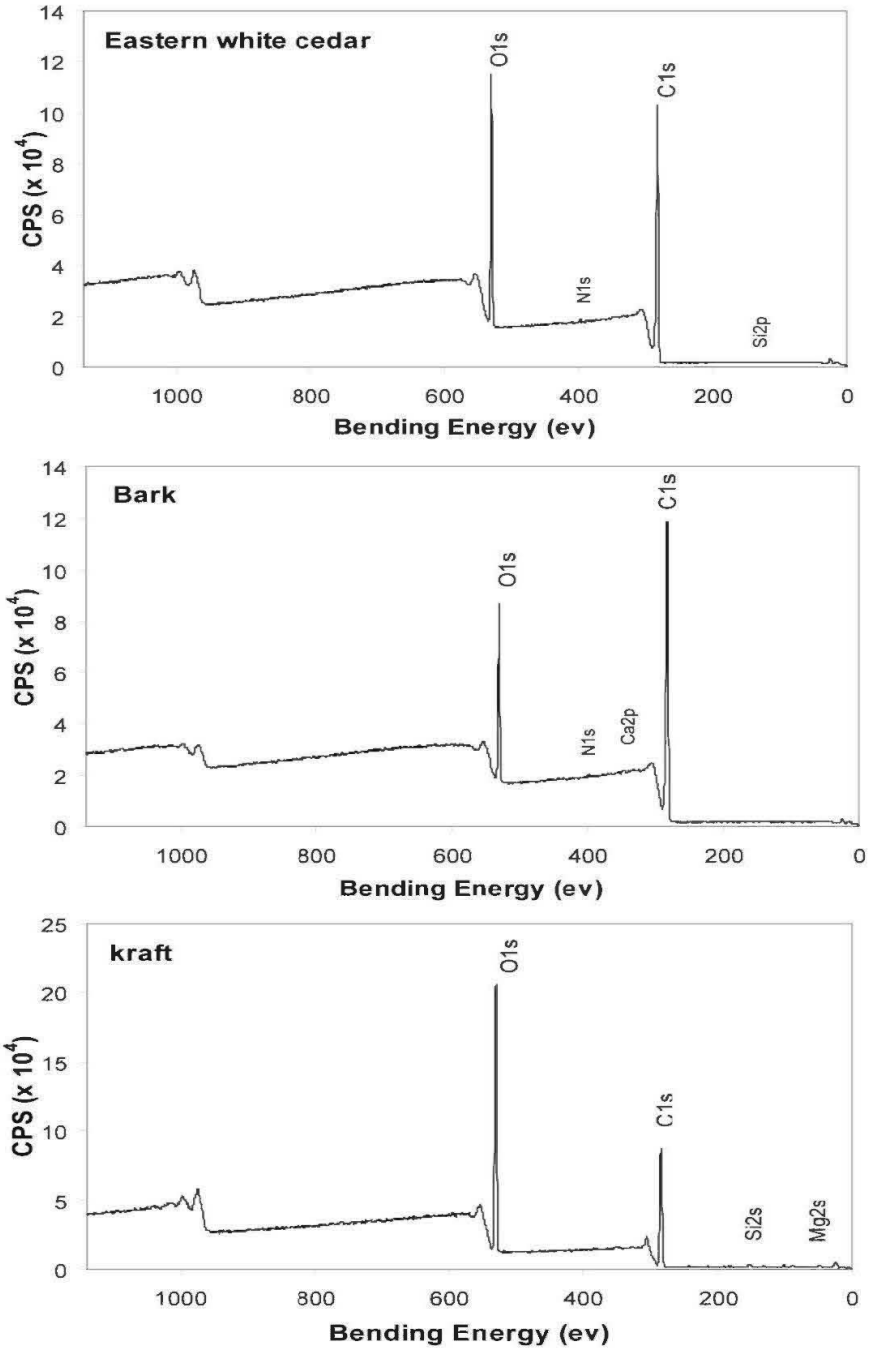

Figure 4.6. X-ray Photoelectron spectroscopic (XPS) survey spectra of different unmodified wood fibers

Table 4.2. Classification of Carbon peak components (C1s) for wood fibers.

Carbon atom class	Bending energy (eV)	Oxidation level	Main wood component	References
C1	285 ± 0.01	C–C and/or C–H	Terpenes, Fatty acids, lignin	(Dorris and Gray, 1978b; Kamdem *et al.*, 1991; Hua *et al.*, 1993)
C2	286.6 ± 0.1	C–O	Celluloses, hemicelluloses, and lignin	(Ahmed *et al.*, 1987; Hua *et al.*, 1993; Jaic *et al.*, 1996)
C3	288 ± 0.3	C=O and/or O–C=O	Fatty acids and their esters	(Dorris and Gray, 1978b)
C4	289 ± 0.6	O–C=O	Resinic acids	(Dorris and Gray, 1978b)

The significant contribution of C2 supports the results from the O/C ratio, suggesting that bleached Kraft fibers are delignified. Thus, exposed surface is essentially rich in carbohydrates, with high content in hydroxyl groups. The lower C1 content in bleached Kraft fiber surfaces arose from the residual lignin. However, assuming that all fatty acids and glycerides were entirely removed during the Kraft pulping process and no contamination occurred during sample preparation, the presence of the C4 class of carbon atoms can be attributed to acetyl groups of hemicelluloses content (Jaic *et al.*, 1996). On the other hand, the low O/C atomic ratio, the significant contribution of C1, and the presence of the C4 class, which were mainly observed in bark fibers, indicate that extractives such as fatty acids and resinic acids govern surface composition.

Theoretically, the atomic ratio of oxygen to carbon in pure carbohydrates (cellulose + hemicelluloses) is 0.83 and without C1 class components , while the O/C atomic ratio

and C1 contribution of the resinic acids, namely abietic acid, are 0.10 and 0.95, respectively (Dorris and Gray, 1978ab; Hua *et al.*, 1993). Assuming that the weight percentage of carbohydrates can be estimated according to their O/C ratio and that extractives content can be related to C1 content, then the theoretical O/C atomic value of pure cellulose and the theoretical C1 contribution in abietic acid was normalized to 100 % as the maximum of carbohydrates and the maximum of extractives, respectively. Hence, a ternary diagram is used to represent the relative percentage of the three components (polysaccharides, lignin, and extractives) of all surface fibers (Figure 4.7).

As expected, Figure 4.7 indicates that the bleached Kraft fiber surface is similar to that of pure cellulose. In fact, bleached Kraft contains 87 % cellulose, 13 % lignin, and no extractives. The fiber surface of jack pine has more carbohydrates and less lignin than eastern white cedar and black spruce. Increasing exposure for carbohydrates means more exposure for hydroxyl groups on the fiber surface, thereby facilitating the formation of ester bonding between fibers and coupling agents during esterification (Figure 4.1). Eastern white cedar and black spruce fibers show approximately the same surface composition, with 34 % carbohydrates, 63 % lignin, and 3 % extractives. However, bark fibers present the most lignin-like exposed surface, with higher content of lignin (73 %) and extractives (5 %). Compared to other mechanical fibers, Hua et al. (1993) reported higher lignin content in CMP and CTMP surfaces, ranging from 50 % to 70 %.

Table 4.2 also presents the O/C atomic ratio and the various peak components of the carbon spectra (C1, C2, C3, and C4) for the treated fiber surfaces, while the curve fitting of the C1 high resolution spectra for untreated and maleic polyethylene treated fibers are presented in Figure 4.8.

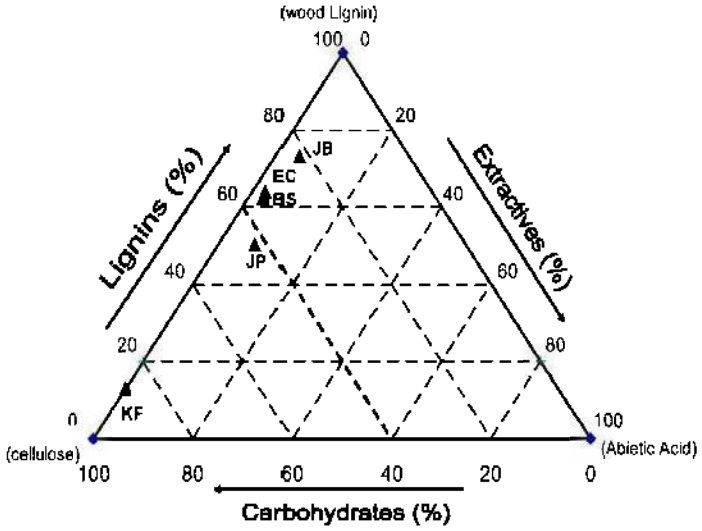

Figure 4.7. Ternary diagram of the surface component fraction of the used fibers (KF: bleached Kraft fiber; JP: jack pine; BS: black spruce; EC: eastern white cedar; JB: jack pine bark).

As expected, treatment of bleached Kraft fibers with MAPE caused a substantial increase in carbon type C1 (C–C and/or C–H) concentration, and consequently a drastic decrease in the O/C atomic ratio (Table 4.2 and Figure 4.8-a). The increased contribution of carbon type C1 and the decrease in O/C atomic ratio following the MAPE treatment might have stemmed from the aliphatic carbons in the MAPE polyethylene chains. This result clearly indicates an effective MAPE attachment to the Kraft fiber surface.

A detailed analysis of the chemical composition of the jack pine maleic polyethylene treated surface is shown in Figure 4.8-b. The contribution of the C1 carbon atoms, which are carbon atoms bonded to carbon or hydrogen only, rose by 31.4 % after MAPE treatment, while both the contribution of C2 carbon and the O/C atomic ratio (Table 4.2) dropped by 26.9 % and 20 %, respectively. These results indicate that unextracted jack pine fibers can react with MAPE, but at lower levels than Kraft

fibers do. The observed decrease in the contribution of the C4 carbon after treatment of the jack pine fibers can be explained by the fact that the resulting ester links are masked by long polyethylene chains, so that they are not readily detected by XPS, which has a probing depth of about 5 nm (Kazayawoko *et al.*, 1999b). It could also be explained by the greater removal of the lipohilic components from the surface during MAPE grafting conducted in a reactor in the presence of an apolair solvent (xylene). In contrast to Kraft and jack pine fibers, bark fibers did not show a clear response to MAPE treatment (Figure 4.8-c). The same findings were observed for unextracted eastern white cedar and black spruce fibers. Lignin concentration variability on the wood fiber surface seems to be the major inhibitor factor for esterification. Its complex three-dimensional structure with only some available reactive hydroxyl groups largely explains its inhibition effect. Hence, based on surface lignin concentration, the fibers can be ranked by their ability to form ester bonds with MAPE as follows:

Kraft <<<<<<<<jack pine <<<black spruce < eastern white cedar <<<< bark

4.5.3 SEM investigations

To corroborate the previous findings, SEM images of the MAPE modified jack pine and bark fiber surfaces are shown in Figure 4.9. For treated jack pine fibers, surfaces appear to be covered by polyethylene. Fiber ends and defibrillated zones are tightly covered by polyethylene. This can be explained by the S2 exposed layer, which is rich in celluloses and hemicelluloses. However, the bark fiber surfaces are fairly clean, i.e. there is little plastic sticking to the bark fiber surfaces. Taken together, these images are in perfect agreement with the XPS analysis. These results partially explain why interfacial adhesion, and consequently the mechanical properties, of wood plastic composites is better for jack pine fibers than for lignin-like surface fibers (bark, eastern white cedar, and black spruce).

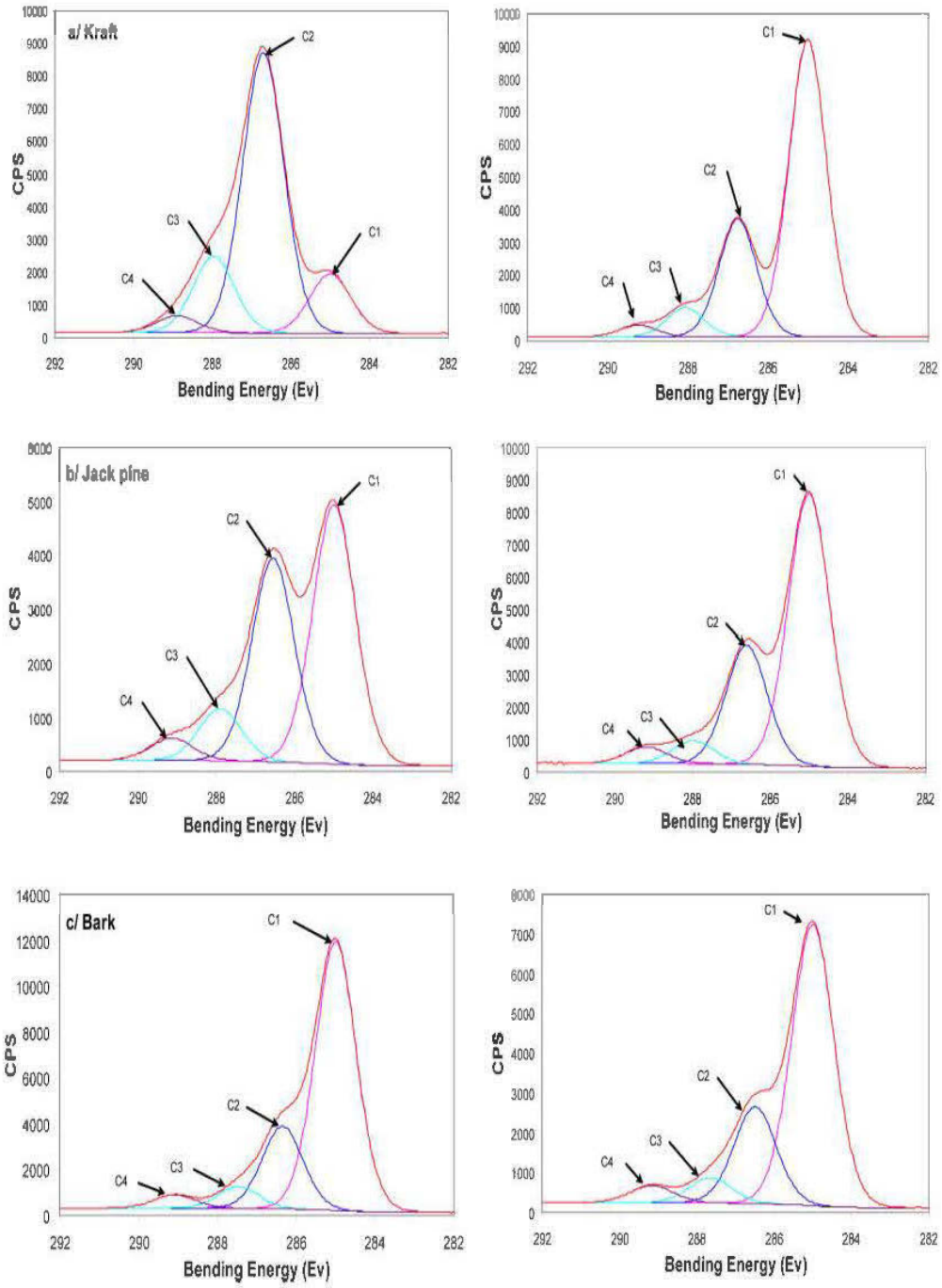

Figure 4.8. C1s high resolution spectra of untreated (left) and maleic polyethylene treated wood fibers (right).

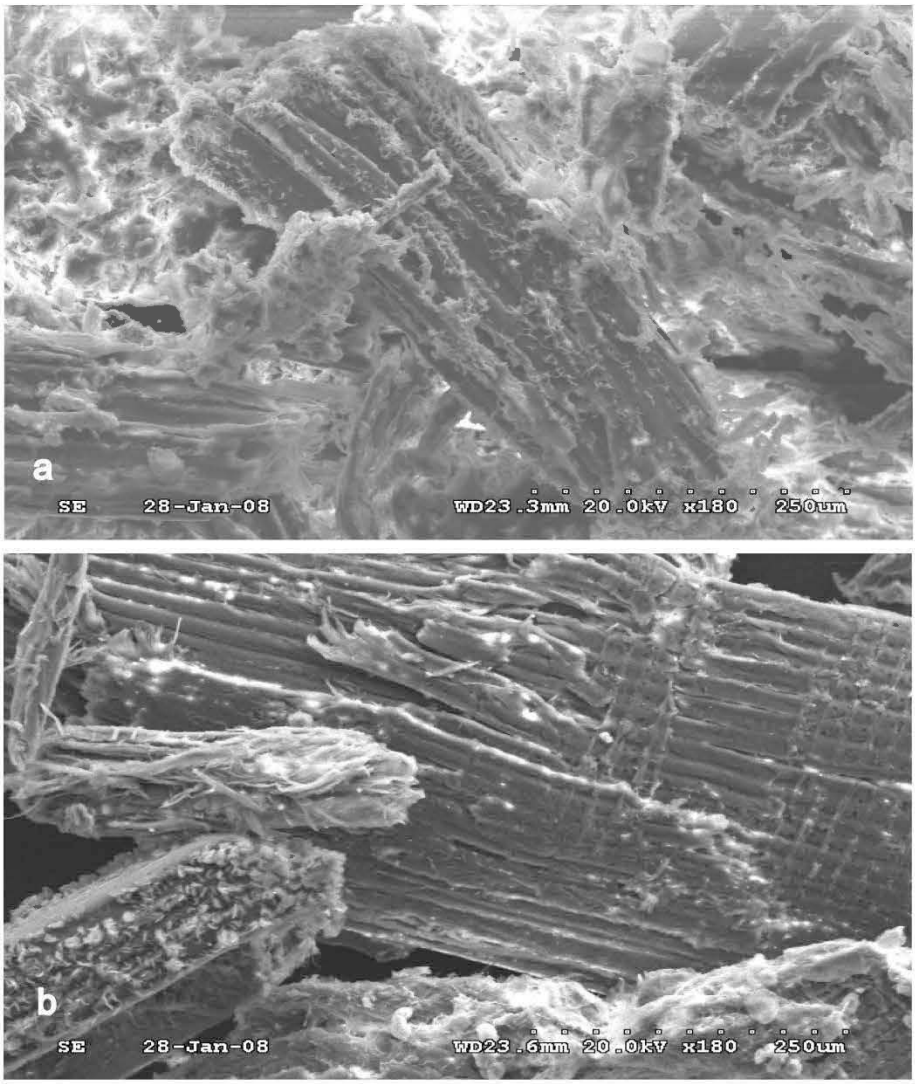

Figure 4.9. SEM images of MAPE treated jack pine wood fiber (a) and jack pine bark fiber (b).

4.6 Conclusion

DRIFTS and XPS were performed to study between-species variability in the chemical composition of wood fiber surfaces. The effect of this variability on the efficiency of the esterification reaction was also examined. Although DRIFTS was successfully used to characterize the chemical composition of the fiber surfaces, it failed to confirm esterification between unextracted wood particles and maleic polyethylene. XPS, which is a highly surface sensitive technique (10–50 Å), was more effective in detecting chemical changes in wood fiber surfaces following MAPE treatment. XPS results were confirmed by SEM imaging. Lignin concentration variability on the fiber surface was found to be the major inhibitor factor for esterification. Jack pine fibers showed the greatest ability to form ester bonds with MAPE due to much lower surface lignin concentration. Bark fibers did not show a clear response to the MAPE treatment, using either DRIFTS or XPS.

Consequently, one of the important considerations in choosing coupling treatments is the type of wood fiber. Once the fiber surface has been clearly characterized, the concentration and chemical structure of coupling agents should be selected, as mentioned earlier.

CHAPTER V

THERMAL SENSITIVITY AND NUCLEATING ABILITY OF WOOD PARTICLES*

5.1 Abstract

Thermal sensitivity, nucleating ability and non-isothermal crystallization of HDPE with different wood fillers were investigated using thermogravimetric analysis and differential scanning calorimetry. Results show that wood degrades at a lower temperature than HDPE. Thermal decomposition behavior was similar across wood species. The most remarkable dissimilarities were observed between wood and bark, in the decomposition rate at processing temperature around 300°C and the peak temperature location for cellulose degradation. The higher degradation rate for bark is explained by the devolatilization of extractives and the degradation of lignin, which are present in higher amount in pine bark. Nucleating ability for various wood fillers was evaluated by crystalline weight fraction, crystal conversion, half-time crystallization and crystallization temperature of the HDPE matrix. Nucleation activity improved with the addition of wood particles to the HDPE matrix. However, no effect of wood species on crystal conversion was found.

---

*

Reprinted in part with permission from Bouafif, H., A. Koubaa, P. Perré, A. Cloutier, and B. Riedl. 2009. "Wood Particle/Composites: Thermal Sensitivity and Nucleating Ability of Wood Particles." J. Appl poly Sci. 113:593-600.

5.2 Résumé

La sensibilité thermique, la capacité de nucléation et la cristallisation non-isotherme du polyéthylène haute densité (PEHD), pour différentes charges de bois, ont été étudiées par analyse thermogravimétrique et par calorimétrie différentielle à balayage. Les résultats ont montré que le bois se dégrade à une température nettement inférieure à celle du PEHD. La cinétique de la décomposition thermique était similaire entre les essences de bois. Les différences les plus remarquables ont été observées entre le bois et l'écorce aux alentours de la température de 300°C qui correspond à la température de dégradation de la cellulose. Le taux élevé de la dégradation de l'écorce est expliqué par le dégazage de matières extractibles et la dégradation de la lignine, qui sont présent en grande quantité dans l'écorce de pin gris. La capacité de nucléation, à différents taux de charges en fibres de bois, a été évaluée grâce à la variation de la fraction cristalline, au taux de conversion en cristal, au demi-temps de conversion et à la température de cristallisation du PEHD. La nucléation a été améliorée avec l'ajout de particules de bois à la matrice du PEHD. Cependant, aucun effet de l'essence de bois sur le taux de conversion en cristal n'a été trouvé.

5.3 Introduction

A common and key limitation to the use of natural fibres in composites is thermal degradation. Knowledge of the appropriate and/or maximum processing temperature is therefore critical for the development of thermosetting and thermoplastic composites. It is known that thermal treatment leads to a variety of physical (Placet *et al.*, 2008) and chemical (Chow, 1971; Hillis, 1984; Tjeerdsma and Militz, 2005; Nguila Inari *et al.*, 2006) changes in wood. Christiansen (1990) reported that overdrying wood reduces bonding to phenol-formaldehyde adhesives. He described three inactivation mechanisms involving physical responses to overdrying: 1)

exudation of extractives to the surface, which lowers wettability by coating the surface; 2) reorientation of wood surface molecules, which reduces wettability, or bonding sites; and 3) irreversible closure of large micropores in cell walls. Sĕrnek et al (2004) attributed surface inactivation to the concentration of non-polar substances, hydrophobic extractives and volatile organic compounds on wood surfaces during the drying process at temperatures above 160°C.

Various analytical methods can be used to assess thermal degradation of wood. Thermogravimetric analysis (TGA) and differential scanning calorimetry (DSC) are two useful methods. Thermal stability is difficult to assess due to the composite nature of wood, which is a mixture of hemicelluloses, cellulose and lignin. Wood also contains extractives, which play a determinant role in the development of wood properties, despite their small content. Thermal degradation of natural fibres can be described as a two-stage process: the first in the temperature range 220–280°C and a second in the range 280–300°C. Hemicelluloses degrade in the low temperature range and cellulose degrades in the high-temperature range (Ramiah, 1970; Müller-Hagedorn *et al.*, 2003; Rath *et al.*, 2003). Ramiah (1970) studied thermal degradation in different cellulose, hemicelluloses and lignin samples. Results calculated from static and dynamic thermogravimetric analysis indicated that the activation energy for thermal degradation for the three components was in the range of 151–251, 63–109 and 54–80 kJ/mole, respectively. Orfão et al. (1999) investigated the thermogravimetric behavior of cellulose, xylan and lignin in inert and oxidizing atmosphere. They concluded that cellulose decomposition rates become measurable at about 225°C in both air and nitrogen, while xylan began decomposing at lower temperatures (160°C). However, fractions corresponding to the low-temperature decomposition of cellulose and hemicelluloses were essentially the same in both gases, at 0.80 and 0.71, respectively. Of the three wood components, lignin begins decomposing at the lowest temperature (110°C). Nevertheless, pyrolysis occurs in an extensive temperature range (up to almost 900°C), at relatively low rates (Ramiah,

1970; Orfão *et al.*, 1999). Similar behavior was reported by Mészàros *et al* (2004) but in the temperature range of 200–600°C. Moreover, the weight-loss profile of lignin depends on the isolation method, the initial degree of condensation (Gardner *et al.*, 1985) and wood species (Faix *et al.*, 1988). Fenner and Lephardt (1981) applied Fourier transform infrared evolved gas analysis (FTIR-EGA) to analyze the volatile compounds formed during thermal decomposition of Kraft pine lignin. They established a number of degradation schemes involving various side reactions. Briefly, they noted that the initial degradation of Kraft lignin occurred from 120 to 300°C from bond fragmentation in the phenyl propane side chains, evidenced by the formation of formic acid, formaldehyde, carbon dioxide, water and sulphur dioxide. The presence of sulphur dioxide supports the argument that sulphur from the Kraft pulping process were incorporated into the lignin structure in the form of sulphoxide and/or sulphone linkages. They observed that 50% of the initial weight was lost in the temperature range 300°C to 480°C at a heating rate of 6 °C/min. Methanol, 2-methoxyphenol (gauiacol), and 2-methoxy-4-alkyl-substituted phenol were the most apparent components evolving in this region, indicating fragmentation of the major chain linkages between the monomeric phenol units in the lignin structure.

Fairbridge *et al* (1975) studied the thermogravimetric behavior of jack pine bark degradation. They noted that the major weight loss began at 180°C. It reached 70 % of the initial sample weight. Inorganic ions are known to greatly influence the thermal degradation of polysaccharides (DeGroot and Shafizadeh, 1984) as well as lignin (Jakab *et al.*, 1993). Mészàros *et al* (2004) associated differences in thermal degradation behavior between wood and bark to chemical composition in terms of inorganic ion content. Because bark has significantly higher mineral matter content than wood, bark pyrolysis showed the lowest decomposition temperature.

Fibre degradation during processing may adversely affect the mechanical properties of composites for two main reasons: (i) it changes the fibre structure, adversely

affecting the mechanical properties, namely its resilience; and (ii) volatile degradation products usually create microvoids across the interface that act as critical flaws and lead to extensive debonding and failure of the material under service (Nabi Saheb and Jog, 2000). In addition, natural fibre degradation generally affects the organoleptic properties of wood-based composites, such as odour and color (Nabi Saheb and Jog, 1999; Wang *et al.*, 2001). Gonzalez and Myers (1993) studied the effect of thermal degradation on the mechanical properties of wood/polymer composites. They observed that, although mechanical properties generally deteriorated as a result of thermal degradation of wood flour, toughness and bending strength were more affected. Wang *et al.* (2001) and Lu *et al* (2004) suggested a suitable combination of processing variables to limit thermal degradation of wood fillers. Furthermore, a short compounding time, an appropriate mixing temperature, and a moderate rotation speed improved the compounding quality of modified blends and the dynamic mechanical properties of the resultant composites (Lu *et al.*, 2004).

It is well known that the presence of a solid surface in contact with semicrystalline polymers during crystallization from the melt induces heterogeneous nucleation. The process comprises two major events: nucleation and crystal growth (Avrami, 1939; Avrami, 1940; Avrami, 1941). For composites based on semicrystalline matrix polymers, crystallinity is an important factor in determining the stiffness and fracture behavior of the crystallized matrix polymer (Joseph *et al.*, 2003). Crystallinity depends on the processing parameters, e.g. crystallinity temperature (T_c), cooling rate, nucleation density, annealing time and fibre type (Thomason and Van Rooyen, 1992; Wang and Liu, 1999). As defined by Billon *et al* (2002), transcrystallization is a nucleation-controlled process that occurs under quiescent conditions in a semicrystalline polymer in contact with other materials (e.g. fibres). At high heterogeneous nucleation ability of the surface, lateral extension is encumbered, and nucleation growth is therefore strained in one direction, i.e. perpendicular to the fibre surface (Thomason and Van Rooyen, 1992; Wang and Liu, 1999). A transcrystalline

layer (TCL) then forms at the fibre/matrix interface. Several researchers have considered that TCL formation improves the interfacial strength and mechanical properties (Zhang *et al.*, 1996; Zafeiropoulos *et al.*, 2001). However, no effect or even a negative effect on interfacial and mechanical properties has been reported in others studies (Wang and Hwang, 1996). Wang and Liu (1999), and Thomason and Van Rooyen (1992) found that transcrystallization depends on fibre type and T_c. Fibre surface micro-roughness appears to be an important factor in the morphology of the transcrystalline layer and the ability of the fibre to induce it (Zafeiropoulos *et al.*, 2001).

A variety of experimental techniques can be used to investigate the crystallization mechanism under isothermal and non-isothermal conditions. The most common are differential scanning calorimetry (DSC) and optical microscopy.

This work is part of a complete investigation of the effect of wood variability on the properties of wood-plastic composite materials. The first main objective was to assess the thermal stability of wood during HDPE melt processing. Thermal sensitivities of various wood types and species were also compared. The second objective was to determine the efficiency of wood filler as a nucleating agent using non-isothermal analysis.

5.4 Experimental

5.4.1 Materials

The five wood particle types (Eastern white cedar (*Thuya occidentalis*) particles, with sapwood particles and heartwood particle treated separately; jack pine (*Pinus banksiana*) particles divided into wood and bark particles; and black spruce (*Picea mariana*) particles) were investigated for thermal stability.

Wood particles (48–100 mesh) were compounded into pellets at 45% by weight with HDPE using co-rotating twin-screw extruder (See **chapter III** for processing conditions). The obtained pellets were used to study the crystallization behavior of the HDPE and to assess the nucleating ability of the wood filler.

5.4.2 Methods

5.4.2.1 Thermogravimetry (TGA)

A TA Instrument SDT 2960 simultaneous TG-DTA apparatus with 0.1µg weight sensitivity was used for the thermogravimetric tests. Samples were tested in a nitrogen environment. Prior to measurements, nitrogen was purged for 10 minutes to establish an inert environment. The sample mass was 15 ± 3 mg. Non-isothermal degradation was then carried out at a 10°C/min heating rate to a final temperature of 600°C.

5.4.2.2 Differential Scanning Calorimetry (DSC)

Crystallization properties were investigated using a Mettler Toledo DSC 822e differential scanning calorimeter (DSC). The thermal program used to determine melting and crystallization behavior is given in Figure 5.1. In stage I, samples were heated from room temperature to 200°C at a rate of 10°C/min under a nitrogen atmosphere and held for 10 min (stage II). In stage III, samples were cooled to room temperature at a cooling rate of 5°C/min. In stage IV, samples were reheated from room temperature to 200°C at a heating rate of 10°C/min and held for 10 min to destroy any residual nuclei (stage V). Finally, samples were cooled at a cooling rate of 5°C/min (stage VI), during which crystallization behavior of the composite materials was recorded. A typical curve for the experimental measurement of HDPE melting and crystallization is presented in Figure 5.1.

Knowing the cooling rate, temperature can be transformed into crystallization time t, and relative crystallinity or crystal conversion at time t, $\chi_c(t)$, can be calculated from the following equation:

$$\chi(t) = \frac{\int_0^t (dH_c/dt)dt}{\int_0^\infty (dH_c/dt)dt} \qquad (5.1)$$

where dH_c is the enthalpy of crystallization measured during an infinitesimal time-lapse dt. The t and ∞ limits are the elapsed time during and at the end of the crystallization process, respectively. Several parameters from the experimental measurement of DSC exotherms are defined as follows:

- t_0 and T_0 are the onset time and onset temperature of crystallization, respectively, measured at the beginning of the primary crystallization stage
- t_e and T_e are the time and the temperature required for the primary crystallization
- $\Delta t = t_e - t_0$, or the broadness of the transition.

Crystallization half-time $t_{1/2}$, or the time required to convert 50% of the crystallizable material, was obtained by plotting $\chi_c(t)$ against (t).

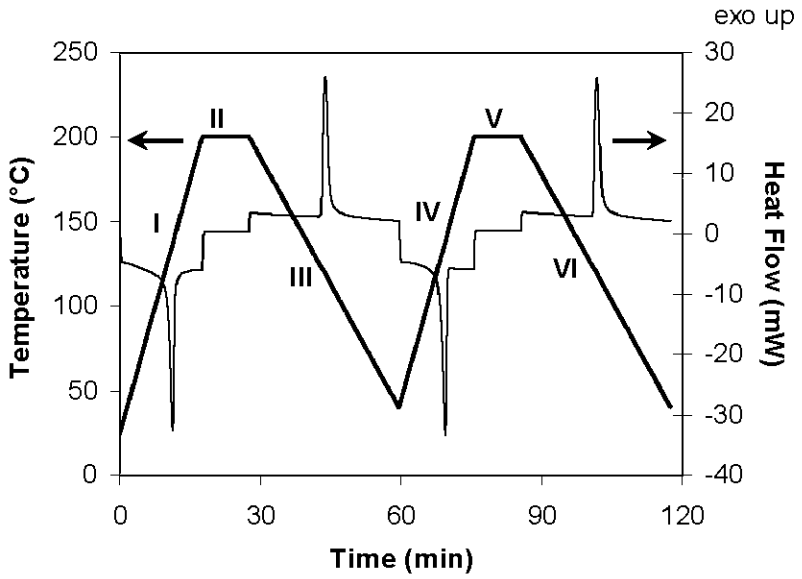

Figure 5.1. Thermal program and typical curve of an experimental measurement of neat HDPE melting and crystallization.

5.5 Results and Discussion

5.5.1 Analysis of thermal sensitivity

Weight loss in % and time derivative of the weight (DTG) in inert atmosphere are reported in Figure 5.2 as functions of temperature for the wood and polymer matrix (HDPE). Consistent with previous findings (Gonzalez and Myers, 1993; Wielage *et al.*, 1999), wood decomposes at lower temperatures than HDPE. The initial weight loss is due to water loss occurring from 60 to 110°C. The thermal decomposition of HDPE can be described by a single-step reaction occurring at 420°C. This simple thermal behavior can be explained by the very homogeneous structure of the thermoplastic, which decomposes in ethylene monomers. On the other hand, wood decomposition curves show two main reaction zones corresponding to (i) devolatilization of materials, with maximum devolatilization rate at about 330–360°C; and (ii) decomposition of the produced char, characterized by lower rates. This late

aspect will not be considered here because our main objective was to clarify the thermal stability of wood fillers during melt processing of wood-plastic composites. A clear distinction between these two reaction zones was not possible for bark, most likely owing to slower decomposition rates over a broader temperature range of the main components (extractives and lignin). In addition, the main DTG peak corresponds to cellulose decomposition, while the shoulder at lower temperature (around 300°C) can be attributed mainly to hemicelluloses decomposition (Mészéros *et al.*, 2004). Lignin decomposes at a lower rate in a wide temperature range (200–600°C) (Jakab *et al.*, 1997).

Because the temperature intervals of component decomposition partially overlap, the DTG curves were deconvoluted into four partial curves by approximating the experimental curve with mixed Lorentzian/Gaussian lineshapes corresponding to the degradation of extractives, hemicelluloses, celluloses and lignin. Corresponding peaks for each region were taken from the literature. Degradation rate characteristics of each component were respected when defining fitting parameters. For example, lignin starts decomposing at the lowest temperature (110°C) and degrades over an extensive temperature range (up to almost 600°C) at relatively low rates (Ramiah, 1970). It was therefore expected that the full width at half maximum (FWHM) would be very large.

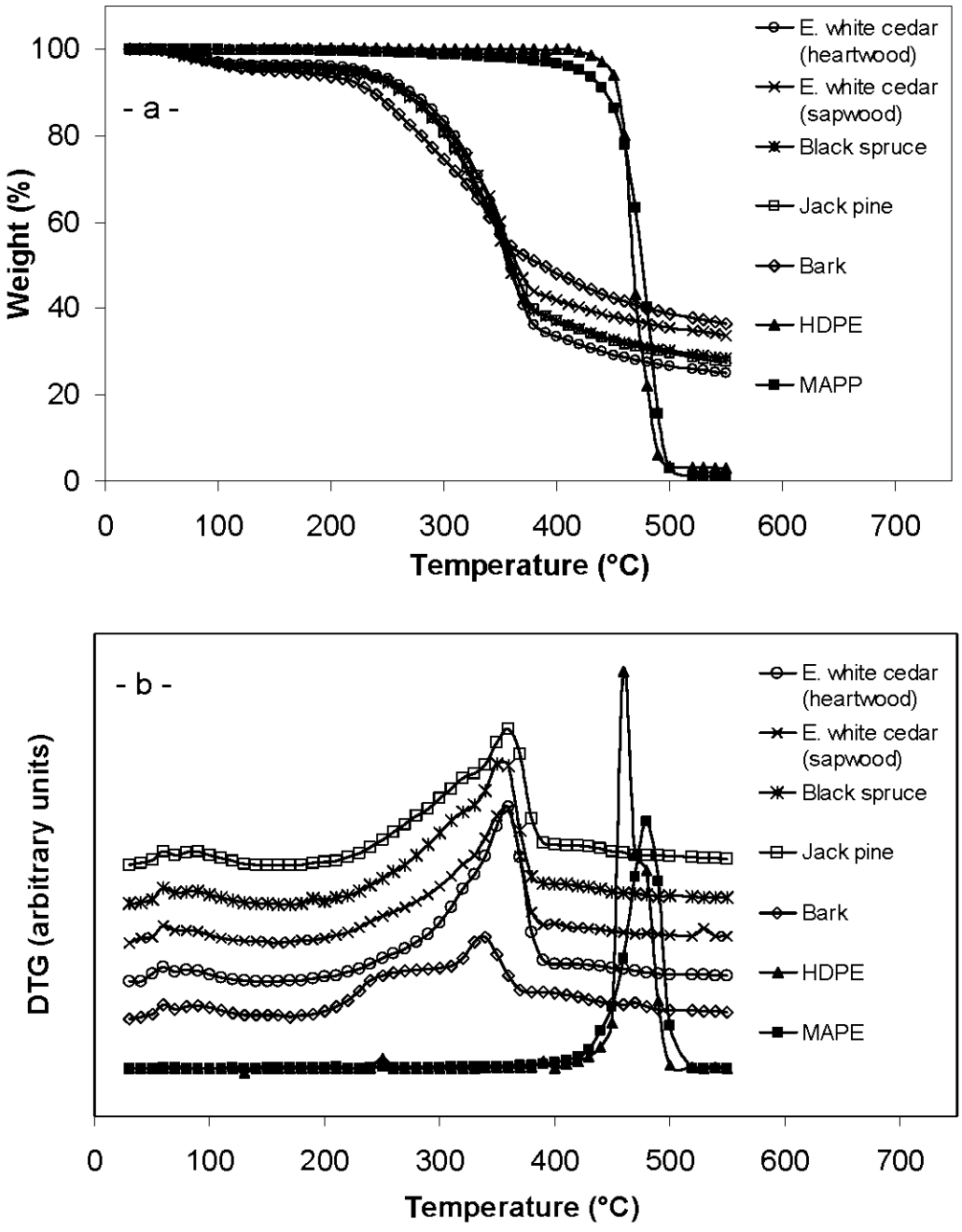

Figure 5.2. Weight loss (a) and time derivative of the weight, DTG (b) in nitrogen environment for different wood species and bark.

Examples of DTG deconvolution of jack pine wood and bark are shown in Figure 5.3, while Table 5.1 summarizes the main characteristic parameters of the regions obtained for the various fillers: the start of extractives, hemicelluloses, celluloses and lignin decomposition were associated with $T_e onset$, $T_h onset$, $T_c onset$, and $T_l onset$, respectively, while *Toffset* designates the end of the decomposition process for each component. Temperature at the peak is indicated by *Tpeak*.

Decomposition is very similar across wood species, and the most remarkable feature is the dissimilarity in DTG characteristics between wood and bark, i.e. decomposition rate around 200°C and location of peak cellulose decomposition. It is noteworthy that bark decomposition not only starts at a lower temperature, but also proceeds at a higher rate. This higher bark decomposition rate can be explained by the devolatilization of extractives and the degradation of lignin, both of which are present in larger content in pine bark. Because these compounds are a mixture of a variety of chemical components, they thermally degrade over a large range of temperatures. Furthermore, bark contains a large amount of highly volatile compounds, including alcohols, simple phenolics, fatty acids and furans, which are characterized by a higher kinetic devolatilization rate at lower temperature ranges (Shafizadeh, 1981; Branca *et al.*, 2006). Other findings support that differences in thermal degradation behavior between wood and bark can be attributed to chemical composition in terms of inorganic ion content (Hosoya *et al.*, 2007). Because bark has significantly higher mineral matter content than wood, bark pyrolysis shows the lowest decomposition temperature (Mészéros *et al.*, 2004). Branca *et al* (2006) confirmed that kinetic degradation of biomaterials depends on the presence of high-molecular-weight components. Hence, an absolute maximum of degradation at high temperatures cannot be achieved with extractives that are less polymerized than cellulose.

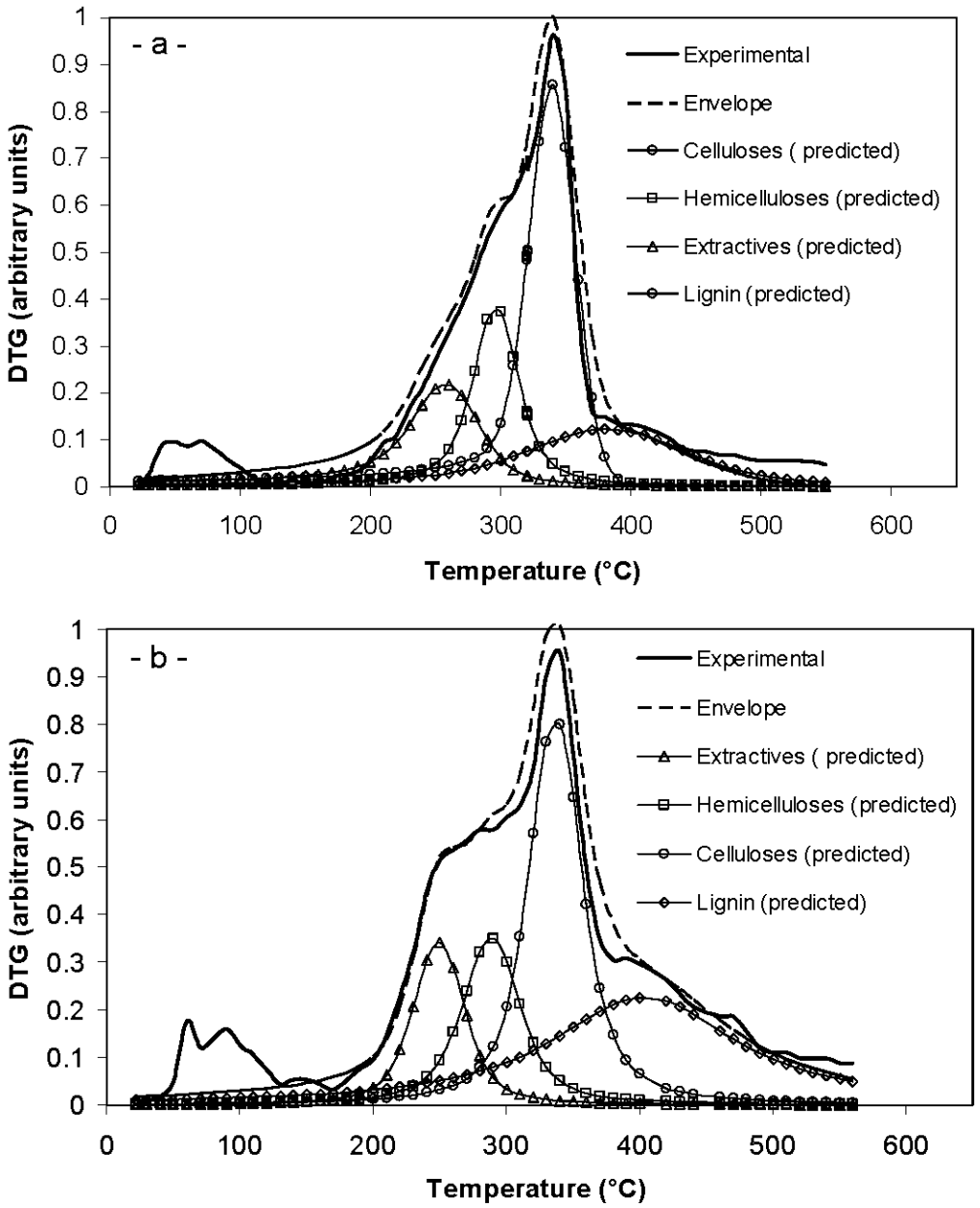

Figure 5.3. Global and component decomposition rates for jack pine wood (a) and bark (b) for a heating rate of 10°C/min as measured and predicted by a mixed Lorentzian/Gaussian model.

Although DTG peak maximums are in agreement with previous findings, the start of hemicelluloses decomposition (onset temperature) and the end of cellulose decomposition (offset temperature) show dissimilarities, mainly due to the deconvolution method. Mészàros *et al* (2004) determined the onset temperature of hemicelluloses decomposition and the offset temperature of cellulose decomposition by extrapolation of the DTG curves. However, their method would be inappropriate in the current study because in most cases, hemicelluloses sub-peaks are overlapped by cellulose decomposition.

5.5.2 Crystallinity and nucleating ability analysis

Crystallization parameters obtained from DSC exotherms are summarized in Table 5.2. The values of the crystalline weight fraction χ_c were obtained using the following relationship:

$$\chi_c(\%) = \frac{\Delta H_f}{\Delta H_f^0} \times \frac{100}{w} \qquad (5.2)$$

where ΔH_f and ΔH_f^0 are the enthalpy of fusion (DSC endotherm) of the samples and the enthalpy of 100% crystalline HDPE, respectively, and w is the mass fraction of HDPE in the composite. DSC analysis of pure HDPE gives a relatively high crystallinity (217.69 J g^{-1} or 75.59 % crystallinity if the enthalpy of 100% crystalline polyethylene is taken as 288 J g^{-1} (Wunderlich, 1973)). Figure 5.4 depicts the crystallization exotherms of HDPE and its various blends at cooling rates of 5°C/min. It is known that the overall crystallization process of a semicrystal polymer is usually divided into two main phases: primary and secondary crystallization. Primary crystallization is the macroscopic expansion of the degree of crystallinity as a result of two consecutive microscopic mechanisms: nucleation and subsequent crystal

growth. Secondary crystallization mainly involves the crystallization of lateral and interfibrillar chains.

Table 5.1. Thermal decomposition parameters for wood components.

Component	Temperature (°C)	Eastern white cedar (sapwood)	Eastern white cedar (heartwood)	Jack pine	Black spruce	Bark (jack pine)
Extractives	T_e *onset*	174	178	171	168	183
	T_e *peak*	254	251	260	254	250
	T_e *offset*	348	351	350	346	340
Hemicelluloses	T_h *onset*	198	201	196	196	200
	T_h *peak*	291	293	298	302	292
	T_h *offset*	382	384	382	386	390
Celluloses	T_c *onset*	281	282	284	278	255
	T_c *peak*	363	361	360	362	338
	T_c *offset*	428	430	423	431	470
Lignin	T_l *onset*	115	115	112	110	115
	T_l *peak*	397	392	391	394	407
	T_l *offset*	> 600	> 600	> 600	> 600	> 600
Decomposition rate around 200°C (%/min)		0.25	0.22	0.21	0.18	0.46

As depicted in Figure 5.4, all obtained exotherms show a dominant sharp exothermic peak at higher temperatures, followed by a shallow tail at lower temperatures. From Figure 5.4 and Table 5.2, the addition of wood particles to HDPE results in an increase in T_c and χ_c of the HDPE matrix. This is due to the nucleating ability of wood particles in the crystallization of HDPE. In fact, during non-isothermal crystallization, the heterogeneous nucleation activity of wood shifts the DSC

exothermic peak towards higher temperature, depending on wood particle type. The highest increase in crystallization temperature (≈ 6°C) is found with the HDPE/black spruce wood particle composites, compared to neat HDPE, and the lowest increase is observed with HDPE/jack pine composites. Consequently, it can be argued that wood particles act as heterogeneous nucleation agents for HDPE. Moreover, Table 5.2 shows that the crystallinity of pure HDPE is slightly increased by the addition of wood particles.

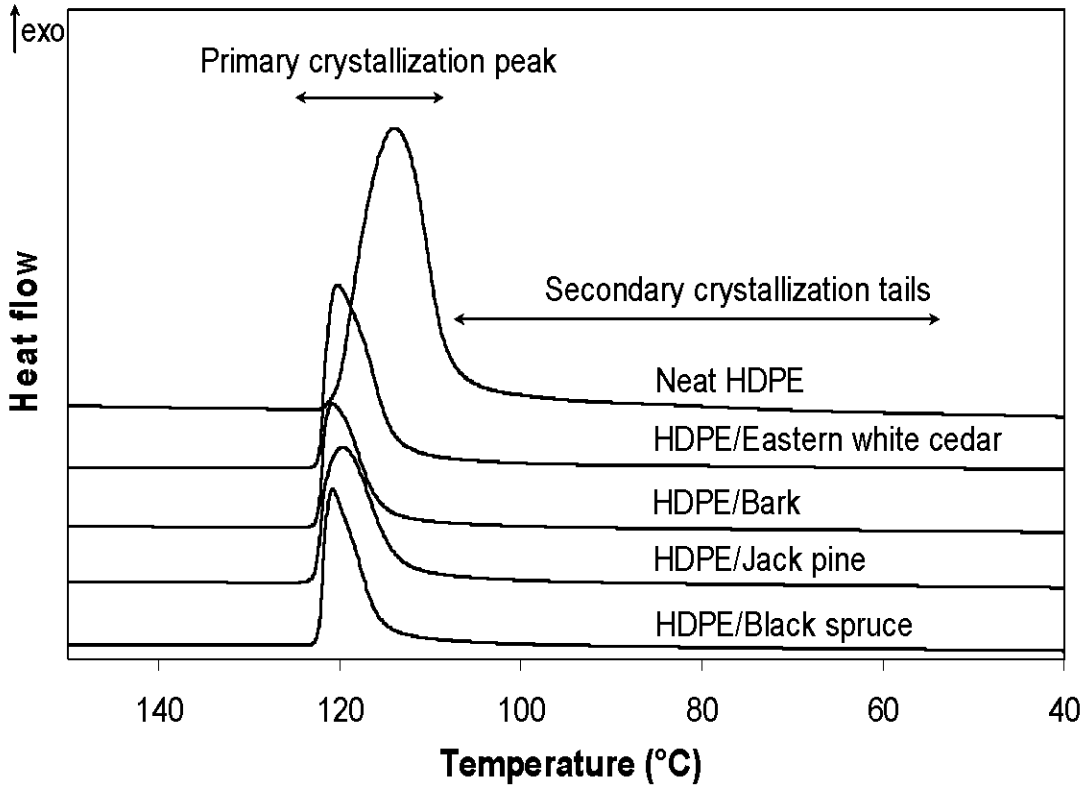

Figure 5.4. Crystallization exotherms of HDPE and its blends at cooling rates of 5°C/min.

The highest crystallinity is obtained with HDPE/jack pine composites (77.4 %). However, the effect is not clear when bark particles are added. Similar findings have been reported by many researchers. Joseph *et al* (2003) observed an increase in

crystallization temperature and crystallinity after the addition of sisal fibres to a polypropylene (PP) matrix. Recently, Borysiak (2007) reported a strong increase in crystallization temperature (5–9°C) when pine or beech wood fibres were added to the polypropylene matrix. Furthermore, it was reported that T_c and crystallinity of the polymer phase is further increased by filler content (Joseph *et al.*, 1999).

Overall crystallization time (Δt_c) of HDPE decreased with the addition of wood particles, from 2.08 min for neat HDPE to 1.65 minutes for HDPE/jack pine particles, and reached 1.4 minutes when black spruce particles were added.

Table 5.2. Non-isothermal parameters for HDPE and various wood particle/HDPE composites determined from DSC exotherms.

Crystallization parameter	Neat HDPE	HDPE/Jack pine	HDPE/ Black spruce	HDPE/Eastern white cedar	HDPE/ Bark
T_0 (°C)	119.60	122.73	122.19	122.05	122.32
t_0 (min)	6,27	5.47	5.64	5.68	5.57
T_c (°C)	115.70	119.63	121.01	120.61	120.87
t_c (min)	6.94	6.26	5.97	6.05	6.22
T_e (°C)	108.27	113.69	115.13	113.87	115.06
t_e (min)	8.35	7.12	7.04	7.27	7.05
Δt_c (min)	2.08	1.65	1.4	1.59	1.48
$T_{1/2}$ (°C)	112.49	117.80	118.75	118.09	118.57
$t_{1/2}$ (min)	7.53	6.6	6.45	6.47	6.55
χ_c(%)	75.59	77.36	76.15	75.97	74.60

The presence of wood particles affected not only the degree of HDPE crystallinity, but also the crystal conversion kinetics. Figure 5.5 shows the variation in measured crystal conversion of HDPE with various wood fillers. It can be seen that all crystal conversion curves have a similar sigmoidal shape. The curvature tails in the upper part of the plot are due to the secondary phase of the crystallization process.

Differences in the crystal conversion kinetics between pure HDPE and its blends are evident during the primary stage of the crystallization process only: crystal conversion increases for HDPE filled with wood particles. This can also be explained by the nucleating ability of wood particles. However, the wood particles used showed a similar effect on crystal conversion, and differences in crystal conversion values were insufficient to allow adequate discrimination between composites.

Half-time ($t_{1/2}$) crystallization of HDPE, a useful parameter to compare the nucleating ability of wood fillers, decreases compared to pure HDPE (Table 5.2). Decline in $t_{1/2}$ has been estimated at around one minute, depending on wood type. Borysiak (2007) concluded that the lower the $t_{1/2}$ values, the higher the nucleating efficiency.

In summary, it can be concluded that nucleation ability improved when wood particles were added to the HDPE matrix. Nucleating efficiency of the filler is considered a critical factor in polymer processing. Composite materials with high nucleating ability shorten the injection moulding time (Borysiak, 2007). Although previous findings are generally in good agreement with our results, a few reports differ. Mucha and Krolikowski (2004) compared the nucleating efficiency of various organic (wood flour, chitosan) and inorganic (carbon black, nano clay particles) fillers in isotactic polypropylene (iPP). They concluded that the presence of chitosan or wood flour hinders the diffusion of iPP macromolecules in the crystallization process and disrupts the creation of the iPP spherulitic structure. Consequently, further investigations are needed to clarify the role of wood surface chemistry on the nucleation activity and crystallization kinetics of polymers. Moreover, it is widely known that polymer nucleation in the presence of substrates is not straightforward; it requires a thorough knowledge of the chemical composition and topography of the surface filler. Mathew *et al.* (2006) examined how size, chemical composition and surface topography of cellulosic materials (microcrystalline cellulose, cellulose fibres and wood flour) affect Polylactic Acid crystallization. Using differential scanning

calorimetry and optical microscopy, they found that microcrystalline cellulose and wood flour had better nucleating ability than cellulose fibres. On the other hand, Borysiak and Doczekalska (2006) reported that the crystal conversion of iPP was highly altered by chemical treatment of the filler surface, with potential consequences for the wood's nucleation ability. Their observations indicated that improved interaction between pine wood and polymeric matrix caused a decrease in the nucleation properties of fillers and iPP crystallization.

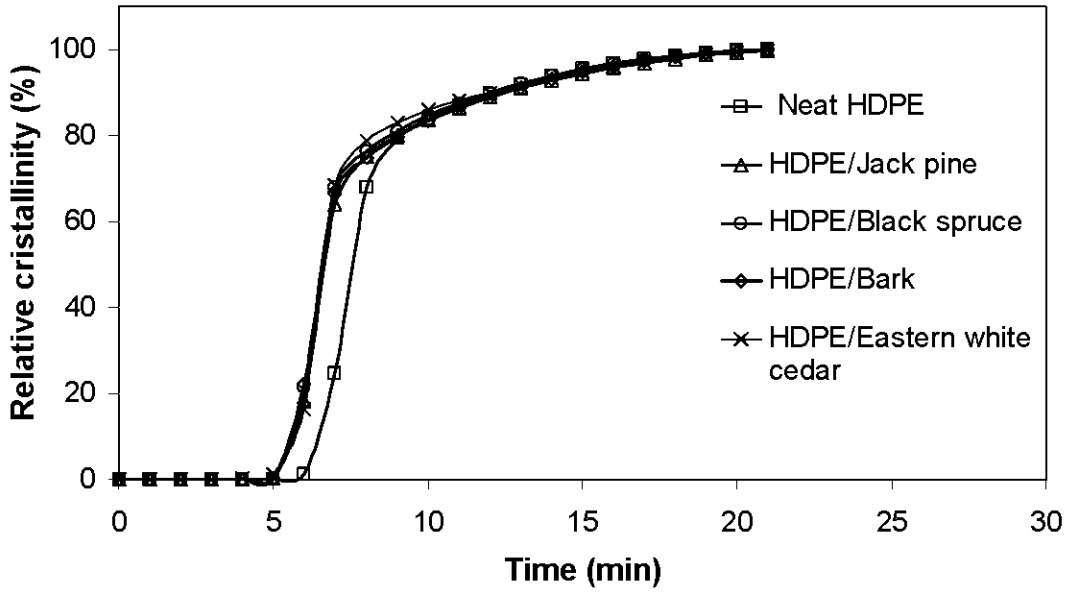

Figure 5.5. Relative crystal conversion of HDPE polymer and its corresponding blends

5.6 Conclusion

The main devolatilization stage of wood fillers occurred at lower temperatures than that of HDPE. Compared to wood, bark decomposition began at a lower temperature and processed at a higher rate. Dissimilarities between wood and bark thermal decomposition were attributed to higher extractives, lignin and inorganic ion contents.

Consequently, the HDPE melt process influenced bark filler decomposition more than wood filler decomposition.

Nucleating activity for various wood fillers was evaluated by the crystalline weight fraction χ_c crystal conversion, half-time of crystallization and crystallization temperature of the HDPE matrix. Nucleation ability was improved by the addition of wood particles to the HDPE matrix. Wood particles showed only a slight effect on crystal conversion, and differences in crystal conversion were insufficient to adequately discriminate between composites. Further investigations are recommended to clarify the role of wood surface chemistry on polymer nucleation and crystallization kinetics.

CHAPTER VI

EFFECTS OF FIBER CHARACTERISTICS ON PHYSICAL AND MECHANICAL PROPERTIES OF WOOD PLASTIC COMPOSITES*

6.1 Abstract:

We investigated the effects of fiber variability, size, and proportion on selected mechanical and physical properties of wood plastic composites. HDPE and fibers were compounded into pellets by twin-screw extrusion and test specimens were prepared by injection molding. All tested properties vary significantly with fiber origin. Higher fiber size produces higher strength and elasticity but lower energy to break and elongation. The effect of fiber size on water uptake is minimal. Increasing fiber load improves the strength and stiffness of the composite but decreases elongation and energy to break. Water uptake increases with increasing fiber proportion.

---

*

Reprinted in part with permission from Bouafif, H., A. Koubaa, P. Perré, and A. Cloutier, "Effects of fiber characteristics on physical and mechanical properties of wood plastic composites" (2009). Composites Part A: Applied Science and Manufacturing 41:131-137

6.2 Résumé

Nous avons étudié les effets de la variabilité des fibres, de la taille et de la proportion sur les propriétés mécaniques et physiques des composites bois-plastique. Le polyéthylène haute densité (PEHD) et les fibres de bois ont été mélangés et mis en granules par extrusion bi-vis, puis des éprouvettes normalisées ont été préparées par moulage par injection. Toutes les propriétés testées varient de façon significative avec l'origine de la fibre. Une forte granulométrie des fibres donne des composites plus résistants et plus rigides, mais moins ténaces et ayant un taux d'élongation à la rupture inférieur. La granulométrie des fibres n'a pas un effet significatif sur le taux d'absorption d'eau des composites bois/plastique. L'augmentation de la charge de fibres améliore la résistance et la rigidité du composite, mais diminue l'allongement et la ténacité. La teneur en eau augmente avec l'augmentation de la charge en fibres de bois dans le mélange.

6.3 Introduction

The effective use of wood-based particles and fibers as fillers or reinforcements in thermoplastic composites requires a fundamental understanding of the structural and chemical characteristics of wood (Stokke and Gardner, 2003). English and Falk (1995) provide a comprehensive overview of the factors that affect the properties of wood-plastic composites (WPC). Although several studies have shown that fiber-polymer compatibility can be enhanced by selecting suitable coupling agents (Maldas *et al.*, 1988a; Bledzki *et al.*, 1998b), compatibility between polar wood fiber and non-polar thermoplastics remains key to extending the application limits of the resultant composites (Zadorecki and Michell, 1989). Another, frequently cited key factor in natural fiber thermoplastic composites is thermal degradation (Burgstaller, 2007). Furthermore, different wood species have different anatomical structures. These structural differences govern the use of these materials in WPC. For example, fiber

dimensions, strength, variability, and structure are important considerations. Maldas et al. (1989b) are among the few researchers who have investigated the effect of wood species on the mechanical properties of wood/thermoplastic composites. They reported that differences in morphology, density, and aspect ratios across wood species account for varying reinforcement properties in thermoplastic composites. Recently, Neagu et al. (2006) investigated the stiffness contribution of various wood fibers to composite materials. They observed a correlation between lignin content and longitudinal Young's modulus, and an optimal lignin content range for maximum fiber stiffness was recorded for softwood Kraft fibers. Several attempts have been made to correlate wood-based particles and fiber properties to WPC properties (Stark and Berger, 1997; Stark and Rowlands, 2003; Bledzki and Faruk, 2006). A high aspect ratio (length/width) is very important in fiber reinforced composites, as it indicates potential strength properties (Rowell *et al.*, 2000). Stark and Berger (1997) investigated the effects of particle size on the properties of polypropylene filled with wood flour. They concluded that melt flow index, heat deflection temperature, notched impact energy, and flexural and tensile modulus and strength increase with increasing particle size. Later, Stark and Rowlands (2003) reported that aspect ratio, rather than particle size, has the greatest effect on strength and stiffness. They suggested that particle size does not affect specific gravity.

Fiber content is an influential factor on WPC processing and properties. Zhang et al. (2007) investigated the effects of fiber content on mixing torque and rheological properties. They concluded that increased wood fiber content results in increased steady state torque and viscosity. Lu and coworkers (2005b) concluded that the mechanical properties of the resultant WPC increase only at low weight percentages of wood filler. They found that tensile and flexural strengths reach a maximum at 15 wt% and 35 wt% wood particle contents, respectively, and gradually decrease with a further increase in wood particle content. Danayadi et al. (2007) reported that, at large wood content, considerable particle aggregation takes place, leading to lower strength

due to the filler's failure to sustain the stress transferred from the polymer to the matrix.

We investigated the effects of wood species, particle size, and fiber proportion on selected physical and mechanical properties of wood particle-reinforced high-density polyethylene (HDPE).

6.4 Composite preparation

WPC were produced in a two-stage process. In the first stage, wood particles were compounded into pellets at 25%, 35%, and 45% by weight with the HDPE, using a co-rotating twin-screw extruder. In the second stage, injection WPC test specimens were produced using a reciprocating screw injection molding machine. All machine settings are shown in **Chapter III**. Specimens were made according to ASTM specifications for tensile, impact, and bending strength testing. Then, Specimens were stored in controlled conditions (50% relative humidity and 23 °C) for 40 hours prior to testing. Tensile and bending tests were performed according to ASTM D638 (2003) and ASTM D790 (2003), respectively. Energy to break is defined as the energy equivalent to the area under the stress-strain curve.

Composites were immersed in water at room temperature for two months. Specimens were weighed at regular intervals using an analytical balance and water uptake was calculated.

As mentioned earlier in Chapter III, experiments were conducted according to an incomplete factorial design. The factors are Species (5 different fibers), Size (three size classes), and Load (3 proportions). Statistical analyses were conducted using a linear univariate procedure in SPSS (5% significance).

6.5 Results and Discussion

Results of the analysis of variance (ANOVA) are shown in Table 6.1. The ANOVA shows that all mechanical properties vary significantly with fiber type, size, and proportion. Water uptake varies significantly with fiber type and proportion. The effect of fiber size on water uptake is not significant, but the interaction between fiber length and fiber proportion is highly significant. This result suggests that the effect of fiber size on water uptake is dependent on fiber proportion.

6.5.1 Effect of fiber type

The mechanical proprieties of the injected wood plastic composites vary significantly with fiber type (Table 6.1). Figures 6.1a and 6.1b illustrate the tensile and flexural modulus of elasticity and maximum strength, respectively, of wood particle-reinforced HDPE composites made with various wood types. WPC made with jack pine and black spruce particles exhibit the highest modulus of elasticity and strength, whereas bark and eastern white cedar WPC show the lowest properties. Average flexural modulus of elasticity ranges from 2.3 GPa to 2.2 GPa for jack pine and black spruce WPC, respectively, while maximum flexural strength is approximately equal (40 MPa) for both species. In other words, both modulus of elasticity and maximum strength of HDPE are enhanced at least 1.5 times when jack pine or black spruce is added.

In a previous investigation, Bouafif et al. (2008c) used the atomic concentration ratio of oxygen to carbon (O/C) on the fiber surface as an initial indication of surface oxidation (Table 6.2). The O/C atomic ratios for eastern white cedar and black spruce fibers are equal (0.28), while jack pine fibers show the most oxidized surface (0.35). Bark fibers show the lowest O/C ratio (0.18). Figure 6.2a shows close relationships between atomic O/C ratio and tensile and flexural strength. Similar tendencies are obtained for the tensile and flexural modulus of elasticity (not shown). The assumed

association of low O/C ratio with a lignin-rich surface (Bouafif *et al.*, 2008c), which prevents the formation of ester bonds between fibers and the coupling agent (MAPE), could explain the lower strength values obtained for the bark composites.

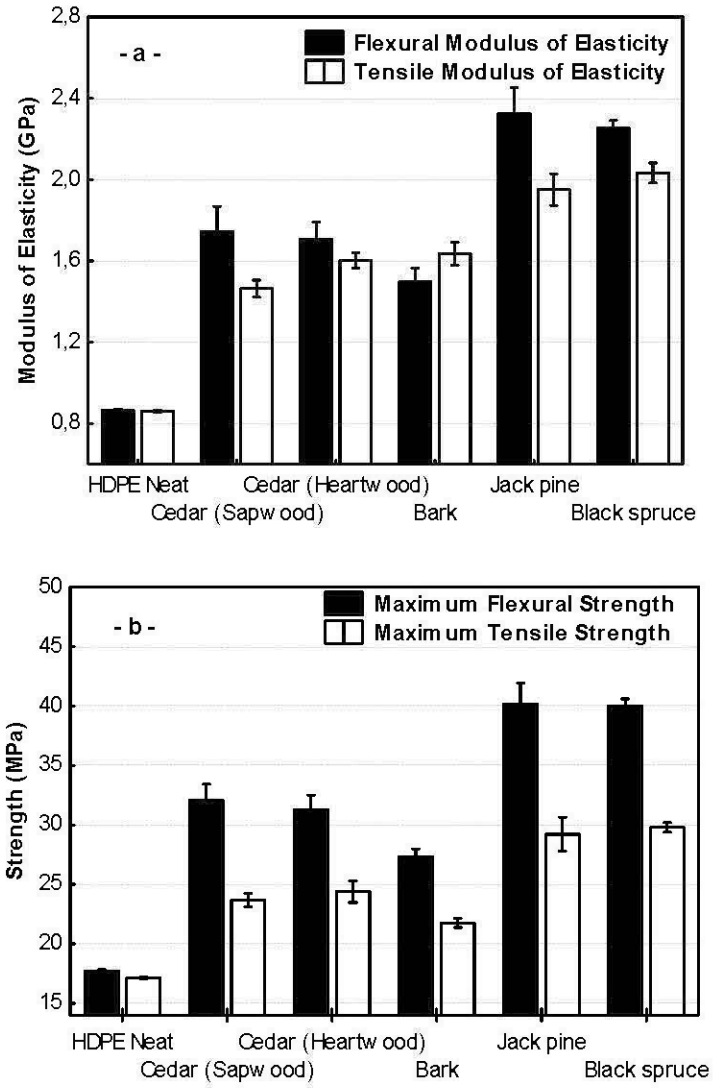

Figure 6.1. Variation in (a) tensile and flexural modulus of elasticity and maximum flexural and tensile strength for wood particle/HDPE injection-molded composites with different filler species at constant fiber load (35%) and particle size (42 mesh).

Table 6.1. Results of the analysis of variance (F values) for selected mechanical and physical properties of wood plastic composites.

	Mechanical properties							Physical properties	
	Tensile				Flexure			Water uptake	
Source	σ	MOE	ε	Energy to break	MOR	MOE	ε	48 hours	4 weeks
Model	96.1**	34.0**	310.7**	186.0**	254.3**	294.2**	201.6**	3.3**	13.3**
Fiber	300.7**	76.4**	279.1**	476.6**	631.5**	667.5**	108.9**	1.7^{ns}	7.9**
Size	224.6**	27.8**	32.1**	29.2**	496.4**	410.3**	117.0**	2.1^{ns}	0.6^{ns}
Proportion	56.7**	166.4**	2214.1**	747.3**	548.7**	1542.1**	1458.8**	17.8**	143.5**
Fiber x Size	72.6**	7.5**	252.4**	183.4**	115.7**	108.5**	116.1**	1.7^{ns}	1.3^{ns}
Fiber x Proportion	12.3**	19.2**	65.4**	22.0**	74.0**	98.7**	44.7**	4.0**	1.8^{ns}
Size x Proportion	16.7**	8.1**	20.3**	16.3**	88.2**	69.5*	4.8**	1.4^{ns}	3.3*
Fiber x Size x Proportion	34.0**	6.1**	14.8**	21.1**	38.5*	32.6**	7.4**	3.5 **	3.6**

** Significant at the 0.01 significance level, * Significant at the 0.05 significance level; ns : non significant at the 0.05 significance level.

Table 6.2. Physical and chemical properties of wood fibers.

Species	Specific gravity	Extractives (%)	Lignin (%)	Carbohydrates (%)	O/C* atomic ratio	Composite crystallinity (%)†
White cedar	0.32	*12%*	25%	67%	0.28	76.0
Jack pine	0.43	3%	27%	70%	0.35	77.4
Black spruce	0.46	3%	25%	72%	0.28	76.2
Jack pine bark	0.40	*10%*	*48%*	*42%*	*0.18*	*74.6*

*Data from Bouafif et al. (Bouafif *et al.*, 2008c)
†Data from Bouafif et al. (Bouafif et *al.*, 2009)

For composites made with semicrystalline matrix polymers, crystallinity is another important factor in determining the stiffness and fracture behavior of the crystallized matrix polymer (Joseph *et al.*, 2003). Crystallinity depends on the processing parameters, e.g., crystallinity temperature, cooling rate, nucleation density, annealing time, and fiber type (Thomason and Van Rooyen, 1992; Wang and Liu, 1999). Bouafif et al. (2009) investigated the efficiency of the same wood filler as a nucleating agent using non-isothermal analysis. Nucleating activity was determined for various wood fillers by the crystalline weight fraction of the HDPE matrix. When tensile and flexural strength were plotted against the crystalline weight fraction (Figure 6.2b), an affinity relationship was established. Other factors could also explain this difference, including the lower intrinsic fiber strength of bark fibers compared to wood fibers.

Figures 6.3a and 6.3b depict the energy to break and elongation at break, respectively, of the obtained composite materials. Composites filled with eastern white cedar sapwood and bark show brittle behavior, with 90% and 60% lower energy to break than black spruce. This result is mainly explained by poor adhesion between the

particles of some species and the HDPE matrix. Because white cedar wood and bark contain high amounts of extractives at the surface compared to jack pine and black spruce, a weak surface boundary layer can be formed, making the coupling agent less effective in forming a cross-linking network with the cellulose (Saputra *et al.*, 2004). This result is observed for bark-particle WPC, which shows the second highest elongation at break after black spruce WPC. This could be explained by the good dispersion of this particle type. Thus, some lipophilic extractives might help to disperse the particles during WPC preparation. These results agree with Maldas et al. (1989b), who reported that differences in morphology, density, and aspect ratios across wood species account for varying reinforcement in thermoplastic composites. It is therefore important to select the appropriate wood species for optimal WPC end use.

Water uptake of the injected WPC varies among the five studied fibers. Bark WPC exhibit lower water absorption compared to those made with wood particles. This result could be explained by the highly different chemical composition of bark fibers compared to wood fibers (Table 6.1). Because bark contains higher hydrophobic volume (lignin and extractives) and lower hydrophilic volume (cellulose and hemicelluloses), it would be expected to show lower water uptake compared to wood fibers (Figure 6.4). Nevertheless, high among-species variation is found in the wood-fiber WPC for water uptake. These differences could be explained by several factors, including wood chemical composition. For example, eastern white cedar heartwood has higher extractive content than its sapwood. Thus, as expected, WPC made with heartwood shows lower water uptake than WPC made with sapwood (Figure 6.4).

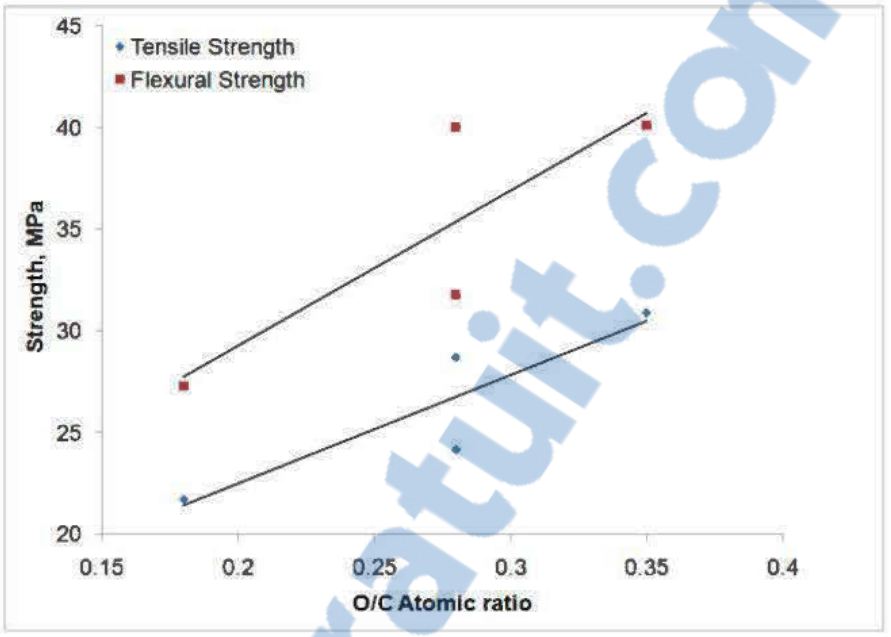

- a -

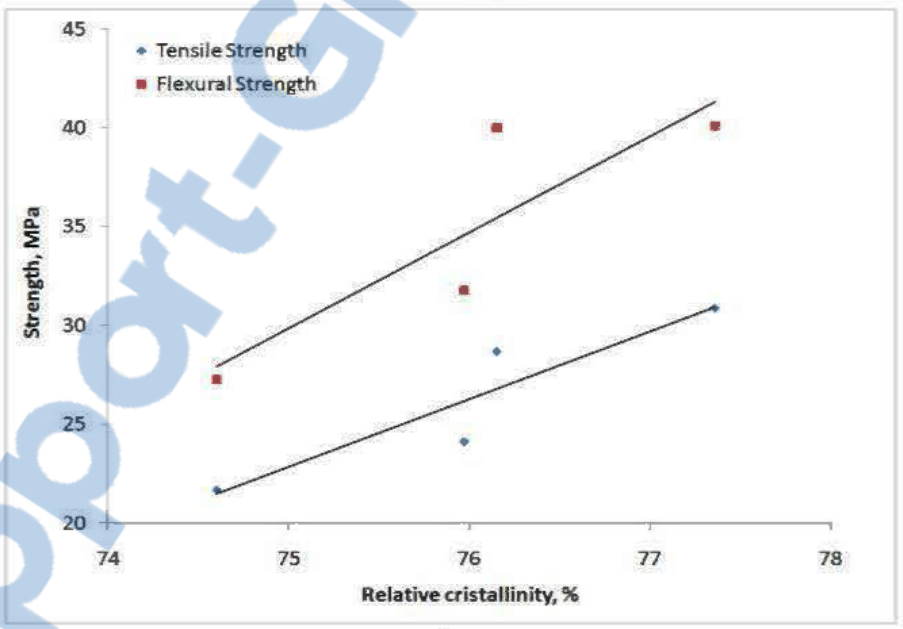

- b -

Figure 6.2. Variation in tensile and flexural strength with (a) O/C ratio and (b) relative crystallinity.

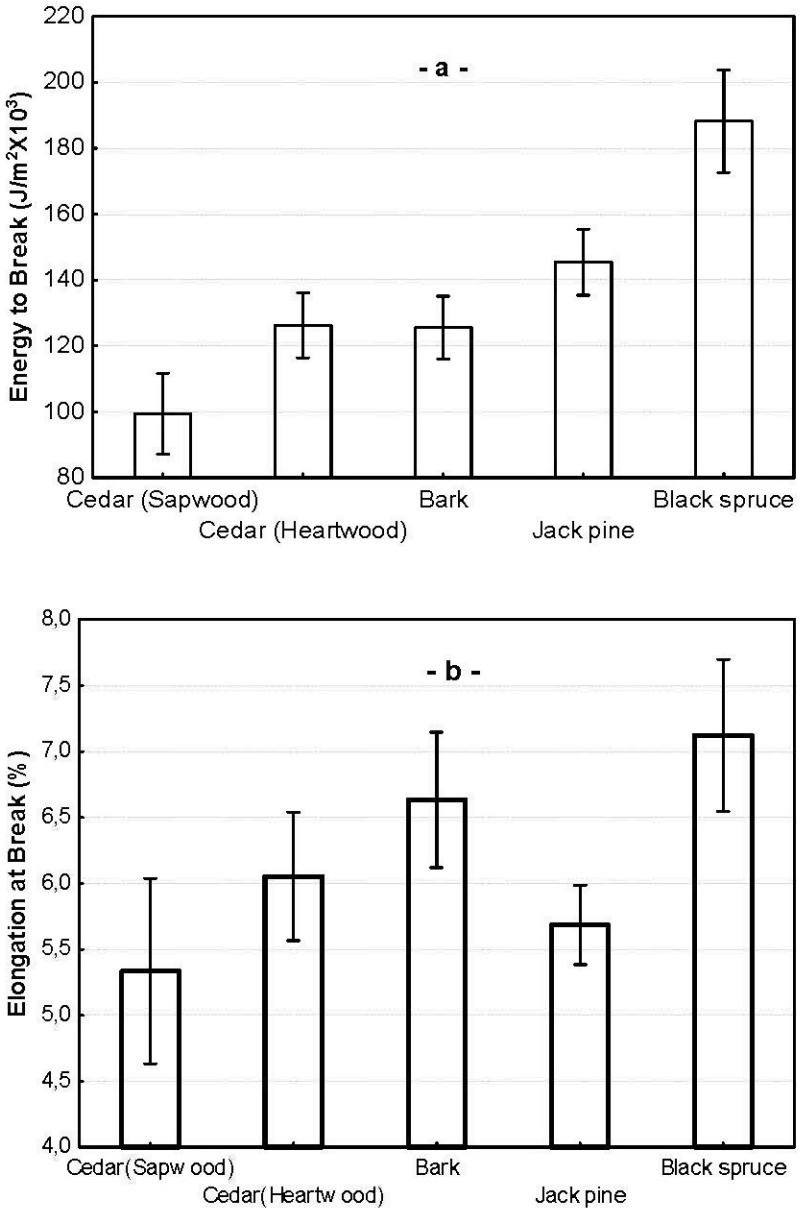

Figure 6.3. Variation in (a) energy to break and (b) maximum tensile elongation at break for wood particle/HDPE injection-molded composites with different filler species at constant load (35%) and particle size (42 mesh).

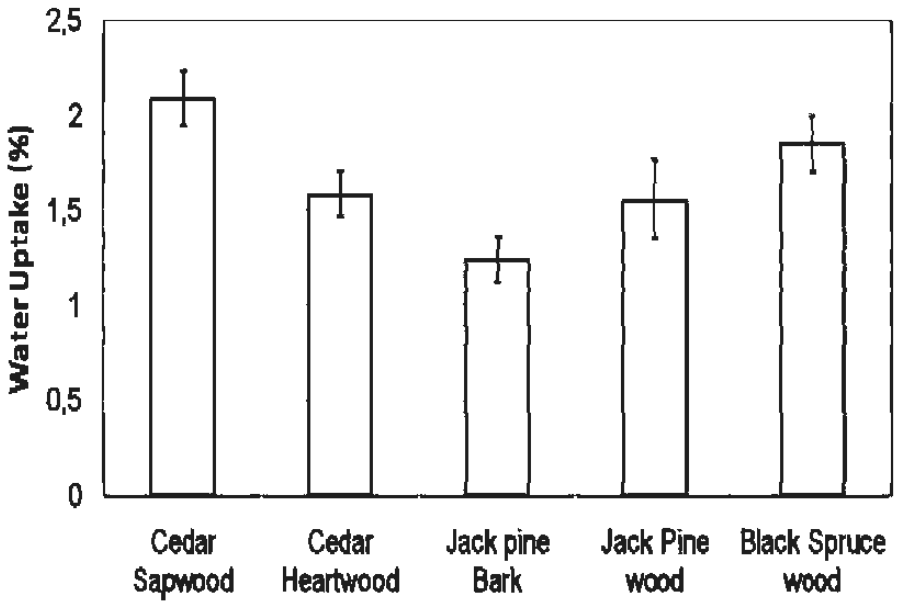

Figure 6.4. Average water uptake in composite materials with various wood fibers after four weeks of water immersion.

6.5.2 Effect of particle size

The effect of particle size on the mechanical properties investigated in this study is highly significant (Table 6.1). In general, increasing fiber size improves the modulus of elasticity and maximum strength in both tensile and flexure tests (Figures 6.5a-6.5d). This result is consistent with previous reports on wood-particle thermoplastic composites (Zaini *et al.*, 1996; Stark and Berger, 1997; Stark and Rowlands, 2003; Dikobe and Luyt, 2007). As for tensile modulus, flexural modulus of elasticity shows a steady increase with increasing particle size at higher filler content (Figure 6.5c). It rises from 2.1 GPa at particle sizes ranging from 100 mesh to 48 mesh (150–300 μm) to 2.7 GPa at average particle size of 24 mesh (≈710 μm) and 45 wt% filler content.

These results are in good agreement with previously reported data (Zaini *et al.*, 1996; Stark and Berger, 1997).

Flexural strength development (Figure 6.5d) also demonstrates that particle size has greater influence at higher fiber load (45 wt%), with approximately 24% higher strength when average particle size increases from 65 mesh to 24 mesh. On the other hand, the incorporation of wood particles in the HDPE matrix steadily increases tensile strength (Figure 6.1b), independently of filler content. When average particle size increases from 65 mesh (≈230 μm) to 24 mesh (≈710 μm), tensile strength improves by 43%, 10%, and 12% at 25 wt%, 35 wt%, and 45 wt% filler content, respectively. Zaini et al. (1996) reported increasing maximum tensile strength with increasing particle size for isotactic polypropylene filled with 250 mesh to 63 mesh oil palm wood flour, while Stark and Rowlands (2003) recommended the use of higher aspect ratio wood fibers, rather than larger size fibers, to increase WPC strength. However, Migneault et al. (2008) showed that maintaining constant fiber diameter and increasing fiber length improves the strength and elasticity of HDPE-filled composites. Stark and Berger (1997) found that larger filler particles (greater than 250 μm) decrease tensile properties.

Figures 6.6a and 6.6b show the energy to break and elongation at break of the resultant composite materials, respectively. Both properties decrease with larger particle size. The effect is more pronounced as particle concentration increases. This is a common tendency, and has been reported with inorganic filler as well (Dubnikova *et al.*, 2004). Moreover, composite strength depends on the debonding process at the fiber end and the fiber's pull-out process during interface failure (Liu *et al.*, 1999). Because of lack of adhesion, crack travels at the weaker wood-polymer interfaces, (as well as through the polymer). The phenomenon is more marked as particle size increases (see appendix 3). As a result, less energy is required to fracture a specimen containing larger particles (Stark and Berger, 1997). In summary,

although incorporating larger particle sizes into the HDPE matrix effectively improves strength properties, this improvement comes at the price of energy to break. Thus, depending on end use, the composite should be optimized for either stiffness or energy to break, by adjusting both filler particle size and concentration.

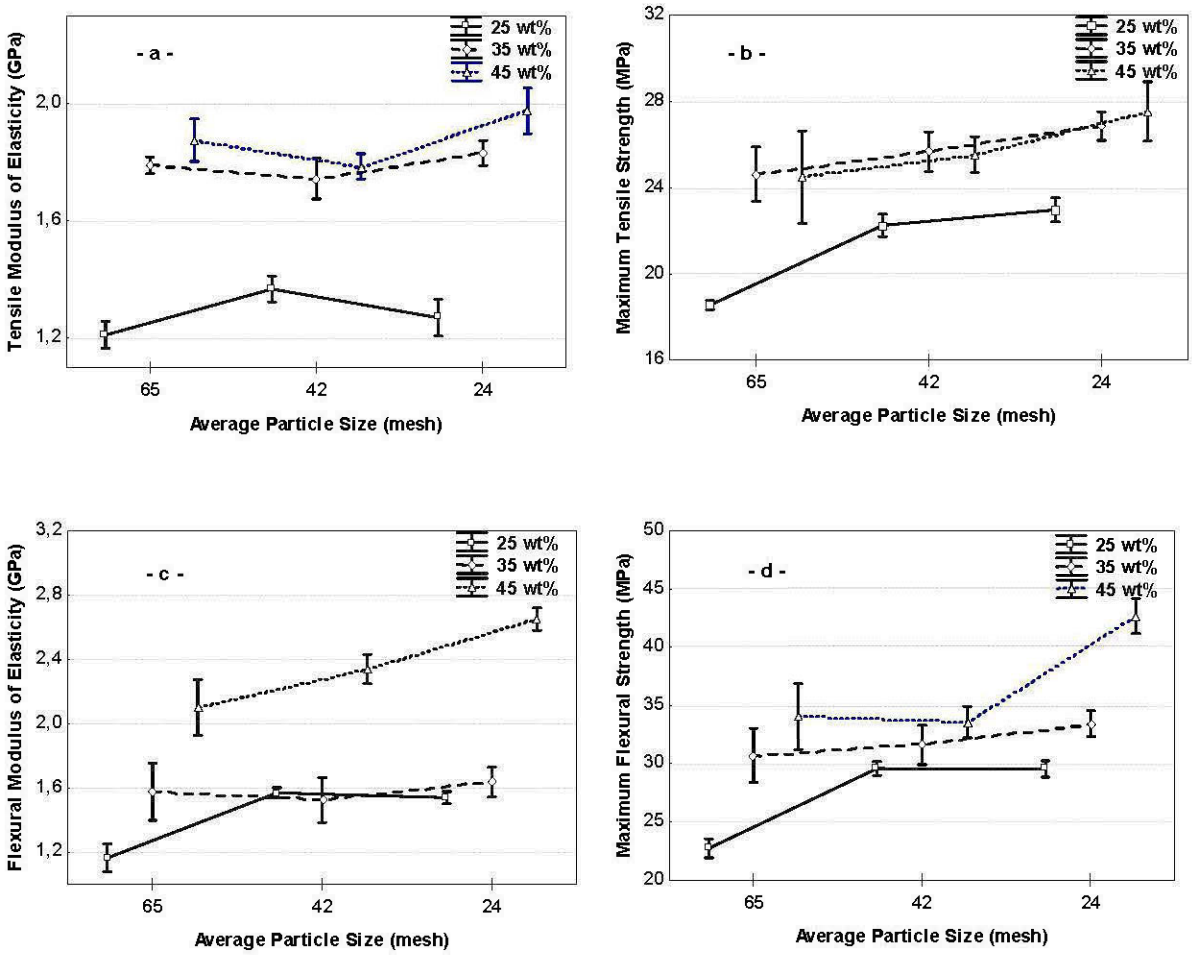

Figure 6.5. Effect of wood particle size with various filler contents on (a) tensile modulus of elasticity (b), tensile strength, (c) flexural modulus of elasticity, and (d) flexural strength of WPC.

The effect of particle size on water uptake is not significant, as shown Table 6.1. However, the interaction between fiber size and fiber proportion is significant. Thus, the effect of fiber length on water uptake is dependent on fiber proportion. At lower proportions, the larger the particle size, the higher the water absorption (Figure 6.7), which is in good agreement with previous reports (Tajvidi *et al.*, 2006b; Steckel *et al.*, 2007). This can be explained in two ways: (i) larger particles lead to greater hydrophilic exposed surfaces; and (ii) poor adhesion between wood particles and the polymer matrix generates void spaces around the wood particles. These voids in the bulk matrix are readily filled with water. At higher proportions, the effect of fiber size is not significant. This could be attributed to the fact that, at high proportions, the effect of fiber size is minimal compared to that of proportion. In addition, fiber size changes during processing. We investigated this development, mainly after compounding (results not shown), and observed that particles with higher aspect ratios are subject to severe damage due to higher shear stresses that develops in the conical counter-rotating intermeshing twin-screw extruder during mixing and compounding. Apparently, particle length distribution after compounding skews towards the shortest particle length.

WPC water absorption tends to increase up to 8 weeks of immersion, as shown in Figure 6.8. This negates the argument that WPC reaches saturation at short and medium immersion times. For example, assuming that moisture is absorbed by wood particles alone, then the average moisture content of wood particles is 10.4% in composites filled with 42 mesh particles at 35 wt%. However, when neat wood particles are immersed in water, moisture content readily exceeds 30%, or fiber saturation. Therefore, WPC water uptake may actually be slowed down rather than delayed.

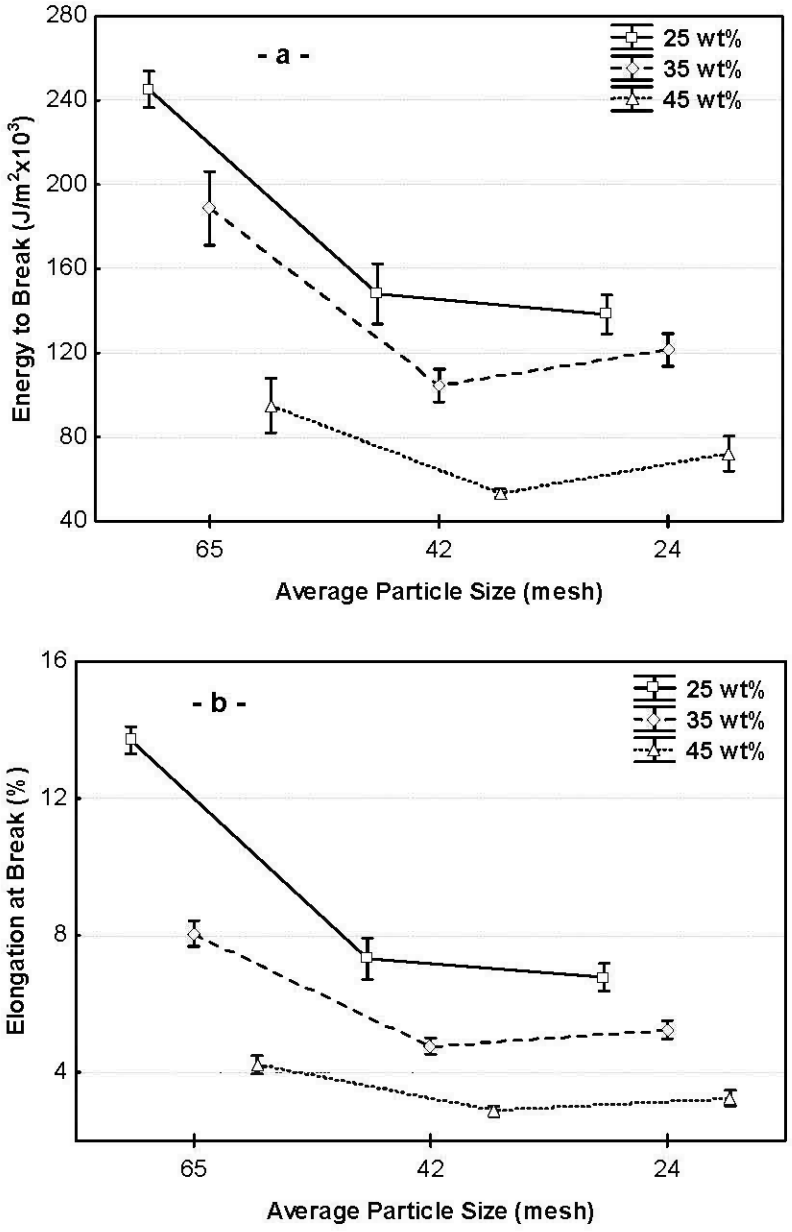

Figure 6.6. Effect of wood particle size and filler content on (a) energy to break (tensile energy) and (b) tensile elongation at break.

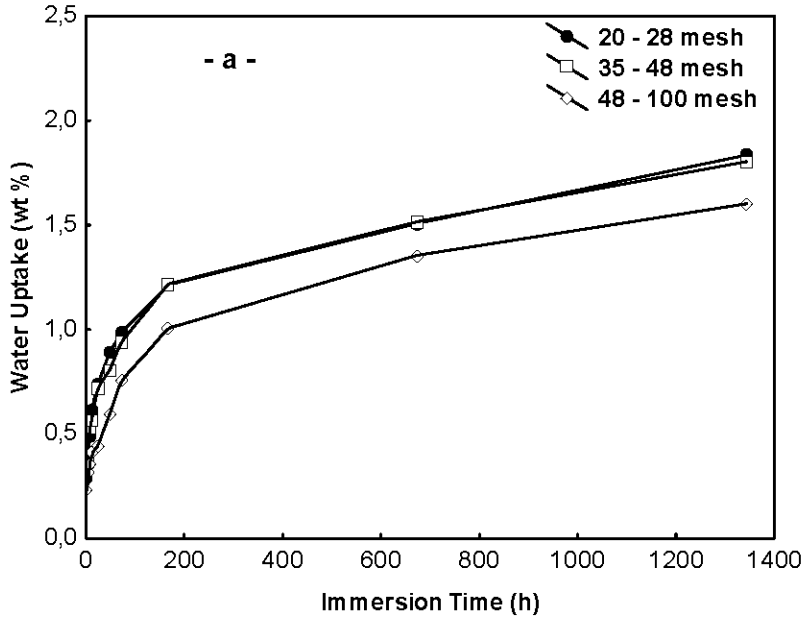

Figure 6.7. Average water uptake in composite materials with wood particle size.

6.5.3 Effect of fiber proportion

As shown in Table 6.1, the effect of fiber proportion is highly significant for all tested properties. In general, high wood particle content yields materials with high rigidity and strength. Figures 6.8a and 6.8b illustrate the effect of fiber content on rigidity and strength properties, respectively, in eastern white cedar particle-based composites. Tensile modulus of elasticity (MOE_T) of the resultant composites increases steadily with wood fiber content, from 0.85 GPa for neat HDPE to 1.75 GPa for WPC with 45 wt% wood content. Loading Neat HDPE with 45 wt% wood fibers increases the flexural modulus of elasticity (MOE_F) by over three times. Compared to neat HDPE, maximum flexural (Fmax) and maximum tensile strength (Rm) of HDPE nearly double with the addition of 45% wood particles. Flexural and tensile strength at break respectively improve by 53% and 18% when wood filler content increases from 25 wt% to 45 wt%. However, wood fibers cause a dramatic decrease in elongation at break after flexion and tensile stress, as shown in Figure 6.9a. Over 400% reduction in elongation at break (ε RB) is recorded at 45% particle content compared to neat

HDPE. These results are in good agreement with previous reports on wood-particle thermoplastic composites (Park and Balatinecz, 1997b; Robin and Breton, 2001). Over 135% reduction in energy to break is recorded at 45% particle content compared to 25% wood-based composites (Figure 6.9b).This reduction in elongation is expected, given that adding fiber changes the viscoelastic behavior of HDPE to a more ductile behavior.

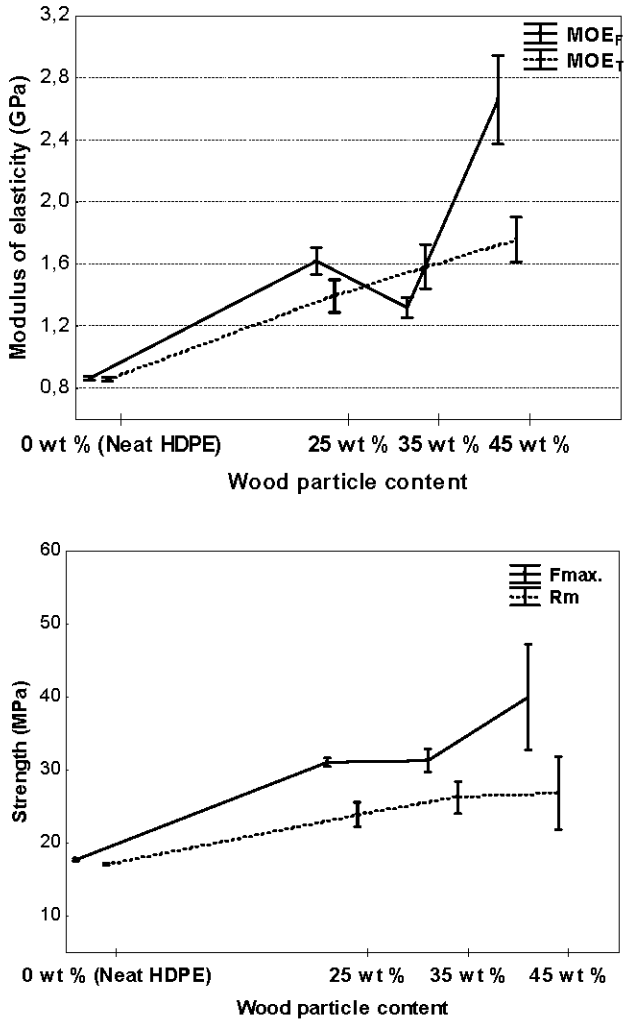

Figure 6.8. Variation in tensile and flexural (a) modulus of elasticity and (b) maximum strength of eastern white cedar-HDPE composites.

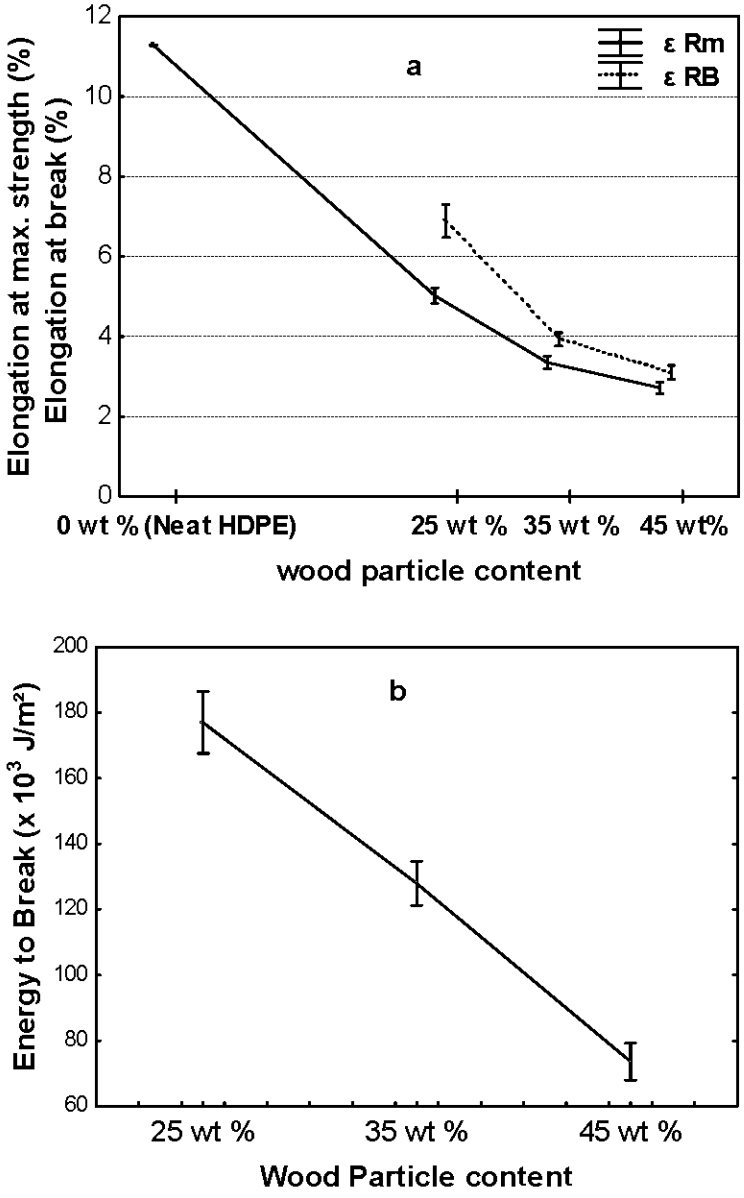

Figure 6.9. Variation in tensile (a) elongation at maximum strength and (b) energy to break of eastern white cedar-HDPE composites.

6.6 Conclusion

Wood fiber variability has a significant effect on the mechanical and physical properties studied. This effect is explained by variations in fiber surface properties, relative crystallinity, thermal degradation, and wood specific gravity. Composites made with bark particles exhibit lower water absorption compared to those made with wood particles. Differences in chemical composition between bark and wood are among the plausible explanations for the differences in water uptake. Increasing fiber size improves strength and stiffness, but reduces elongation and energy to break. The effect of fiber size on water uptake is minimal compared to the effects of fiber origin and proportion. Increasing fiber proportion improves the strength and stiffness of composites, but decreases elongation and energy to break. Water uptake increases substantially with increasing fiber proportion. Composites made with bark particles exhibit lower water absorption compared to those made with wood particles. Differences in chemical composition between bark and wood are among the plausible explanations for the differences in water uptake.

CHAPTER VII

EFFECTS OF PROCESSING METHODS ON WOOD PARTICLE DEVELOPMENT AND LENGTH DISTRIBUTION: CONSEQUENCES ON MECHANICAL PROPERTIES OF WOOD/THERMOPLASTIC COMPOSITES*

7.1 Abstract

The relationship between structure and properties of high-density polyethylene (HDPE) filled with wood particles and processing techniques—injection molding, compression molding, and extrusion was investigated. Wood particles were hammer-milled, sieved, and compounded into pellets at 35% by weight with HDPE using a twin-screw extruder. Coupling agent (ethylene-maleic anhydride copolymer) was added at 2% by wood filler weight. The pellets were used to produce test samples using the three processing techniques. The sensitivity of jack pine and several other wood particles (eastern white cedar, black spruce, and jack pine bark) to composite processing was analyzed. Bark particles showed higher propensity to generate fines than wood particles, possibly because of a higher thermal sensitivity. The major

---

*

Reprinted in part with permission from Bouafif, H., A. Koubaa, P. Perré, and A. Cloutier (2010), "Effects of Processing Methods on Wood Particle Development and Length Distribution: Consequences on Mechanical Properties of Wood/Thermoplastic Composites". Wood and Fiber Science 42(1):9 pages *(in press)*

reduction in mean particle length was found to occur in the compounding process. Extrusion and injection molding contributed to particle length reduction to a lesser extent. Conversely, compression molding did not cause significant damage to wood particles. Stiffness and strength increased linearly with weight-averaged length.

7.2 Résumé

La relation entre la structure et les propriétés du polyéthylène haute densité (PEHD) renforcé de particules de bois et les procédés de mise en forme par : moulage par injection, moulage par compression et extrusion a été étudié. Les échantillons de bois ont été broyés, tamisés, mélangé à 35% avec le PEHD et mise en granules en utilisant une extrudeuse bi-vis. Un agent de couplage (copolymère éthylène-anhydride maléique) a été ajouté à 2%. Les granules ont été utilisées pour produire des éprouvettes normalisées en utilisant les trois procédés de mise en forme. La vulnérabilité du pin gris, ainsi que d'autres particules de bois (thuya occidental, épinette noire écorce de pin gris), face aux procédés de mise en forme des composite a été analysée. Les particules d'écorce ont montré une plus forte aptitude à se désintégrer en particules fines à cause de leur sensibilité au gradient thermique élevé généré lors du procédé de mis en forme. La plus grande attrition en longueur chez les particules a été observée suite au procédé de mélange par extrusion double vis. L'extrusion et le moulage par injection ont contribué à la réduction de la longueur des particules de façon moins importante. Inversement, le moulage par compression ne cause pas de dommages significatifs aux particules de bois. La rigidité et la résistance varie linéairement avec la distribution de la longueur des fibres dans le mélange.

7.3 Introduction

The relationships among processing methods, structures, and properties of wood-fiber or flour–polymer composites have been widely studied (Xanthos 1983; Park and Balatinecz 1997; Barbosa and Kenny 2000; Balasuriya et al 2001; Kim et al 2004). Balasuriya et al (2001) investigated the structure–property relationship of wood-flake/high-density polyethylene (HDPE) composites in relation to the matrix agent

melt flow behavior and processing technique, namely twin-screw compounding and mechanical blending. It was found that the structure of the twin-screw compounded composites, based on medium melt-flow-index HDPE, consistently achieved better flake wetting and distribution and therefore produced higher mechanical properties than mechanically blended composites or twin-screw compounded composites with a low melt-flow index. Xanthos (1983) reported that the compounding procedure improves adhesion through the use of a coupling agent and at the same time produced minimum degradation of the wood flour. Stark et al (2004) studied the effect of the processing method (ie injection molding, extrusion, or extrusion followed by planing) on the surface and weathering characteristics of wood-flour/HDPE composites. It was concluded that lightness after weathering was not dependent on the manufacturing method. However, composites with more wood component at the surface (ie planed samples) exhibited a larger percentage of total loss in flexural modulus of elasticity and strength after weathering.

Compounding is a preprocess in thermoplastic injection molding, whereby the polymer and wood filler are mixed together by counterrotating screws in an extrusion machine. The compound is then extruded and chopped into pellets, which are ready for injection molding. The compounding process directly influences the compounding quality of wood–polymer blends and the coupling agent performance in the resultant composites (Lu et al 2005). However, the compounding of thermoplastics with wood flour or natural fibers presents many drawbacks because of the temperature and shear sensitivity of the thermoplastic matrix, the presence of moisture in the cellulosic fibers, and the critical process temperature limitations of the wood filler. Ali et al (2003) reported that during mixing and compounding, the higher shear stresses that developed in a counterrotating conical intermeshing twin-screw extruder that was used to disperse the fibers caused a substantial reduction in both fiber diameter and length. Fu and Lauke (1996) verified that the postcompounding processes, namely extrusion and injection molding, also led to fiber damage, and the end result was an asymmetric fiber length distribution with a tail at higher fiber lengths.

In contrast to numerous studies on inorganic fillers, there are few studies that document the effect of processing conditions on fiber-length distribution and mechanical properties of woodfiber reinforced thermoplastic matrices. Bigg (1985) found that a single-screw compounder did less damage to inorganic filler than a twinscrew compounder under similar processing conditions when the polymer was in pellet form. Conversely, when the polymer was supplied as a powder, the twin-screw compounder did less damage to fiber. Subsequently, Grillo et al (1993) proved that compounding short glass fibers in a corotating twin-screw extruder required process design optimization (i.e. screw configuration assembly and die) to yield a material with suitable mechanical properties. They also found that certain physical mechanical properties such as notched Izod were highly correlated with the degree of damage to the glass fibers, whereas flexural properties were a function of preserved glass length as well as fiber–matrix adhesion. The study concluded that reduction in glass abrasion requires a very gentle screw configuration and minimal average shear rate in the extruder and die, whereas good adhesion is promoted by complete glass wetting, requiring an effective mixing screw and die restriction. Recently, Yilmazer and Cansever (2002) studied the effect of screw speed and feed rate (in different combinations). Results showed that the average fiber length decreased when the shear rate increased through screw speed and/or feed rate. Consequently, impact strength, tensile modulus, and tensile strength increased, but the elongation at the breaking point decreased with a decrease in the average fiber length. In addition, lower shear history and melt temperature during the primary compounding operations of such composites generally result in better mechanical properties of the finished product (Bledzki and Faruk 2004; Kasliwal and Jones 2004). Increased screw rotational speed or reduced processing temperature has been shown to reduce fiber dimensions (Fu et al 2001; Ali et al 2003; Bledzki and Faruk 2004).

As mentioned, the separation processes of natural fibers and the composite processing method influence fiber degradation and hence fiberlength distribution (FLD). FLD is controlled by a number of factors, including original fiber length, fiber content, die

and mold geometry, and processing conditions (Fu and Lauke 1996; Fu et al 1999, 2001). Because the mechanical properties such as strength, elastic modulus, and fracture toughness of short-fiber reinforced thermoplastics are critically dependent on FLD (Fu and Lauke 1996; Fu et al 1999), several methods have been used to accurately characterize the geometric distribution of fibers. Characterization of a sample for FLD before processing is rather straightforward. Nevertheless, it is much more complicated when fibers are blended into a thermoplastic matrix. To study the relationships between the mechanical properties and FLD of short-fiber reinforced thermoplastics, Fu et al (2001) used a statistical cumulative fiber length distribution model, whereas Suzuki (2003) used a probabilistic approach based on the projection length of the fiber to the composite surface. Clemons et al (1999) successfully characterized the FLD of postprocessing residual fibers using solvent extraction followed by optical measurement techniques. Results of these studies indicated that fiber lengths were reduced by one-half when they were compounded in a high-intensity thermokinetic mixer followed by injection molding. Recently, Balasuriya et al (2001) used an optical microscope with an image analyzer to determine the wood-flake length/width distribution after processing. They also measured length and width distributions before compounding by projecting images of the flakes onto a large screen.

Because the intrinsic characteristics of wood fillers vary with the chemical composition of the species involved, the vulnerability of different wood species to processing conditions can be expected to vary. A few studies have highlighted the relationship between variability in wood fiber structure and damage levels during mixing. Neagu et al (2006) investigated the stiffness contribution of various wood fibers to the resulting composite materials. The study concluded that unbleached fibers are more suitable than bleached fibers for use as stiffening reinforcement. A correlation between lignin content and fiber longitudinal Young's modulus was observed, and the optimal lignin content range at which fiber stiffness attains a maximum was identified for softwood kraft fibers. Moreover, they found that

hardwood fibers showed a higher reinforcement potential than softwood fibers. This article presents the correlations among processing, structure, and properties of woodparticle reinforced HDPE composites. Initially, the study explores the vulnerability of wood filler to the environment prevailing during polymeric processing by comparing the susceptibility of different softwood particles to the damage exerted by high shear stresses that developed during processing. The physical properties of the finished composites were analyzed for the degree of particle damage. Finally, the relationship among processing techniques (compounding, extrusion, and molding), structure, and some mechanical properties of wood-particle reinforced HDPE are highlighted.

7.4 Experimental

7.4.1 Characterization of particle length distribution after processing

Pieces of composites were randomly chosen (see **Chapter III** for composite preparation). The procedure used to separate the wood particles from the polymer matrix was as follows: 250 mL of xylene was placed in a 500-mL reactor and gently stirred with a magnetic stirrer while heating to 130 – 140°C. After reaching this temperature, pieces of composites (25 g) were placed in the reactor and allowed to react for 2 h. After the reaction, the mixture was filtered to recover the wood particles. The obtained material was soxhlet- extracted with xylene for 12 h to remove the unreacted anhydride and oven-dried at 70°C for 24 h. Finally, a dilute suspension of recovered particles was analyzed with a Fiber Quality Analyzer (FQA) (OpTest, Hawkesbury, Canada). FQA is an optical device used to characterize the length distribution and aspect ratio of wood fibers. Weight-averaged particle lengths were calculated according to the following equation (Robertson et al 1999):

$$L_W = \frac{\sum_{i=1}^{n} l_i}{\sum_{i=1}^{n} l_i^2} \qquad (7.1)$$

Where,

L_W is the weight-averaged length

l_i is the effective length of i^{th} particle

n is the total number of particles analysed

7.4.2 Mechanical measurement

Specimens were stored under controlled conditions (50% RH and 23°C) for 40 h before testing. Only specimens having 35 wt% of wood fillers and 42-mesh particles were analyzed in this study. Tensile tests and bending tests were conducted according to ASTM D638-03 (ASTM 2003a) and ASTM D790-03 (ASTM 2003b), respectively.

7.5 Results and discussion

7.5.1 Development of wood particle reinforced HDPE

To eliminate processing variables, all wood particles (except bark particles) were produced under nearly identical hammer-milling conditions. As shown in Figure 7.1, the vulnerability of wood to a F1 hammer-milling process depends on species. Eastern white cedar showed the lowest mean length (0.8 mm) after hammer milling. This apparent weakness of eastern white cedar during processing became more evident when compared with the structural properties of solid wood. *Table 7.1* shows some mechanical properties of solid wood. It confirms that the weakness of white cedar is mainly because of its low density (320 kg/m^3). In good agreement with previous reports (Hernandez et al 2002; Ali et al 2003; Kasliwal and Jones 2004), the

higher shear stresses that developed in the counter-rotating conical intermeshing twin-screw extruder during mixing and compounding caused a reduction in both particle length (Figure 7.1) and diameter (Figure 7.2).

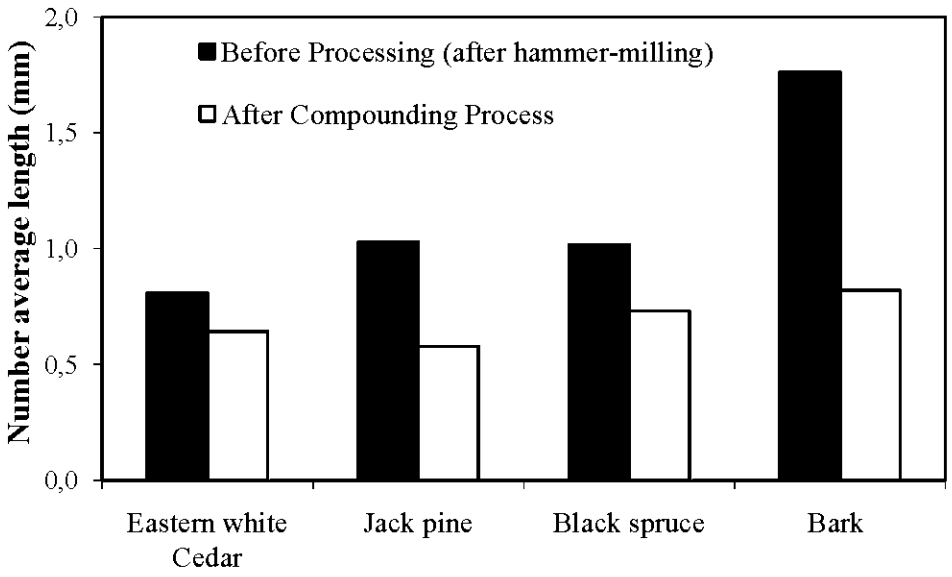

Figure 7.1. Effect of compounding process on the effective mean length of various wood particles.

The final products, after the compounding process, appear to have comparable geometric means regardless of wood species or initial dimensions. Apparently, wood particle mean length and aspect depend solely on compounding process conditions. Visual examination of the compounded samples showed that after a residence time of 240 s and a screw speed of 240 rpm **(see Chapter III)**, the blend appeared to have been homogenized with no aggregated particles present. At this stage, the composites showed pseudoplastic behavior, which can be explained as follows. Initially, particles that are randomly oriented are subjected to shear. Particle length continues to diminish progressively through friction between the material and both the screw and barrel. After reaching the shortest length, the particles tend to align themselves in the direction of flow **(see Appendix 4)**. Therefore, the extent of particle degradation

decreases and averaged particle length appears to be constant regardless of species or initial dimension.

The development of the effective length and aspect ratio of jack pine particles in relation to processing methods are shown in *Figure 7.3a* and *Figure 7.3b*, respectively. The particles are dramatically shortened after the compounding process. The particle damage that occurs in injection molding or in single-screw extrusion is much lower than in twin-screw compounding. Similar effects have been reported by Yilmazer and Cansever (2002) and Bigg (1985), in which short inorganic fibers were used. After injection molding, neither the number average length nor the aspect ratio appears to be influenced by the process. This is primarily from the lack of shear stress and friction during compression.

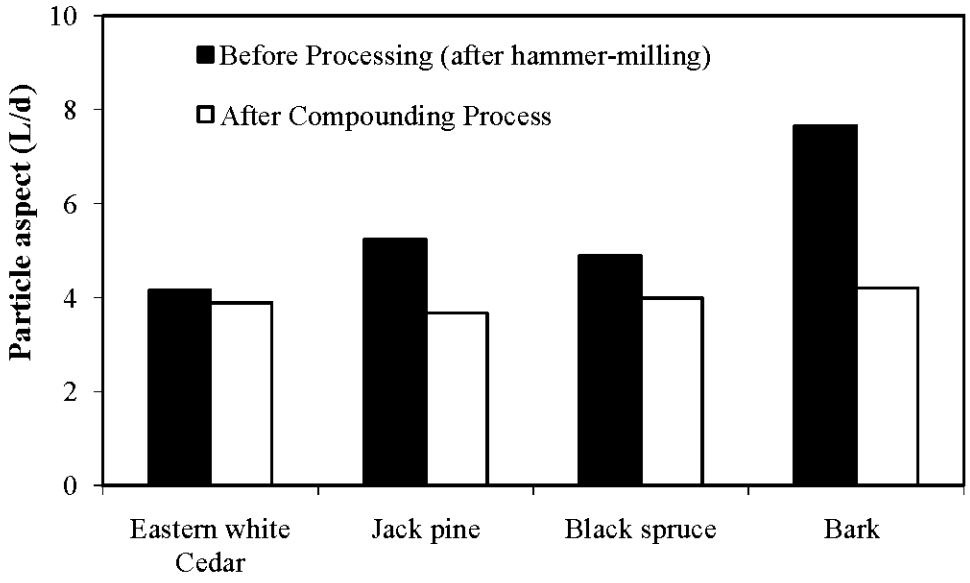

Figure 7.2. Effect of compounding process on the mean aspect ratio of various wood particles.

Table 7.1. Strength properties of the used wood species (Green et al 1999).

	Specific gravity	Modulus of Rupture (kPa)	Modulus of elasticity (MPa)	Work to maximum Load (kJ/m^3)
Eastern white cedar	0.32	47	6.4	41
Jack pine	0.43	68	9.3	57
Black spruce	0.46	74	11.1	72

7.5.2 Characterization of particle length distribution

Figures 7.4 and 7.5 depict the number-average particle- size distribution for jack pine after each stage of processing. It was assumed that molding compression did not have a major impact on the size distribution. The analyzed particles were sieved through mesh 35 to 48 before compounding. In Figure 7.4, the longest particles (greater than 2.4 mm) completely vanished after compounding. Moreover, particles with lengths greater than 1.2 mm were severely damaged from compounding. The aspect ratio showed a symmetric distribution with 4 being the modal value (Figure 7.5). After compounding, the particle length distribution skewed toward the shortest particle length without modifying the original distribution before processing. However, the average length diminished slightly after the single-screw extrusion and molding injection processes, and particle length distribution exhibited a dramatic shift toward an asymmetric character with a tail on the longer fiber sizes.

Higher shear stresses developed in the compounding process directly attack the wood particles, which consist of wood fibers. In this process, the particle structure is disrupted, resulting in more refined particles. Injection molding and single-screw extrusion attack shives by breaking the extremities of the disintegrated fibers. As a consequence, the number of fines is greatly increased, as shown in Figure 7.4 and *Table 7.2.* Bark particles showed higher propensity to produce fines than wood particles *(Table 7.2)*. The fraction of bark fines having effective lengths of 0.1 – 0.5

mm doubled as a result of compounding (*Table 7.2*). Among the three wood types, the fines fraction increased almost equally by approximately 46%.

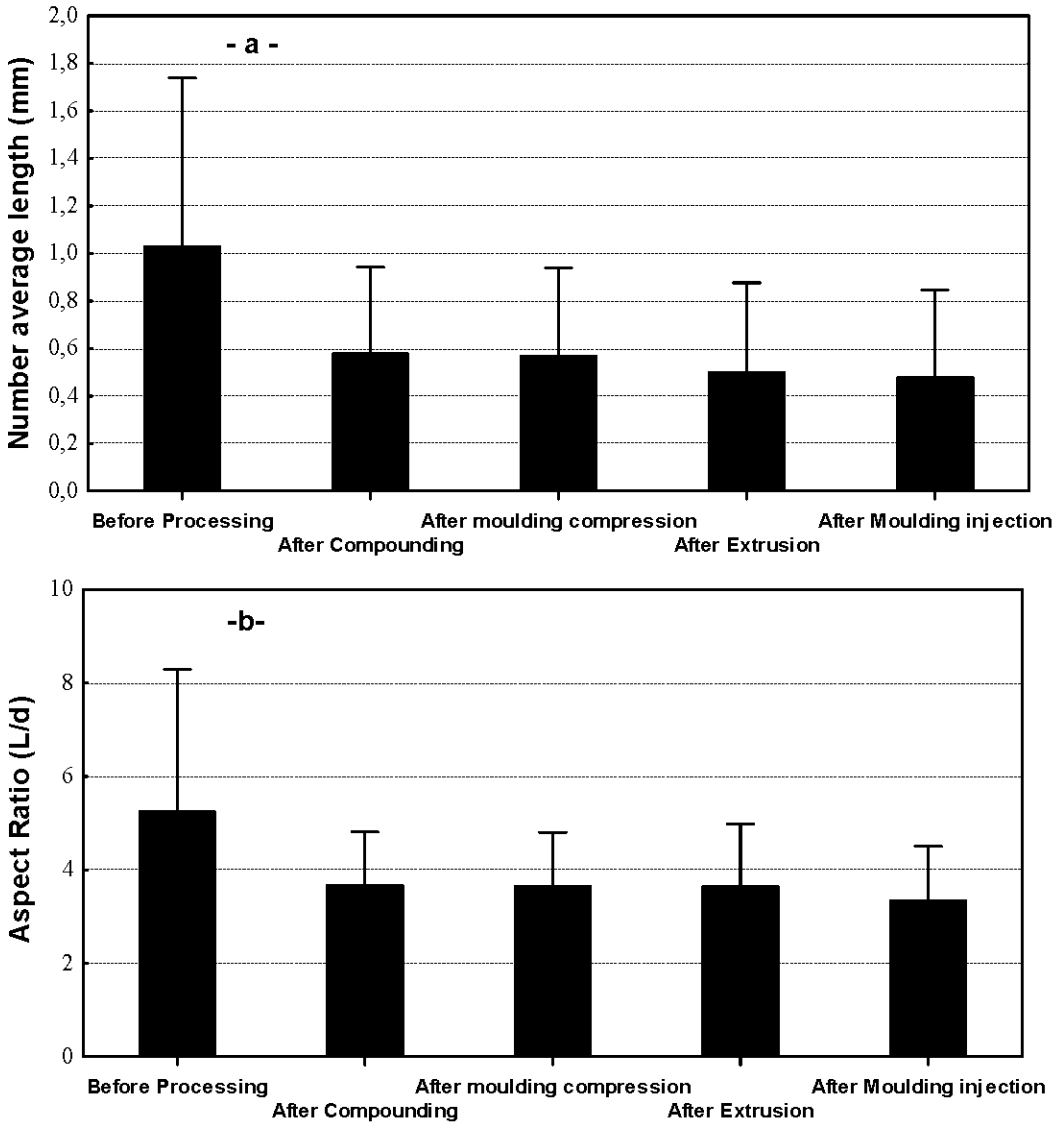

Figure 7.3. Development of (a) the effective length and (b) aspect ratio of jack pine particles in relation to composite processing techniques.

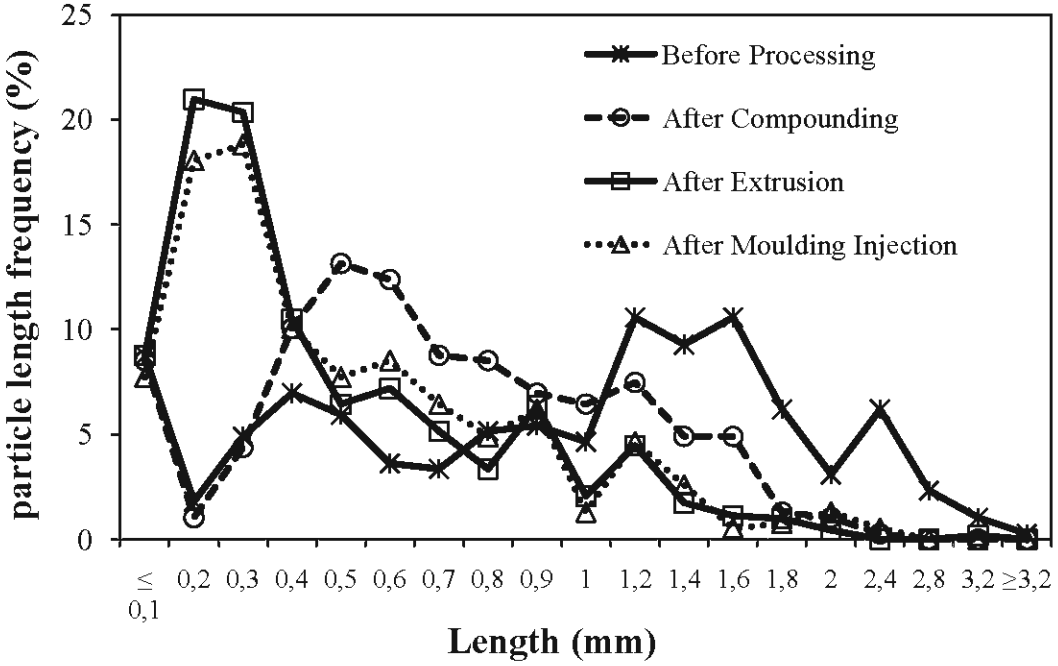

Figure 7.4. Length distribution of processed Jack pine particles.

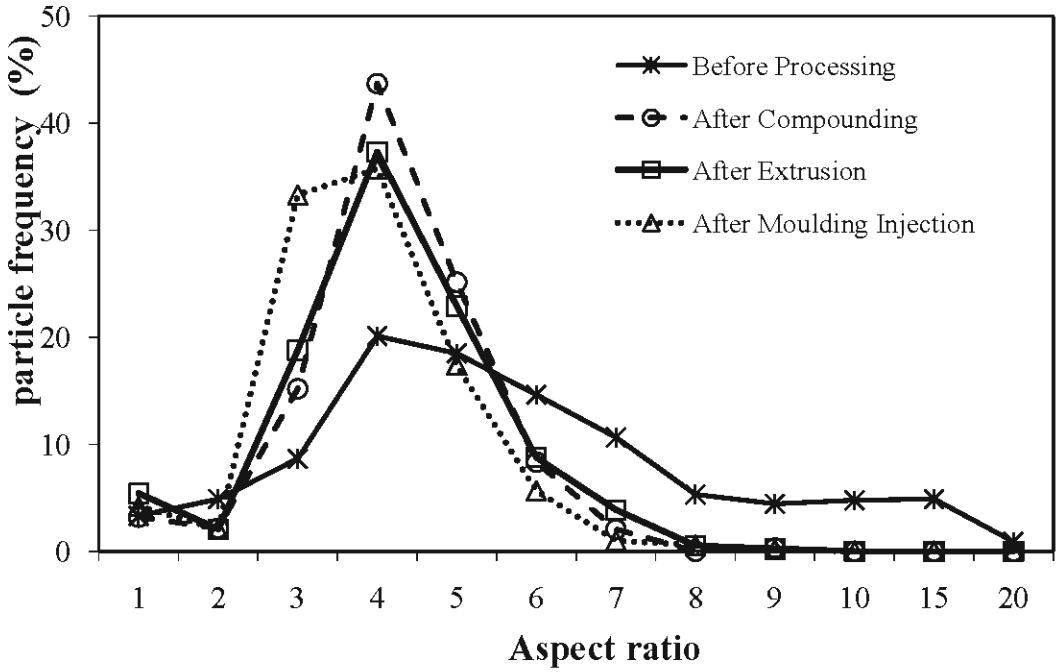

Figure 7.5. Aspect ratio distribution of processed Jack pine particles.

Table 7.2. Fines frequency (0.1< Length ≤0.5mm) before and after compounding process.

Species	Before processing	After compounding	Change (in %)
Jack pine	19.6	28.6	46.0
Eastern white cedar	26.1	38.7	48.4
Black spruce	21.10	30.9	46.3
Bark	10.5	21.9	109.1

7.5.3 Effect of *Weight length* and fines on mechanical properties

Weight average particle length was taken into consideration since it imparts emphasis to the longer particles in the sample and gives less emphasis to the fines. Linear regression was used to model the relationship between weight-averaged length of wood particles, stiffness (*Figure 7.6a*) and strength (*Figure 7.6b*) of the composites. As expected, both stiffness and strength depicted good correlations with the weight-averaged length of particles at 35% wood particle content. Maximum flexural strength (MOR (flexion)) show the best correlation (R^2 = 0.9) with the L_W (Figure 6.b). Maximum tensile strength (MOR (tensile)) was also highly correlated with L_W (R^2 = 0.83). These results are consistent with the literature. Indeed, (Bledzki and Faruk 2003) had observed that the tensile, flexural, charpy impact and impact properties of wood fibre reinforced polypropylene composites were positively influenced by fiber length. (Lee et al 2001) found the same behaviour when studying tensile and flexural modulus of wood-fiber/polypropylene prepreg sheets.

Effective average length, in contrast to weight-averaged length, is the widely used factor when characterizing mechanical properties of wood fibre reinforced polymer composites (Fu and Lauke 1996; Fu et al 1999; Lee et al 2001; Juhlin et al 2002). However, after going through the processing cycle, particles in the polymer matrix are crushed and squeezed. This significantly affects particle length distribution, even

if the effective mean length is not changed. Therefore, weight-averaged length, which is directly related to the occurrence of long particles, is a more suitable parameter to be considered than the effective mean length when characterizing the effect of a reinforcing material on mechanical properties of the produced polymer composite.

As discussed earlier in this study, the higher shear stresses developed during processing caused damage on particles and led to a higher content of fines in the material. *Figure 7.7a* and *7.7b* show the effect of fines content on stiffness and strength of the composite material, respectively. Composites with 35wt% of wood particles were studied. Results show that 20 % of fines content seems to produce optimum strength and stiffness properties. Fine loads bellows 20% seem to play a reinforcing task in the composites materials. Loads above would have a deteriorating effect on both stiffness and strength. These results were in harmony with several studies in which load transfer across the fibre ends was considered as the significant parameter in the micromechanics of wood plastic composites, since the reinforcing fibres are typically very short and of low aspect ratio (Sretenovic *et al.*, 2006). In addition, emphasis on both long particles and fines occurrence must be taken into consideration when composites with good mechanical properties will be developed. Furthermore, when the same processing conditions were maintained, these two factors were directly related to the wood particles strength in terms of resistance to the fracture exerted by different shear stresses during the composites processes.

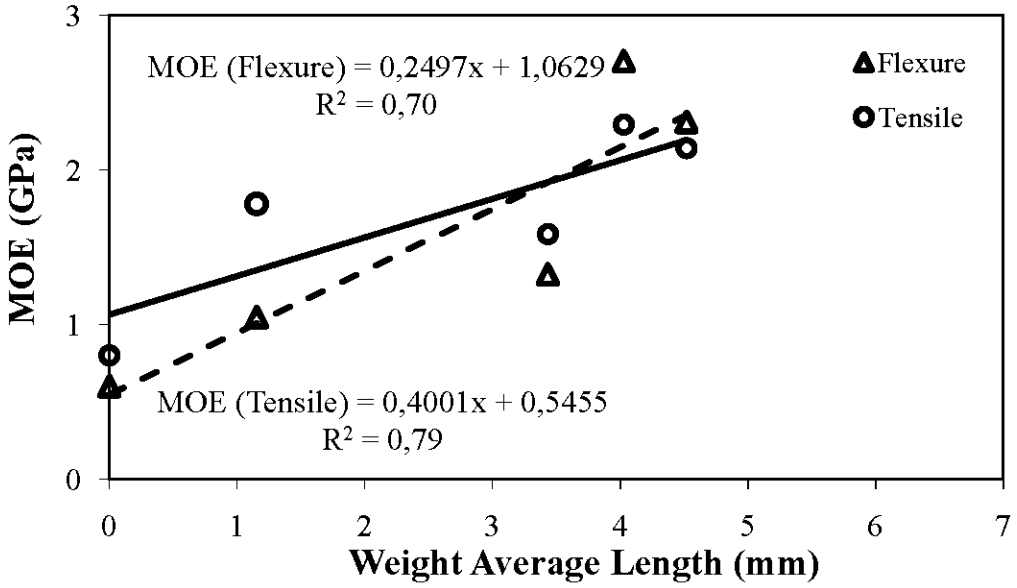

- a -

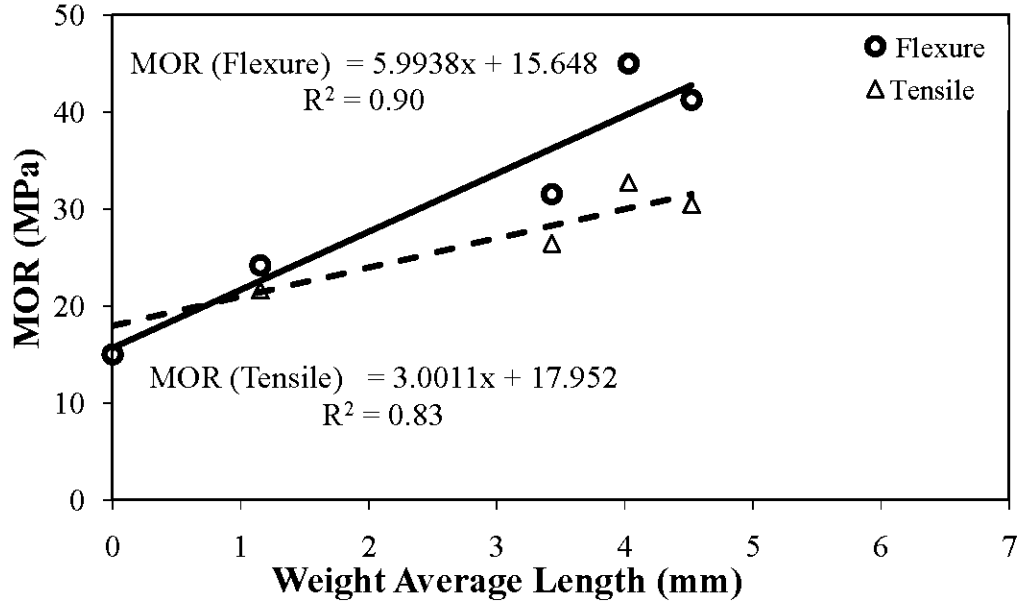

- b -

Figure 7.6. Relationships between (a) stiffness, (b) strength and weight average length in wood particle based composites.

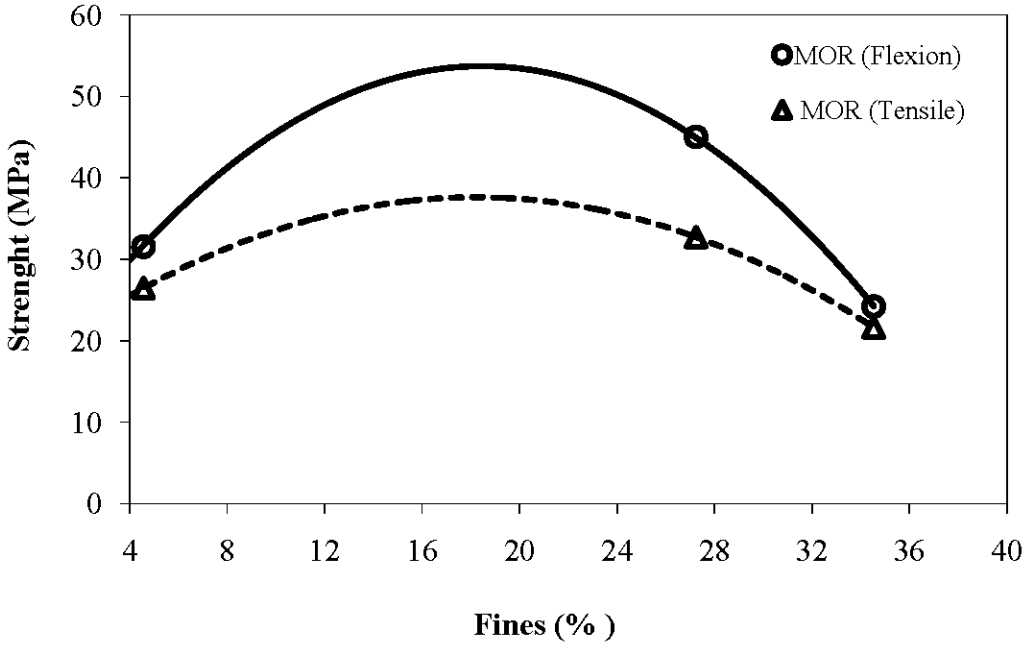

- a -

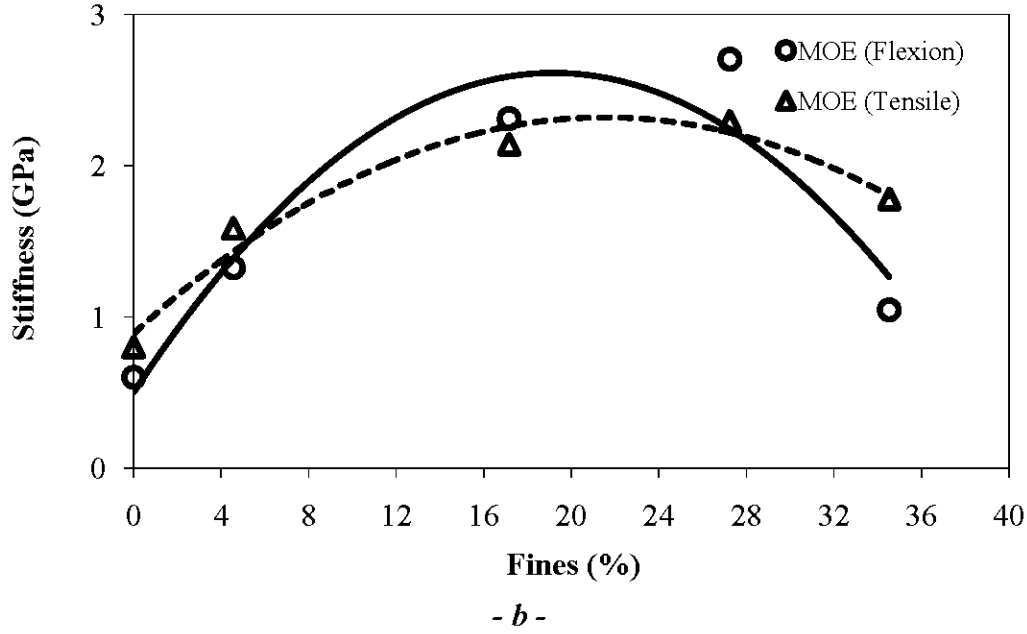

- b -

Figure 7.7. -a- Effects of fines occurrence on strengths, -b- stiffness of wood particle based composites made with 35wt% of jack pine wood particles.

7.6 Conclusion

Vulnerability of wood to composite manufacturing processes significantly depends on intrinsic characteristics of the wood species involved. The major reduction in the effective mean length of the wood particles was found to be associated with compounding process. The subsequent processes, such as extrusion, moulding injection and moulding compression had relatively mild effect towards particle size reduction. This observation explains the increased percentage of fines in the finished composite as compared to the original wood particle size distribution. Bark particles showed the highest susceptibility to generate fines than the wood particles used in this study. This may be due to its low intrinsic strength and highest thermal sensitivity. Thus, the selection of natural lignocellulosic materials for composite reinforcement could be based on intrinsic strength and thermal sensitivity of the material for a given end use. Bark and eastern white Cedar wood-based composites, containing high extractives content, are well known for their weak stiffness and strengths. It is suggested that weight-averaged particle length and particle length distribution, mainly in terms of fines content, must be simultaneously considered for characterizing the effect of composite manufacturing processes on particle length attrition. This would also be helpful in determining mechanical properties of the composite manufactured. In order to maximize the reinforcing effect of wood particles, fines occurrence must be kept under 20% of the reinforcing material while the longer particle occurrence could be as high as possible.

CHAPTER VIII

EFFECTS OF WOOD FILLER ADDITION AND PROCESSING METHOD ON THE DYNAMIC MECHANICAL PROPERTIES OF WOOD PARTICLE/HDPE COMPOSITES

8.1 Abstract

The effects of wood filler characteristics and processing methods on the dynamic mechanical properties of wood particle/HDPE composites were investigated. Storage modulus (E′) decreased with an increase in temperature. Jack pine-based composites showed the highest storage modulus, attributed to better interfacial adhesion between jack pine wood fiber and HDPE matrix. In HDPE, the α-relaxation peak marginally shifted to high temperature regions with the addition of wood fiber and resultant loss modulus (E″) increased by 17% to 30%, indicating more viscous dissipation. Slow cooling and quenching of extruded samples significantly affected α-peak temperature. E′ increased with increasing frequency, whereas tan δ and E″ decreased. Moreover, α-peak tended to shift to lower temperatures as frequency decreased. A slight increase in ΔE was detected after wood particle addition, which may be explained by the increase in crystallinity due to the nucleation efficiency of wood filler.

8.2 Résumé

Les effets des caractéristiques du bois, comme élément de renfort, et les procédés de mise en forme sur les propriétés mécaniques dynamiques des composites bois/PEHD ont été étudiés. Le module de stockage (E ') diminue avec une augmentation de la température. Les composites à base de fibres de pin gris ont montré le module de stockage le plus élevé, ceci a été attribué à la meilleure adhésion entre les fibres de bois de pin gris et la matrice PEHD. Le pic de relaxation-α a légèrement décalé vers les régions à haute température avec l'ajout de fibre de bois. Le module de perte (E") qui en résulte a augmenté de 17% à 30%, indiquant ainsi plus de dissipation visqueuse. La vitesse de refroidissement des échantillons extrudés affecte la température du pic α. E' augmente avec une augmentation de la fréquence de sollicitation, alors que le facteur des pertes (tan δ) et E" ont diminué. En outre, la température relative au pic α a diminué en réponse à une diminution de la fréquence. La légère augmentation de l'énergie d'activation (ΔE), détectée après l'ajout de particules de bois, a été expliquée par l'augmentation de la cristallinité due à l'efficacité de nucléation des particules de bois.

8.3 Introduction

Recently, the production and application of wood fiber and natural fiber reinforced thermoplastic polymers, or wood polymer composites (WPC), have increased considerably (Bledzki *et al.*, 1998a; Bledzki *et al.*, 1998b). Today, application fields for these materials are practically unlimited. For instance, WPC products are used in window and door profiles, decking, garden furniture, and the automotive industry (Ashori, 2008). This growing interest in lignocellulosic fibers is mainly due to their economical production, few equipment requirements, biodegradability, and their availability in large quantities and in various forms. Considerable amounts of wood fiber can be added to commodity thermoplastic matrices, offering economically

advantageous solutions (Maldas *et al.*, 1988b; Raj *et al.*, 1990; Bledzki *et al.*, 1998a; Bledzki *et al.*, 1998b; Bledzki and Gassan, 1999; Takatani *et al.*, 2000; Stokke and Gardner, 2003; El-Meligy *et al.*, 2004; Wester, 2005) and environmental benefits(Bogoeva-Gaceva *et al.*, 2007).

Because wood-reinforced thermoplastic composite materials can endure various types of dynamic stressing during service, studies on the dynamic mechanical properties of these materials are of great importance. Similar to previous findings on static mechanical properties (Bouafif *et al.*, 2008b; Bouafif *et al.*, 2008a; Migneault *et al.*, 2009), dynamic mechanical properties, based on material viscoelasticity, depend on the intrinsic wood filler characteristics, including fiber loading, type, aspect, and orientation, fiber-matrix compatibility, and processing method (Reussmann and Mieck, 1999; Saha *et al.*, 1999; Kim *et al.*, 2000; Tajvidi, 2005; Jacob *et al.*, 2006; Mohanty *et al.*, 2006; Tajvidi *et al.*, 2006a). According to the International Confederation for Thermal Analysis (ICTA), dynamic mechanical analysis (DMA) is defined as "*a technique in which dynamic modulus and/or damping of a substance under oscillatory load is measured as a function of temperature whilst the substance is subjected to a controlled temperature program.*" This technique separates the dynamic response of materials into two distinct parts: an elastic part (E'), which is a measure of the maximum energy stored in the material during one oscillation cycle, and a damping component (E''), which is the dissipating energy.

The mechanical relaxation behavior of polyethylene (PE) has been extensively studied through low-frequency dynamic mechanical spectra (Boyer, 1973; Boyd, 1976; Popli *et al.*, 1984a; Sha *et al.*, 1991; Matthews *et al.*, 1999; Pegoretti *et al.*, 2000). Boyd (1985) gave a comprehensive review of relaxation processes in semi-crystalline polymers as well as methods for phase assignment of mechanical relaxation. It is well known that PE undergoes three major transitions related to molecular processes either in the amorphous or crystalline phase. (i) The α-relaxation

in the temperature range from 50 °C to 120 °C is associated with an interlamellar shear process. (ii) The β- transition, which peaks at about -20 °C, is generally attributed to branched and amorphous structures, and is absent in entirely linear polyethylene, i.e., HDPE. However, under special quenching conditions that yield amorphous phases, the β-transition can also be observed in linear PE (Khanna *et al.*, 1985; Matthews *et al.*, 1999). (iii) The γ-relaxation depicts a peak transition at about -125 °C. It is assumed to correspond to the glass-transition temperature (Tg) and is caused by small, local, short-range segmental motion of amorphous material involving possibly three or four methylene groups (Khanna *et al.*, 1985). The study of these different transitions and the processes involved, using dynamic tests over a wide range of temperatures and frequencies, is critically important in understanding the mechanical performance of semicrystalline polymers and their composites.

Saha et al. (1999) investigated chemically modified jute fiber-reinforced polyester composites using dynamic mechanical analysis (DMA) over a wide temperature range. They concluded that the cyanoethylation of jute fibers strongly increased the storage modulus and thermal transition temperature of the composites, indicating higher stiffness compared to a composite made with unmodified fiber. Moreover, the addition of jute fiber (unmodified and modified) considerably reduced tan δ peak height. Similarly, Jacob et al. (2006) observed an increased storage modulus with d weight fraction increase of sisal/oil palm hybrid fibers, indicating increased stiffness imparted by the natural fibers, whereas damping property decreased. In another study involving biofibers, Geethamma et al. (2005) reported that composites with poor interfacial bonding tended to dissipate more energy than those with good interfacial bonding. Moreover, Hristov and Vasileva (2003) showed that the tan δ peak temperature of a compatibilized wood fiber-polypropylene system increased over that of composites without coupling agent. These findings were corroborated by a recent study by Mohanty et al. (2006), who reported increased storage modulus and loss modulus peak with fiber reinforcement and the addition of coupling agent. However,

the damping properties of treated and untreated composites decreased compared to the virgin matrix. Geethamma et al. (2005) studied the influence of frequency on the mechanical transitions of natural rubber and its composites reinforced with short coir fibers. They reported that tan δ and E″ decreased with increased frequency, whereas E′ increased. They explained that, in low frequency range, the molecules have time to slip past one another and flow occurs. This liquid-like behavior causes increased damping.

The present study systematically investigated the effects of intrinsic characteristics and processing methods of wood fiber reinforcement in high-density polyethylene. The main focus was on the additional effects of wood particle loading, type, size, and processing method, based on the theory of relaxation transitions in high-density polyethylene. Composites were subjected to periodic stress using dynamic mechanical analyzer to investigate variations in storage modulus, loss modulus, and damping properties as a function of temperature. The dynamic mechanical behavior of wood fiber/HDPE composites as a function of frequency was also investigated.

8.4 Experimental

8.4.1 DMA testing

Virgin HDPE specimens and treated composites having dimensions of 35 x 12.5 x 3.2 mm were subjected to dynamic mechanical testing using a Dynamic Mechanical Analyzer (DMA 2980, TA Instruments). Measurements were initially performed with a temperature ramp/single frequency method, using a dual cantilever measuring system, similar to 3-point bending system except that sample ends were clamped and corresponding viscoelastic properties were determined as a function of temperature. Temperature range varied from -130 °C to 110 °C with an equilibrate time of 10 min at -130 °C followed by a heating rate of 3 °C/min under nitrogen flow. Samples were scanned at a fixed frequency of 1 Hz with 0.2% static strain and 0.1% dynamic strain.

Measurements were then performed with a temperature ramp/multi-frequency method using the same system as for the initial measurements. Frequency sweeping was stepped in logarithmic increments from 0.1 Hz to 10 Hz and temperature range varied from 35 °C to 110 °C. Equilibrate time and heating rate were maintained the same as for the initial measurements.

8.5 Results and Discussion

8.5.1 Storage modulus

The storage modulus in viscoelastic solids measures the stored energy, representing the elastic portion. It is analogous to Young's modulus or the elastic modulus, a measure of elastic stiffness. Figure 8.1a shows the variation in storage modulus as a function of temperature and wood particle content in injection molded composites. As expected, the modulus of the virgin matrix increased appreciably with the addition of wood particles. This confirms the finding that HDPE matrix stiffness increases through the reinforcing effect of the wood particle component, which improves the material's elastic behavior (George *et al.*, 1996; Bouafif *et al.*, 2008b). Thus, the higher the percentage of added wood, the higher the increment in storage modulus of the composite. On the other hand, as shown in Figure 8.1, storage modulus decreased in all samples with increasing temperature and dropped significantly at higher temperatures (> 40 °C). Mohanty et al. (2006) proposed that higher moduli maintained at higher temperatures were probably due to the presence of wood fibers, which reduced material flexibility by introducing constraint on the segmental mobility of polymeric molecules at relaxation temperatures. However, filled composites showed greater thermal stability than virgin HDPE, as the falling rate of the matrix modulus increased with increasing filler content.

Storage moduli of composites made with different wood particle species are shown in Figure 8.1b. As can be seen, jack pine-based composites showed the highest modulus.

This behavior can be attributed to better interfacial adhesion between jack pine wood fibers and HDPE matrix. In a previous study and under the same conditions, we concluded that this compatibility between jack pine wood fibers and HDPE matrix was the result of esterification efficiency between hydroxyl groups on the fiber surface and coupling agent (MAPE) (Bouafif *et al.*, 2008c). It is noteworthy that, at temperatures higher than 75 °C, the storage modulus of the jack pine-HDPE composites fell rapidly and reached the same values as for eastern white cedar-based composites. This can be primarily explained by the onset of the debonding process and interface failure due to the precocity of the melting point of the ethylene-maleic anhydride copolymers, reported at from 104 °C to 107 °C. The storage modulus of the bark-based composites showed a different behavior, especially in the positive temperature range, where it dropped more swiftly.

However, composites filled with coarse particles (24 mesh) showed higher storage modulus (Figure 8.1c). The effect was significant only for composites with higher filler content (45 wt%), whereas with lower filler content, the effect of particle size on storage modulus was ambiguous. Compression molded samples showed the highest storage modulus, followed by injection molded samples. Extruded composites showed by far the lowest E′ values. Whereas void volumes in the inner structure of extruded samples (Figure 8.2d) (see also appendix 6) can explain their weaker behavior, the cooling rate of HDPE composites at the end of the manufacturing process can explain the high E′ values of compression molded composites (Khanna *et al.*, 1985; Matthews *et al.*, 1999; Pegoretti *et al.*, 2000).

8.5.2 Loss modulus

The dynamic loss modulus or viscous modulus E" in viscoelastic solids measures the energy dissipated as heat due to relaxation in the viscous portion (Meyer and Chawla, 1999). It is widely used to clarify internal motion mechanisms (Popli and Mandelkern, 1983; Popli *et al.*, 1984a; Khanna *et al.*, 1985; Sha *et al.*, 1991; George *et al.*, 1996;

Pegoretti *et al.*, 2000). Before analyzing the effects of the intrinsic characteristics of wood fillers and processing methods on the dynamic mechanical behavior of wood-based composites, the significance of mechanical loss peaks and their relationship to the physical and structural parameters of the HDPE virgin matrix is discussed.

According to Khanna *et al.* (1985), analysis of the loss modulus of polyethylene prior to melting reveals three peaks known as the α, β, and γ transitions (Figure 8.2a). The α-transition is associated with chain segment mobility in the crystalline phases, which is probably due to reorientation of defects in the crystals rather than in the discrete (or bulk) amorphous phase (Mohanty *et al.*, 2006). For the studied HDPE, α-peak was observed at 46.79 ±1.07 °C. Similarly, Boyd (1985) and Khanna et al. (1985) reported that α-peak location in temperature (T_α) was very sensitive to thermal history. In addition, most findings on α-relaxation confirm Boyd's mechanism, in which α-relaxation was attributed to the deformation of interfacial regions (chain folds, loops, tie molecules). In other words, T_α depends on crystallite thickness. Thicker crystals (lamellae) therefore produce higher-temperature relaxation (Khanna *et al.*, 1985).

The β-transition occurred at -35.8 ± 0.49 °C (Figure 8.2a) in the studied HDPE matrix. However, in contrast to the α-transition, the β-relaxation lacks a clear peak. Although the β –relaxation is commonly attributed to the motion of branches in the amorphous matrix (Boyd, 1984; Popli *et al.*, 1984a; Khanna *et al.*, 1985), the true origin of the β–relaxation remains highly controversial. Three main hypotheses (Sha *et al.*, 1991) have been proposed to explain its origin: (i) diffusional motion of branch points, (ii) relaxation of crystalline-amorphous interfacial components (Popli and Mandelkern, 1983), and (iii) glass-rubber transition of the constrained amorphous component. The third view was strongly supported by Khanna et al. (1985) and Boyer (Boyer, 1973), who considered the β–relaxation as the glass transition in polyethylene. In this study, it was assumed that the more intense β-relaxation peak could be simply explained by the higher amorphous fraction. The γ-relaxation for HDPE is shown at -108.50± 1.57 °C. Although it is commonly agreed that γ-relaxation occurs in both

semicrystalline and completely amorphous state, the origin of this relaxation remains contested. Boyd (1984) suggested that the γ-relaxation has its origin in relatively localized molecular motions.

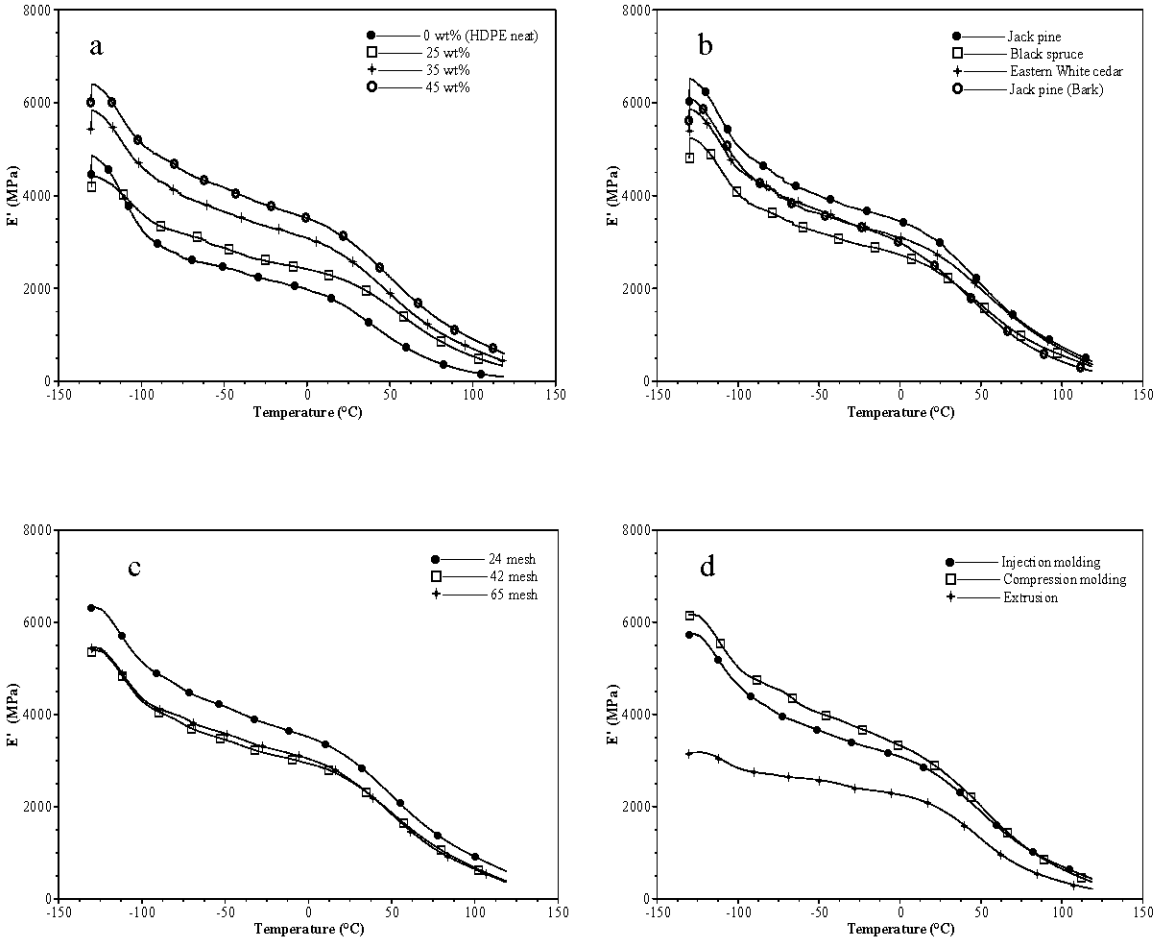

Figure 8.1. Storage modulus of (a) eastern white cedar particle(42 mesh)/HDPE composites, (b) wood particle(35 wt%, 24 mesh)-based composites (c) jack pine(35 wt%)/HDPE composites, and (d) jack pine(35wt%, 24 mesh)/HDPE composites

Table 8.1 presents the maximum temperature of α- and γ-relaxation peaks for virgin HDPE and its composites by load, type, filler size, and processing method. The α-relaxation peak for HDPE exhibited a marginal shift to high temperature regions with the addition of wood fibers and MAPE (Figure 8.2a, Table 8.1). Moreover, resultant E″ at this temperature increased by 17% to 30%, indicating more viscous dissipation with the addition of wood filler. These results are in good agreement with previous findings (Saha *et al.*, 1999; Mohanty *et al.*, 2006). Sha et al. (1991) found that α-transition temperature increased with decreasing branching, whereas Laredo *et al.* (1999) suggested that the location of the α-transition depended primarily on crystallite thickness, and crystallinity level and the supermolecular structure did not significantly influence the transition location. On the other hand, when structural and chemical factors were incorporated in the chain, such as branching or copolymerization with non-crystallizable units, i.e., MAPE, transition intensity decreased (Sha *et al.*, 1991). Accordingly, broader α-transition regions could only be attributed to inhibition of the relaxation process within the composites with the addition of wood particles (Mohanty *et al.*, 2006). Wood particle nucleation offers another plausible explanation of the broader α-transition regions. Thus, Bouafif *et al.* (2009) showed that adding wood particles affected HDPE crystallinity.

Figure 8.2b plots E'' versus temperature of various wood particle-based composites. The two main observations emerging from Figure 8.2b and Table 8.1 are that (i) the jack pine/HDPE composite shows the highest corresponding loss modulus; (ii) eastern white cedar shows an upward shift to high temperature regions (55.95±2.18 °C). The broadening of the α-transition region for the jack pine-based composite can be attributed to higher HDPE crystallinity due to the higher nucleation efficiency of jack pine wood particles. However, the higher peak temperature shift in eastern white cedar-based composites remains unexplained.

Figure 8.2c shows the effect of particle size on the mechanical relaxation behavior of wood/HDPE composites. At the same filler content, HDPE matrix filled with coarse particles (24 mesh) showed a marginal broadening of the α-transition region. Moreover, the transition location was somewhat similar in composites with different particle sizes (Table 8.1).

As expected, more differences in the α-transition region were detected in composites made with different processing methods (Figure 8.2d, Table 8.1). The temperature location of the α-peak in extruded samples shifted by, only 2.6 °C from the maximum temperature of the α-transition in virgin HDPE. Furthermore, the corresponding loss modulus was almost 70% smaller than those of injection and compression molded composites. It was mentioned above that slow-cooled composites (compressed and injection molded samples) have higher storage modulus, attributed to increased crystallinity (Khanna *et al.*, 1985; Matthews *et al.*, 1999). Accordingly, quenched composites (extruded samples) contain higher amorphous fractions. This is confirmed by the β–relaxation peak occurring at around -35 °C, which is commonly attributed to the relaxation of crystalline-amorphous interfacial components. In addition, fast cooling or quenching of the samples significantly affects the α-peak, while the lower dynamic moduli of the extruded samples is attributed to the presence of voids at the interface that weaken the bonds and produce composites of lower stiffness and strength. The intensity of γ- peak relaxation increased with the addition of wood particles, indicating mainly the involvement of the amorphous phase with the maleated co-polymers (MAPE). The γ-peak temperature decreased with the addition of wood fibers (Figure 8.2, Table 8.1). This result is in good agreement with those of Mohanty *et al.* (2006), who reported that γ- peak temperature decreased with the addition of either treated or untreated jute fibers in HDPE matrix.

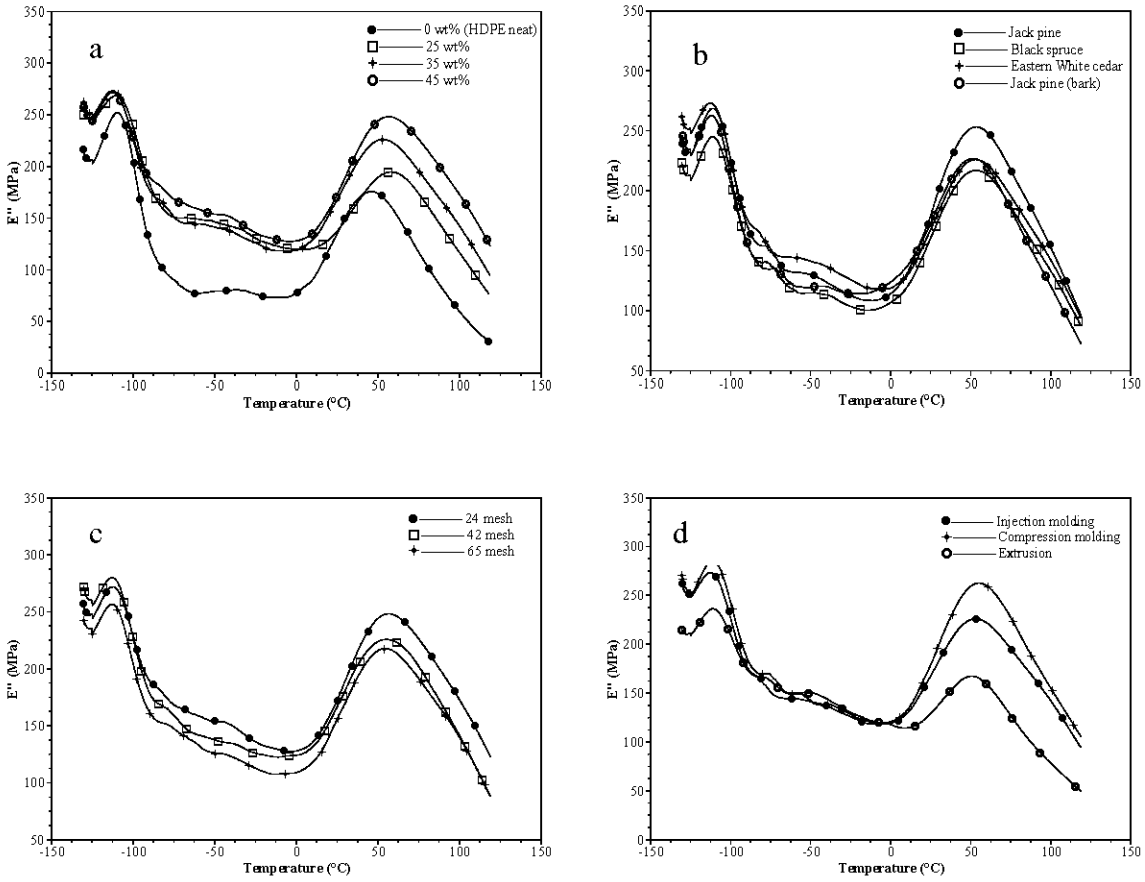

Figure 8.2. Loss modulus of (a) eastern white cedar particle (42 mesh)/HDPE composites, (b) wood particle (35 wt%, 24 mesh)-based composites (c) jack pine (35 wt%)/HDPE composites and (d) jack pine(35wt%, 24 mesh)/HDPE composites.

8.5.3 Frequency–temperature dependence

Figure 8.3 presents some E′, E″, and damping factors (tanδ) plotted against temperature using the frequency scanning method for the 45 wt% eastern white cedar/HDPE composites. The test objective was limited to just the α-peak of the temperature regions. As it can be seen, E′ increases with increased frequency,

whereas tan δ and E″ decrease for both HDPE and composites. Moreover, α-peak (maximum of E″) tends to shift to lower temperatures as frequency decreases. Based on the time–temperature principle in viscoelastic materials whereby the effect of longer time (lower frequency) is equivalent to that of higher temperature, frequency–temperature dependence can be expressed by the Arrhenius equation, as follows:

$$Ln(\omega) = \mathrm{A}e^{-\Delta E/RT} \qquad (8.1)$$

where ΔE is the relaxation activation energy corresponding to the potential barrier hindering molecular motion, and R denotes the universal gas constant.

Figure 8.4 presents examples of Arrhenius plots of α-relaxation peaks for composites with various filler properties. All curves showed slightly similar slopes, and curves varied only by temperature intercept. This result was expected because the slope, as expressed in the linear form of the Arrhenius equation (1), is directed by the activation energy, which is typical for the polymer. Moreover, the above-presented analysis of the effect of wood filler characteristics on α-transition remains valid. Table 8.2 compiles the activation energy results for all investigated composites, taking into account wood filler characteristics (content, type, shape, and processing method). The calculated activation energy of HDPE was equal to 82.93±3.22 KJ/mol, which is in the same range as those reported in previous studies: 50–140 KJ/mol (Stadler *et al.*, 2005), 65–80 KJ/mol (Boiko and Sherman, 1998), and 79–106 KJ/mol (Matsuo *et al.*, 1988). A slight increase in ΔE was detected after wood particle addition, which can also be explained by increased crystallinity. Only the extruded composites showed substantial lower activation energy. This can be explained by the quenching water of the extruded samples, which affected HDPE crystallinity. The potential barrier for molecular arrangements consequently decreased because fewer cooperative motions among neighboring chains were required (Stadler *et al.*, 2005).

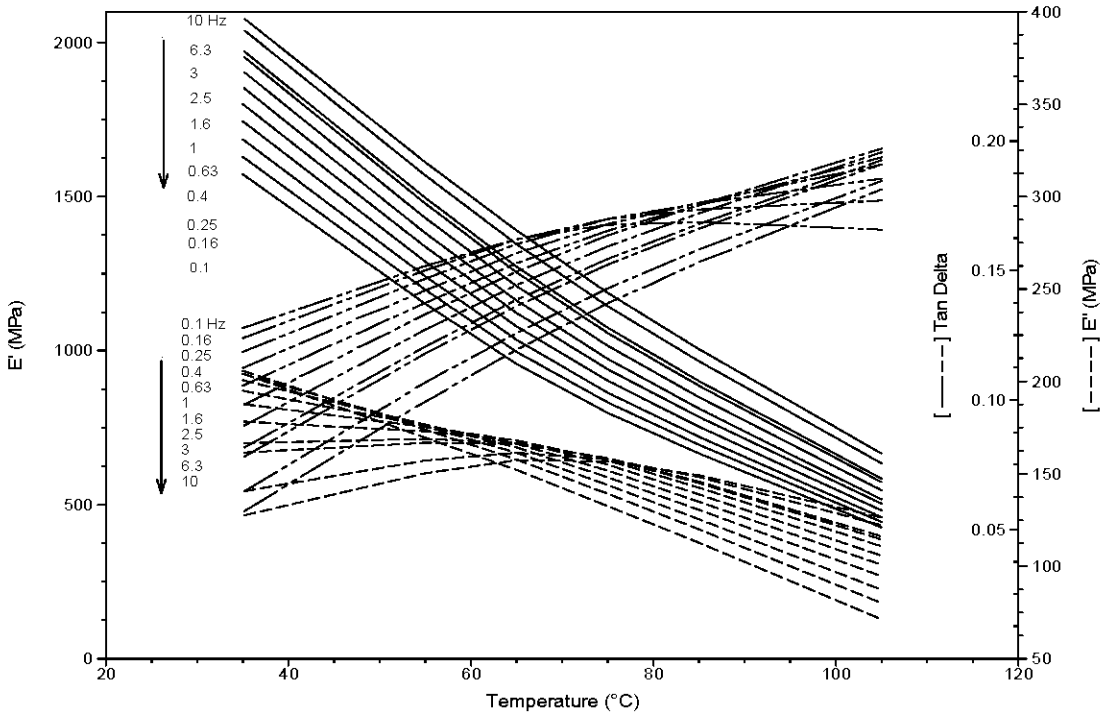

Figure 8.3. Example of dynamic mechanical behavior of injection molded jack pine (35 wt%, 24 mesh)/HDPE composites as a function of temperature and frequency sweeping.

Table 8.1. Localization of α- and γ- peak temperature relaxations and corresponding dynamic moduli of various composite designs.

		α-relaxation						γ-relaxation					
		T_α (°C)		E'_α (MPa)		E''_α (MPa)		T_γ (°C)		E'_γ (MPa)		E''_γ (MPa)	
		Mean	SD	Mean	SD	Mean	SD	Mean	SD	Mean	SD	Mean	SD
Load	0 wt% (HDPE neat)	46.8	1.1	989	74	166.9	11.5	-108.5	1.6	3558	449	254.9	4.3
	25 wt%	52.6	4. 6	1408	111	201.9	11.9	-110.7	0.4	4459	257	254.5	11.1
	35 wt%	53.2	2.7	1664	106	226.8	13.9	-111.4	0.5	5065	183	260.7	15.3
	45 wt%	54. 8	1.3	1802	141	235.0	13.9	-112.1	0.6	5366	499	267.0	12.6
Species	Jack pine	53.5	2.2	1770	168	226.6	12.9	-111.5	0.5	5086	548	256.3	5.9
	Eastern white cedar	56.0	2.7	1634	227	221.0	21.9	-111.4	1.0	4817	521	269.4	10.3
	Black spruce	51.9	2.4	1570	225	205.8	15.9	-110.5	0.6	4652	354	241.7	4.7
	Bark	51.3	2.5	1571	198	221.5	19.6	-111.5	0.8	5095	528	256.6	12.7
Particle size	24 mesh	53.6	2.7	1685	245	222.0	24.2	-111.3	0.8	5021	698	262.0	13.5
	42 mesh	53.6	4.3	1537	156	212.0	14.7	-111.4	1.1	4694	282	260.1	16.7
	65 mesh	53.1	3.0	1612	195	226.8	16.6	-111.5	0.8	5095	379	259.1	11.6
Processing method	Injection molding	53.5	3.2	1615	205	220.3	19.3	-111.4	0.9	4940	507	260.5	13. 5
	Compression molding	53.4	0.7	1575	100	222.5	10.0	-110.2	0.2	4686	103	249.8	11. 7
	Extrusion	49.4	1.8	1186	372	156.0	47.7	-110.4	1.8	2919	429	229.2	78.4

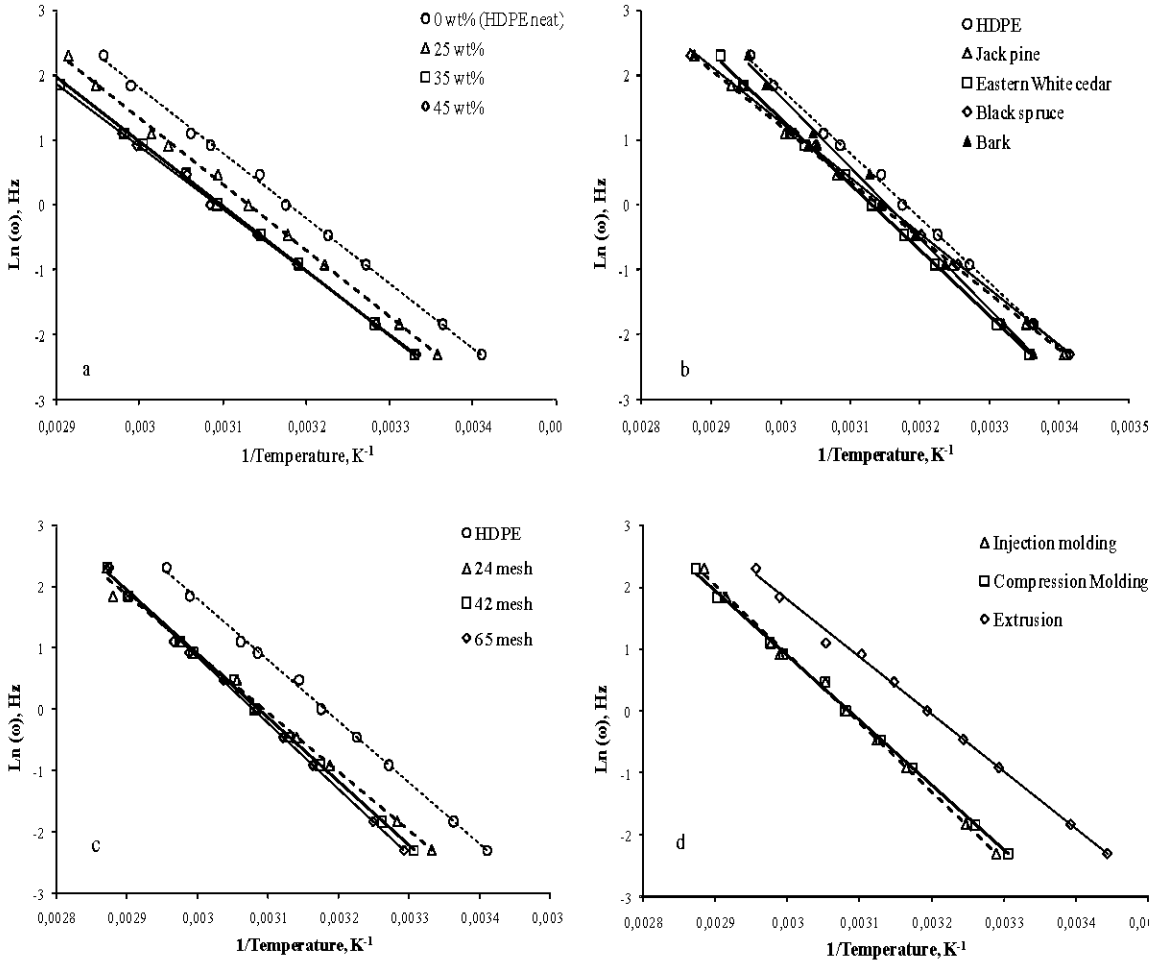

Figure 8.4. Examples of Arrhenius plots for α-relaxation peaks of (a) eastern white cedar particle(42 mesh)/HDPE composites, (b) wood particle(35 wt%, 24 mesh)-based composites (c) jack pine(35 wt%)/HDPE composites, and (d) jack pine (35 wt%, 24 mesh)/HDPE composites

Table 8.2. Activation energy for the α-relaxation in HDPE and its composites.

Composite design		α-transition ΔE (KJ/mol)	
		Mean	SD
Load	0 wt% (HDPE neat)	82.93	3.22
	25 wt%	84.48	4.17
	35 wt%	85.43	4.04
	45 wt%	85.68	3.88
Species	Jack pine	85.82	5.01
	Eastern white cedar	83.84	4.32
	Black spruce	83.53	3.33
	Bark	83.75	5.22
Particle size	24 mesh	84.36	3.88
	42 mesh	84.76	3.59
	65 mesh	85.27	4.31
Processing method	Injection molding	86.53	5.11
	Compression molding	84.99	4.99
	Extrusion	79.73	6.22

8.6 Conclusion

The mechanical and dynamic mechanical properties of wood particle/HDPE composites were investigated. Increased stiffness of the HDPE matrix due to the reinforcing effect of wood particles was observed. The higher the percentage of added wood, the higher is the increment in the storage modulus of the composites. However, storage modulus decreased with increased temperature in all samples. Jack pine-based composites showed the highest storage modulus, attributable to better interfacial adhesion between jack pine wood fibers and matrix. Composites filled with coarse particles (24 mesh) showed higher storage moduli. The α-relaxation peak of HDPE exhibited a marginal shift to higher temperature regions with the addition of wood fibers, while the resultant E″ increased by 17% to 30%, indicating more viscous dissipation with the addition of wood filler.

The effect of particle size on the mechanical relaxation behavior of wood/HDPE composites showed a marginal broadening of the α-transition region with coarse particles (24 mesh). The intensity of γ- peak relaxation increased with the addition of wood particles, indicating mainly the involvement of the amorphous phase with maleated polyethylene (MAPE) co-polymers. However, intensity decreased with the incorporation of wood fibers. Quenching of the extruded samples significantly affected α-peak temperature, while the lower dynamic moduli of these samples was attributed to the presence of voids at the interface that weaken bonds and produce composites of lower stiffness and strength.

E′ increased with increasing frequency, whereas tan δ and E″ decreased in both HDPE and composites. It was also found that α-peak tended to shift to lower temperatures as frequency decreased. Finally, a slight increase in ΔE was detected after wood particle addition, which may be explained by the increased in crystallinity due to the nucleation efficiency of wood filler.

CHAPTER IX

CREEP BEHAVIOR OF HDPE/WOOD PARTICLE COMPOSITES

9.1 Abstract

The effect of wood particle type, size, content and processing conditions on the creep behavior of wood particles/high density polyethylene (HDPE) composites has been investigated. Short-term creep tests at different temperature levels were carried out and modeled using Bürger's model and Findley's power law. The relative creep of the composites increases with increasing temperature which is explained by the mobility of the amorphous bulk and tie molecules of HDPE. Wood particle addition generally reduces the creep level. Jack pine fibers based composites exhibited the best creep reduction. This behavior is related to the chemical composition on the surface of wood fibers and the efficiency of the adhesion mechanism between fibers and HDPE. Master curves, constructed by applying the time-temperature superposition principal (TTSP), depict non similar tendencies with Findley-extrapolated data. Results from the short-term creep measurement were used to predict the dynamic mechanical behavior. A good agreement between calculated and predicted values was observed only at moderate frequency (0.5 to 1.5 Hz). The use of a continuous retardation spectrum is recommended to better predict the dynamic mechanical properties of the investigated wood based composites.

9.2 Résumé

L'effet de l'essence de bois, la taille et la teneur en particules dans le mélange ainsi que les méthodes de mise en forme sur le comportement au fluage des composites bois/polyéthylène haute densité (PEHD) a été étudiée. Les essais de fluage à court terme pour différentes températures ont été étudiés moyennant le recours au modèle de Burger et la loi de puissance de Findley. Le fluage des composites augmente avec la température. Ceci s'explique par la mobilité des molécules dans la fraction amorphe du PEHD. Globalement, les particules de bois permettent de réduire le niveau de fluage des composites. Les composites à base de fibres de pin gris ont montrée une meilleure résistance au fluage. La variation de la résistance au fluage entre les composites est lié à la composition chimique de la surface des fibres du bois et donc, l'efficacité du mécanisme d'adhésion entre les fibres et le PEHD. Les Courbes maîtresses, construites en appliquant le principe de superposition temps-température (TTSP), ont présentées des divergences avec celle obtenues par extrapolation de la loi de Findley. Les résultats de mesure du fluage à court terme ont été utilisés pour prédire le comportement mécanique dynamique. Une bonne concordance entre les valeurs calculées et les valeurs prédites n'a été observée qu'à des fréquences modérées (0,5 à 1,5 Hz). L'utilisation d'un spectre continu de temps de retard est recommandée pour mieux prédire les propriétés mécaniques dynamiques des composites bois/plastiques.

9.3 Introduction

The effect of service environment on material performance can be divided into 3 main categories: (i) Micro-structural changes, such as physical aging; (ii) Chemical effects, such as oxidation and (iii) Mechanical effects, such as creep and rupture. The micro-structural changes can lead to weakening of the material, and therefore can indirectly lead to failure, while oxidation and creep can directly lead to material

failure in service. Creep is defined as a time dependent deformation which occurs under stress. Generally, unsteady structures change during long-term service and this leads to reduction in creep strength. Therefore, many of the strengthening mechanisms that are effective at fixed room conditions (static mode) become ineffective in service where temperature and/or humidity change persistently (dynamic mode).

Commonly known as viscoelastic deformation, creep of polymers occurs as a result of the molecular motions in backbone polymer arrangement. However, creep of the reinforced polymer matrix (composites) arises, not only when molecular chain of the polymer matrix moves but also when the reinforcement components dislocate or slide. As time progresses, the creep deformation may exceed the limit for structures. Creep rupture (so called stress rupture) occurs long after the load has been applied.

Thermoplastics reinforced with wood fillers are enjoying rapid growth due to their advantages, such as light weight, reasonable strength, durability and stiffness. Their processing is flexible, economical, and ecological. However, creep and creep rupture considerations are essential especially in structural applications of wood-fiber/thermoplastic composites.

Recently, few studies on polymer matrix composites creep behavior have been reported. Park and Balatinecz (1998) investigated the effect of wetting agent, temperature, and wood-fiber concentration, on creep behavior of wood-fiber polypropylene (PP) composites. They concluded that the addition of a wetting agent greatly reduced the creep at high stress level, but had little effect at a lower stress level, while the extent of relative creep increased with increasing temperature. On the other hand, the relative creep of the composites decreased with an increase in wood-fiber concentration. However, the composite showed relatively large creep compared with that of solid wood. More recently, Nuñez *et al.* (2004) reported that, at very high

filler concentrations, the creep deformation was generally raised because of filler-wetting and dispersion problems. Sain *et al.* (2000) studied the creep behavior of unmodified and functionally modified wood/ thermoplastic fiber composites. They reported that Maleic or maleimide modification of wood fiber improved transient creep behavior of PP-wood fiber composite but did not show practically any effect on instantaneous creep.

Acha *et al.* (2007) investigated the effect of the interfacial adhesion on the creep and dynamic mechanical behavior of PP–jute composites. They found that the highest creep deformation was exhibited for the composites prepared from esterified samples, while creep strain and deformation of samples prepared with compatibilizers showed the lowest values. Govindarajan *et al.* (1996) compared the influence of two different void volume fractions on the creep behavior of compression molded polymer/woven graphite fiber composites at elevated temperature levels. They noted that the lower void content implies a higher modulus, due to more matrix material, and so enables lesser elastic and creep strains. In addition, the creep performance of short wood fiber reinforced thermoplastics is greatly affected by the nature of the stress transfer which itself depends on the fiber–matrix interfacial force of interaction, as well as on the nature of the interface.

Although the effects of interfacial properties, chemical composition, stress level, time, and temperature help to predict the short- and long-term creep behavior of wood-fiber/thermoplastic composites in structural applications, studies that take into account the geometrical effect of wood fibers and the processing conditions are still scarce. Therefore, the aim of this work is to investigate the creep performance of wood particle-HDPE composites, taking into account the wood particle type, shape and concentration as well as the processing conditions. Then, the viscoelastic behavior of the investigated materials was modeled using mechanical analogies and the accuracy of the predictions was discussed. The fitting parameters for the Bürger's

model were finally used to predict the dynamic mechanical behavior of the composites.

9.4 Theoretical background

The creep compliance, J(t, σ (t), T), is frequently used to describe the creep behaviour of a material. This function is usually assumed to depend on creep time, real stress and temperature. In the domain of linear viscoelasticity, the dependence on real stress vanishes. A schematic curve of creep compliance vs. time at constant temperature over a very wide time scale is shown in Figure 9.1. In this case of a typical amorphous polymer, the creep compliance can be divided into four stages :(i) glassy status in which the compliance is almost independent of time;(ii) viscoelastic behavior where the compliance is time dependent; (iii) rubbery behavior where the compliance presents a plateau; (iv) and finally, the polymer behaves as a viscous liquid.

9.4.1 Bürger's Model

The common practice to simulate the combined viscous and elastic behavior of a material is the use of mechanical analogies that include viscous elements (dashpots) and elastic elements (springs). Bürger's model (Figure 9.2) is widely used to analyze the viscoelasticity of materials with a Maxwell and a Kelvin unit connected in series. When a constant stress is applied, the total strain ε_B at time t is the sum of the strains in the three constitutive units (Figure 9.2). For N Kelvin's elements, the generalized form of ε_B is given in equation 1 (see (Ward, 1983) for detailed deduction).

$$\varepsilon_B(t) = \frac{\sigma}{E_M} + \sum_{i=1}^{N} \frac{\sigma}{E_{K_i}} \cdot \left[1 - e^{-t/\tau_i}\right] + \frac{\sigma}{\eta_M} \cdot t \qquad (9.1)$$

Where E_M and η_M are the modulus of elasticity and viscosity of the Maxwell spring and dashpot, respectively; E_{K_i} and η_{K_i} are the modulus of elasticity of the spring and the viscosity of the dashpot of the i[th] Kelvin-Voigt element, respectively; σ is the stress level, applied at $t = 0$; and $\tau_i = E_{K_i} / \eta_{K_i}$ the retardation time of the i[th] element.

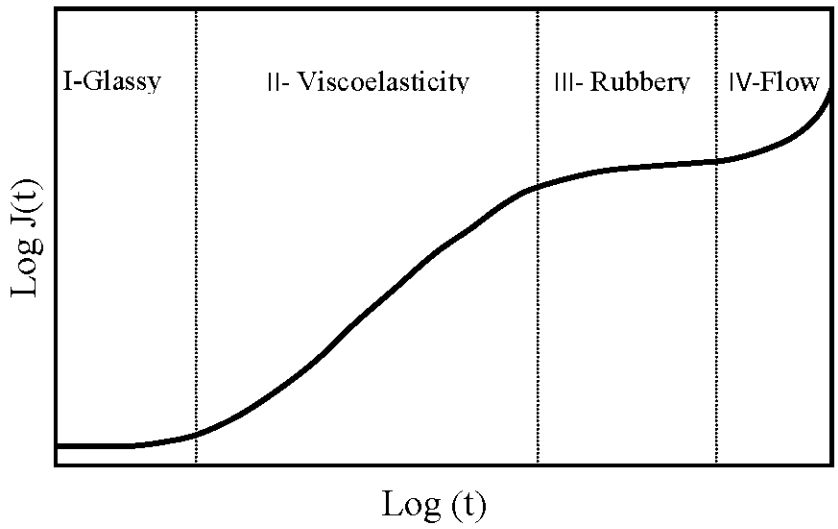

Figure 9.1. Scheme of the curve of the creep compliance vs. time.

Assuming that the study of the material behavior is limited to the linear viscoelastic region, at a unique temperature level, the creep compliance is a function of time only:

$$J(t) = \frac{1}{E_M} + \sum_{i=1}^{N} \frac{1}{E_{K_i}} \cdot \left[1 - e^{-t/\tau_i} \right] + \frac{1}{\eta_M} \cdot t \qquad (9.2)$$

The first term of the right-hand side of equation (2) is constant and describes the instantaneous elastic deformation of the Maxwell element. The second term is the delayed elasticity of the Kelvin elements which have the sum of $1/E_{K_i}$ as asymptote; the third term is the viscous flow which increases linearly as soon as the load is applied. The material parameters E_M, η_M, E_{K_i} and η_{K_i} were found from the best

fitting with experimental data using a nonlinear least-squares optimization algorithm. The variation of the simulated parameters will constitutively show the effect of wood particle filler, load, shape and processing conditions.

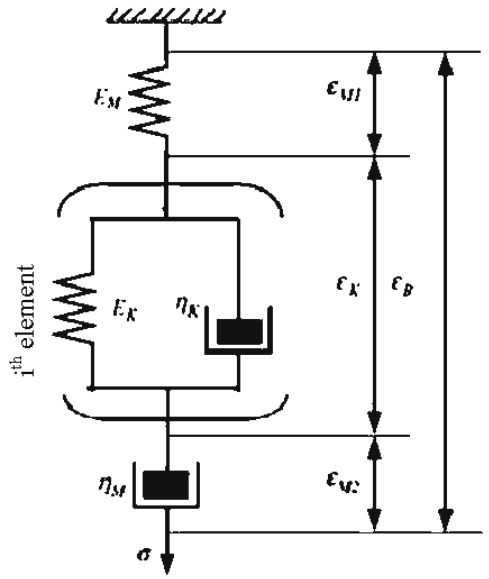

Figure 9.2. Schematic diagram of the generalized Burgers model.

9.4.2 Findley power law

The Findley power law is also widely used to express strain-time relationship for viscoelastic materials (Park and Balatinecz, 1998; Cyras *et al.*, 2002; Nunez *et al.*, 2004). The advantage of the following empirical power equation is the fact that it can describe the creep behavior under constant load of many polymers over a large time scale with few parameters:

$$\varepsilon_F(t) = a + bt^n \qquad (9.3)$$

Where a, b and n are empirical parameters.

J(t) can be simply deduced from equation (3), as a dimensionless strain :

$$J(t) = A + Bt^n \qquad (9.4)$$

Where A = a/σ and B = b/σ.

Many creep experiments intend to predict long-term creep from short-time tests. Assuming that the polymer does not change its structure with time, the time-temperature-superposition (TTS) principle is the most acceptable method to predict viscoelastic behaviour. TTS implies that the viscoelastic behavior at one temperature can be related to that at another temperature by a change in the time scale. Thus, the creep curves obtained at different temperatures are superposed by horizontal shifts along a logarithmic time scale (ln a_T) to obtain a master curve. The shift factor can be calculated by means of the Williams-Landel-Ferry (WLF) equation (equation9.5) or the Arrhenius equation (equation 6) (Ward, 1983) :

$$\ln a_T = -\frac{C_1(T - T_{ref})}{C_2 + (T - T_{ref})} \qquad (9.5)$$

Where; C_1 and C_2 are constants dependent on the material. T_{ref} is the reference temperature.

$$\ln a_T = \frac{\Delta H}{2.303R}\left(\frac{1}{T} - \frac{1}{T_{ref}}\right) \qquad (9.6)$$

Where ΔH is an activation energy and R is the universal gas constant.

9.4.3 Harmonic tests

Bürger's model can be used to predict the mechanical response of the material in the linear viscoelastic region for a harmonic test of frequency ω (Nunez *et al.*, 2004):

$$J'(\omega) = \frac{1}{E_M} + \sum_{i=1}^{N} \frac{E_{K_i}}{E_{K_i}^2 + (\eta_{K_i} \cdot \omega)^2} \tag{9.7}$$

$$J''(\omega) = \sum_{i=1}^{N} \frac{\eta_{K_i} \cdot \omega}{E_{K_i}^2 + (\eta_{K_i} \cdot \omega)^2} + \frac{1}{\eta_M \cdot \omega} \tag{9.8}$$

$$E'(\omega) = \frac{J'(\omega)}{J'(\omega)^2 + J''(\omega)^2} \tag{9.9}$$

$$E''(\omega) = \frac{J''(\omega)}{J'(\omega)^2 + J''(\omega)^2} \tag{9.10}$$

$$\tan\delta = \frac{E''}{E'} = \frac{J''}{J'} \tag{9.11}$$

Where ω is the frequency, J′ and J″ are the storage and loss compliance, respectively; E′ and E″ are the storage and loss modulus, respectively, and *tanδ* is the damping factor.

9.5 Experimental

9.5.1 Creep Tests

A TA Instruments Dynamic Mechanical Analyzer (DMA 2980) was used in the short-time creep experiments for a test duration of 15 minutes. The tests were carried out in the creep mode, using a dual cantilever measuring clamp. The tests were carried out in seven temperature scanning mode from 35°C to 105°C by a step of 10°C. The equilibrium time was five minutes.

9.5.2 Dynamic Mechanical Tests

The same equipment reported for the short-time creep tests are used. In these experiments, the storage modulus (E′), loss modulus (E″) and phase lag (tanδ) were measured. Frequency sweeping was stepped in logarithmic increments from 0.1 Hz to 10 Hz. Equilibrate time and heating rate were maintained the same as for the short-time creep measurements.

9.5.3 Simulation method

The functions of the Bürger's model with four undetermined parameters (N = 1) and the Findley power law with three undetermined parameters were defined by using the non-linear curve fit function in Maple 11 (Maplesolft, ON, Canada). The simulation was performed by the program using a least square approximation procedure.

9.6 Results and discussions

9.6.1 Effect of Temperature

The representative experimental curves of creep compliance vs. creep time of the 35 wt% of 24 mesh eastern White cedar wood particles based composites, tested at different temperature levels between 35°C and 105°C, are presented in Figure 9.3. The fitted curves by using both Bürger's model and Findley power law are in good agreement with the experimental data for each temperature level. Note however that the Findley power law gives a better trend at long time, especially for the higher temperature level. The modeling parameters are listed in Table 9.1.

Table 9.1. Fitting parameters of Burgers and Findley models. Composites made with 35 wt% of eastern white cedar (24 mesh)

T (°C)	Bürgers Model				τ (s)	Findley Model		
	E_M (GPa)	E_K (GPa.)	η_K (GPa.s)	η_M (GPa.s)		A	B	n
35	1.67	2.99	136.71	3115.26	45.66	$4{,}64 \times 10^{-11}$	$4{,}61 \times 10^{-10}$	0,136
45	1.37	2.21	101.02	2398.08	45.66	$1{,}68 \times 10^{-11}$	$7{,}65 \times 10^{-10}$	0,117
55	1.15	1.73	72.21	1930.50	41.67	$-5{,}74 \times 10^{-10}$	$1{,}28 \times 10^{-09}$	0,095
65	1.01	1.33	49.32	1686.34	37.04	$-1{,}59 \times 10^{-10}$	$2{,}45 \times 10^{-09}$	0,065
75	0.79	1.33	41.61	1560.06	31.25	$-4{,}03 \times 10^{-09}$	$5{,}08 \times 10^{-09}$	0,037
85	0.65	1.24	33.41	1430.62	27.03	$-8{,}98 \times 10^{-09}$	$1{,}03 \times 10^{-09}$	0,021
95	0.53	1.16	29.07	1277.14	25.00	$-5{,}87 \times 10^{-09}$	$7{,}55 \times 10^{-09}$	0,030
105	0.42	1.07	27.45	1079.91	25.64	$-1{,}41 \times 10^{-09}$	$3{,}57 \times 10^{-09}$	0,062

Figure 9.3 exhibits a strong temperature dependence of the short term creep behavior. The same comment remains valid for all experimental conditions. The creep compliance is often large at higher test temperatures. It is well documented that this viscoelastic response depends on the material structure, which is a strongly dependent on the testing temperature (Boyer, 1973; Khanna *et al.*, 1985; Read and Tomlins, 1997). As the temperature increases, the mobility of the amorphous bulk and tie molecules increases. Consequently, isostress creep compliance increases. It is noteworthy, that the analyzed temperature range remains below the melting temperature (≈ 135°C). Thus, no changes in the crystallinity were expected. In addition, the creep response is associated to the softening of the amorphous phase (folds, loops, tie molecules) which without the crystal mobility is rigidly fixed. This mechanical relaxation is so called α-relaxation. It is observed between about 20 and 60 °C for HDPE (Khanna *et al.*, 1985). According to the constitutive Eq. (9.2), the modulus E_M of the Maxwell spring determines the instantaneous elastic creep strain, which could be immediately recovered on the removal of stress, while η_M,

represented the irrecoverable creep. E_M and η_M are strongly dependent on temperature (Table 9.2). η_M at 35°C is, approximately, three times greater than that at 105°C. This is obviously the effect of thermal activation. At 35°C, the viscous flow is not activated and remains low for the experimental time range, while large instantaneous creep compliance occurred at 105°C because reptation of many thermally activated polymer chains under the external stress becomes possible. These results are in agreement with those reported by Nuñez *et al.* (2004). However, Yang *et al.* (2006) did not observe any dependence between η_M and temperature for the tensile creep resistance of polyamide 66 nanocomposites.

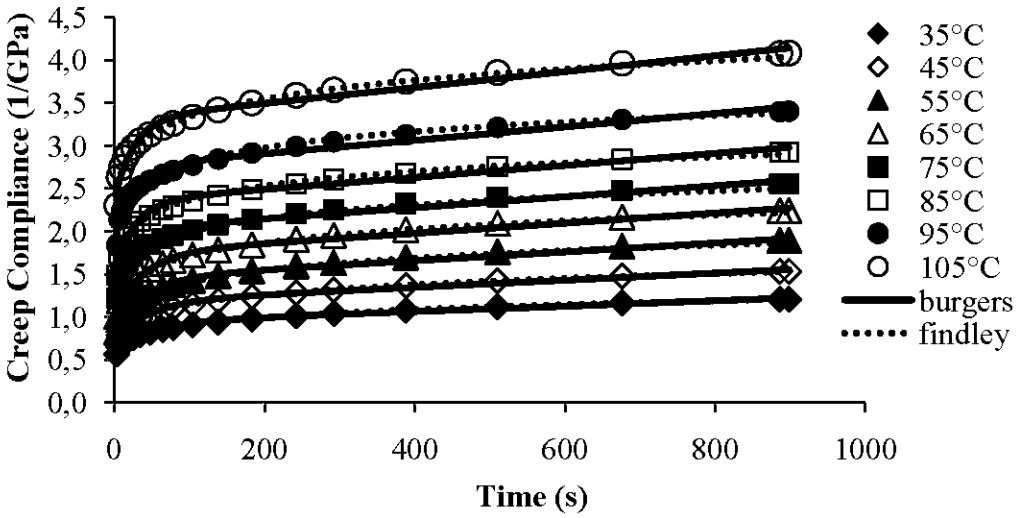

Figure 9.3. Creep compliance of composites containing 35 wt% of eastern white cedar (24 mesh) at different test temperatures.

The retardant elasticity E_K and viscosity η_K depict a similar dependency: they decrease with increasing temperature. In others words, the compliance of the Kelvin unit, corresponding to the constitutive viscoelastic creep model, increased with increasing temperature. Yang et al. (2006) associated E_K and η_K to the stiffness and viscosity of amorphous polymer chains in short term, respectively.

At the elapsed test time of 15 min, the creep compliance varies linearly with temperature (Figure 9.4), except for the extruded composites. For the latter, the creep compliance presents rather an exponential increase with temperature above 75°C. The unexpected creep behavior of the extruded samples was explained by the presence of void volumes in the material bulk (see appendix 6.). More explication on these imperfections, which occur during manufacturing, will be highlighted in the following subsections.

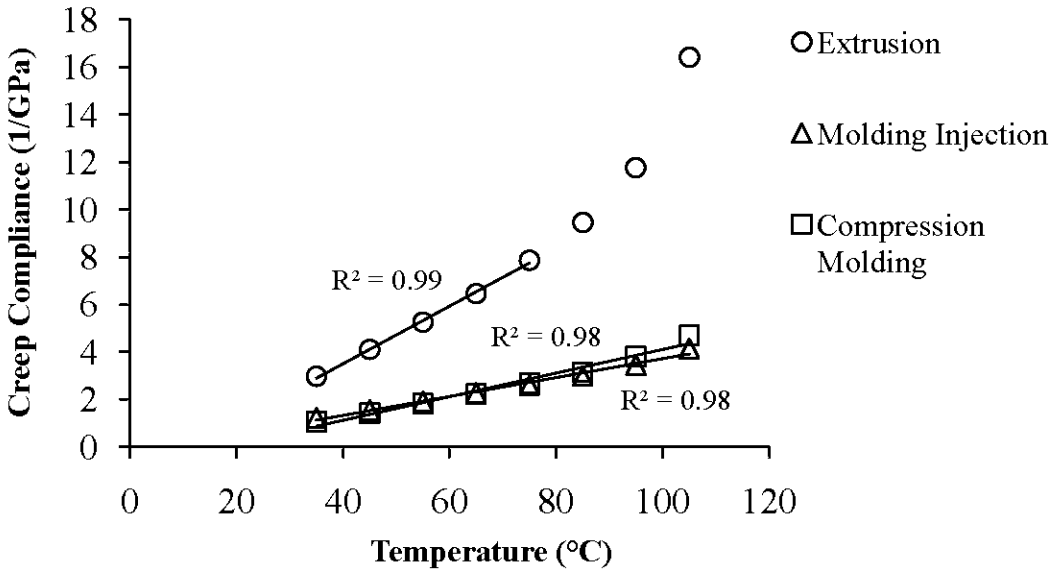

Figure 9.4. Creep compliance vs. temperature for black spruce based composites (35wt%, 42 mesh) made with different processes

9.6.2 Effect of wood species

Figure 9.5 shows the short term creep-compliance curves of molding injected composites made with different wood types at 45 wt% fiber content. The highest creep compliance is exhibited for the composites prepared from bark fibers, followed by the composites made with white cedar and black spruce wood fibers. Jack pine composites exhibit the lowest values. This behavior can be directly related to the

chemical composition of surface of the wood fibers and efficiency of the adhesion mechanism between wood fibers and HDPE matrix. In order to corroborate this, Bouafif et al. (2008c) investigated the effect of the variability in chemical composition of surface properties of the same wood fibers on esterification efficiency, using X-ray photoelectron spectroscopy (XPS). They concluded that lignin concentration variability on the wood fiber surface seems to be the major inhibitor factor for the occurrence of esterification. More specifically, its complex three-dimensional structure, with only some available reactive hydroxyl groups, largely explains its inhibition effect. In addition, the higher is the ability to form ester bonds with MAPE; the lower is the creep compliance.

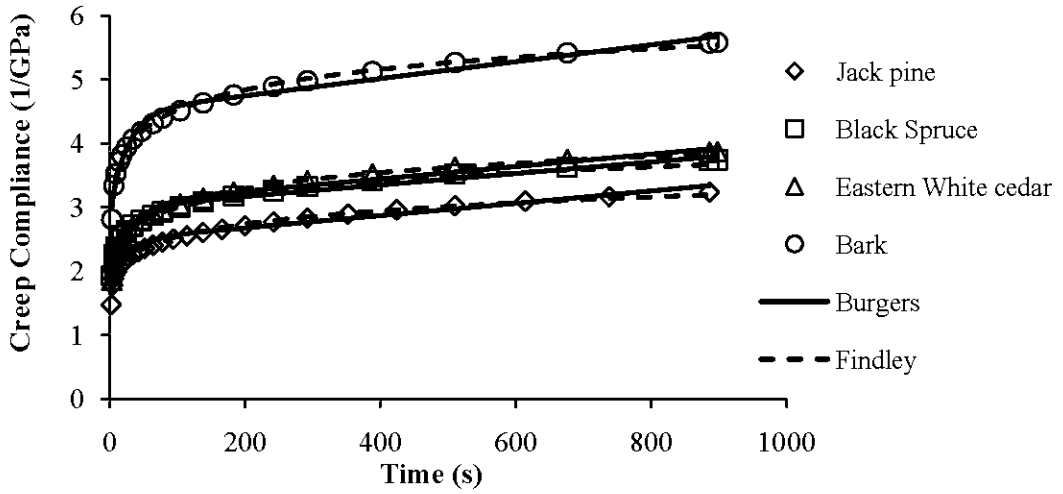

Figure 9.5. Creep compliance of composites made with 35% (24 mesh) of different wood particle reinforcement.

9.6.3 Effect of particle load

Figure 9.6 shows the short term creep tests performed on 24 mesh White cedar based composites prepared with different wood particle loads. The creep compliance decreases as the wood particle content increases. This behavior is expected from the

increased rigidity of the composites. However, the creep compliance of samples containing 35 or 45 wt% of reinforcement differs slightly, specifically at higher temperatures. At 105°C, (Figure 9.6c), an opposite behavior has been observed for samples made with 45wt%, which depicted great creep compliance values than those made with 35 wt%. This indicates that no additional reinforcement is obtained using more than 35 wt% of fibers, because the matrix did not wet the wood particle completely which might result in stress concentration. This is more pronounced for composites made with larger particles, which is in good agreement with previous findings (Nunez *et al.*, 2004; Acha *et al.*, 2007; Cyras *et al.*, 2002).

In general, the composites have higher values of E_M compared to neat matrix under each test temperature. However, E_M depicts relatively small changes between composites, especially at higher temperatures. η_M, so called steady state viscosity, showed the same pattern of variation as that of E_M., while a slight changes are observed when wood particle concentration exceeds 35 wt%, confirming a steady state of the creep behavior regardless the filler concentration.

At a given test temperature, E_K and η_K increased with increasing wood particle load (Table 9.2) which suggests that the creep resistance of the Kelvin unit increased with increasing wood particle content. This consistent variation of E_K and η_K with filler content led to a nearly constant retardant time τ at a given test temperature (Table 9.2).

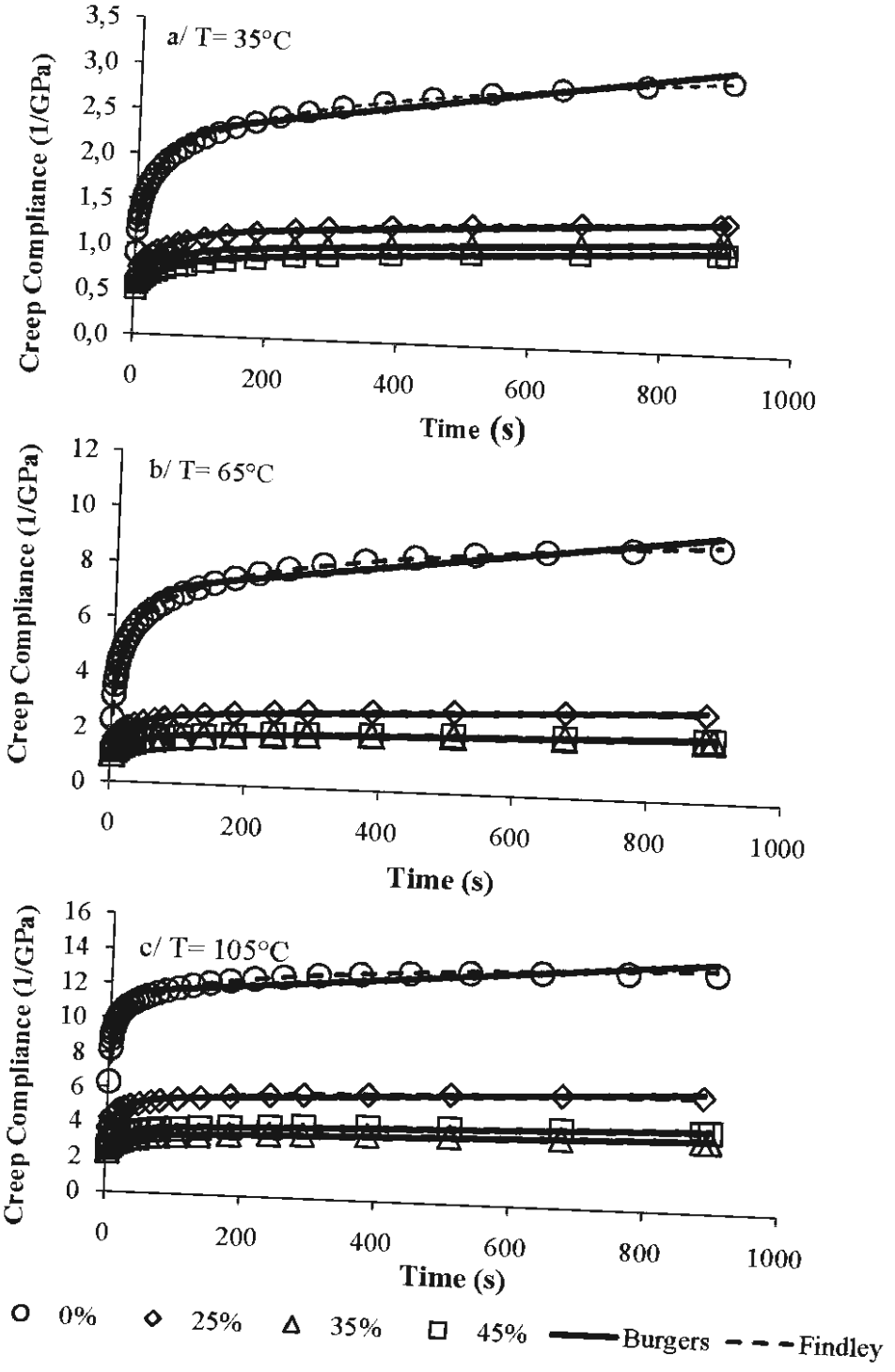

Figure 9.6. Short term creep tests for composites containing 24 mesh white cedar at different wood particle loads

Table 9.2. Fitting parameters of Burgers and Findley models for composites made with 24 mesh eastern white cedar and different wood particle content.

Load (wt %)	T (°C)	Bürgers Model				τ (s)	Findely Model		
		E_M (GPa)	E_K (GPa.)	η_K (GPa.s)	η_M (GPa.s)		A	B	n
0 % (neat HDPE)	35	0.87	0.95	30.58	989.12	32.26	-1.25×10^{-09}	2.21×10^{-09}	0.096
	65	0.33	0.26	7.26	336.81	27.93	-3.46×10^{-08}	3.70×10^{-08}	0.025
	105	0.14	0.23	2.48	316.56	10.96	-1.86×10^{-08}	2.63×10^{-08}	0.031
25%	35	1.47	2.27	103.31	2813.73	45.45	-4.86×10^{-10}	1.02×10^{-09}	0.093
	65	0.72	0.95	32.62	1082.84	34.25	-6.04×10^{-09}	7.10×10^{-09}	0.038
	105	0.27	0.63	15.07	606.06	23.81	-6.74×10^{-09}	1.01×10^{-08}	0.040
35%	35	1.67	2.99	136.71	3115.26	45.66	4.64×10^{-11}	4.61×10^{-10}	0.136
	65	1.01	1.33	49.32	1686.34	37.04	-1.59×10^{-10}	2.45×10^{-09}	0.065
	105	0.42	1.07	27.45	1079.91	25.64	-1.41×10^{-09}	3.57×10^{-09}	0.062
45%	35	1.87	3.27	163.40	3201.02	50.00	1.16×10^{-10}	3.39×10^{-10}	0.158
	65	0.98	1.40	55.94	1588.81	40.00	-1.24×10^{-09}	2.05×10^{-09}	0.079
	105	0.39	0.90	25.29	916.59	28.25	-1.87×10^{-09}	4.18×10^{-09}	0.064

9.6.4 Effect of particle size

Short term creep compliance did not show notable dissimilarities when compared with different wood particle size, although a slightly higher creep resistance was observed at lower test temperatures with injection molded composites made with 65 mesh wood particle size (Figure 9.7 a and b). This result could be explained by the fact that, in higher wood filler content (45 wt%), fine particles seems to be more recovered with the polymer and well dispersed than coarse particles leading to more rigid composites. At higher temperatures, creep behavior was the same regardless wood particle size (Figure 9.7c).

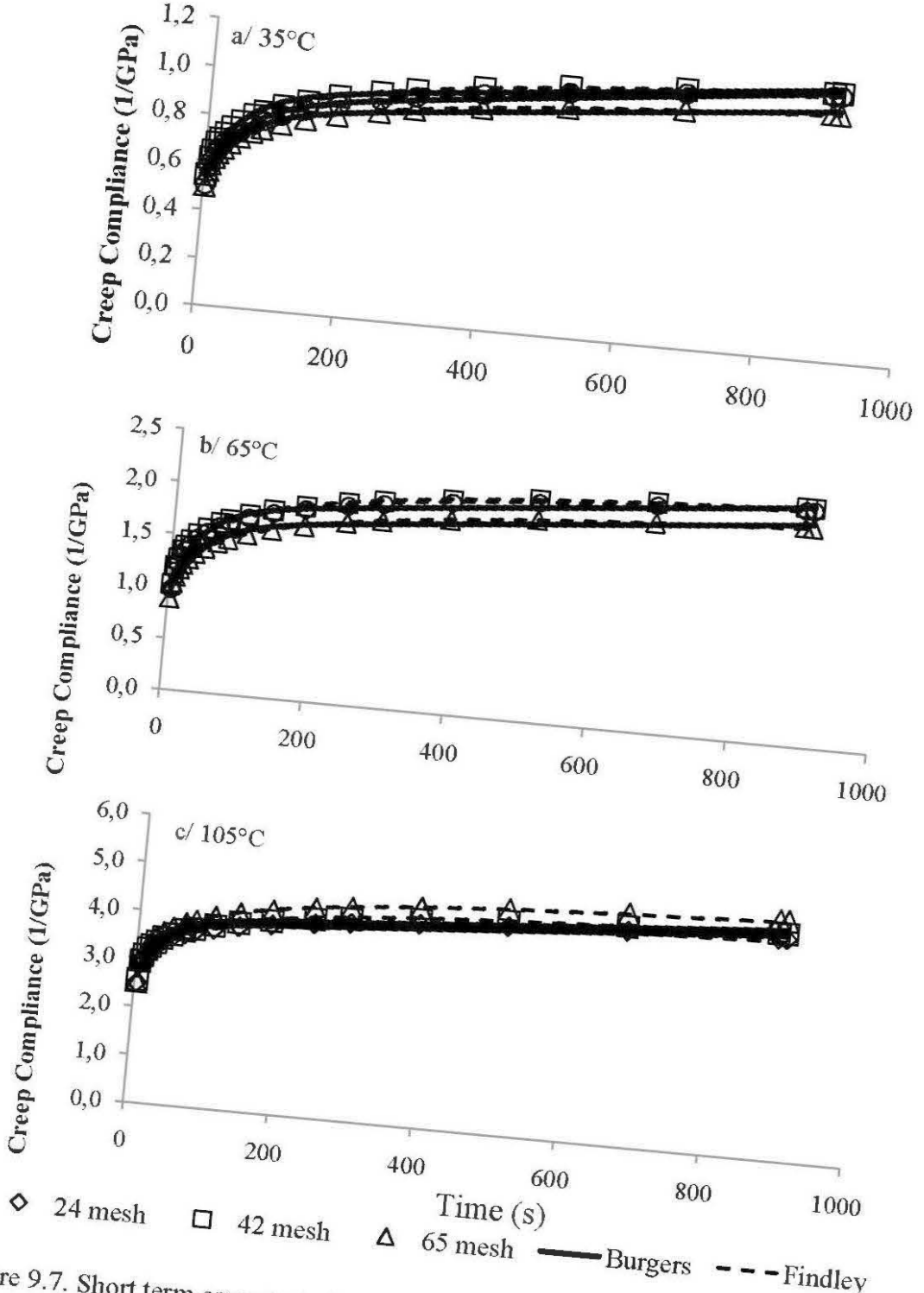

Figure 9.7. Short term creep tests for composites containing 45 wt % White cedar particles in different sizes.

9.6.5 Effect of processing conditions

As mentioned above, creep behavior was greatly influenced by processing conditions. Figure 9.8 depictes the variation of the creep compliance of composites made with 35 wt% black spruce wood particles (24 mesh), at three different test temperatures. For all test conditions, extruded composites showed the lowest creep resistance (the largest creep compliance). Injection molded composites showed nearly the same creep behavior as the compression molded samples. At lower temperatures (Figure 9.8a), injection molded composites had somewhat the highest creep resistance values. At intermediate temperatures (Figure 9.8b), no difference in creep behavior could be observed between composites made with different processes. At higher temperatures, creep behavior has been inversed, showing more creep resistance for compression molded composites. Although dissimilarities were limited in short term tests, it could be pronounced in long term measurement tests. In a previous study, Bouafif *et al.* (2008a) reported that the used mono-vis extruder yielded samples with distortions and surface defects as well as important void volumes in the inner structure (see appendix 6). This may explain the soft-like behavior of the extruded composites. According to the concept of crystal orientation in the toughening mechanism (Galeski, 2003), the higher creep resistance for injection molded composites may be explained by the presence of flow induced crystal orientation, due to the alignment of molecular chains in a polymer melt flow. This oriented morphology is retained upon crystallization of the HDPE. An increase of temperature results in mechanical α-relaxation process occurring in the amorphous phase that requires mobility of the crystals (Khanna *et al.*, 1985; Read, 1989). Thus, crystal orientation is disturbed and, as a result, creep resistance decreases. The creep resistance performance of the compression molded composites can be explained by the densification at the sides of the samples when full molding pressure was applied leading to structure with particles in the skin layer closely compacted and without voids.

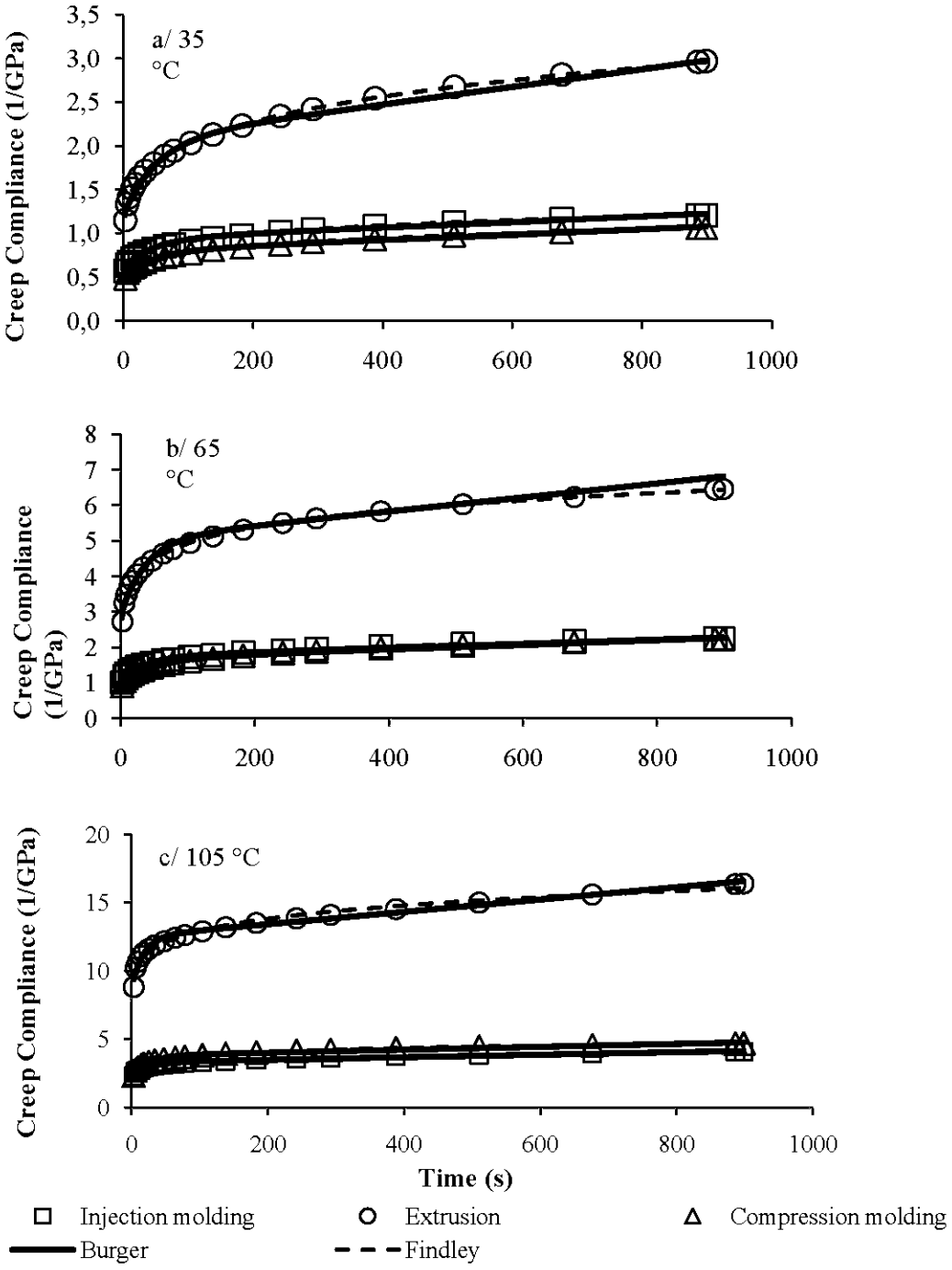

Figure 9.8. Short term creep tests for composites made with different processes. Composites containing 35wt% black spruce wood particles (24 mesh).

Table 9.3 includes the calculated values for the Bürgers and Findley fitting parameters corresponding to Figure 9.8. Similar values were observed for samples made from injection molding and compression molding processes. However, lower values of the retardant elasticity E_K and viscosity η_K of the Kelvin unit for the extruded composites clearly indicated a weaker material and imperfect inner structure.

Table 9.3. Fitting parameters of Burgers and Findley models in different processing conditions. Composites containing 35wt% black spruce wood particles (24 mesh)

Process	T (°c)	Bürgers Model				τ (s)	Findely Model		
		E_M (GPa)	E_K (GPa.)	η_K (GPa.s)	η_M (GPa.s)		A	B	n
Injection molding	35	1.70	3.00	140.71	3155.2	46.97	4.84×10^{-11}	4.31×10^{-10}	0.141
	65	1.02	1.43	48.92	1716.3	34.17	-1.62×10^{-09}	2.50×10^{-09}	0.069
	105	0.44	1.11	28.15	1109.9	25.35	-1.44×10^{-09}	3.62×10^{-09}	0.064
Compression molding	35	1.95	3.52	174.02	3217.5	49.50	1.85×10^{-10}	2.58×10^{-10}	0.179
	65	1.04	1.42	67.77	1521.0	47.85	-2.60×10^{-10}	1.03×10^{-09}	0.130
	105	0.42	0.70	18.13	930.49	25.84	-1.44×10^{-08}	1.65×10^{-08}	0.022
Extrusion	35	0.83	1.16	60.30	989.81	52.08	4.25×10^{-10}	6.12×10^{-10}	0.209
	65	0.35	0.47	17.37	502.26	37.31	-1.07×10^{-08}	1.29×10^{-08}	0.042
	105	0.11	0.27	4.75	221.09	17.70	3.83×10^{-09}	4.90×10^{-09}	0.134

9.6.6 Limit of Bürger's model to predict long time creep behavior

In this subsection, creep tests were carried out for 24 hours and in a fixed temperature of 95°C, in order to assess the creep behavior of composites in high temperature and more large time scale as well as the applicability of the used model in this stage.

Data from the first 10h creep test were used to determine constants corresponding to constitutive equation (1), with two elements (N=1), and equation (4). The tests were continued uninterrupted for 24h. Then, the calculated constants have been used to simulate creep behavior for the 24h creep tests. Although the fitted curves agreed satisfactory with the experimental data within the applied time period, i.e., 10 h, the prediction of the Findley power law led to a more adequate fit than the Burgers model over the investigated period. Figure 9.9 shows large deviation of the Burgers-fitted curve from the experimental data. Similar behavior was obtained for all investigated materials. Thus, choosing the appropriate creep equation to describe the time dependence becomes an important consideration. Consequently, Findley power law model was considered.

9.6.7 Time-Temperature Superposition (TTSP) and Long-Term Creep prediction

TTSP is an interesting concept to assess the long-term performance of various materials through short-term testing (Cessna Jr, 1971; Markovitz, 1974; Nunez *et al.*, 2004; Placet *et al.*, 2007). The superposition technique exploits molecules seeking to attain a state of thermodynamic equilibrium under temperature variation scale. To predict long-term behavior, the creep compliance data at various temperatures were shifted according to the TTSP. The reference temperature selected was 35°C. The master curves constructed from short-term data for various investigated composites are shown in Figure 9.10. It was assumed that ageing could be neglected in these conditions. Special interest has been given to the impact of processing conditions,

filler content and particle size on the long term creep behavior. Continuous curves in Figure 9.10 represent the extrapolation of the short term curves fitted by Findley model at 35°C. Although the master curves were successfully established, a disparity between the extrapolated of the short term curves fitted by Findley model and the master curves was observed for some investigated composites. Table 9.4 contains a compilation of limit creep time, at which mismatching between creep compliance data were shifted according to the TTSP and data extrapolated from Findley model.

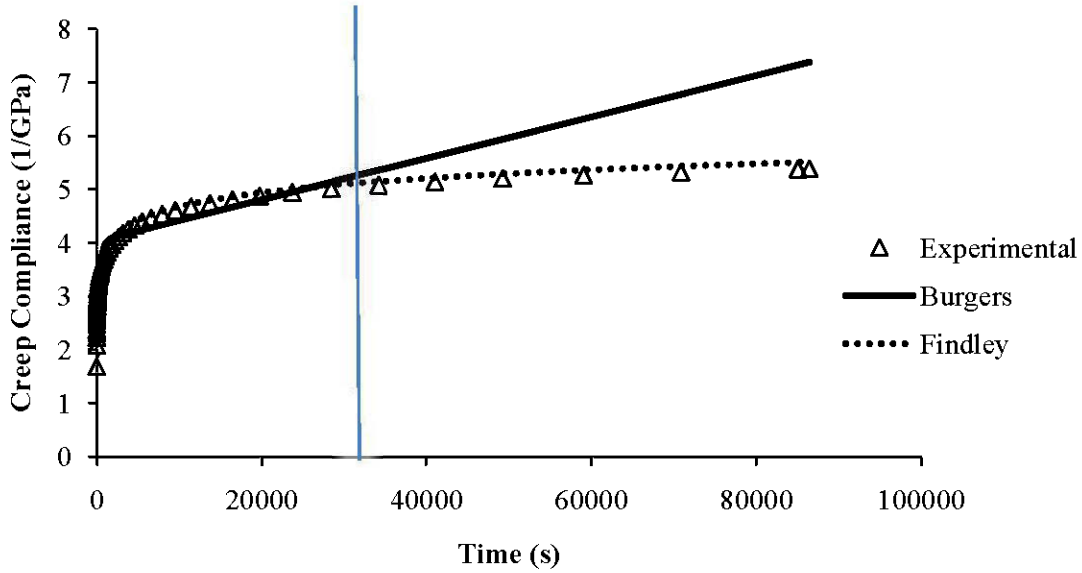

Figure 9.9. Comparison of the prediction ability of the Burgers model (n=2) and Findley power law at 95°C for molding-injected composites containing 35%wt white cedar.

Figure 9.10-a depicts a satisfactory parity between master curve and predicted Findley curve for injected molding composites. This parity continues until creep time test reaches roughly 167 days. However, in the case of compressed molding samples, creep behavior was predicted with concordance by both methods for only 30 testing days. On the other hand, extruded composite data - extrapolated from Findley model - failed to predict precisely long term creep behavior. This can be explained by the initial conditions that have been used to calculate constants. These conditions were

greatly influenced by the weakest inner structure of the composites due to the formation of void volumes (see appendix 6).

Figure 9.10b showed a satisfactory concordance between master curve and predicted Findley curve for filled HDPE composites. However, the dissimilarities in the case of unfilled HDPE matrix showed that Findley power law could not predict the accelerated accumulation of creep deformations which are the macroscopic manifestation of molecular relaxations.

Figure 9.10c shows that Findley power law failed to predict long term creep behavior of the coarse particle (24 mesh) based composites only by extrapolating initial conditions. As mentioned previously, lack in the interfacial adhesion could provide the most plausible explanation.

Table 9.4. Compilation of the time limit of Findley power law in predicting creep compliance behavior.

Sample design		Time limit of Findley power law in predicting creep compliance behavior (Days)
Eastern white cedar wood particles : 42 mesh	0%	0.01
	25%	0.13
	35%	2.25
	45%	1.85
Eastern white cedar wood particles: 45wt %, 24 mesh	injection	166.6
	extrusion	0.11
	compression	29.1
Eastern white cedar wood particles: 45%	24 mesh	1,85
	42 mesh	166,6
	65 mesh	312,5

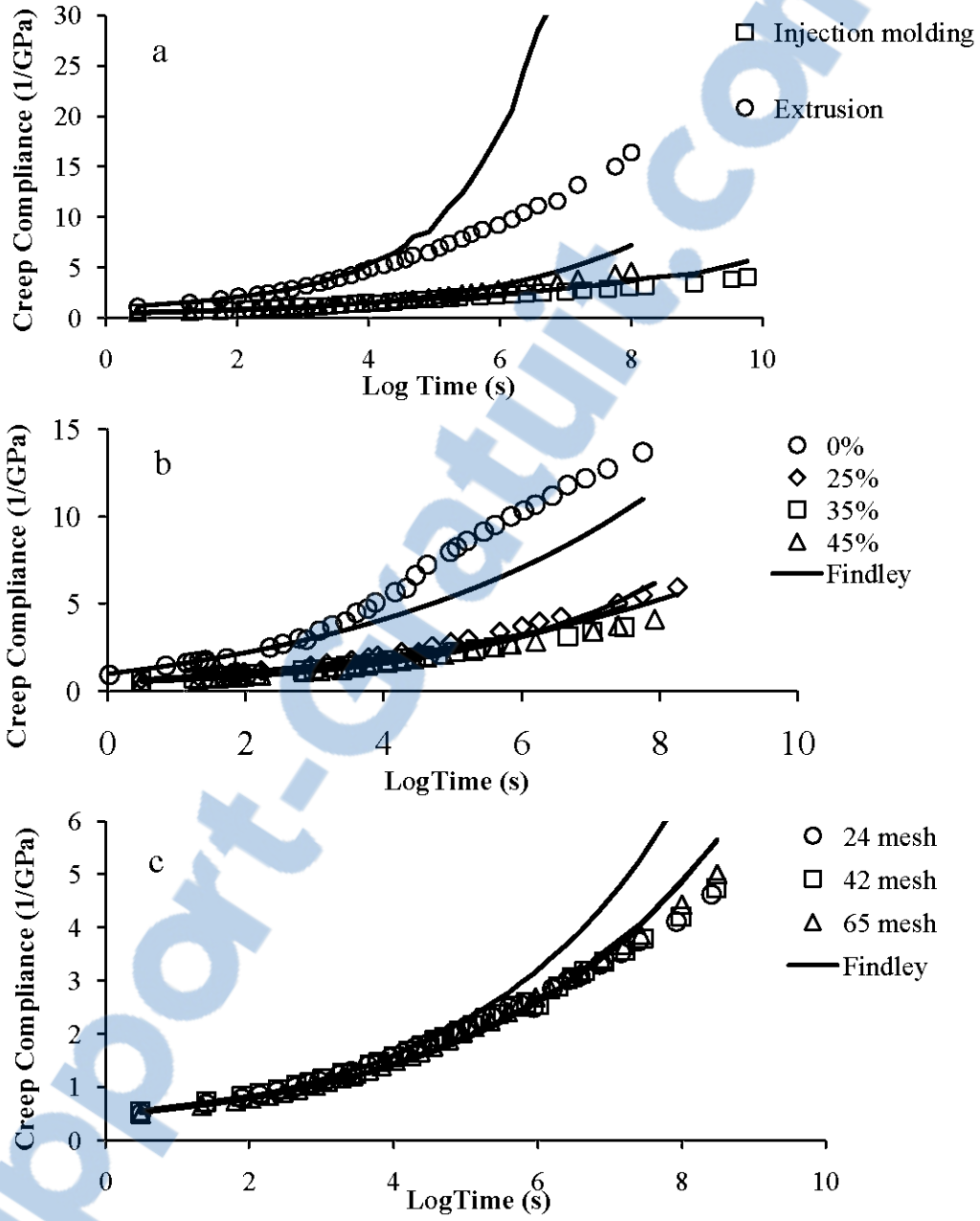

Figure 9.10. Predicting long term creep compliance by TTSP method and Findley power law extrapolation. Tref = 35°C.

9.6.8 Prediction of dynamic mechanic behavior

As the master curve envelops an open spectrum of time, many retardation times were needed to obtain a good description of the retardant part of the mechanical system (E_K and η_K). The use of Bürger's model with multiple Kelvin-Voigt elements applied to the creep master curve was needed to represent accurately the creep behavior of the material composites. As expected, Figure 9.11 shows that the higher is the Kelvin-Voigt elements number, the better is the fitting of the creep compliance. Thus, ten Kelvin-Voigt elements (n=11) were retained to fit master curves at 95°C for 35wt% black spruce based composites (24 mesh).

The retardation times related to the Kelvin-Voigt elements were fixed at 5, 50, 500, 1000, 1500, 3000, 5000, 7500, 10000 and 15000 seconds. The dynamic mechanical response of the material was calculated using equations 9.9, 9.10 and 9.15 and the best fitting parameters obtained for the Bürgers model from the creep master curve at 90°C. Physical ageing was neglected. In Figure 9.12, predicted values were plotted against the experimental data obtained, directly, from the dynamic mechanical machine. Good agreement has been observed at moderate frequency (0.5 to 1.5 Hz). However, differences between observed and predicted values became more apparent at higher frequencies. Such difference may be due to the inaccuracies in basic creep function, namely in the selection of discrete retardation spectrum. Further investigations are needed and should consider continuous retardation spectrum to better predict the dynamic mechanical properties of the investigated wood based composites.

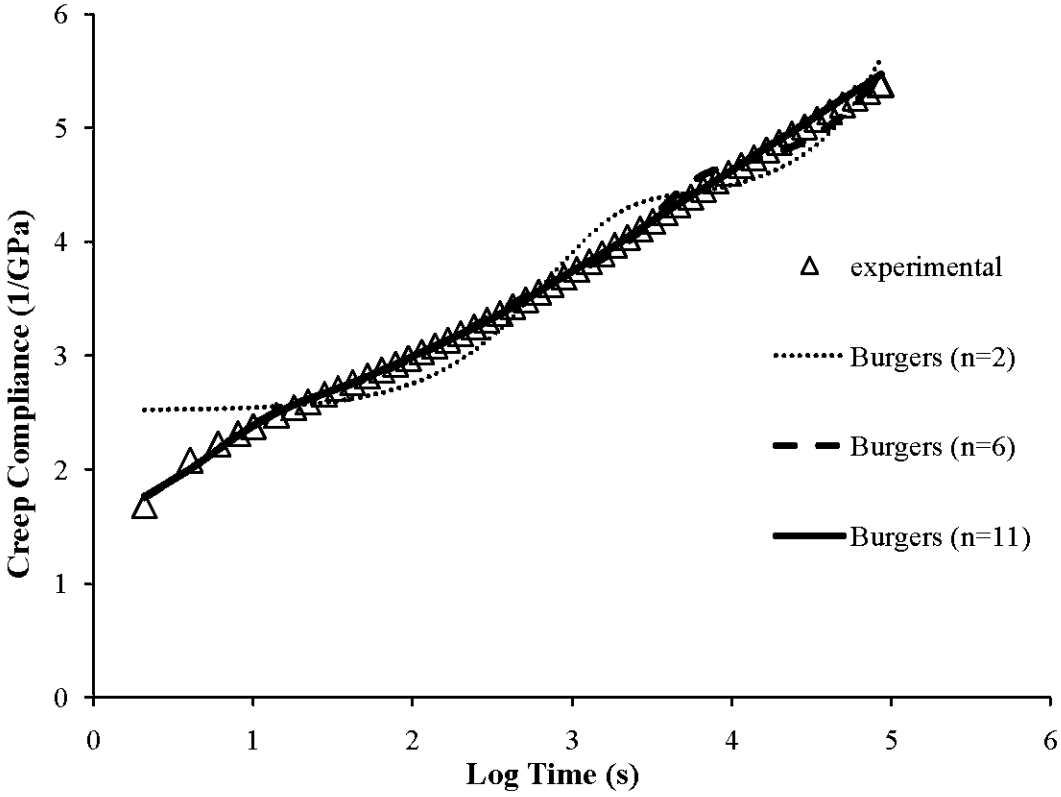

Figure 9.11. Short term master curve from long-term creep data. Continuous lines represent the calculated Burgers model with different numbers of Kelvin-voigt elements.

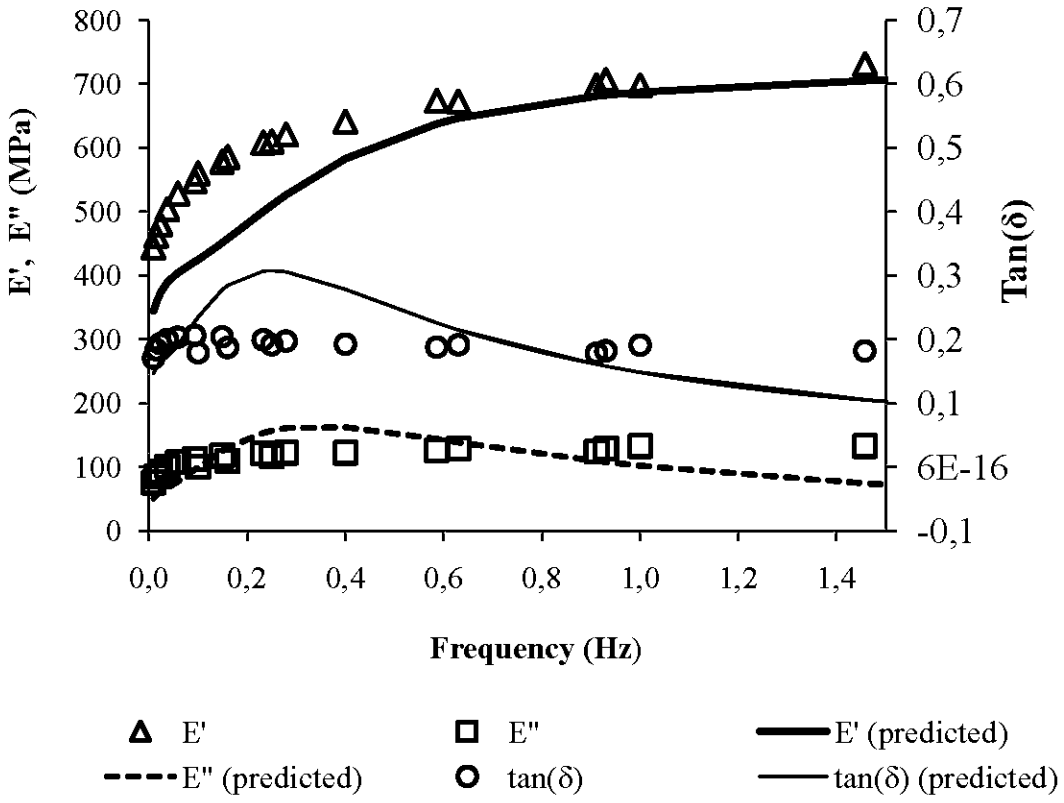

Figure 9.12. Dynamic mechanical behavior of composites made with 35wt% black spruce particles (42 mesh). Continuous lines are the curves calculated (Equations 13, 14 and 15) from the results of modeling the creep master curve at 95°C by Burgers model (n= 11).

9.7 Conclusion

The effects of temperature, wood content, wood particles type and size as well as processing methods on the creep behavior of wood particle-HDPE composites were studied. Creep deformation of HDPE and its wood based composites were satisfactorily modeled by using Burgers' model, the Findley model and time-temperature superposition method. Creep resistance of the investigated composites

was analyzed through the simulating parameters of the Burgers' model. It was shown that the relative creep of the composites increased with an increase in temperature. This was explained by the mobility of the amorphous bulk and tie molecules of the HDPE. Jack pine fibers based composites exhibited the better creep resistance. This behavior was related to the chemical composition of wood fiber surface and the efficiency of the adhesion mechanism between wood fibers and HDPE matrix. The creep compliance decreases as the wood particle content increases, as expected from the increased rigidity of the composites. Dynamic mechanical behavior could be successfully deducted from Burgers' model simulation, but only at moderate frequency tests.

CHAPITRE X

CONCLUSION GÉNÉRALE

Le potentiel de l'utilisation des fibres de bois issues de la première transformation, comme éléments de renfort des polymères thermoplastiques, a été étudié. En particulier, les effets de la variabilité intrinsèque des fibres de bois sur la performance des composites qui en résultent, tel que l'effet de l'essence, l'effet du bois de duramen ou de l'aubier, l'effet de l'écorce, etc., ont été analysés.

L'analyse comparative de la composition de la surface des fibres de bois a été établie moyennant le recours à la spectroscopie infrarouge à transformée de Fourier, couplée à la technique de réflectance diffuse (DRIFTS) et la spectroscopie de photoélectrons avec rayons X (XPS). L'analyse des spectres issus de ces deux techniques montrent une grande variabilité dans la composition de la surface, non seulement entre les espèces mais aussi entre les fibres d'une même espèce (aubier *versus* duramen, ou bois *versus* écorce). Les résultats de l'XPS ont montré que le traitement des fibres avec polyéthylène greffé anhydride maléique (MAPE) a été plus efficace avec les fibres du pin gris. La variation de la concentration en lignine sur la surface des fibres a été montrée comme principal facteur qui inhibe la réaction d'estérification entre les fibres de bois et le HDPE.

L'analyse thermogravimétrique et l'analyse par calorimétrie différentielle à balayage ont été utilisées pour évaluer la stabilité thermique et le pouvoir de nucléation (pouvoir d'initier la cristallisation du HDPE) des particules de bois, respectivement. Les résultats ont montré que la cinétique de la décomposition thermique est similaire pour toutes les fibres de bois. Cependant, des divergences ont été observées entre le bois et l'écorce aux alentours de 300°C.

Il a été montré également que le processus de nucléation du HDPE semi-cristallin a été stimulé par l'addition des particules de bois, mais aucun effet de la variation de l'essence de bois sur le rendement de conversion en cristal du HDPE n'a été observé.

Les propriétés mécaniques et physiques des échantillons de composites varient significativement avec l'essence des fibres. Des particules de bois de grande taille aboutissent à des composites rigides mais ayant une faible énergie de rupture par rapport à des échantillons de même formulation mais qui sont renforcés avec des particules de bois de faible taille. En outre, l'augmentation de la charge en particules de bois améliore la résistance et la rigidité du composite mais diminue l'élongation et l'énergie à la rupture. L'effet de la taille des particules sur la rétention de l'eau, pour un même taux de charge, était minime en comparaison avec l'effet de la variation du taux de charge.

Le développement des particules de bois au cours des différents procédés de fabrication des composites a été étudié. Il a été montré que la vulnérabilité des particules de bois dépend essentiellement de la densité et de la structure des parois des trachéides qui dépendent, entre autre de l'essence. Une nette réduction du facteur forme des particules a été observée après le procédé de mise en granules, tandis que l'extrusion et l'injection influencent plutôt la distribution en augmentant la fréquence des particules fines. À cause de leur sensibilité thermique, les particules d'écorce ont montré une grande susceptibilité à générer de fines particules. La rigidité et la résistance augmentent linéairement avec la taille des particules. Réciproquement, pour aboutir à un effet de renforcement optimal, le pourcentage d'occurrence des particules fines dans la matrice thermoplastique devrait être inférieur à 20% de l'ensemble des particules de bois.

L'effet des caractéristiques des fibres de bois et des procédés de mise en forme sur les propriétés mécaniques dynamiques des composites bois/HDPE a été enquêté. Le module de stockage (E′) diminue avec l'augmentation de la température. La bonne adhésion interfaciale entre les fibres du pin gris et le HDPE explique les valeurs élevées du module de stockage de leur composite. Le pic de la relaxation α du HDPE évolue vers les hautes températures avec l'addition des fibres de bois. De même, le module de perte augmente entre 17% et 30% indiquant une plus grande dissipation due à une augmentation de la viscosité.

La vitesse de refroidissement des composites affecte aussi la température du pic α. E′ augmente avec une augmentation de la fréquence des oscillations, tandis que tan δ et E″ diminuent. En outre, la température du pic α tend à diminuer quand la fréquence diminue. Une légère augmentation de ΔE a été observée suite à l'ajout des fibres de bois. Cela a été expliqué par une augmentation de la cristallinité due au pouvoir de nucléation des particules de bois.

Le fluage à court terme a été simulé moyennant le recours aux modèles analogiques de Bürger et de Findley. Le fluage des composites bois/HDPE augmente avec l'augmentation de la température et il est expliqué par les mouvements de la chaîne moléculaire de la partie amorphe du HDPE. L'ajout des fibres de bois réduit le degré de fluage en réduisant la mobilité de la chaîne moléculaire. Les composites à base de fibres de pin gris ont montré une meilleure résistance au fluage. Ce comportement a été expliqué par l'efficacité de l'adhésion entre les fibres de bois et le polymère. Les résultats des tests de fluage à court terme ont été utilisés aussi pour prédire les propriétés mécaniques dynamiques des composites. Une bonne conformité entre les valeurs mesurées et les valeurs prédites a été observée seulement pour des fréquences modérées (entre 0,5 et 1,5 Hz).

En conclusion, les objectifs de cette étude, bien qu'ils soient très diversifiés, ont été atteints. En effet, on sait aujourd'hui que l'utilisation des fibres d'une telle essence plutôt qu'une autre permettra d'avoir un matériau composite d'une meilleure performance. Par ailleurs, il est important de considérer des pratiques de sélection à la source des fibres issues des résidus de la première transformation. Il est important de noter aussi que l'écorce a montré des potentiels en faveur d'une gestion plus responsable de cette matière. Une utilisation de cette matière à des proportions bien étudiées avec les fibres de bois pourrait être envisageable compte tenu de leurs caractéristiques chimiques (par exemple leur teneur en acides gras) qui leur permettent de se disperser facilement lors du procédé de mise en granules ou de

mélange. Toutefois, comme dans tous les cas d'études sur les composites où les fibres naturelles sont l'élément de renfort ou de charge, l'amélioration de l'interface demeure la principale recommandation afin d'élargir le spectre d'utilisation des matériaux composites bois thermoplastiques vers des applications structurales.

En fin, les travaux de recherche sur les matériaux composites bois/plastiques doivent élargir la liste des fibres non-conventionnelles qui peuvent être utilisées ou réutilisées dans la fabrication de nouveaux matériaux de valeur ajoutée. Les fibres issues des boues papetières pourront donner le bon exemple d'une telle démarche et ce, au même niveau que de penser à la matière plastique de recyclage.

RÉFÉRENCES CITÉES

Acha, B. A., M. M. Reboredo and N. E. Marcovich (2007). "Creep and dynamic mechanical behavior of PP-jute composites: Effect of the interfacial adhesion." Composites Part A: Applied Science and Manufacturing **38**(6): 1507-1516.

Agarwal, U. P. (2006). "Raman imaging to investigate ultrastructure and composition of plant cell walls: Distribution of lignin and cellulose in black spruce wood (Picea mariana)." Planta **224**(5): 1141-1153.

Ahmed, A., A. Adnot, J. L. Grandmaison, J. Doucet and S. Kaliaguine (1987). "ESCA analysis of cellulosic materials." Cellulose Chemistry and Technology **21**: 483-492.

Ajuong, E. M. A. and M. C. Breese (1998). "Fourier Transform Infrared characterization of Pai wood (Afzelia africana Smith) extractives." FTIR-Charakterisierung der Extraktstoffe von Apa-Holz (Afzelia africana Smith) **56**(2): 139-142.

Ajuong, E. M. A. and M. Redington (2004). "Fourier transform infrared analyses of Bog and modern oak wood (Quercus petraea) extractives." Wood Science and Technology **38**(3): 181-190.

Åkerholm, M. and L. Salmén (2001). "Interactions between wood polymers studied by dynamic FT-IR spectroscopy." Polymer **42**(3): 963-969.

Ali, R., S. Iannace and L. Nicolais (2003). "Effect of processing conditions on mechanical and viscoelastic properties of biocomposites." Journal of Applied Polymer Science **88**(7): 1637-1642.

Andrieu, S. and P. Müller (2005). Les surfaces solides : concepts et méthodes, EDP Sciences Editions. 511 P.

Anonymous (2003). Current and Emerging Applications for Natural & Wood Fiber Composites. Natural & Wood Fiber composites. Exton, PA, Principia Partners p.

Anonymous (2005). Estimated Production, Consumption and Surplus Mill Wood Residues in Canada - 2004. A National Report. C. F. Service. Ottawa, Natural Resources Canada 73 p.

Ashori, A. (2008). "Wood-plastic composites as promising green-composites for automotive industries!" Bioresource Technology **99**(11): 4661-4667.

Avrami, M. (1939). "Kinetics of phase change. I: General theory." The Journal of Chemical Physics 7(12): 1103-1112.

Avrami, M. (1940). "Kinetics of phase change. II Transformation-time relations for random distribution of nuclei." The Journal of Chemical Physics **8**(2): 212-224.

Avrami, M. (1941). "Granulation, phase change, and microstructure kinetics of phase change. III." The Journal of Chemical Physics **9**(2): 177-184.

Baïlon, J.-P. and J.-M. Dorlot (2000). DES Matériaux. Montréal, Presses Internationales Polytechnique. 736 P.

Balasuriya, P. W., L. Ye and Y. W. Mai (2001). "Mechanical properties of wood flake-polyethylene composites. Part I: Effects of processing methods and matrix melt flow behaviour." Composites Part A: Applied Science and Manufacturing **32**(5): 619-629.

Balasuriya, P. W., L. Ye, Y. W. Mai and J. Wu (2002). "Mechanical properties of wood flake-polyethylene composites. II. Interface modification." Journal of Applied Polymer Science **83**(12): 2505-2521.

Banks, W. B. (1970). "Some factors affecting the permeability of Scots pine and Norway spruce." J. Inst. Wood Sci. **5**(1): 10-17.

Barbosa, S. E. and J. M. Kenny (2000). "Processing of short-fiber reinforced polypropylene. I. Influence of processing conditions on the morphology of extruded filaments." Polymer Engineering and Science **40**(1): 11-22.

Barker, B. and N. L. Owen (1999). "Identifying Softwoods and Hardwoods by Infrared Spectroscopy." Journal of Chemical Education **76**(12): 1706-1709.

Bengtsson, M., P. Gatenholm and K. Oksman (2005). "The effect of crosslinking on the properties of polyethylene/wood flour composites." Composites Science and Technology **65**(10): 1468-1479.

Bertaud, F. and B. Holmbom (2004). "Chemical composition of earlywood and latewood in Norway spruce heartwood, sapwood and transition zone wood." Wood Science and Technology **38**(4): 245-256.

Bhattacharya, A. and B. N. Misra (2004). "Grafting: A versatile means to modify polymers: Techniques, factors and applications." Progress in Polymer Science (Oxford) **29**(8): 767-814.

Bigg, D. M. (1985). "EFFECT OF COMPOUNDING ON THE PROPERTIES OF SHORT FIBER REINFORCED INJECTION MOLDABLE THERMOPLASTIC COMPOSITES." Polymer Composites **6**(1): 20-28.

Billon, N., V. Henaff and J. M. Haudin (2002). "Transcrystallinity effects in high-density polyethylene. II. Determination of kinetics parameters." Journal of Applied Polymer Science **86**(3): 734-742.

Bledzki, A. K. and O. Faruk (2003). "Wood fibre reinforced polypropylene composites: Effect of fibre geometry and coupling agent on physico-mechanical properties." Applied Composite Materials **10**(6): 365-379.

Bledzki, A. K. and O. Faruk (2004). "Wood fiber reinforced polypropylene composites: Compression and injection molding process." Polymer - Plastics Technology and Engineering **43**(3): 871-888.

Bledzki, A. K. and O. Faruk (2006). "Microcellular injection molded wood fiber-PP composites: Part II - Effect of wood fiber length and content on cell morphology and physico-mechanical properties." Journal of Cellular Plastics **42**(1): 77-88.

Bledzki, A. K. and J. Gassan (1999). "Composites reinforced with cellulose based fibres." Progress in Polymer Science (Oxford) **24**(2): 221-274.

Bledzki, A. K., J. Gassan and S. Theis (1998a). "Wood-filled thermoplastic composites." Mechanics of Composite Materials **34**(6): 563-568.

Bledzki, A. K., M. Letman, A. Viksne and L. Rence (2005). "A comparison of compounding processes and wood type for wood fibre - PP composites." Composites Part A: Applied Science and Manufacturing **36**(6): 789-797.

Bledzki, A. K., S. Reihmane and J. Gassan (1996). "Properties and modification methods for vegetable fibers for natural fiber composites." Journal of Applied Polymer Science **59**(8): 1329-1336.

Bledzki, A. K., S. Reihmane and J. Gassan (1998b). "Thermoplastics reinforced with wood fillers: a literature review." Polymer - Plastics Technology and Engineering **37**(4): 451-468.

Bogoeva-Gaceva, G., M. Avella, M. Malinconico, A. Buzarovska, A. Grozdanov, G. Gentile and M. E. Errico (2007). "Natural fiber eco-composites." Polymer Composites **28**(1): 98-107.

Boiko, Y. M. and M. Y. Sherman (1998). "Dynamic mechanical behavior of oriented films of high-density polyethylene." Polymer Science - Series A **40**(2): 143-149.

Borysiak, S. (2007). "Determination of nucleating ability ofwood for non-isothermal crystallisation of polypropylene." Journal of Thermal Analysis and Calorimetry **88**(2): 455-462.

Borysiak, S. and B. Doczekalska (2006). "Influence of chemical modification of wood on the crystallisation of polypropylene." Holz als Roh - und Werkstoff **64**(6): 451-454.

Bouafif, H., A. Koubaa, P. Perre and A. Cloutier (2008a). Effects of fiber characteristics on the physical and mechanical properties of wood plastic composites. The 9th International Conference on Flow Processes in Composite Materials. Montreal-Quebec p.

Bouafif, H., A. Koubaa, P. Perre and A. Cloutier (2008b). Effects of processing method and fiber load on wood plastic composites properties. Proceedings of the Polymer Processing Society 24th Annual Meeting ~ PPS-24 ~ Salerno-Italy.

Bouafif, H., A. Koubaa, P. Perré, A. Cloutier and B. Riedl (2008c). "Analysis of Among-Species Variability in Wood Fiber Surface Using DRIFTS and XPS: Effects on Esterification Efficiency." Journal of Wood Chemistry and Technology **28**(4): 296 - 315.

Bouafif, H., A. Koubaa, P. Perré, A. Cloutier and B. Riedl (2009). "Wood particle/high-density polyethylene composites: Thermal sensitivity and nucleating ability of wood particles." Journal of Applied Polymer Science **113**(1): 593-600.

Bouza, R., C. Marco, Z. Martin, M. A. Gomez, G. Ellis and L. Barral (2006). "Dynamic crystallization of polypropylene and wood-based composites." Journal of Applied Polymer Science **102**(6): 6028-6036.

Boyd, R. H. (1976). "Molecular interpretation of relaxation in polyethylene." American Chemical Society, Polymer Preprints, Division of Polymer Chemistry **17**(2): 125-130.

Boyd, R. H. (1984). "Strengths of the mechanical alpha-, beta-, and gamma-relaxation processes in linear polyethylene." Macromolecules **17**(4): 903-911.

Boyer, R. F. (1973). "Glass temperatures of polyethylene." Macromolecules **6**(2): 288-299.

Branca, C., C. Di Blasi and R. Elefante (2006). "Devolatilization of conventional pyrolysis oils generated from biomass and cellulose." Energy and Fuels **20**(5): 2253-2261.

Bräs, I., L. T. Lemos, A. Alves and M. F. R. Pereira (2004). "Application of pine bark as a sorbent for organic pollutants in effluents." Management of Environmental Quality **15**(5): 491-501.

Burgstaller, C. (2007). "Processing of thermal sensitive materials - A case study for wood plastic composites." Monatshefte fur Chemie **138**(4): 343-346.

Carlborn, K. and L. M. Matuana (2006). "Functionalization of wood particles through a reactive extrusion process." Journal of Applied Polymer Science **101**(5): 3131-3142.

Carlsson, L. A. and T. Lindstrom (2005). "A shear-lag approach to the tensile strength of paper." Composites Science and Technology **65**(2): 183-189.

Carvalho, M. G., P. J. Ferreira, A. A. Martins and M. M. Figueiredo (1997). "A comparative study of two automated techniques for measuring fiber length." Tappi journal **80**(2): 137-142.

Caulfield, D. F., C. Clemons, R. E. Jacobson and R. M. Rowell (2005). Wood-thermoplastic composites. *in* Handbook of wood chemistry, wood composites. R. M. Rowell (Ed.). Boca Raton, Taylor and Francis**:** 365-380.

Cessna Jr, L. C. (1971). "STRESS-TIME SUPERPOSITION OF CREEP DATA FOR POLYPROPYLENE AND COUPLED GLASS-REINFORCED POLYPROPYLENE." Polymer Engineering and Science **11**(3): 211-219.

Chen, R. and K. A. Jakes (2002). "Effect of pressing on the infrared spectra of single cotton fibers." Applied Spectroscopy **56**(5): 646-650.

Chow, S. Z. (1971). "Infrared spectral characteristics and surface inactivation of wood at high temperatures." Wood Science and Technology **5**(1): 27-39.

Christiansen, A. W. (1990). "How overdrying wood reduces its bonding to phenol-formaldehyde adhesives: a critical review of the literature. Part I, physiscal responses." Wood and Fiber Science **22**(4): 441-459.

Chtourou, H., B. Riedl and A. Ait-Kadi (1992). "Reinforcement of recycled polyolefins with wood fibers." Journal of Reinforced Plastics and Composites **11**(4): 372-394.

Chuai, C., K. Almdal, L. Poulsen and D. Plackett (2001). "Conifer fibers as reinforcing materials for polypropylene-based composites." Journal of Applied Polymer Science **80**(14): 2833-2841.

Clemons, C. (2002). "Wood-plastic composites in the United States: The interfacing of two industries." Forest Products Journal **52**(6): 10-18.

Clemons, C. M., D. F. Caulfield and A. J. Giacomin (1999). "Dynamic fracture toughness of cellulose-fiber-reinforced polypropylene: Preliminary

investigation of microstructural effects." Journal of Elastomers and Plastics **31**(4): 367-378.

Colom, X. and F. Carrillo (2005). "Comparative study of wood samples of the northern area of Catalonia by FTIR." Journal of Wood Chemistry and Technology **25**(1-2): 1-11.

Colthup, N. B., L. Daly and S. E. Wiberley (1975). Introduction to infrared and Raman spectroscopy. New York, Academic Press. 523 P.

Core, H. A., W. A. Cote and A. C. Day (1979). Wood structure and identification, Syracuse University Press. P.

Cornel, J., C. Lindenberg and M. Mazzotti (2008). "Quantitative application of in situ ATR-FTIR and raman spectroscopy in crystallization processes." Industrial and Engineering Chemistry Research **47**(14): 4870-4882.

Cyras, V. P., J. F. Martucci, S. Iannace and A. Vazquez (2002). "Influence of the fiber content and the processing conditions on the flexural creep behavior of sisal-PCL-starch composites." Journal of Thermoplastic Composite Materials **15**(3): 253-265.

D638-03, A. (2003). Standard Test Method for Tensile Properties of Plastics. A. International. West Conshohocken p.

D790-03, A. (2003). Standard Test Method for Flexural properties of unreinforced and Reinforced plastics and Electrical Insulating Materials Plastics. A. International. West Conshohocken p.

Daniel, G. and T. Nilsson (1984). "Studies on the S2 layer of Pinus silvestris." Swedish Univ. Agri. Sc., Dept. For. Prod. Report **154**: 1-33.

Dányádi, L., T. Janecska, Z. Szabó, G. Nagy, J. Móczó and B. Pukánszky (2007). "Wood flour filled PP composites: Compatibilization and adhesion." Composites Science and Technology **67**(13): 2838-2846.

De Meijer, M., S. Haemers, W. Cobben and H. Militz (2000). "Surface energy determinations of wood: Comparison of methods and wood species." Langmuir **16**(24): 9352-9359.

Degallaix, S., M. Boussuge and B. Ilschner (2007). Caractérisation expérimentale des matériaux, Press Polytechniques et Universitaires Romandes. 402 P.

DeGroot, W. F. and F. Shafizadeh (1984). "Influence of exchangeable cations on the carbonization of biomass." Journal of Analytical and Applied Pyrolysis **6**(3): 217-232.

Dikobe, D. G. and A. S. Luyt (2007). "Effect of filler content and size on the properties of ethylene vinyl acetate copolymer-wood fiber composites." Journal of Applied Polymer Science **103**(6): 3645-3654.

Dominkovics, Z., L. Dányádi and B. Pukánszky (2007). "Surface modification of wood flour and its effect on the properties of PP/wood composites." Composites Part A: Applied Science and Manufacturing **38**(8): 1893-1901.

Donaldson, L. A. (1991). "Seasonal changes in lignin distribution during tracheid development in Pinus radiata D. Don." Wood Science and Technology **25**(1): 15-24.

Donaldson, L. A. (1995). "Cell wall fracture properties in relation to lignin distribution and cell dimensions among three genetic groups of radiata pine." Wood Science and Technology **29**(1): 51-63.

Donaldson, L. A. (2001). "Lignification and lignin topochemistry - An ultrastructural view." Phytochemistry **57**(6): 859-873.

Donaldson, L. A. (2002). "Abnormal lignin distribution in wood from severely drought stressed Pinus radiata trees." IAWA Journal **23**(2): 161-178.

Dorris, G. M. and D. G. Gray (1978a). "The surface analysis of paper and wood fibers by ESCA I." Cellulose Chemistry and Technology **12**: 9-23.

dorris, G. M. and D. G. gray (1978b). "The surface analysis of paper and wood fibers by ESCA II." cellulose Chemistry and Technology **12**: 721-734.

Downes, G. M., J. V. Ward and N. D. Turvey (1991). "Lignin distribution across tracheid cell walls of poorly lignified wood from deformed copper deficient Pinus radiata (D. Don)." Wood Science and Technology **25**(1): 7-14.

Drumond, W. S., C. G. MothÃ© and S. H. Wang (2006). "Quantitative analysis of biodegradable amphiphilic poly(L-lactide)-block- poly(ethyleneglycol)-blockpoly(L-lactide) by using TG, FTIR and NMR." Journal of Thermal Analysis and Calorimetry **85**(1): 173-177.

Dubnikova, I. L., S. M. Berezina and A. V. Antonov (2004). "Effect of rigid particle size on the toughness of filled polypropylene." Journal of Applied Polymer Science **94**(5): 1917-1926.

El-Meligy, M. G., W. K. El-Zawawy and M. M. Ibrahim (2004). "Lignocellulosic composite." Polymers for Advanced Technologies **15**(12): 738-745.

Ellis, W. D. and J. L. O'Dell (1999). "Wood-polymer composites made with acrylic monomers, isocyanate, and maleic anhydride." Journal of Applied Polymer Science **73**(12): 2493-2505.

Emons, A. M. C. and B. M. Mulder (1998). "The making of the architecture of the plant cell wall: How cells exploit geometry." Proceedings of the National Academy of Sciences of the United States of America **95**(12): 7215-7219.

Emons, A. M. C. and B. M. Mulder (2000). "How the deposition of cellulose microfibrils builds cell wall architecture." Trends in Plant Science **5**(1): 35-40.

English, B. W. and R. H. Falk (1995). Factors that Affect the Application of Woodfiber-Plastic Composites. Proceedings of the woodfiber-Plastic Composites Conference, Madison, Wisconsin, Forest Product Society.

Escobar, W. G. (2008). "Influence od Wood Species on Properties of Wood/HDPE Composites." Department of Civil Environmental Engineering. Washihgton State University. PhD thesis. 134 P.

Fahlén, J. and L. Salmén (2002). "On the lamellar structure of the tracheid cell wall." Plant Biology **4**(3): 339-345.

Faibridge, C., R. A. Ross and P. Spooner (1975). "A thermogravimetric study of the pyrolysis of the bark and chemically-modified bark of jack pine, pinus banksiana lamb." Wood Science and Technology **9**(4): 257-274.

Faix, O. and J. H. Böttcher (1992). "The influence of particle size and concentration in transmission and diffuse reflectance spectroscopy of wood." Holz als Roh - und Werkstoff **50**: 221-226.

Faix, O., E. Jakab, F. Till and T. Székely (1988). "Study on low mass thermal degradation products of milled wood lignins by thermogravimetry-mass-spectrometry." Wood Science and Technology **22**(4): 323-334.

Fenner, R. A. and J. O. Lephardt (1981). "Examination of the thermal decomposition of Kraft pine lignin by Fourier transform infrared evolved gas analysis." Journal of Agricultural and Food Chemistry **29**(4): 846-849.

Fergus, B. J., A. R. Procter, J. A. N. Scott and D. A. I. Goring (1969). "The distribution of lignin in sprucewood as determined by ultraviolet microscopy." Wood Science and Technology **3**(2): 117-138.

Ferraz, A., J. Baeza, J. Rodriguez and J. Freer (2000). "Estimating the chemical composition of biodegraded pine and eucalyptus wood by DRIFT spectroscopy and multivariate analysis." Bioresource Technology 74(3): 201-212.

Frihart, C. R. (2005). wood adhesion and adhesives. *in* Handbook of Wood chemistry and Wood composites. R. M. Rowell (Ed.). Boca Raton, CRC Press. **1:** 215 - 278.

Fu, S. Y., X. Hu and C. Y. Yue (1999). "Effects of fiber length and orientation distributions on the mechanical properties of short-fiber-reinforced polymers - a review." Materials Science Research International **5**(2): 74-83.

Fu, S. Y. and B. Lauke (1996). "Effects of fiber length and fiber orientation distributions on the tensile strength of short-fiber-reinforced polymers." Composites Science and Technology **56**(10): 1179-1190.

Fu, S. Y., C. Y. Yue, X. Hu and Y. W. Mai (2001). "Characterization of fiber length distribution of short-fiber reinforced thermoplastics." Journal of Materials Science Letters **20**(1): 31-33.

Fukazawa, K. and H. Imagawa (1981). "Quantitative analysis of lignin using an UV microscopic image analyser. variation within one growth increment." Wood Science and Technology **15**(1): 45-55.

Galeski, A. (2003). "Strength and toughness of crystalline polymer systems." Progress in Polymer Science (Oxford) **28**(12): 1643-1699.

Gardner, D. J., T. P. Schultz and G. D. McGinnis (1985). "Pyrolytic behavior of selected lignin preparations." Journal of Wood Chemistry and Technology **5**(1): 85-110.

Gassan, J. and A. K. Bledzki (1997). "The influence of fiber-surface treatment on the mechanical properties of jute-polypropylene composites." Composites Part A: Applied Science and Manufacturing **28**(12): 1001-1005.

Gauthier, R., C. Joly, A. C. Coupas, H. Gauthier and M. Escoubes (1998). "Interfaces in polyolefin/cellulosic fiber composites: Chemical coupling, morphology, correlation with adhesion and aging in moisture." Polymer Composites **19**(3): 287-300.

Geethamma, V. G., G. Kalaprasad, G. Groeninckx and S. Thomas (2005). "Dynamic mechanical behavior of short coir fiber reinforced natural rubber composites." Composites Part A: Applied Science and Manufacturing **36**(11): 1499-1506.

George, J., S. S. Bhagawan and S. Thomas (1996). "Thermogravimetric and dynamic mechanical thermal analysis of pineapple fibre reinforced polyethylene composites." Journal of Thermal Analysis **47**(4): 1121-1140.

Gérardin, P., M. Petri, M. Petrissans, J. Lambert and J. J. Ehrhrardt (2007). "Evolution of wood surface free energy after heat treatment." Polymer Degradation and Stability **92**(4): 653-657.

Gibson, L. J. and F. Ashby (1997). Cellular Solids, Structure and Properties. Cambridge, University Press. 532 P.

Gindl, M. and S. Tschegg (2002). "Significance of the acidity of wood to the surface free energy components of different wood species." Langmuir **18**(8): 3209-3212.

Gonzalez, C. and G. E. Myers (1993). "Thermal degradation of wood fillers at the melt-processing temperatures of wood-plastic composites: effects on wood mechanical properties and production of volatiles." International Journal of Polymeric Materials **23**(1-2): 67-85.

Gordon, M. H. and R. Macrae (1989). Instrumental analysis in the biological sciences., Blackie & Son Ltd. 256 P.

Govindarajan, S., N. A. Langrana and G. J. Weng (1996). "The influence of imperfections on the creep behavior of woven polymer composites at elevated temperatures." Finite Elements in Analysis and Design **23**(2-4): 333-347.

Grillo, J., P. Andersen and E. Papazoglou (1993). "Experimental studies for optimizing screw and die design when compounding fiberglass strand on the co-rotating twin screw extruder." Journal of Reinforced Plastics and Composites **12**(3): 311-326.

Guay, D., N. R. Sutherland, W. Rantanen, N. Malandri, A. Stephens, K. Mattingly and M. Schneider (2005). Comparison of fiber length analyzers. 2005 TAPPI Practical Papermaking Conference, Milwaukee, WI.

Gupta, B. S., I. Reiniati and M. P. G. Laborie (2007). "Surface properties and adhesion of wood fiber reinforced thermoplastic composites." Colloids and Surfaces A: Physicochemical and Engineering Aspects **302**(1-3): 388-395.

Harper, D. and M. Wolcott (2004). "Interaction between coupling agent and lubricants in wood-polypropylene composites." Composites Part A: Applied Science and Manufacturing **35**(3): 385-394.

Haussard, M., I. Gaballah, N. Kanari, P. De Donato, O. Barre?s and F. Villieras (2003). "Separation of hydrocarbons and lipid from water using treated bark." Water Research **37**(2): 362-374.

Hillis, W. E. (1984). "High temperature and chemical effects on wood stability - Part 1: General considerations." Wood Science and Technology **18**(4): 281-293.

Horne, P. A. and P. T. Williams (1996). "Influence of temperature on the products from the flash pyrolysis of biomass." Fuel **75**(9): 1051-1059.

Hosoya, T., H. Kawamoto and S. Saka (2007). "Influence of inorganic matter on wood pyrolysis at gasification temperature." Journal of Wood Science **53**(4): 351-357.

Hristov, V. and S. Vasileva (2003). "Dynamic mechanical and thermal properties of modified poly(propylene) wood fiber composites." Macromolecular Materials and Engineering **288**(10): 798-806.

Hua, X., S. Kaliaguine, B. V. Kokta and A. Adnot (1993). "Surface analysis of explosion pulps by ESCA. Parte 1: Carbon (1s) spectra and oxygen to carbon ratios." Wood Science and Technology **27**: 449-459.

Hunter, A. J. (1993). "On movement of water through wood - The diffusion coefficient." Wood Science and Technology **27**(6): 401-408.

Ichazo, M. N., C. Albano, J. GonzÃ¡lez, R. Perera and M. V. Candal (2001). "Polypropylene/wood flour composites: Treatments and properties." Composite Structures **54**(2-3): 207-214.

Jacob, M., B. Francis, S. Thomas and K. T. Varughese (2006). "Dynamical mechanical analysis of sisal/oil palm hybrid fiber-reinforced natural rubber composites." Polymer Composites **27**(6): 671-680.

Jaic, M., R. Zivanovic, T. Stevanovic-Janezic and A. Dekanski (1996). "Comparison of surface properties of beech and oakwood as determined by ESCA method." Holz als Roh - und Werkstoff **54**: 37-41.

Jakab, E., O. Faix and F. Till (1997). "Thermal decomposition of milled wood lignins studied by thermogravimetry/mass spectrometry." Journal of Analytical and Applied Pyrolysis **40-41**: 171-186.

Jakab, E., O. Faix, F. Till and T. Szekely (1993). "Effect of cations on the thermal decomposition of lignins." Journal of Analytical and Applied Pyrolysis **25**: 185-194.

Jakab, E., G. Värhegyi and O. Faix (2000). "Thermal decomposition of polypropylene in the presence of wood-derived materials." Journal of Analytical and Applied Pyrolysis **56**(2): 273-285.

Johansson, L. S., J. Campbell, K. Koljonen, M. Kleen and J. Buchert (2004). "On surface distributions in natural cellulosic fibres." Surface and Interface Analysis **36**(8): 706-710.

Johansson, L. S., J. M. Campbell, K. Koljonen and P. Stenius (1999). "Evaluation of surface lignin on cellulose fibers with XPS." Applied Surface Science **144-145**(0): 92-95.

Joseph, P. V., K. Joseph and S. Thomas (1999). "Effect of processing variables on the mechanical properties of sisal-fiber-reinforced polypropylene composites." Composites Science and Technology **59**(11): 1625-1640.

Joseph, P. V., K. Joseph, S. Thomas, C. K. S. Pillai, V. S. Prasad, G. Groeninckx and M. Sarkissova (2003). "The thermal and crystallisation studies of short sisal fibre reinforced polypropylene composites." Composites Part A: Applied Science and Manufacturing **34**(3): 253-266.

Juhlin, E., X. Chen and T. D. Papathanasiou (2002). On the effects of fiber length and spatial distribution on the stiffness of short-fiber reinforced composites. Polymers and Polymer Composites **10**(3): 205-210.

Kamdem, D. P., B. Riedl, A. Adnot and S. Kaliaguine (1991). "ESCA spectroscopy of poly (methyl methacrylate) grafted onto wood fibers." Journal of Applied Polymer Science **43**(10): 1901-1912.

Karlsson, H. (2008). "New technique for measurement of fibre properties including vessel cells and mix of fibre species." Appita Journal **61**(3): 192-196.

Kasliwal, S. G. and J. W. Jones (2004). Gentle compounding of natural fiber filled PVC composites. Annual Technical Conference - ANTEC, Conference Proceedings.

Kazayawoko, M., J. J. Balatinecz and L. M. Matuana (1999a). "Surface modification and adhesion mechanisms in woodfiber-polypropylene composites." Journal of Materials Science **34**(24): 6189-6199.

Kazayawoko, M., J. J. Balatinecz and R. N. S. Sodhi (1999b). "X-ray photoelectron spectroscopy of maleated polypropylene treated wood fibers in a high-intensity thermokinetic mixer." Wood Science and Technology **33**(5): 359-372.

Kazayawoko, M., J. J. Balatinecz and R. T. Woodhams (1997). "Diffuse reflectance Fourier transform infrared spectra of wood fibers treated with maleated polypropylenes." Journal of Applied Polymer Science **66**(6): 1163-1173.

Keener, T. J., R. K. Stuart and T. K. Brown (2004). "Maleated coupling agents for natural fibre composites." Composites Part A: Applied Science and Manufacturing **35**(3): 357-362.

Kelly, A. and W. R. Tyson (1965). "Tensile properties of fibre-reinforced metals: Copper/tungsten and copper/molybdenum." Journal of the Mechanics and Physics of Solids **13**(6).

Khanna, Y. P., E. A. Turi, T. J. Taylor, V. V. Vickroy and R. F. Abbott (1985). "Dynamic mechanical relaxations in polyethylene." Macromolecules **18**(6): 1302-1309.

Kim, J. I., S. H. Ryu and Y. W. Chang (2000). "Mechanical and dynamic mechanical properties of waste rubber powder/HDPE composite." Journal of Applied Polymer Science 77(12): 2595-2602.

Kim, Y. S., G. Guo, K. H. Wang, C. B. Park and F. W. Maine (2004). Processing/structure/property relationships for artificial wood made from stretched PP/wood-fiber composites. Annual Technical Conference - ANTEC, Conference Proceedings, Chicago, IL.

Koljonen, K. (2004). "Effect of surface properties of fibers on some paper properties of mechanical and chemical pulp." department of forest product technology. Helsinki University of Technology. thesis. P.

Koljonen, K. and P. Stenius (2005). "Surface characterisation of single fibres from mechanical pulps by contact angle measurements." Nordic Pulp and Paper Research Journal **20**(1): 107-113.

Koubaa, A., B. Riedl and Z. Koran (1996). "Surface analysis of press dried-CTMP paper samples by electron spectroscopy for chemical analysis." Journal of Applied Polymer Science **61**(3): 545-552.

Kubat, J., M. Rigdahl and M. Welander (1990). "Characterization of interfacial interactions in high density polyethylene filled with glass spheres using dynamic-mechanical analysis." Journal of Applied Polymer Science **39**(7): 1527-1539.

Kutnar, A., F. A. Kamke, M. Petri and M. Sernek (2008). "The influence of viscoelastic thermal compression on the chemistry and surface energetics of wood." Colloids and Surfaces A: Physicochemical and Engineering Aspects **329**(1-2): 82-86.

Laine, C., X. Wang, M. Tenkanen and A. Varhimo (2004). "Changes in the fiber wall during refining of bleached pine kraft pulp." Holzforschung **58**(3): 233-240.

Laredo, E., N. Suarez, A. Bello, B. Rojas De Gáscue, M. A. Gomez and J. M. G. Fatou (1999). "?, ? and ? relaxations of functionalized HD polyethylene: A TSDC and a mechanical study." Polymer **40**(23): 6405-6416.

Le Digabel, F. and L. Avěrous (2006). "Effects of lignin content on the properties of lignocellulose-based biocomposites." Carbohydrate Polymers **66**(4): 537-545.

Lee, B. J., A. G. McDonald and B. James (2001). "Influence of fiber length on the mechanical properties of wood-fiber/polypropylene prepreg sheets." Materials Research Innovations **4**(2-3): 97-103.

Lee, C. L. (1961). "Crystallinity of wood cellulose fibers." For. Prod. J. **11**: 108-112.

Li, Q. and L. M. Matuana (2003a). "Effectiveness of Maleated and Acrylic Acid-Functionalized Polyolefin Coupling Agents for HDPE-Wood-Flour Composites." Journal of Thermoplastic Composite Materials **16**(6): 551-564.

Li, Q. and L. M. Matuana (2003b). "Surface of cellulosic materials modified with functionalized polyethylene coupling agents." Journal of Applied Polymer Science **88**(2): 278-286.

Lindström, H. (1997). "Fiber length, tracheid diameter, and latewood percentage in norway spruce: development from pith outwards." Wood and Fiber Science **29**(1): 21-34.

Lindström, H., J. W. Evans and S. P. Verrill (1998). "Influence of Cambial Age and Growth Conditions on Microfibril Angle in Young Norway Spruce (Picea abies [L.] Karst.)." Holzforschung **52**(6): 573-581.

Liu, F. P., T. G. Rials and J. Simonsen (1998). "Relationship of wood surface energy to surface composition." Langmuir **14**(2): 536-541.

Liu, F. P., M. P. Wolcott, D. J. Gardner and T. G. Rials (1995). "Characterization of the interface between cellulosic fibers and a thermoplastic matrix." Composite Interfaces **2**(6): 419-432.

Liu, Y. H., J. Q. Xu and H. J. Ding (1999). "Mechanical behavior of a fiber end in short fiber reinforced composites." International Journal of Engineering Science **37**(6): 753-770.

Lu, J. Z., I. I. Negulescu and Q. Wu (2005a). "Maleated wood-fiber/high-density-polyethylene composites: Coupling mechanisms and interfacial characterization." Composite Interfaces **12**(1-2): 125-140.

Lu, J. Z. and Q. Wu (2005). "Surface and interfacial characterization of wood-PVC composite: Imaging morphology and wetting behavior." Wood and Fiber Science **37**(1): 95-111.

Lu, J. Z., Q. Wu and H. S. McNabb Jr (2000). "Chemical coupling in wood fiber and polymer composites: A review of coupling agents and treatments." Wood and Fiber Science **32**(1): 88-104.

Lu, J. Z., Q. Wu and I. I. Negulescu (2004). "Wood-fiber/high-density-polyethylene composites: Compounding process." Journal of Applied Polymer Science **93**(6): 2570-2578.

Lu, J. Z., Q. Wu and I. I. Negulescu (2005b). "Wood-fiber/high-density-polyethylene composites: Coupling agent performance." Journal of Applied Polymer Science **96**(1): 93-102.

Lu, Z. (2003). "Chemical Coupling in Wood-Polymer Composites." Forestry, Wildlife, & Fisheries. Louisiana State University. Doctor of Philosophy (Ph.D.) thesis. 238 P.

Luo, J., Z. Tang and J. Zhou (2006). "Preparation and properties of HDPE/lignin composite." Hecheng Shuzhi Ji Suliao/China Synthetic Resin and Plastics **23**(2): 39-42.

Mahlberg, R., L. Paajanen, A. Nurmi, A. KivistÃ¶, K. Koskela and R. M. Rowell (2001a). "Effect of chemical modification of wood on the mechanical and adhesion properties of wood fiber/polypropylene fiber and

polypropylene/veneer composites." Holz als Roh - und Werkstoff **59**(5): 319-326.

Mahlberg, R., L. Paajanen, A. Nurmi, A. Kivistö, K. Koskela and R. M. Rowell (2001b). "Effect of chemical modification of wood on the mechanical and adhesion properties of wood fiber/polypropylene fiber and polypropylene/veneer composites." Holz als Roh - und Werkstoff **59**(5): 319-326.

Maldas, D. and B. V. Kokta (1990). "Effects of coating treatments on the mechanical behavior of wood-fiber-filled polystyrene composites. I. Use of polyethylene and isocyanate as coating components." Journal of Applied Polymer Science **40**(5-6): 917-928.

Maldas, D. and B. V. Kokta (1991). "Surface modification of wood fibers using maleic anhydride and isocyanate as coating components and their performance in polystyrene composites." Journal of Adhesion Science and Technology **5**(9): 727-740.

Maldas, D., B. V. Kokta and C. Daneault (1989a). "Influence of coupling agents and treatments on the mechanical properties of cellulose fiber-polystyrene composites." J. Appl. Polym. Sci. **37**: 751-775.

Maldas, D., B. V. Kokta and C. Daneault (1989b). "Thermoplastic composites of polystyrene: effect of different wood species on mechanical properties." Journal of Applied Polymer Science **38**(3): 413-439.

Maldas, D., B. V. Kokta, R. G. Raj and C. Daneault (1988a). "Improvement of the mechanical properties of sawdust wood fibre-polystyrene composites by chemical treatment." Polymer **29**(7): 1255-1265.

Maldas, D., B. V. Kokta, R. G. Raj and S. T. Sean (1988b). "Use of wood fibres as reinforcing fillers for polystyrene." Materials Science & Engineering A: Structural Materials: Properties, Microstructure and Processing **A104**: 235-244.

Malkov, S., V. Kuzmin, V. Baltakhinov and P. Tikka (2003). "Modelling the process of water penetration into softwood chips." Journal of Pulp and Paper Science **29**(4): 137-143.

Marcovich, N. E., M. M. Reboredo and M. I. Aranguren (1996). "Composites from sawdust and unsaturated polyester." Journal of Applied Polymer Science **61**(1): 119-124.

Markovitz, H. (1974). "SUPERPOSITION IN RHEOLOGY." J Polym Sci Polym Symp(50): 431-456.

Mathew, A. P., K. Oksman and M. Sain (2006). "The effect of morphology and chemical characteristics of cellulose reinforcements on the crystallinity of polylactic acid." Journal of Applied Polymer Science **101**(1): 300-310.

Matsuo, M., C. Sawatari and T. Ohhata (1988). "Dynamic mechanical studies on crystal dispersion using ultradrawn polyethylene films." Macromolecules **21**(5): 1317-1324.

Matthews, R. G., A. P. Unwin, I. M. Ward and G. Capaccio (1999). "Comparison of the dynamic mechanical relaxation behavior of linear low- and high-density polyethylenes." Journal of Macromolecular Science - Physics **B38**(1-2): 123-143.

Matuana, L. M., J. J. Balatinecz, R. N. S. Sodhi and C. B. Park (2001). "Surface characterization of esterified cellulosic fibers by XPS and FTIR spectroscopy." Wood Science and Technology **35**(3): 191-201.

Matuana, L. M., R. T. Woodhams, J. J. Balatinecz and C. B. Park (1998). "Influence of interfacial interactions on the properties of PVC/cellulosic fiber composites." Polymer Composites **19**(4): 446-455.

Mészéros, E., E. Jakab, G. Vàrhegyi, P. Szepesváry and B. Marosvölgyi (2004). "Comparative study of the thermal behavior of wood and bark of young shoots obtained from an energy plantation." Journal of Analytical and Applied Pyrolysis **72**(2): 317-328.

Meyer, M. A. and K. K. Chawla (1999). Mechanical Behavior of Materials. **Upper Saddle River** New Jersey, Pearson Prentice Hall. P.

Migneault, S., A. Koubaa, F. Erchiqui, A. Chaala, K. Englund, C. Krause and M. Wolcott (2008). "Effect of fiber length on processing and properties of extruded wood-fiber/HDPE composites." Journal of Applied Polymer Science **110**(2): 1085-1092.

Migneault, S., A. Koubaa, F. Erchiqui, A. Chaala, K. Englund and M. P. Wolcott (2009). "Effects of processing method and fiber size on the structure and properties of wood-plastic composites." Composites Part A: Applied Science and Manufacturing **40**(1): 80-85.

Moëll, M. K. and L. A. Donaldson (2001). "Comparison of segmentation methods for digital image analysis of confocal microscope images to measure tracheid cell dimensions." IAWA Journal **22**(3): 267-288.

Mohammed-Ziegler, I., Z. Ho?rvo?lgyi, A. To?th, W. Forsling and A. Holmgren (2006). "Wettability and spectroscopic characterization of silylated wood samples." Polymers for Advanced Technologies **17**(11-12): 932-939.

Mohanty, S., S. K. Verma and S. K. Nayak (2006). "Dynamic mechanical and thermal properties of MAPE treated jute/HDPE composites." Composites Science and Technology **66**(3-4): 538-547.

Mohlin, U. B. (1997). "Fibre development during mechanical pulp refining." Journal of Pulp and Paper Science **23**(1).

Moore, A. K. and N. L. Owen (2001). "Infrared spectroscopic studies of solid wood." Applied Spectroscopy Reviews **36**(1): 65-86.

Mucha, M. and Z. Krölikowski (2004). "The effect of fillers on crystallization kinetics of polypropylene." Wpyw Napeniaczy Na Kinetyke Krystalizacji Polipropylenu **25**(3 II): 1373-1379.

Müller-Hagedorn, M., H. Bockhorn, L. Krebs and U. Müller (2003). "A comparative kinetic study on the pyrolysis of three different wood species." Journal of Analytical and Applied Pyrolysis **68-69**: 231-249.

Nabi Saheb, D. and J. P. Jog (1999). "Natural fiber polymer composites: A review." Advances in Polymer Technology **18**(4): 351-363.

Nabi Saheb, D. and J. P. Jog (2000). "Compatibilization of PBT/polyolefin blends: Mechanical and dynamic mechanical properties." Advances in Polymer Technology **19**(1): 41-53.

Nardin, M. and J. Schultz (1993). "Effect of elastic moduli and interfacial adhesion energy on the critical fibre aspect ratio in single-fibre composites." Journal of Materials Science Letters **12**(16): 1245-1247.

Neagu, R. C., E. K. Gamstedt and F. Berthold (2006). "Stiffness contribution of various wood fibers to composite materials." Journal of Composite Materials **40**(8): 663-699.

Newman, R. H. (2004). "Homogeneity in cellulose crystallinity between samples of Pinus radiata wood." Holzforschung **58**(1): 91-96.

Nguila Inari, G., M. Petrissans, J. Lambert, J. J. Ehrhardt and P. Gérardin (2006). "XPS characterization of wood chemical composition after heat-treatment." Surface and Interface Analysis **38**(10): 1336-1342.

Nunez, A. J., N. E. Marcovich and M. I. Aranguren (2004). "Analysis of the creep behavior of polypropylene-woodflour composites." Polymer Engineering and Science **44**(8): 1594-1603.

Nuopponen, M. H., G. M. Birch, R. J. Sykes, S. J. Lee and D. Stewart (2006). "Estimation of wood density and chemical composition by means of diffuse reflectance mid-infrared fourier transform (DRIFT-MIR) spectroscopy." Journal of Agricultural and Food Chemistry **54**(1): 34-40.

Olson, J. A., A. G. Robertson, T. D. Finnigan and R. R. H. Turner (1995). "Analyzer for fibre shape and length." Journal of Pulp and Paper Science **21**(11).

Olsson, T., M. Megnis, J. Varna and H. Lindberg (2001). "Study of the transverse liquid flow paths in pine and spruce using scanning electron microscopy." Journal of Wood Science **47**(4): 282-288.

Orfão, J. J. M., F. J. A. Antunes and J. L. Figueiredo (1999). "Pyrolysis kinetics of lignocellulosic materials - Three independent reactions model." Fuel **78**(3): 349-358.

Palaniyandi, V. and J. Simonsen (2007). "Effect of compatibilizers on the crystallization kinetics of cellulose-filled high density polyethylene." Composite Interfaces **14**(1): 73-83.

Pandey, K. K. (1999). "A Study of Chemical Structure of Soft and Hardwood and Wood Polymers by FTIR Spectroscopy." Journal of Applied Polymer Science **71**(12): 1969-1975.

Pandey, K. K. and A. J. Pitman (2004). "Examination of the lignin content in a softwood and a hardwood decayed by a brown-rot fungus with the acetyl bromide method and Fourier transform infrared spectroscopy." Journal of Polymer Science, Part A: Polymer Chemistry **42**(10): 2340-2346.

Pandey, K. K. and K. S. Theagarajan (1997). "Analysis of wood surfaces and ground wood by diffuse reflectance (DRIFT) and photoacoustic (PAS) Fourier transform infrared spectroscopic techniques." Holz als Roh - und Werkstoff **55**(6): 383-390.

Panshin, A. J. and C. De-Zeeuw (1980). Text Book of Wood Technology. New York, McGraw-Hill Inc. 722 P.

Papp, G., E. Barta, E. Preklet, L. Tolvaj, O. Berkesi, T. Nagy and S. Szatma?ri (2005). "Changes in DRIFT spectra of wood irradiated by UV laser as a function of energy." Journal of Photochemistry and Photobiology A: Chemistry **173**(2): 137-142.

Park, B. D. and J. J. Balatinecz (1997a). "A comparison of compounding Processes for wood-fiber/thermoplastic composites." Polymer Composites **18**(3): 425-431.

Park, B. D. and J. J. Balatinecz (1997b). "Mechanical properties of wood-fiber/toughened isotactic polypropylene composites." Polymer Composites **18**(1): 79-89.

Park, B. D. and J. J. Balatinecz (1998). "Short term flexural creep behavior of wood-fiber/polypropylene composites." Polymer Composites **19**(4): 377-382.

Paunikallio, T., J. Kasanen, M. Suvanto and T. T. Pakkanen (2003). "Influence of maleated polypropylene on mechanical properties of composite made of viscose fiber and polypropylene." Journal of Applied Polymer Science **87**(12): 1895-1900.

Pegoretti, A., M. Ashkar, C. Migliaresi and G. Marom (2000). "Relaxation processes in polyethylene fibre-reinforced polyethylene composites." Composites Science and Technology **60**(8): 1181-1189.

Placet, V., J. Passard and P. Perré (2007). "Viscoelastic properties of green wood across the grain measured by harmonic tests in the range 0-95°C: Hardwood vs. softwood and normal wood vs. reaction wood." Holzforschung **61**(5): 548-557.

Placet, V., J. Passard and P. Perré (2008). "Viscoelastic properties of wood across the grain measured under water-saturated conditions up to 135 °C: evidence of thermal degradation." Journal of Materials Science **43**(9): 3210-3217.

Polovka, M., J. Polovkova, K. Viza?rova, S. Kirschnerova, L. Bielikova and M. Vrs?ka (2006). "The application of FTIR spectroscopy on characterization of paper samples, modified by Bookkeeper process." Vibrational Spectroscopy **41**(1): 112-117.

Popli, R. and L. Mandelkern (1983). "The transition in ethylene copolymers: The ?-transition." Polymer Bulletin **9**(6-7): 260-267.

Popli, R., L. Mandelkern and R. S. Benson (1984a). "Dynamic mechanical studies of *alpha* and *beta* relaxations of polyethylenes " Journal of polymer science. Part A-2, Polymer physics **22**(3): 407-448.

Popli, R., L. Mandelkern and R. S. Benson (1984b). "DYNAMIC MECHANICAL STUDIES OF alpha AND beta RELAXATIONS OF POLYETHYLENES." Journal of polymer science. Part A-2, Polymer physics **22**(3): 407-448.

Pranovich, A., J. Konn and B. Holmbom (2005). Variation in spatial distribution of organic and inorganic compounds across annual growth rings of Norway spruce and aspen. Appita Annual Conference.

Pritchard, G. (2004). "Two technologies merge: Wood plastic composites." Plastics, Additives and Compounding **6**(4): 18-21.

Rahman, M. M., S. Fujiwara and Y. Kanagawa (2005). "Variations in volume and dimensions of rays and their effect on wood properties of teak." Wood and Fiber Science **37**(3): 497-504.

Raiskila, S., M. Pulkkinen, T. Laakso, K. Fagerstedt, M. Lo?ija, R. Mahlberg, L. Paajanen, A. C. Ritschkoff and P. Saranpa?a (2007). "FTIR spectroscopic prediction of Klason and acid soluble lignin variation in norway spruce cutting clones." Silva Fennica **41**(2): 351-371.

Raj, R. G., B. V. Kokta and C. Daneault (1990). "Wood flour as a low-cost reinforcing filler for polyethylene: studies on mechanical properties." Journal of Materials Science **25**(3): 1851-1855.

Raj, R. G., B. V. Kokta, D. Maldas and C. Daneault (1988). "Use of wood fibers in thermoplastic composites. VI. Isocyanate as a bonding agent for polyethylene-wood fiber composites." Polymer Composites **9**(6): 404-411.

Ramakrishna, S., Z. Ming Huang, G. V. Kumar, A. W. Batchelor and J. Mayer (2004). An introduction to biocomposites, Imperial College Press. 223 P.

Ramiah, M. V. (1970). "Thermogravimetric and differential thermal analysis of cellulose, hemicellulose and lignin." Journal of Applied Polymer Science **14**(5): 1323-1337.

Rath, J., M. G. Wolfinger, G. Steiner, G. Krammer, F. Barontini and V. Cozzani (2003). "Heat of wood pyrolysis." Fuel **82**(1): 81-91.

Rauvanto, I., J. Pere and K. Henricson (2006). "Fibre damage in unbleached reinforcement pulp - The effect of hemicelluloses and lignin on the susceptibility of fibres to damage during oxygen delignification." Nordic Pulp and Paper Research Journal **21**(3): 328-335.

Razi, P. S., R. Portier and A. Raman (1999). "Studies on polymer-wood interface bonding: effect of coupling agents and surface modification." Journal of Composite Materials **33**(12): 1064-1079.

Read, B. E. (1989). "Mechanical relaxation in isotactic polypropylene." Polymer **30**(8): 1439-1445.

Read, B. E. and P. E. Tomlins (1997). "Creep and physical aging of injection molded, fiber reinforced polypropylene." Polymer Engineering and Science **37**(9): 1572-1581.

Reme, P. A. and T. Helle (2001). "Quantitative assessment of mechanical fibre dimensions during defibration and fibre development." Journal of Pulp and Paper Science **27**(1): 1-7.

Reme, P. A. and T. Helle (2002). "Assessment of transverse dimensions of wood tracheids using SEM and image analysis." Holz als Roh - und Werkstoff **60**(4): 277-282.

Reussmann, T. and K. P. Mieck (1999). "Dynamic-mechanical analysis of natural fiber reinforced plastics." Advanced Engineering Materials **1**(2): 140-141.

Robertson, G., J. Olson, P. Allen, B. Chan and R. Seth (1999). "Measurement of fiber length, coarseness, and shape with the fiber quality analyzer." Tappi journal **82**(10): 93-98.

Robin, J. J. and Y. Breton (2001). "Reinforcement of recycled polyethylene with wood fibers heat treated." Journal of Reinforced Plastics and Composites **20**(14): 1253-1262.

Robinson, I. M. and J. M. Robinson (1994). "The influence of fibre aspect ratio on the deformation of discontinuous fibre-reinforced composites." Journal of Materials Science **29**(18): 4663-4677.

Rodrigues, J., O. Faix and H. Pereira (1998). "Determination of lignin content of Eucalyptus globulus wood using FTIR spectroscopy." Holzforschung **52**(1): 46-50.

Rodrigues, J., O. Puls and H. Pereira (2001). "Determination of monosaccharide composition of Eucalyptus globulus wood by FTIR spectroscopy." Holzforschung **55**(3): 265-269.

Rowell, R. M. (2004). Solid wood processing/Chemical Modification. *in* Encyclopedia of forest sciences. H. Burley, J. Evans and J. A. Youngquist (Ed.). San Diego, Elsevier Ltd. **3:** 1269-1274.

Rowell, R. M., J. S. Han and J. S. Rowell (2000). Characterization and Factors Effecting Fiber Properties. Natural Polymers and Agrofibers Composites, Sãn Carlos, Brazil.

Rowell, R. M., P. Roger, J. S. Han, J. S. Rowell and M. A. Tshabalala (2005). cell wall chemistry. *in* Handbook of wood chemistry and wood composites. R. M. Rowell (Ed.). Boca Raton, Fla, CRC Press: 35-74.

Ruel, K., V. Chevalier-billosta, F. Guittemin, J. B. Sierra and J. P. Joseleau (2006). "The wood cell wall at the ultrastructural scale formation and topochemical organization." Maderas: Ciencia y Tecnologia **8**(2): 107-116.

Saha, A. K., S. Das, D. Bhatta and B. C. Mitra (1999). "Study of Jute Fiber Reinforced Polyester Composites by Dynamic Mechanical Analysis." Journal of Applied Polymer Science 7**1**(9): 1505-1513.

Sain, M. M., J. Balatinecz and S. Law (2000). "Creep fatigue in engineered wood fiber and plastic compositions." Journal of Applied Polymer Science 77(2): 260-268.

Sain, M. M., B. V. Kokta and C. Imbert (1994). "Structure-property relationships of wood fiber-filled polypropylene composite." Polymer - Plastics Technology and Engineering **33**(1): 89-104.

Saka, S. and R. J. Thomas (1982a). "Evaluation of the quantitative assay of lignin distribution by SEM-EDXA-technique." Wood Science and Technology **16**(1): 1-18.

Saka, S. and R. J. Thomas (1982b). "A study of lignification in loblolly pine tracheids by the SEM-EDXA technique." Wood Science and Technology **16**(3): 167-179.

Salmén, L. (2004). "Micromechanical understanding of the cell-wall structure." Comptes Rendus - Biologies **32**7(9-10): 873-880.

Salmén, L. and I. Burgert (2009). "Cell wall features with regard to mechanical performance. A review. COST Action E35 2004-2008: Wood machining - Micromechanics and fracture." Holzforschung **63**(2): 121-129.

Salmen, L. and A.-M. Olsson (1997). Interaction between hemicelluloses, lignin and cellulose; Structure-property relations. Proceedings of the ACM Workshop on Role-Based Access Control, Montreal, Can, ACM.

Salmén, L. and A. M. Olsson (1998). "Interaction between hemicelluloses, lignin and cellulose: Structure-property relationships." Journal of Pulp and Paper Science **24**(3): 99-103.

Sanschagrin, B., S. T. Sean and B. V. Kokta (1988). Mechanical properties of cellulose fibers reinforced thermoplastics. Society of the Plastics Industry, Reinforced Plastics/Composites Institute, Annual Conference - Proceedings, Cincinnati, OH, USA, Publ by SPI.

Saputra, H., J. Simonsen and K. Li (2004). "Effect of extractives on the flexural properties of wood/plastic composites." Composite Interfaces **11**(7): 515-524.

Sernek, M., F. A. Kamke and W. G. Glasser (2004). "Comparative analysis of inactivated wood surface." Holzforschung **58**(1): 22-31.

Sha, H., X. Zhang and I. R. Harrison (1991). "A dynamic mechanical thermal analysis (DMTA) study of polyethylenes." Thermochimica Acta **192**(C): 233-242.

Shafizadeh, F. (1981). "Basic principles of direct combustion." Biomass Conversion Processes for Energy and Fuels: 103-124.

Shafizadeh, F. (1982). "INTRODUCTION TO PYROLYSIS OF BIOMASS." Journal of Analytical and Applied Pyrolysis **3**(4): 283-305.

Shafizadeh, F. and A. G. W. Bradbury (1979). "THERMAL DEGRADATION OF CELLULOSE IN AIR AND NITROGEN AT LOW TEMPERATURES." J Appl Polym Sci **23**(5): 1431-1442.

Sheshkali, H. R. Z., H. Assempour and H. Nazockdast (2007). "Parameters affecting the grafting reaction and side reactions involved in the free-radical melt grafting of maleic anhydride onto high-density polyethylene." Journal of Applied Polymer Science **105**(4): 1869-1881.

Silverstein, R. M. (2005). The spectrometric identification of organic compounds. Hoboken, N.J, John Wiley & Sons. 512 P.

Simonsen, J., R. Jacobsen and R. Rowell (1998). "Wood-fiber reinforcement of styrene-maleic anhydride copolymers." Journal of Applied Polymer Science **68**(10): 1567-1573.

Sinn, G., M. Gindl, A. Reiterer and S. Stanzl-Tschegg (2004). "Changes in the surface properties of wood due to sanding." Holzforschung **58**(3): 246-251.

Sirviö, J. and P. Kärenlampi (2001). "The effects of maturity and growth rate on the properties of spruce wood tracheids." Wood Science and Technology **35**(6): 541-554.

Smith, M. J., H. Dai and K. Ramani (2002). "Wood-thermoplastic adhesive interface - Method of characterization and results." International Journal of Adhesion and Adhesives **22**(3): 197-204.

Smith, P. M. and M. P. Wolcott (2006). "Opportunities for wood/natural fiber-plastic composites in residential and industrial applications." Forest Products Journal **56**(3): 4-11.

Solomon, P. R. and R. M. Carangelo (1982). "FTIR analaysis of coal. 1. techniques and determination of hydroxyl concentrations." Fuel **61**(7): 663-669.

Sombatsompop, N., A. Kositchaiyong and E. Wimolmala (2006). "Experimental analysis of temperature and crystallinity profiles of wood sawdust/polypropylene composites during cooling." Journal of Applied Polymer Science **102**(2): 1896-1905.

Sombatsompop, N., C. Yotinwattanakumtorn and C. Thongpin (2005). "Influence of type and concentration of maleic anhydride grafted polypropylene and impact modifiers on mechanical properties of PP/wood sawdust composites." Journal of Applied Polymer Science **97**(2): 475-484.

Sorvari, J., E. Sjöström, A. Klemola and J. E. Laine (1986). "Chemical characterization of wood constituents, especially lignin, in fractions separated from middle lamella and secondary wall of Norway spruce (Picea abies)." Wood Science and Technology **20**(1): 35-51.

Sretenovic, A., U. Mu?ller and W. Gindl (2006). "Mechanism of stress transfer in a single wood fibre-LDPE composite by means of electronic laser speckle

interferometry." Composites Part A: Applied Science and Manufacturing **37**(9): 1406-1412.

Stadler, F. J., J. Kaschta and H. Münstedt (2005). "Dynamic-mechanical behavior of polyethylenes and ethene-/?-olefin- copolymers. Part I. ??-relaxation." Polymer **46**(23): 10311-10320.

Stamm, A. J. (1953). "Diffusion and penetration mechanism of liquids into wood." Pulp and Paper Magazine of Canada **54**(2): 10.

Stark, N. M. and M. J. Berger (1997). Effect of Particle Size on Properties of Wood-Flour Reinforced Polypropylene Composites. Fourth International Conference on Woodfiber-Plastic Composites. Madison, Wisconsin, Forest Product Society p.

Stark, N. M., L. M. Matuana and C. M. Clemons (2004). "Effect of processing method on surface and weathering characteristics of wood-flour/HDPE composites." Journal of Applied Polymer Science **93**(3): 1021-1030.

Stark, N. M. and R. E. Rowlands (2003). "Effects of wood fiber characteristics on mechanical properties of wood/polypropylene composites." Wood and Fiber Science **35**(2): 167-174.

Steckel, V., C. M. Clemons and H. Thoemen (2007). "Effects of material parameters on the diffusion and sorption properties of wood-flour/polypropylene composites." Journal of Applied Polymer Science **103**(2): 752-763.

Stokke, D. D. and D. J. Gardner (2003). "Fundamental aspects of wood as a component of thermoplastic composites." Journal of Vinyl and Additive Technology **9**(2): 96-104.

Sturtevant, J. M. (1987). "Biochemical applications of differential scanning calorimetry." Annu. Rev. Phys. Chem. **38**: 463-488.

Suzuki, H. (2003). "Probabilistic study of visible length of fibers under the surface of a short fiber reinforced composite." Nippon Kikai Gakkai Ronbunshu, A Hen/Transactions of the Japan Society of Mechanical Engineers, Part A **69**(4): 719-726.

Tajvidi, M. (2005). "Static and dynamic mechanical properties of a kenaf fiber-wood flour/polypropylene hybrid composite." Journal of Applied Polymer Science **98**(2): 665-672.

Tajvidi, M., R. H. Falk and J. C. Hermanson (2006a). "Effect of natural fibers on thermal and mechanical properties of natural fiber polypropylene composites studied by dynamic mechanical analysis." Journal of Applied Polymer Science **101**(6): 4341-4349.

Tajvidi, M., S. K. Najafi and N. Moteei (2006b). "Long-term water uptake behavior of natural fiber/polypropylene composites." Journal of Applied Polymer Science **99**(5): 2199-2203.

Takatani, M., H. Ito, S. Ohsugi, T. Kitayama, M. Saegusa, S. Kawai and T. Okamoto (2000). "Effect of lignocellulosic materials on the properties of thermoplastic polymer/wood composites." Holzforschung **54**(2): 197-200.

Takeshita, H., K. Ishida, Y. Kamiishi, F. Yoshii and T. Kume (2000). "About the surface characteristics of natural fibres." Macromolecular Materials and Engineering **283**: 132-139.

Tesoro, F. O., E. T. Choong and O. K. Kimbler (1974). "Relative permeability and the gross pore structure of wood." Wood and Fiber **6**(3): 226-236.

Thomason, J. L. and A. A. Van Rooyen (1992). "Transcrystallized interphase in thermoplastic composites - Part I Influence of fibre type and crystallization temperature." Journal of Materials Science **27**(4): 889-896.

Tjeerdsma, B. F. and H. Militz (2005). "Chemical changes in hydrothermal treated wood: FTIR analysis of combined hydrothermal and dry heat-treated wood." Holz als Roh - und Werkstoff **63**(2): 102-111.

Toivanen, T. J. and R. Alén (2006). "Variations in the chemical composition within pine (Pinus sylvestris) trunks determined by diffuse reflectance infrared spectroscopy and chemometrics." Cellulose **13**(1): 53-61.

Tokoh, C., K. Takabe, J. Sugiyama and M. Fujita (2002). "CP/MAS 13C NMR and electron diffraction study of bacterial cellulose structure affected by cell wall polysaccharides." Cellulose **9**(3-4): 351-360.

Tserki, V., N. E. Zafeiropoulos, F. Simon and C. Panayiotou (2005). "A study of the effect of acetylation and propionylation surface treatments on natural fibres." Composites Part A: Applied Science and Manufacturing **36**(8): 1110-1118.

Tucker, M. P., Q. A. Nguyen, F. P. Eddy, K. L. Kadam, L. M. Gedvilas and J. D. Webb (2001). "Fourier transform infrared quantitative analysis of sugars and lignin in pretreated softwood solid residues." Applied Biochemistry and Biotechnology - Part A Enzyme Engineering and Biotechnology **91-93**: 51-61.

Tze, W. T. Y., D. J. Gardner, C. P. Tripp and S. C. O'Neill (2006). "Cellulose fiber/polymer adhesion: Effects of fiber/matrix interfacial chemistry on the micromechanics of the interphase." Journal of Adhesion Science and Technology **20**(15): 1649-1668.

Tze, W. T. Y., S. C. O'Neill, C. P. Tripp, D. J. Gardner and S. M. Shaler (2007). "Evaluation of load trasfer in the cellulosic-fiber/polymer interphase using a micro-Raman tensile test." Wood and Fiber Science **39**(1): 184-195.

Wang, C. and L. M. Hwang (1996). "Transcrystallization of PTFE fiber/PP composites. II. Effect of transcrystallinity on the interfacial strength." Journal of Polymer Science, Part B: Polymer Physics **34**(8): 1435-1442.

Wang, C. and C. R. Liu (1999). "Transcrystallization of polypropylene composites: nucleating ability of fibres." Polymer **40**(2): 289-298.

Wang, Y., H. C. Chan, S. M. Lai and H. F. Shen (2001). "Twin screw compounding of PE-HD wood flour composites." International Polymer Processing **16**(2): 100-107.

Ward, I. M. (1983). *Mechanical Properties of Solid Polymers*. Chichester. P.

Watanabe, U. (1998). "Liquid penetration of precompressed wood VI: Anatomical characterization of pit fractures." Journal of Wood Science **44**(2): 158-162.

Wester, D. (2005). "Hot new technology marries wood and plastic." Timber Producer(9): 12-14.

Westermark, U., O. Lidbrandt and I. Eriksson (1988). "Lignin distribution in spruce (Picea abies) determined by mercurization with SEM-EDXA technique." Wood Science and Technology **22**(3): 243-250.

Wielage, B., T. Lampke, G. Marx, K. Nestler and D. Starke (1999). "Thermogravimetric and differential scanning calorimetric analysis of natural fibres and polypropylene." Thermochimica Acta **337**(1-2): 169-177.

Wimmer, R., B. H. Lucas, T. Y. Tsui and W. C. Oliver (1997). "Longitudinal hardness and Young's modulus of spruce tracheid secondary walls using nanoindentation technique." Wood Science and Technology **31**(2): 131-141.

Wolkenhauer, A., G. Avramidis, E. Hauswald, H. Militz and W. Viöl (2009). "Sanding vs. plasma treatment of aged wood: A comparison with respect to surface energy." International Journal of Adhesion and Adhesives **29**(1): 18-22.

Wunderlich, B. (1973). Macromolecular Physics II. New York, Academic Press. 476 P.

Xanthos, M. (1983). "PROCESSING CONDITIONS AND COUPLING AGENT EFFECTS IN POLYPROPYLENE/WOOD FLOUR COMPOSITES." Plastics and Rubber Processing and Applications **3**(3): 223-228.

Yang, J. L., Z. Zhang, A. K. Schlarb and K. Friedrich (2006). "On the characterization of tensile creep resistance of polyamide 66 nanocomposites. Part II: Modeling and prediction of long-term performance." Polymer **47**(19): 6745-6758.

Yilmazer, U. and M. Cansever (2002). "Effects of processing conditions on the fiber length distribution and mechanical properties of glass fiber reinforced nylon-6." Polymer Composites **23**(1): 61-71.

Yip-wah, C. (2001). Practical guide to surface science and spectroscopy. New York, Academic Press. 186 P.

Yuan, Q., D. Wu, J. Gotama and S. Bateman (2008). "Wood fiber reinforced polyethylene and polypropylene composites with high modulus and impact strength." Journal of Thermoplastic Composite Materials **21**(3): 195-208.

Zadorecki, P. and A. J. Michell (1989). "Future prospects for wood cellulose as reinforcement in organic polymer composites." Polymer Composites **10**(2): 69-77.

Zafeiropoulos, N. E., C. A. Baillie and F. L. Matthews (2001). "Study of transcrystallinity and its effect on the interface in flax fibre reinforced composite materials." Composites Part A: Applied Science and Manufacturing **32**(3-4): 525-543.

Zaini, M. J., M. Y. A. Fuad, Z. Ismail, M. S. Mansor and J. Mustafah (1996). "The effect of filler content and size on the mechanical properties of polypropylene/oil palm wood flour composites." Polymer International **40**(1): 51-55.

Zhang, M., J. Xu, Z. Zhang, H. Zeng and X. Xiong (1996). "Effect of transcrystallinity on tensile behaviour of discontinuous carbon fibre reinforced semicrystalline thermoplastic composites." Polymer **37**(23): 5151-5158.

Zhang, S. Y., Y. Zhang, M. Bousmina, M. Sain and P. Choi (2007). "Effects of raw fiber materials, fiber content, and coupling agent content on selected properties of polyethylene/wood fiber composites." Polymer Engineering and Science **47**(10): 1678-1687.

Zhang, Y., H. Toghiani, J. Zhang, Y. Xue and C. U. Pittman Jr (2009). "Studies of surface-modified wood flour/polypropylene composites." Journal of Materials Science: 1-9.

APPENDIXES

Appendix1 : Machine settings of the Coperion Werner & Pfleiderer ZSK-25 WLE co-rotating twin-screw extruder (Stuttgart, Germany) used for compounding.

Compounding	Screw speed	Flow rate	Torque	Pressure	Melting temperature
25% Eastern white Cedar(sapwood)20-28 mesh/73% HDPE /2% MAPE	200 RPM	10 Kg/Hr	38 %	210 PSI	196 °C
35% Eastern white Cedar(sapwood)20-28 mesh/63% HDPE /2% MAPE	200 RPM	10 Kg/Hr	44%	255 PSI	199 °C
45% Eastern white Cedar(sapwood)20-28 mesh/53% HDPE /2% MAPE	200 RPM	10 Kg/Hr	49%	345 PSI	202 °C
25% eastern white Cedar(sapwood)35-48 mesh/73% HDPE /2% MAPE	200 RPM	10 Kg/Hr	38 %	205 PSI	196 °C
35% Eastern white Cedar(sapwood)35-48 mesh/63% HDPE /2% MAPE	200 RPM	10 Kg/Hr	41 %	231 PSI	199 °C
45% Eastern white Cedar(sapwood)35-48mesh/53% HDPE /2% MAPE	200 RPM	10 Kg/Hr	46 %	345 PSI	201 °C
25% Eastern white Cedar(sapwood)48-100 mesh/73% HDPE /2% MAPE	200 RPM	10 Kg/Hr	29 %	142 PSI	194 °C
35% Eastern white Cedar(sapwood)48-100 mesh/63% HDPE /2% MAPE	200 RPM	10 Kg/Hr	34 %	170 PSI	196 °C
45% Eastern white Cedar(sapwood)48-100 mesh/53% HDPE /2% MAPE	125 RPM	10 Kg/Hr	15 %	54 PSI	192 °C
25% Eastern white Cedar(heartwood)20-28 mesh/73% HDPE /2% MAPE	250 RPM	15 Kg/Hr	84 %	242 PSI	204 °C
35% Eastern white Cedar(heartwood)20-28 mesh/63% HDPE /2% MAPE	250 RPM	15 Kg/Hr	86 %	232 PSI	211 °C
45% Eastern white Cedar(heartwood)20-28 mesh/53% HDPE /2% MAPE	250 RPM	15 Kg/Hr	90 %	300 PSI	216 °C
25% Eastern white Cedar(heartwood)35-48 mesh/73% HDPE /2% MAPE	250 RPM	15 Kg/Hr	79 %	248 PSI	200 °C

(Continued)

35% Eastern white Cedar(heartwood)35-48 mesh/63% HDPE /2% MAPE	275 RPM	15 Kg/Hr	82 %	249 PSI	206 °C
45% Eastern white Cedar(heartwood)35-48mesh/53% HDPE /2% MAPE	250 RPM	10Kg/Hr	76 %	202 PSI	200 °C
25% Eastern white Cedar(heartwood)48-100 mesh/73% HDPE /2% MAPE	200 RPM	10 Kg/Hr	65 %	165 PSI	198 °C
35% Eastern white Cedar(heartwood)48-100 mesh/63% HDPE /2% MAPE	200 RPM	10 Kg/Hr	72 %	250 PSI	200 °C
45% Eastern white Cedar(heartwood)48-100 mesh/53% HDPE /2% MAPE	200 RPM	5 Kg/Hr	45 %	145 PSI	197 °C
25% Black spruce 35-48 mesh/73% HDPE /2% MAPE	240 RPM	15 Kg/Hr	84 %	235 PSI	204 °C
35% Black spruce 20-28 mesh/63% HDPE /2% MAPE	260 RPM	15 Kg/Hr	85 %	240 PSI	209 °C
35% Black spruce 48-100 mesh/63% HDPE /2% MAPE	250 RPM	15 Kg/Hr	82 %	225 PSI	205 °C
25% Jack pine 20-28 mesh/73% HDPE /2% MAPE	240 RPM	15 Kg/Hr	82 %	230 PSI	201 °C
35% Jack pine 20-28 mesh/63% HDPE /2% MAPE	240 RPM	12 Kg/Hr	75 %	235 PSI	204 °C
45% Jack pine 48-100 mesh/53% HDPE /2% MAPE	240 RPM	10 Kg/Hr	73 %	234 PSI	207 °C
25% Jack pine bark 20-28 mesh/73% HDPE /2% MAPE	240 RPM	15 Kg/Hr	76 %	212 PSI	202 °C
35% Jack pine bark 20-28 mesh/63% HDPE /2% MAPE	250 RPM	15 Kg/Hr	78 %	241 PSI	204 °C
45% Jack pine bark20-28 mesh/53% HDPE /2% MAPE	260 RPM	15 Kg/Hr	80 %	270 PSI	207 °C
25% Jack pine bark 35-48 mesh/73% HDPE /2% MAPE	240 RPM	15 Kg/Hr	76 %	214 PSI	202 °C
35% Jack pine bark 35-48 mesh/63% HDPE /2% MAPE	240 RPM	15 Kg/Hr	77 %	231 PSI	204 °C

(Continued)

45% Jack pine bark 35-48mesh/53% HDPE /2% MAPE	250 RPM	15 Kg/Hr	78 %	260 PSI	205 °C
25% Jack pine bark 48-100 mesh/73% HDPE /2% MAPE	240 RPM	15 Kg/Hr	76 %	211 PSI	201 °C
35% Jack pine bark 48-100 mesh/63% HDPE /2% MAPE	240 RPM	15 Kg/Hr	76 %	238 PSI	202 °C
45% Jack pine bark 48-100 mesh/53% HDPE /2% MAPE	250 RPM	15 Kg/Hr	76 %	265 PSI	203 °C

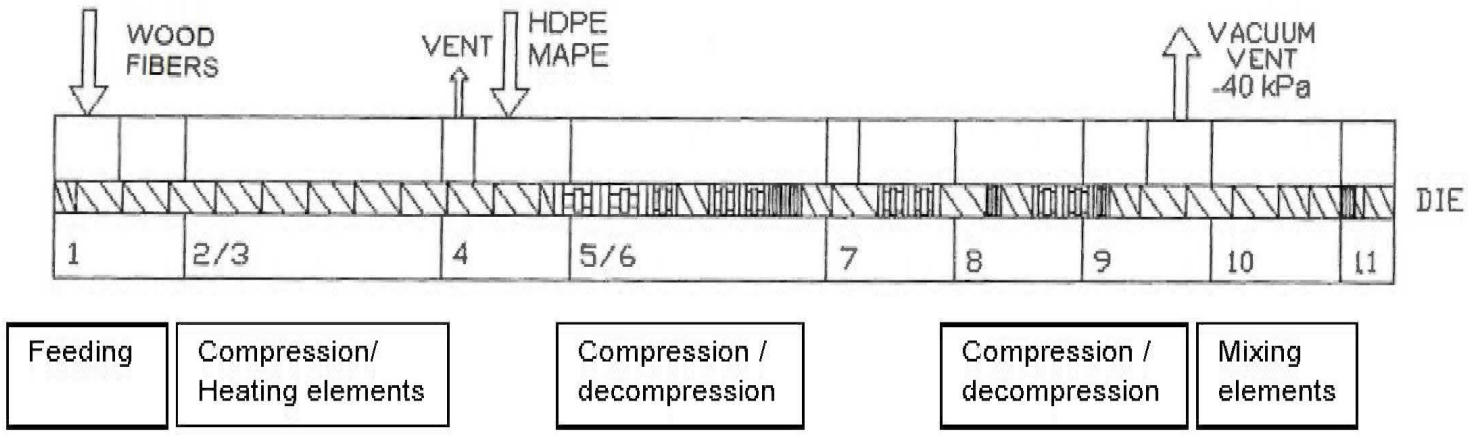

Appendix 2: Multi stage screw profile on co-rotating intermeshing twin-screw extruder.

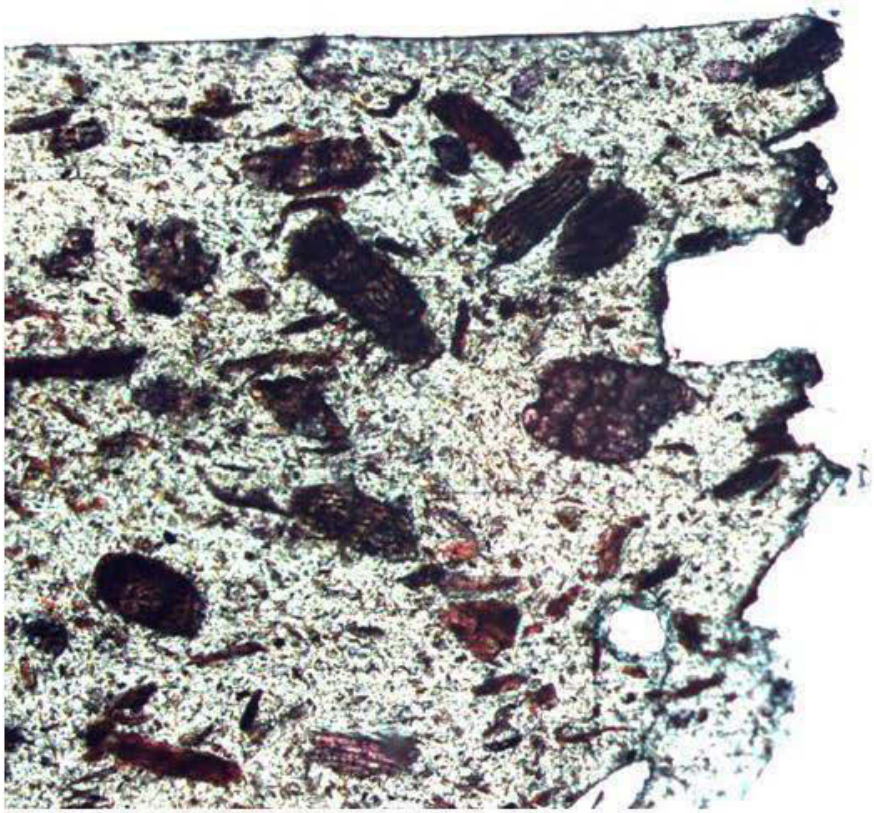

Appendix 3. Example of failure plane due to lack of adhesion between wood particles and HDPE (x5). Composite is made of 25 wt% eastern cedar heartwood particles (28 mesh size).

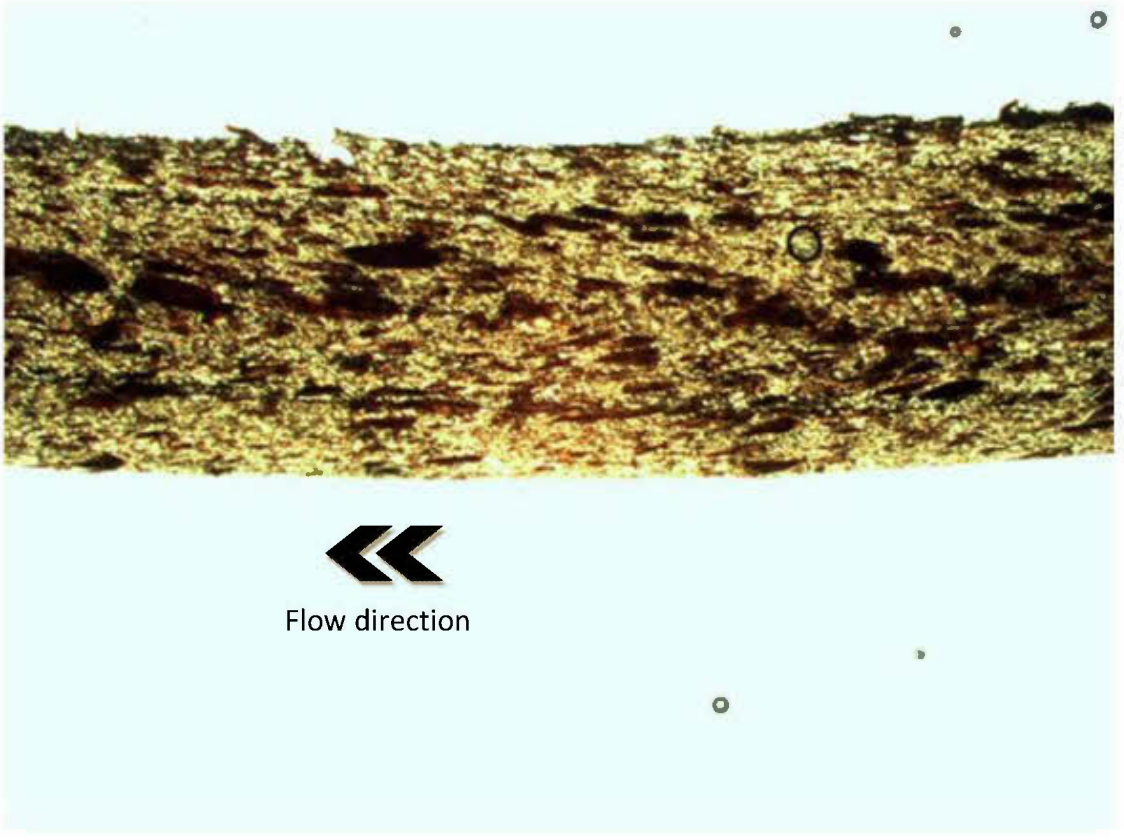

Appendix 4. Example of optical microscope enhancement (x1.5) showing the alignment of the wood particles in the direction of flow in an injected composite (35 wt% of jack pine wood particles).

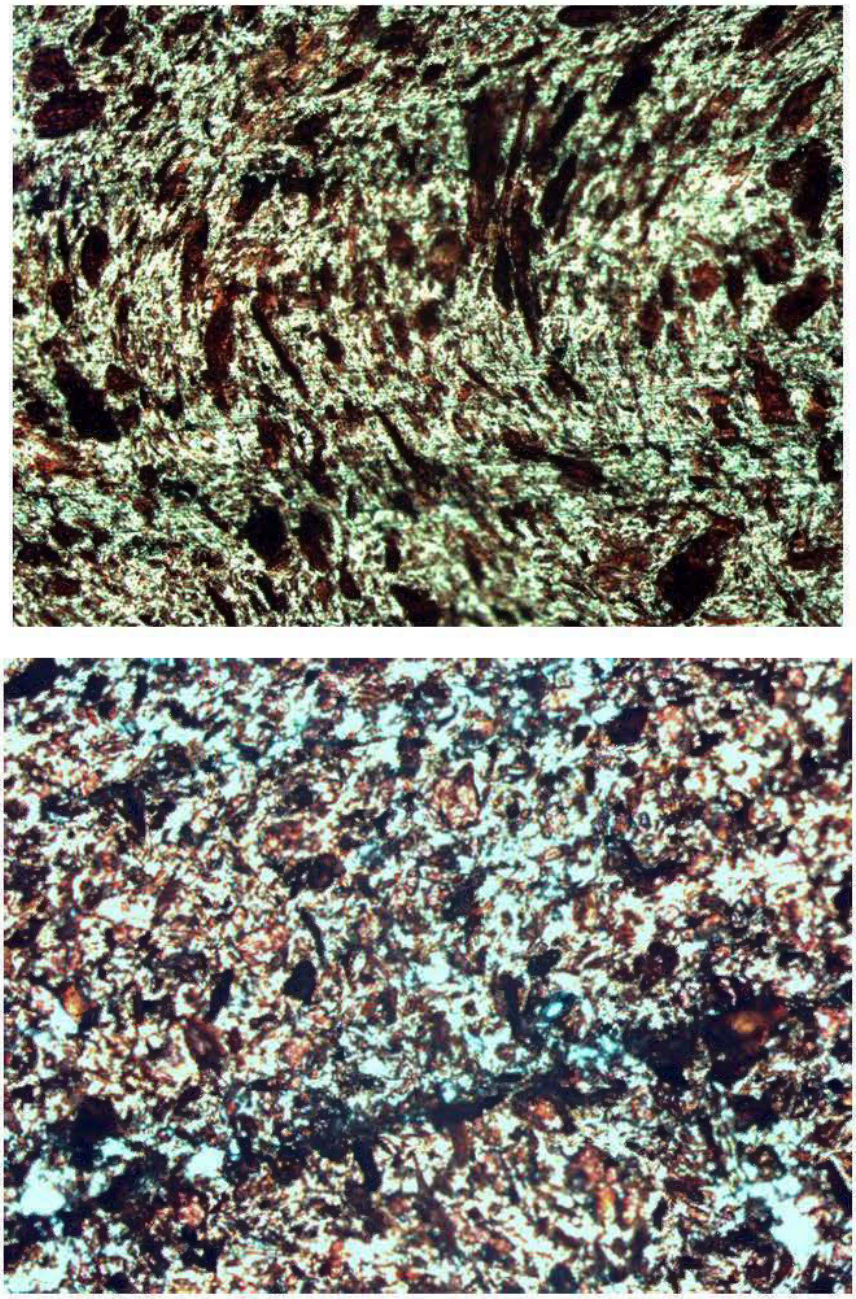

Appendix 5. Example of transversal section (x5)of the structure of an injected moulding composite made with 45 wt% jack pine wood particle (top) and bark particle (bottom). Initially mean size of the particles was 42 mesh.

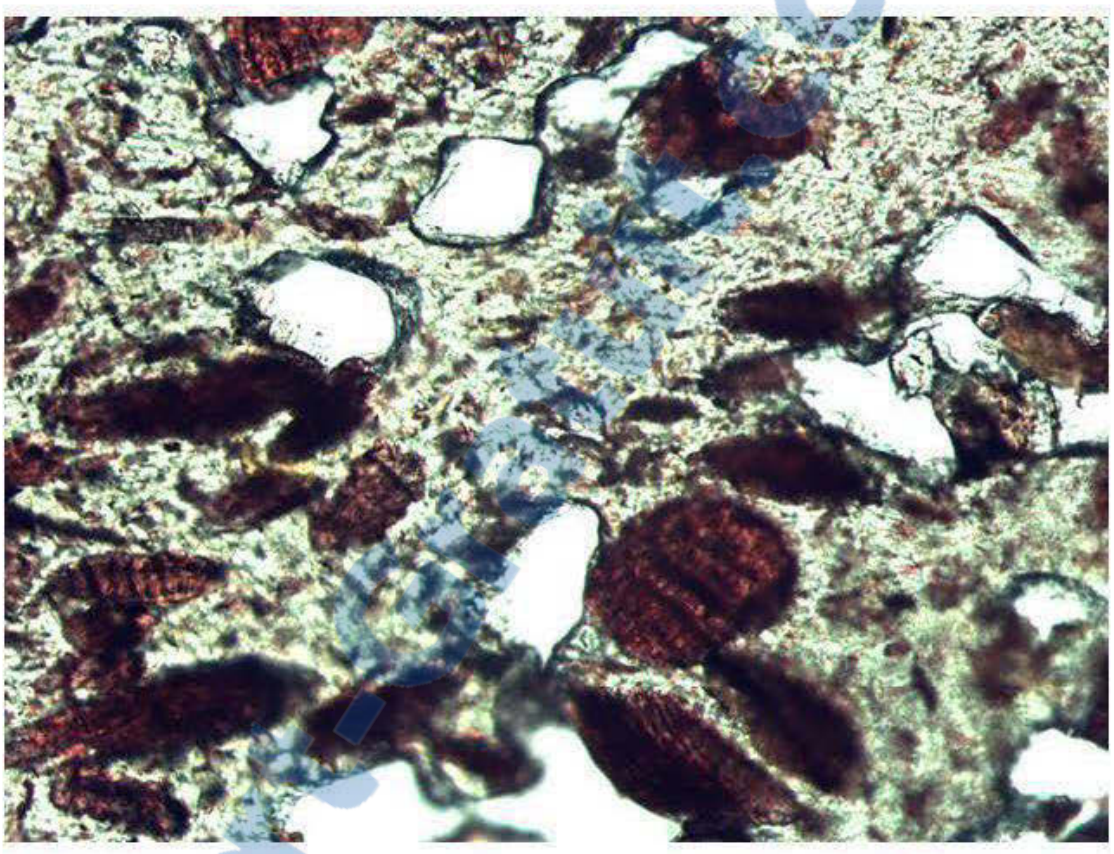

Appendix 6. Optical microscopic section (x10) of an extruded sample showing the existence of voids, which weaken the bonds and produce composites of lower stiffness and strength. Composite here is made of 25wt% black spruce particle having 42 mesh size.